Slurry, Solution and Speciation Analysis By Inductively Coupled Plasma Atomic Emission Spectrometry

by

KAREN LORRAINE O'HANLON

A thesis submitted to the University of Plymouth
in partial fulfilment for the degree of

DOCTOR OF PHILOSOPHY

Department of Environmental Sciences
Faculty of Science

In collaboration with
The Perkin-Elmer Corp.
761 Main Ave., Norwalk, CT 06897, USA

September 1996

Slurry, Solution and Speciation Analysis By ICP-AES

ABSTRACT

Karen Lorraine O'Hanlon

Inductively coupled plasma atomic emission spectrometry has been investigated for solution, slurry and speciation analysis. It has been shown that it is possible to optimise a simultaneous multielement analysis for slurry and solution samples using solid state detection and optimisation algorithms. A range of certified reference materials have been analysed using optimum conditions and results were in good agreement with certified values. Slurry nebulisation has been used for the first time in the analysis of NIST SRM 'Total Diet' and carbon black samples. Both radially and axially viewed ICP spectrometers were used in these studies.

Modifications of the mass transport efficiency of solutions and slurries through the sample introduction system was illustrated upon EIE addition. The transport phenomenon was found to be dependent on the matrix element and not on the analyte of interest. A decrease in transport efficiency was found to be related to the mass of the EIE added.

Solution and slurry atom and ion line intensity ratios obtained from an axially viewed ICP were used to illustrate emission enhancement when Mg was used as the thermometric species of interest. Enhancement was found to be spatially dependent and the energy transfer processes governing excitation were modified upon EIE addition. The magnitude of the enhancement effects for solutions and slurries differed, once transport effects had been negated, and this was attributed to variations in atomisation efficiency. A radially viewed ICP spectrometer was also used to monitor the effect of EIEs on solutions and slurries. The Abel integral technique was used to transform lateral profiles and Fe atom line ratios were calculated. 'Real' enhancement effects were apparent upon EIE addition when transport effects had again been negated.

The plasma excitation temperature was used as a physical marker to determine the effect of EIE addition on solutions and slurries of Fe. The variation in T_{exc} upon EIE addition was small but showed an increasing trend from Li to Cs. Radially obtained values of T_{exc} were lower than literature values whereas preliminary values obtained axially compared well.

It has been demonstrated that transient signal data may be obtained from an array-based spectrometer for speciation studies. The feasibility of reverse phase and size exclusion HPLC-ICP-AES has been demonstrated for the separation of a selection of organosilicon species of various molecular weights. Detection limits were in the range 0.1 to 5 $\mu g\ ml^{-1}$ for a radially viewed plasma. The use of axial viewing when aspirating organic solvents as part of the mobile phase yields higher limits of detection owing to the noise that is measured.

LIST OF CONTENTS

LIST OF TABLES

LIST OF FIGURES

Chapter 5

ACKNOWLEDGEMENTS

I would like to thank my supervisors, Dr. Mike Foulkes and Prof. Les Ebdon for their continuous support, encouragement and friendship throughout the past three years. I also wish to thank the University of Plymouth and The Perkin-Elmer Corporation for their financial support.

I gratefully acknowledge Prof. Akbar Montaser for donating the Abel inversion computer program used in this study. I would also like to thank Juan Ivaldi of the Perkin-Elmer Corp. for technical assistance regarding the Optima 3000 instruments. Thanks also go to Dennis Yates, Chris Hanna and Ken Fredeen of The Perkin-Elmer Corp. for negotiating my trips to the US.

I would like to thank my friends at the University of Plymouth and the Perkin-Elmer Corp., USA, my husband Richard for his support throughout and my parents for their encouragement.

AUTHOR'S DECLARATION

At no time during the registration for the degree of Doctor of Philosophy has the author been registered for any other university award.

This study was financed with the aid of a studentship from the University of Plymouth.

A programme of advanced study was undertaken, which included instruction in ICP atomic emission theory and instrument operation and a supervised study in Basic programming.

Relevant scientific seminars and conferences were regularly attended at which work was often presented, external institutions were visited for consultation purposes and several papers prepared for publication.

Publications arising from this project:

"Optimised Simultaneous Multi-Element Analysis of Environmental Slurry Samples by Inductively Coupled Plasma Atomic Emission Spectrometry Using a Segmented Array Charge-Coupled Device Detector"; Ebdon, L., Foulkes, M.E. and O'Hanlon, K., Anal. Chim. Acta, 1995, 311, 123.

ICP Application Study No. 81, "The Analysis of NIST SRM Total Diet by Slurry Nebulization ICP-OES", O'Hanlon, K. and Barnes, K.W., The Perkin-Elmer Corp., Norwalk, CT, USA, 1995.

"The Effect of Easily Ionisable Elements on Solutions and Slurries in an Axially Viewed Inductively Coupled Plasma"; O'Hanlon, K., Ebdon, L. and Foulkes, M.E., J. Anal. At. Spectrom., 1996, 11,427.

ICP Application Study No. 83, "The Analysis of Sulphur in Carbon Black by Slurry Nebulization ICP-OES", O'Hanlon, K. and Barnes, K.W., The Perkin-Elmer Corp.,Norwalk, CT, USA, 1996.

"Slurry Nebulization Into Plasmas - A Review", O'Hanlon, K., Ebdon, L. and Foulkes, M.E., J. Anal. At. Spectrom., 1996 (in press).

"The Effect of Easily Ionisable Elements on the Mass Transport Efficiency of Solutions and Slurries", O'Hanlon, K., Ebdon, L. and Foulkes, M.E., J. Anal. At. Spectrom., 1996 (in press).

"The Effect of Easily Ionisable Elements on Emission Intensity and Excitation Temperature for Solutions and Slurries in a Radially Viewed Inductively Coupled Plasma with Simultaneous Detection Capability"., O'Hanlon, K., Ebdon, L. and Foulkes, M.E., J. Anal. At. Spectrom., 1996 (in press).

Presentations and conferences attended (P = poster presentation, L = lecture presentation):

Perkin-Elmer Environmental Symposium, London, UK, April 1994 (L).

R and D Topics in Analytical Chemistry Meeting, University of Hertfordshire, UK, July 1994 (P).

7th BNASS, University of Hull, UK, July 1994 (P).

European Winter Conference on Plasma Spectrochemistry, Cambridge, UK, January 1995 (P).

R and D Topics in Analytical Chemistry Meeting, University of Hull, UK, July 1995 (P).

SAC 95, University of Hull, UK, July 1995 (P and L).

European Winter Conference on Plasma Spectrochemistry, Ft. Lauderdale, Florida, USA, January, 1996 (L).

8th BNASS, University of East Anglia, Norwich, UK, July, 1996 (L).

Signed Karen J Howles

Date 30th October 1996

Chapter 1 - Introduction

1.1 Slurry Nebulisation into Plasmas

It is well established that the method of sample presentation into plasmas is the critical step in an analytical procedure (1). The most conventional method of introducing samples to plasmas is by nebulisation of dissolved samples. Traditionally, samples have been prepared as solutions using digestion steps such as fusion or acid dissolution. This facilitates introduction, calibration and homogenisation. Many analytical samples are, however, of an intractable nature, such as silicaceous minerals, refractory compounds and ceramics. Methods based on, for example, fusion and on digestion using acids can result in incomplete dissolution of the sample, evaporative losses of the more volatile elements and contamination problems. Dissolution can also be time consuming and sample preparation time often exceeds analysis time. Hazardous and concentrated acids such as HF and $HClO_4$ may be required to digest samples. In addition, achieving a true multi-element dissolution for certain samples may be difficult, as is the case for geological materials which contain a variety of minerals. The direct introduction of solids or slurries into plasmas would circumvent these difficulties and markedly reduce sample preparation time by combining matrix destruction, analyte atomisation and excitation in a single step. Analytical plasmas are, in general, higher temperature sources than conventional combustion flames, a prerequisite if complex solid matrices are to be efficiently atomised, ionised and excited.

The introduction of solid samples into the plasma may be implemented using a number of well established techniques such as the 'swirl cup' (2), fluidised bed chamber (3), the direct sample insertion device (4-6), 'spark discharges' (7-9) and laser ablation (10-12). Another approach to solid sample introduction involves the nebulisation of (usually aqueous) suspensions of fine powders into the ICP and is termed 'slurry nebulisation'. Slurry sample nebulisation is an alternative technique to solution nebulisation and has received particular attention in recent years. The technique offers many of

the same advantages of other solid sample introduction techniques, such as elimination of complex dissolution procedures and the avoidance of hazardous chemicals. In addition, the technique is simple to implement, is inexpensive and requires little instrument modification. The most significant advantage of slurry nebulisation is that it can be calibrated using aqueous solutions in an analogous way to solution nebulisation. As other solid sampling techniques are plagued by problematic calibration procedures, slurry nebulisation has attracted the interest of analytical spectroscopists in a wide range of application areas. In the last decade, the technique of slurry nebulisation has been adapted for different samples and many of the early difficulties of achieving a homogenous and stable dispersion have been overcome.

1.2 Plasma Techniques Used in Slurry Analysis

Slurry nebulisation has been implemented using a variety of plasma techniques. The most common is Inductively Coupled Plasma Atomic Emission Spectrometry (ICP-AES) with numerous papers reporting a wide variety of studies (13 - 67). Inductively Coupled Plasma Mass Spectrometry (ICP-MS) has been increasingly used in recent years, although less work has been published in this area (64 - 80) due to it being a younger spectroscopic technique. Direct Current Plasma (DCP) Emission Spectrometry was used for earlier studies into slurry sample introduction (14,81 - 87) but recent analytical trends have favoured the use of modern ICP-AES and ICP-MS instrumentation. This may be attributed to the low limits of detection attainable in the 'hotter' ICP, fewer matrix effects and instrument availability. One paper has even reported the introduction of slurries into a microwave induced plasma (MIP) (88) despite the significantly lower kinetic temperature of this plasma compared to most ICPs.

Electrothermal vaporisation (ETV) has developed into a popular tool for the analysis of trace elements in recent years. The technique enables the possible separation of matrix constituents using particular temperature and

time components before transportation of the analyte into the ICP via a stream of argon. Several papers regarding slurry 'nebulisation' ETV coupled with ICP-AES have been published (89 - 91) as well as the use of ETV-ICP-MS (92, 93) which offers superior limits of detection.

A survey of solid sampling in ICP-MS has been written by Bauman (94). Slurry sample nebulisation is compared in this paper to other solid sample introduction techniques such as ETV, direct sample insertion and laser ablation. Darke and Tyson (95) also compare ETV and laser ablation with slurry nebulisation. A study of the literature with regards to the application of the slurry technique to biological materials has been made by de Benzo and co-workers (96).

1.3 Slurry Preparation

1.3.1 Grinding Methods

It is now accepted that, unless the sample from which a slurry is to be prepared is of a naturally small mean diameter (as with clays), then it must be ground in order to reduce the solid particle size. The transport efficiency of the slurry particle through the sample introduction system and the behaviour of the particle in the plasma in terms of atomisation and excitation must be identical to a solution of equivalent concentration if aqueous calibration is to be used. The particle size is the limiting parameter for efficient slurry nebulisation and theoretically the maximum particle size of the slurry must be such that a single solid particle may occupy an aerosol droplet (56). To achieve a particle size distribution that would yield results similar to those of an equivalent, equimolar aqueous solution, a wide range of grinding techniques have been employed in the literature (97).

The technique of choice and the actual grinding time depends on the sample being prepared. Table 1.1 lists the various mills and size reduction methods that have been used to date, with varying degrees of success, to grind a wide range of materials. The particle size ranges that result are also tabulated. The

GRINDING METHOD	SAMPLE	GRINDING TIME	RESULTING PARTICLE SIZE	COMMENTS	REFERENCE
Bottle and Bead Method	Geological materials	40 mins	<60 µm	1.00 g of sample ground with 10 g of beads	63
	Geological/ Refractory Materials	15 hours (overnight)	<5 µm	Aqua regia added to prevent sample loss	77
	Refractory Samples	-	<10 µm	Beads:sample mass ratio = 10:1. Dispersant added prior to grinding	38
	Firebrick Plant Material	2 hours 4 hours	2 - 2.5 µm <2 µm	0.5 g dm^{-3} $Na_4P_2O_7$ added Material ashed before grinding	56
	Coals	Overnight	<8 µm	Varied in efficiency for different samples	73
	Ores and minerals	1 hour	<8 µm	Technique compared to micronising mill	27
	Ores	30 minutes	<6 µm	Acetone added	13

Table 1.1 - Grinding methods used in the preparation of slurries for introduction into plasmas.

GRINDING METHOD	SAMPLE	GRINDING TIME	RESULTING PARTICLE SIZE	COMMENTS	REFERENCE
	Soils	3 hours	<8 µm	Dispersant added before grinding	33
	Soils and sediments	12 hours	<50 µm	Lithium (as chloride) added as ionisation buffer	86
	Soils, zeolite, catalysts	24 hours	<3 µm	Materials may be reduced to <8 µm with 2 hours grinding	72
	Slags	3 hours	<10 µm	Sample ground in ball mill for 3 hours and sieved before bottle and bead method	47
	Agricultural samples	Overnight	<5 µm	Recovery 95 % of equivalent aqueous solution	83
	Spinach, garlic and pollen	1 hour	-	Agate spheres used with varying amounts of PTFE	89
Micronising Mill	Silicate Rocks	8 hours	<3 µm	4 g of sample ground in mill	75

Table 1.1 (cont.) - Grinding methods used in the preparation of slurries for introduction into plasmas.

GRINDING METHOD	SAMPLE	GRINDING TIME	RESULTING PARTICLE SIZE	COMMENTS	REFERENCE
	Ores and minerals	10- 15 minutes	<8 µm	Produced a similar slurry distribution to 1 hour grinding by bottle and bead method	27
	Coal	20 - 30 minutes	6 µm	Sample weighed directly onto agate grinding pellets	22
	Coal	30 minutes	<25 µm	Samples ground to <38 µm in Tema Disc mill initially	23
	Coal	10 minutes	<20 µm	Dispersant added to ten times original weight of coal powder	82
	Biological samples	30 minutes	3 µm	0.5 g sample and nylon coated stainless steel beads used	76
	Whole plant tissue	30 minutes	5.7 µm	Homogeniser used for 4 minutes. Alumina milling aid added.	84

Table 1.1 (cont.) - Grinding methods used in the preparation of slurries for introduction into plasmas.

GRINDING METHOD	SAMPLE	GRINDING TIME	RESULTING PARTICLE SIZE	COMMENTS	REFERENCE
Mixing Mill	Plant tissue	15 minutes	27 - 154 µm	Samples oven dried at 80°C for 6 hours before grinding	44
	Estuarine sediments	30 minutes	<2 µm	1.5 ml agate vial and agate ball used	45
Puck Type Grinder	Geological and refractory materials	-	<10 µm	80 % of particles <10 µm, majority less than 5 µm	39
Puck Type Grinder then Rotary Grinder	Geological materials	10 minutes in puck type then 40 minutes in rotary grinder	<2 µm	Samples ground initially to 75 µm in puck grinder then for various periods in rotary grinder	25
Grinding Mill	Silicon Carbide	10 minutes	<38 µm	4 g of sample ground	57
Vibration Pot Mill	Geochemical Materials	16 hours (overnight)	7 - 10 µm	beads:sample mass ratio = 10:1	66

Table 1.1 (cont.) - Grinding methods used in the preparation of slurries for introduction into plasmas.

choice of grinding or milling agent is important and will effect analytical accuracy. The grinding material should be harder than the material being ground and should not contain elements that will interfere with an analysis.

It is known that materials containing a large proportion of brittle, hard composites can be ground efficiently and make excellent slurries if the correct grinder/dispersant is chosen. This is the case for some geological samples such as rocks, sediments and soils (69). However, some materials which have a high measure of hardness (MOH) value, such as silicates and other refractories, may be difficult to grind. The attrition materials used in mills and grinders, such as zirconia and tungsten carbide, may have comparable MOH values resulting in poor grinding efficiencies and even contamination if long periods of size reduction are employed. In addition, rock samples are invariably composed of a variety of minerals which generally have different grain sizes, MOH values and friabilities (77). Grinding may therefore reduce the particle size of some of the minerals to a lesser extent than others. This will result in poor analytical accuracy for some elements after aspiration of the slurry into the plasma. Fractionation in the sample introduction system may also occur for samples where particle size varies with sample composition (38). Generally grinding procedures, which produce more uniform particle size, e.g. ball mills, are therefore preferred to techniques which may produce a wide range of particle sizes.

A review by de Benzo *et al.* (96) discusses the importance of preparing a homogenous and representative sample for biological materials. The authors argue that trace elements in biological samples may be evenly distributed in the lattices of the sample matrix or they may be present as discrete particles found irregularly throughout the matrix. Trace elements are present as salts in most biological tissue and liquids or are bound to proteins, vitamins and enzymes. Total sample dissolution ensures elemental homogeneity but for biological slurry samples the homogeneity depends on the distribution of the element of interest in the original material and the method of grinding. Poor precision is obtained if there is difficulty obtaining a homogenous slurry but

this may be overcome, for instance, by taking all the tissue from one part of the plant or animal.

Biological materials that contain a high degree of fibrous material may be resistant to grinding. In addition, some plants may contain components that can appreciably increase the viscosity of slurries at relatively low sample loadings (83). Charring the samples by placing them in a muffle furnace at temperatures in the region of 200 - 300^{0}C breaks down this fibrous structure and enables grinding of the material to the required particle size range (83). Losses due to the volatility of certain species must also be considered if the charring technique is used and consequently lower temperatures are recommended.

1.3.2 Dispersion of Slurries

Preparing slurries in aqueous solution alone is unsuitable for the majority of samples due to flocculation effects which result in rapid sedimentation of the finely powdered material. It is therefore essential to prepare a stable and homogenous slurry that will achieve a stable, homogenous aerosol for introduction into the plasma yielding accurate and precise analytical results. This is achieved by employing stabilising agents, commonly termed 'dispersants' or 'surfactants'.

Table 1.2 shows the different dispersants that have been used in the preparation of slurries from a wide variety of samples. Dispersants fall into two main categories - non-ionic, e.g. Triton X-100; and ionic e.g Sodium hexametaphosphate. In addition, ionic dispersants may be cationic (e.g. Cetrimide) or anionic (e.g. Dispersal T) in character. If the surface of the solid in the preferred liquid carrier is lyophobic, the powder will be difficult to disperse. If it is lyophilic the powder disperses easily (98). To obtain a suitable dispersion of lyophobic particles, stabilising agents are added to wet the surface so that the particle becomes lyophilic. There have been few in depth studies in the literature regarding the stabilising effect of dispersants.

DISPERSANT	CONCENTRATION	SAMPLE	REFERENCE
Aerosol OT	0.5 g dm^{-3}	Plant material	56
	0.1 % m/v	Coal	65, 73
Ammonia	0.35 % v/v	Slags	47
	0.35 % v/v	Kaolin clay	28,30, 85
Darvan-7	0.5 % m/m	Ceramics	61
Darvan-C	0.5 % m/m	Ceramics	61
Dolapix PC-33	0.5 % m/m	Ceramics	61
Glycerine + 0.5 N HCl	40 %	ZrO_2	36
Glycerol + Kodak photoflow	40 % v/v 2 % v/v	Ceramic, geological and refractory materials	39
Sodium hexametaphosphate	0.1 % m/v	Refractory samples, sulphide ore	27,38
Sodium hexametaphosphate + monoisopropanolamine	0.1 % m/v 0.02 % m/v	TiO_2	29
Tetrasodium pyrophosphate	0.05 % m/v	Soils, catalysts, geological samples, firebrick	72
	0.1 % m/v	geochemical materials silicon nitride,	66, 77
	1% m/v	soils	33
	0.5 g dm^{-3}	firebrick, sediment	43, 56

Table 1.2 - Dispersants used to stabilise slurries for nebulisation into plasmas

DISPERSANT	CONCENTRATION	SAMPLE	REFERENCE
Triton X-100	0.005 % v/v	Coal, total diet, oyster tissue, lobster hepatopancreas	92, 93
	0.01 % v/v	Soils, milk, plant tissue sediments	83 45
	0.05 % v/v	Tea leaves	59
	0.1 % v/v	Milk powder, soils, sediments, silicate rocks, silicon carbide	71 78, 86 75 57
	0.5 % v/v	Whole plant tissue, coal	84 15, 22, 82
	1% v/v	Coal, biological samples	23,24 76
Xylene	100 %	Airborne particulate matter	16
HCl	1 % m/m	Silicon nitride	60
	2 mol l^{-1}	Clays	17
H_2SO_4	2% v/v	Biological samples	41
HNO_3	1% m/m	Zeolites	90
	10% m/m	Lobster hepatopancreas, marine sediment	88
	0.01 M	Citrus and tomato leaves	44
	1 M	Marine sediment	52

Table 1.2 (cont.) - Dispersants used to stabilise slurries for nebulisation into plasmas

DISPERSANT	CONCENTRATION	SAMPLE	REFERENCE
HNO_3 + NaCl	1 M 0.1 M	Clays	48
NaCl	0.1 M	Clay minerals	40
None		Animal tissue. Geological materials, Clays, Si_3N_4 Al_2O_3 SiC Foods ZrO_2 Ores and flotation feeds	81 25, 55, 63 25 35, 42 70 70 89 50 18

Table 1.2 (cont.) - Dispersants used to stabilise slurries for nebulisation into plasmas

Fariñas *et al.* published an excellent study on the colloidal stability of ceramic suspensions for the nebulisation of slurries for ICP-AES (61). The authors report a case study using alumina slurries when different pH conditions and dispersing agents were used. The paper shows the different types of stabilising additives available for ceramic suspensions and also the best use of them. The authors explain the electrostatic stabilising mechanism in detail and state that in a ceramic suspension, H^+ and OH^- ions determine the potential. In the case of Al_2O_3, the charge on the surface of any slurry particle is negative resulting in the attraction of protons to the surface and creating a gradient of concentration (of protons) from the particle surface to the liquid. Conversely, the OH^- ion concentration is decreased near the surface of the particle and increases with distance from the surface. A charged layer, known as the electrical double layer is formed because of the potential gradient set up. The surface potential of the particle may be changed according to the Nernst equation by changing the concentration of the potential determining ion. The relative adsorption of ions onto the surface of the slurry particle will alter as a result.

At a particular concentration of the potential determining ion the positive and negative surface activities will be equal and the overall potential at the surface of the particle will be zero. In this scenario, no double layer exists and agglomeration of the particles is observed at a concentration known as the isoelectric point. This demonstrates the important role a dispersant plays when added to a slurry. The potential at the surface of a slurry particle is known as the zeta potential. A slurry is only stable when the zeta potential is high and significantly removed from the isoelectric point. The addition of a dispersant causes the zeta potential to change and ultimately acts to stabilise the slurry. Clearly the concentration of a dispersant must be controlled, as an excess can be detrimental to the slurry stability and be a cause of coagulation. Triton X-100 was found not to stabilise alumina slurries and no real dispersion was achieved with 'Kodak photoflow' in glycerol. The dispersant PKV-5088 was unable to prevent sedimentation of alumina despite being commonly used to disperse nonoxide ceramics. Three dispersants,

Dolapix PC-33, Darvan-C and Darvan-7 were found to produce the desired dispersion of an alumina slurry. The precision of the ICP-AES measurement was found to be directly related to the stability offered by the dispersant system. The authors state that the dispersant additive may yield the required stability providing an electrostatic stabilising mechanism by either i) controlling the pH (using potential determining ions), ii) using inorganic electrolytes or iii) using a polyelectrolyte where long chain polymers adsorbed onto the surface of particles prevent contact between them.

In the same paper the influence of pH on the slurry stability was examined by plotting the zeta potential versus pH for Al_2O_3. The pH was altered by the addition of NH_4OH and the point of maximum zeta potential evaluated. Optimum conditions for the preparation of the homogenous alumina slurry was pH 4 - 5 and it was concluded that pH is the parameter that controls stability. As the stability of the slurry increases, so too does the emission intensity and the RSD of the values are lower. Fuller and co-workers described how the pH of an ore slurry was adjusted to between 6 and 7 to maintain stability (13).

Lobiński *et al.* (50) attempted to stabilise a ZrO_2 slurry by optimising the pH. Two optima were found at pH 1 - 2 and pH 10 - 11. The addition of an acidic medium gave a broader optimum and so in further preparations all slurries were acidified to pH 2.

Ebdon and Collier (28) investigated three dispersants commonly used in the stabilisation of kaolin slurries: Calgon (sodium hexametaphosphate), Dispex and aqueous ammonia solution. Aqueous ammonia was found to be the most effective in dispersing the irregular, flat, plate-like kaolin particles. Equivalent slurry and aqueous atomisation efficiencies for Mg were obtained. Dilute ammonia solution (0.35%) was also found to be the most effective dispersant in the analysis of slags in a study by Fernandez *et al.* (47). Triton X-100, sodium pyrophosphate and ammonia were compared - ammonia producing the most stable emission signals for all the elements under investigation.

Some early studies concerning the viability of slurry nebulisation as an alternative sample introduction technique did not realise the importance of the addition of dispersant as a slurry stabilising agent. Halicz and Brenner (25) prepared slurries of silicate materials in the absence of a dispersant. Poor analyte signal intensity ratios were obtained and calibration functions were not consistent. Further work (55, 63) concluded that slurries of particle size less that 1.5 and 2.0 μm did not behave similarly to aqueous aerosols. Again, a surfactant was not introduced to stabilise the slurry and poor recoveries when compared to solutions of equivalent concentration are consistent with the effect from agglomeration.

Biological samples have also been prepared for analysis using ETV-ICP-AES without the use of dispersants (89). However, PTFE was used as a fluorinating agent to eliminate memory effects and appears to act as a solid dispersant as the recoveries of Mo were found to be very good for all the certified reference materials analysed.

1.3.3 Magnetic Stirring and Vortex Mixing

Magnetic stirring of a slurry is frequently performed, after preparation and dispersion, whilst the slurry is being pumped to the sample introduction system (47, 59). This ensures a homogenous distribution of the solid material in the liquid phase and prevents sedimentation of particles. Errors caused by sedimentation are directly related to particle size and the presence of dense solid particles of varying composition may cause differential sedimentation.

Many geological materials contain magnetic, iron containing minerals such as magnetite (Fe_3O_4). The use of magnetic stirring would result in migration and even adhesion of some slurry particles to a magnetic stirring bar (99). Vortex mixing may be used in these instances as an alternative and effective method to ensure homogeneity of slurry samples before aspiration into the ICP (63).

1.3.4 Ultrasonic Agitation

Slurries have been homogenised using ultrasonic agitation as an alternative to grinding the sample, or in addition to grinding. Samples that do not require grinding are well documented in the literature. Ebdon and Collier (28) prepared slurries of 0.2 % m/v unground kaolin samples, dispersed with 0.35 % m/v NH_3. Slurries were placed in an ultrasonic bath for 30 minutes and particles were found to be less that 2 μm in diameter.

It has been reported that the analyte of interest may be partially extracted into the liquid phase, owing to the ultrasonic action, when slurries are prepared in an acidic medium. Manickum and Verbeek (59) determined the concentration of Al, Ba, Mg, and Mn in tea leaves by ICP-AES slurry nebulisation. The sample was sonicated for 5 minutes with a solution containing 10 mol l^{-1} HCl and Triton X-100. It was found that between 50 and 60 % of the total Al and Ba and between 66 and 77 % of the total Mg and Mn was extracted during this 5 minute dispersion period. The authors noted that similar amounts of analyte elements are leached in the usual 5 minute brewing time of tea made with boiling water.

1.4 Influence of Slurry Particle Size on Analytical Performance

It is well known that the particle size distribution of a slurry is the limiting factor controlling analytical recovery (56). Slurry nebulisation into plasmas requires that both the analyte transport efficiency of the slurry particle through the sample introduction system and the atomisation efficiency of that particle in the plasma must be identical to that of a solution (56). If these criteria are fulfilled then simple aqueous calibration may be used.

Ebdon *et al.* (38) measured transport and atomisation efficiencies directly from emission intensity data. Magnesium of known concentration was absorbed onto a silica-based cation exchange material. Magnesium and

silicon emission signals were compared to those of the equivalent solution. The magnesium recovery was used as a measure of the slurry transport efficiency relative to the solution and was found to depend on slurry particle size. A transport efficiency of 3-4% was obtained for particles of 10 μm diameter. This transport efficiency improved to 14 - 15% when the particle size was 5 μm. Neither particle size range was found to model the atomisation of solutions under the plasma conditions used.

Vien and Fry (84) discussed the effect of slurry particle size on analytical recovery for plant tissue samples using DCP emission spectrometry. They state that for aerosol transport through a modified DCP spray chamber, particles larger than 23 μm will not be delivered to the plasma. Instead, they settle out of the aerosol stream and exit the spray chamber via the drain. Using a laser diffractometer, the median plant particle diameter was measured to be 85 μm which exceeded the spray chamber cut off limit. By milling the sample using an abrasive milling aid, the particle size distribution was much improved and the elemental recovery for Cu was found to be 94 %. No correction factors, standard addition, matrix matching or lithium buffering were necessary.

Fernandez *et al.* (47) measured the particle size distribution effect on the 'atomisation efficiency' of Ca, Mg, Al, Fe, Mn, Ti, Na and K in slags using ICP-AES. The sample was ground in a ball mill for increasing periods of time. It was observed that suspensions prepared from different particle size ranges produced different emission intensities for the elements in question. The emission signal was found to increase with grinding time but not to the same extent for the various elements, indicating that the slag was a multicomponent material.

Raeymaekers and co-workers collected solid Al_2O_3 particles from a slurry aerosol onto membrane filters at the top of the torch injector in the absence of an ICP discharge (31). The mean diameters of the particles were found to be

below 17 μm. Emission signals for an Al_2O_3 powder, a refractory oxide of low grain size, showed good agreement with those of an Al solution.

Ebdon *et al.* (38) performed fundamental studies of refractory samples using ICP-AES. Particle size effects were studied using alumina. Slurries of known composition with size distributions exceeding 90 % (by volume) less than 8 μm but of various size fractions, were analysed for their aluminium content. The finest particle size alumina slurry (100 % less than 2.5 μm) gave 99 % recovery indicating that transport and atomisation efficiencies of the slurry are close to that of a solution. For samples difficult to atomise, a particle size of less than 5 μm (the bulk being less than 3 μm) was optimal. Conditions which brought about a longer residence time in the plasma also aided atomisation.

In the work of Darke *et al.* (66), calculated recoveries for SARM 5, a rock material, were low for a wide range of elements. A high proportion of the particles were in the range 7 - 10 μm and it was concluded that reduction of the particle size should improve the ICP-AES results.

Ebdon and Collier (30) used a variety of spray chambers and torches with different diameter injectors to study particle size effects in kaolin slurry nebulisation. Using a 3 mm i.d. injector tube enabled the analysis of kaolin slurries with particles up to 8 μm in diameter. Recoveries were comparable to equivalent solutions. It was suggested that even when particles greater than 8 μm reached the plasma they were only partially atomised or pass through the plasma without being atomised. In a separate paper (28) the same authors illustrated the effects of nebuliser design, particle size, dispersants and viscosity in the analysis of kaolin by slurry nebulisation.

Recently (56), Goodall *et al.* introduced the size occupancy diameter (SOD) model which assumes that the maximum allowable particle size is that which allows the occupation of every aerosol droplet by one solid particle. For slurries to give comparable recoveries to those of solutions it was stated that the particle size distribution of the slurry should not exceed 2.9 μm for a

material of density 1 g cm^{-3} or 1.5 µm for a material of density 7 g cm^{-3} for a given double pass spray chamber. The solid particle size in the slurry was stated to be the fundamental limiting factor for efficient slurry nebulisation into the ICP.

Ebdon and Collier (28) found a wide particle size range to be the major cause of low recoveries for a kaolin sample using ICP-AES. The particle size distribution of post-spray-chamber kaolin was measured and a cut off point of 2 µm for particle size was calculated. Halicz and Brenner (25) also found that increased signal ratios corresponded to reduced particle size. For a basalt rock slurry, elemental intensity ratios increased sharply with grinding time.

Isozaki (43) found that the slurry particle size coupled with nebuliser gas flow rate influences sensitivity and accuracy in the determination of iron in silicon nitride by ICP-AES. Approximately 90 % of the slurry particles were found to be below 2.3 µm, 4.4 µm and 8.5 µm for 3 different silicon nitride samples, respectively. The authors concluded that the particle size for this particular sample should be below 10 µm. Broekaert and co-workers (70) discussed the possibilities and limitations of the slurry technique for ICP-AES and ICP-MS. They found that the particle size of the slurry is of major importance and concluded that slurry particle size should be below the 5 - 10 µm level. Lobiński *et al.* (50) looked at the effect of particle size on the solution/slurry emission ratio for ten ZrO_2 powders using ICP-AES. For samples with particles smaller that 10 µm a full recovery was obtained. Mochizuki *et al.* (75) illustrated that sensitivity, precision and accuracy were dependent on the slurry particle size for rare earth element determination in silicate rocks. The emission count rate was shown to increase with increasing grinding time.

The role of particle size on the efficiency of vaporisation and atomisation of botanical sample slurries using fluorination-slurry sampling ETV-ICP-AES has been investigated (91). Recoveries were obtained by comparing elemental intensities from the plant slurries with those obtained when the samples were acid digested. The recovery increased with decreasing particle size. When the

average particle size was less than 170 μm the recovery was approximately 100 %. This work concluded that the use of *in situ* fluorination yields excellent recoveries for larger particle sizes.

1.5 Solid Particle Size Distribution Measurements

The particle size distribution of a fine powdered sample may be determined by examining a suspension of that material. Various methods have been used to measure the particle size distribution of slurries to ensure suitability of the slurry before analysis by plasma techniques. Often, the method by which the particle size is measured depends on the instrumentation available so there is no rigid methodology to follow for a particular sample. Table 1.3 lists the techniques that are documented in the literature together with the particle size range that was measured for the particular sample.

Optical microscopy should be used to check the dispersion of a slurry. It is useful to analyse slurries in this manner immediately prior to sample introduction into the plasma to ensure that loose agglomeration of particles has not occurred.

1.6 The Influence of Slurry Concentration

The concentration of the slurry is an important factor to consider during preparation. Slurries may be diluted but only within a limited range as precision may be degraded with slurries that are highly diluted. This is because of the smaller number of particles in the total volume which remain after dilution has been performed. Ebdon and Wilkinson (23) prepared coal slurries in the concentration range 1 - 25 % m/v for analysis by ICP-AES. The effect of sample pumping rate with varying concentration was optimised. For an argon plasma, the signal to background ratio increased linearly with increasing slurry concentration up to 20 % m/v. The effects of viscosity and non-Newtonian rheological phenomena should be considered for very concentrated slurries.

PARTICLE SIZE MEASUREMENT METHOD	SAMPLE	PARTICLE SIZE DISTRIBUTION	COMMENTS	REFERENCE
Automated Electron Probe Microanalysis	Al_2O_3	<0.3 μm	No particles larger that 16 μm observed	37, 49
	TiO_2 powder	<5 μm	Number of particles sized = 500	29
	ZrO_2 powder	<1.4 μm	Before analysis, slurries filtered through a Nucleopore membrane	50
Coulter Counter	Firebrick, Plant material	2 - 2.5 μm <2 μm	Optical microscopy showed aggregation of 5 - 10 particles for plant material	56
	Geochemical materials	7 - 10 μm	Particle size effects observed	66
	Kaolin	Various fractions from 0.5 μm up to 50 μm	Particle size distribution measured for various fractions	28, 30
	Ores	<6 μm	-	13
	Refractory Samples	<10 μm	Slurry does not model atomisation of an equivalent solution	38

Table 1.3 - Techniques used to measure the particle size distribution of slurries before nebulisation into plasmas

PARTICLE SIZE MEASUREMENT METHOD	SAMPLE	PARTICLE SIZE DISTRIBUTION	COMMENTS	REFERENCE
	Soils, zeolites, catalysts	<3 μm	-	72
	Whole coal	<25	Various size fractions analysed	23
	Whole Coal	Two samples <2 μm and two <10 μm	Various certified coals analysed	65
Laser Diffractometer	Coal	<8 μm	Particle size distributions measured for various coals	73
	Coal	6 μm	Non-intrusive aerosol droplet size measurements also performed using the diffractometer	22
	Geological Samples	<2 μm	Particle size analyser used	55
	Whole Plant tissue	5.7 μm	Diffractometer could not distinguish between milling aid and plant tissue	84
	Refractory oxide powders	<20 μm	Sub μm condensates and remolten larger particles identified	31

Table 1.3 (cont.) - Techniques used to measure the particle size distribution of slurries before nebulisation into plasmas

PARTICLE SIZE MEASUREMENT METHOD	SAMPLE	PARTICLE SIZE DISTRIBUTION	COMMENTS	REFERENCE
Photosedimentometer	Slags	<10 µm	-	47
SEM	Geological Materials	<2 µm	Silicate rocks and glass samples analysed	25, 63
	Botanical Samples	<400 µm	Samples prepared by sieving	91
Optical Microscopy (430X magnification)	Coal	<20 µm	Particles obtained from different grinding techniques differentiated	82
Submicron Particle Sizer	Biological Samples	3 µm	Flour powder analysed successfully whereas liver and pine needles posed problems	76
X-Ray Diffraction	Rock samples	<0.2 - 45 µm	Particle size and mineralogy detected by XRD	48

Table 1.3 (cont.) - Techniques used to measure the particle size distribution of slurries before nebulisation into plasmas

SAMPLE	ELEMENTS DETERMINED	PLASMA TECHNIQUE	DISPERSANT USED	COMMENTS	REFERENCE
Plant Materials	Ca, Mg, Mn, P	ICP-AES	1 g dm^{-3} Aerosol OT	Sample ashed before grinding	56
	Cu, Mn, Pb, Zn	DCP-AES	0.01% Triton X-100	Carbonisation procedure used for fibrous material	83
Refractory Oxide Powders	Al, Cu, Fe, Mg, Nb, Si, Zr	ICP-AES	0.01% SHMP and monoisopropan-olamine	Slurry technique compared with direct insertion and electroerosion techniques	29
Refractory Samples	Cu, Zn, Pb, Sn, Ag, Fe, Mo, As, Zr	ICP-AES	0.1% Sodium hexametaphosphate	Fundamental studies carried out	38
Rice Flour	Mn, Fe, Co, Ni, Cu, Zn, As, Se, Br, Rb, Mo, Cd, Pb	ICP-MS	1% Triton X-100	Acceptable Accuracy and precision obtained	76
Rocks	Si, Ca, Mg, Fe, Al, Ti, Mn	ICP-AES	-	Grinding time and particle size effects investigated	25
	Al, K, Na, Si, Ba, Mn, Sr, Ti, Ca, Mg, Cu	ICP-AES and ICP-MS	0.1 % $Na_4P_2O_7$	Poor recoveries due to large particle size of slurry	66
Slags	Si, Ca, Mg, Al, Fe, Mn, Ti, Na, K	ICP-AES	0.35 % ammonia	Calibration performed using reference slag	47

Table 3.1 (continued) Applications of Slurry Nebulisation Into Plasmas

Williams *et al.* (72) prepared slurries of refractory compounds for nebulisation into an ICP mass spectrometer. Slurries of 1 g per 100 ml were originally prepared but it was found that, after 30 minutes of nebulisation, partial blockage of the sampling cone occurred due to the deposition of particles. Two dilutions (0.05 g 100 ml^{-1} and 0.0001 g 100 ml^{-1}) of the slurry were therefore made prior to the analysis for minor/trace level elements and for major elements. No blocking problems were encountered after dilution was carried out.

Mochizuki and co-workers analysed rare earth elements in silicate rocks using ICP-MS (75). Again, the use of slurries with a high solids concentration resulted in deposition on the sampling cone and the analytical signal fell with time. The authors state that the upper limit of concentration depends on the sample matrix being analysed. Refractory compounds deposit on the sampling cone and cause the sensitivity of the analysis to decrease with time. The low content of refractory inorganic compounds in biological samples allows the aspiration of relatively high slurry concentrations.

Conventionally, acid dissolution procedures produce solutions with 1 % sample content. Clearly the ability to use slurries with a sample content of 20 % or more yields major advantages in trace analysis.

1.7 Modifications to the Sample Introduction System

1.7.1 Introduction

The effective introduction of a slurry sample into a plasma is a critical step if comparable recoveries to equivalent solutions are to be obtained. The sample introduction system consists of three basic parts; a nebuliser, which produces a fine aerosol of solution and, if of the correct design, slurry particles (100); a spray chamber, which removes relatively large particles (101); and a torch, which enables the sample to travel to the plasma via an injector. Other parts may be added to the sample introduction system to improve sample throughput and transport efficiencies if desired. These may include

desolvation devices, tandem sources, the use of a sheathing gas or flow injection.

1.7.2 Nebulisers

The efficient nebulisation of a sample is the most critical step in the sample introduction system. There are many examples in the literature of various nebulisers and their customised counterparts which are all designed to improve transport efficiencies and are suited to particular samples.

The nebulisation of slurries into a plasma requires a nebuliser that is unlikely to clog when solid particles are passed through it. The most popular designs for use with slurries and dissolved high solids are based on the V-Groove 'Babington-type' nebuliser (13,23,28,37). The sample is pumped down a groove containing a small aperture through which argon gas flows at high velocity. This causes the sample to shatter into an aerosol of small droplets. The high velocity of the argon gas ensures efficient nebulisation and prevents blocking of the small orifice. Examples of typical aerosol size distributions are illustrated and discussed in detail in a paper by Ebdon *et al.* (34). There are many variations of this v-groove nebuliser including one design with an integral impact bead (30) and another design based on a cooled Babington nebuliser (79) both of which serve to reduce noise levels in the resultant spectra.

Algeo and coworkers (19) introduced a modified Babington type nebuliser with sample heater for use in the analysis of metals in lubricating oils by ICP-AES. The heating action on the droplet occurred as the sample was introduced into the nebuliser and served to increase the aerosol output. It also reduced the variation in emission intensity that arose due to differences in oil type and viscosity. Metallic particles in lubricating oils were also analysed by Saba *et al.* (14) who investigated the efficiencies of various nebuliser/spray chamber combinations. A ceramic nebuliser and horn-like glass spray chamber were found to be the most efficient of all the systems studied.

The Ebdon nebuliser (28,30,56,73,78) is a commonly used v-groove variation of the Babington nebuliser. It has been shown to give excellent performance in slurry nebulisation (23,24,28) and is of a robust one-piece design. The diameter of the gas orifice is 0.2 mm to enable a high velocity gas flow for nebulisation.

A V-groove Babington-type nebuliser has been used successfully with an MIP (88). This design of nebuliser contained a very small (0.1 mm diameter) gas orifice, a solution orifice of 0.8 mm diameter and an impact bead to break up large droplets. Both the Hildebrand Grid and Maximum Dissolved Solids nebulisers have been described for use in ICP-AES slurry work (48). The former contains a fine platinum grid upon which the slurry is laid and the aerosol is formed when the argon passes through the grid, while the latter is based on the v-groove design. Fuller *et al.* (13) used a cross flow slot type nebuliser for the continuous aspiration of slurries over 10 % m/v into the DCP with success.

Rademeyer and co-workers have developed a rotating disc nebuliser for solution and slurry sample introduction ICP-AES (46). The nebuliser is not based on pneumatic or ultrasonic principles but around the action of a planar spinning disc. The disc is rotated at high frequency and particles are placed on the disc. The disc is contained within container walls. The high frequency spinning causes the particles to be swept outwards resulting in an area of reduced pressure at the disc surface. If a gas flow is introduced above the centre of the disc, the low pressure will be counteracted and the gas spirals outwards and upwards, taking the sample droplets/particles with it. Turbulence occurs, resulting in mixing of the sample with the gas and the sample is introduced to a spray chamber.

1.7.3 Spray chambers

As in the case of nebulisers, there have been many spray chambers designed and used exclusively for the introduction of slurries into plasmas. The spray chamber separates the droplets that emerge from the nebuliser. Large droplets are rejected and removed via a drain whilst small droplets are allowed to pass to the plasma torch. Approximately 1-2% of the sample reaches the plasma; the rest is pumped out of the spray chamber. There are two more popular designs of spray chamber used for solution and slurry analysis (101); i) the 'Scott' type 'double pass' design that consists of a chamber with an inner barrel and ii) the 'single pass' which is a single chamber sometimes containing a baffle or impact bead which aids the production of small droplets.

Cooled spray chambers have also been used to improve analytical recoveries. Williams and co-workers (72) used a single pass water-cooled spray chamber, maintained at 13° C. Ebdon *et al.* (73) employed a Scott double pass water-cooled spray chamber constructed from glass in the analysis of coal by ICP-MS. Cooled spray chambers offer advantages in noise reduction as they act to lower the vapour loading in the plasma so precision is improved.

The influence of spray chamber temperature has been measured by Pollman *et al.* (79). Their spray chamber design enabled the temperature to be constantly maintained between 5 and 25 °C. The authors found that in the analysis of Al_2O_3 slurries by ICP-MS, the RSD of the analyte signal improved upon cooling of the spray chamber.

Gervais and Salin (45) have developed a heated spray chamber followed by condenser for slurry sample introduction ICP-AES. Both the nebuliser and spray chamber are control heated with a heating coil/thermocouple arrangement. An internal condenser follows the spray chamber. No sample

overloading was observed and detection limits were improved by a factor of 10.

McCurdy and co-workers (22,82) designed a spray chamber configuration without impact beads or baffles. The performance of the modified spray chamber was compared to that of an unaltered spray chamber in the analysis of coal by ICP-AES. The impactor bead was found to have a minor effect on the sample droplet size passing through the system. Mohamed *et al.* (81) designed a novel, single-pass, glass spray chamber for use with a v-groove nebuliser for a DCP.

A 'reduced volume' spray chamber has been designed (33) which excelled in performance over a conventional Scott double pass spray chamber. The spray chamber has minimal volume and does not introduce excessive spectral noise. Ebdon and Wilkinson (23,24) reported using a recycling spray chamber to conserve sample solution when using high sample flow rates. The waste from a conventional double pass chamber was collected into a slurry reservoir and continuously presented to the nebuliser for aspiration into the ICP.

Ebdon and Collier (30) compared the designs of four spray chambers; a conventional double pass, a cyclone, a 'straight-through' and 'direct' spray chamber. The cyclone is a vortex type chamber which has been used previously for the aspiration of solutions into the ICP. The 'straight-through' prototype design had minimum impact surfaces thus allowing larger particles to reach the plasma. The 'direct' spray chamber allowed large particles to directly enter the torch injector and minimised impaction processes. It was found that the spray chambers filtered out the majority of particles, particularly the larger ones. The 'straight-through' spray chamber was chosen for further studies.

1.7.4 Torches

Torches have been modified for slurry sample introduction in the work of Verbeek and Brenner (32) and Varga and co-workers (35). In the former paper, an 'extended torch' was designed which extended 6.5 cm above the injector tip. Emission for slurry nebulisation was found to be spread over a greater range of height when compared with a Trassy-Mermet torch. No appreciable improvement in SBR values was obtained. Varga *et al.* (35) stated that an extended torch can eliminate carbon contamination from the air in the analysis of Si_3N_4 by ICP-AES.

Ebdon and Collier (30) investigated the effect of various torch injector tubes on analyte sample transport. Capillary tubes of 2.2, 3 and 4 mm internal diameter (i.d.) were used along with a 2 mm i.d. jet injector tube. The authors found that the internal diameter of the injector dictated the mean particle droplet size of the aerosol entering the plasma. The 4 mm and jet injector tubes were found to be unsuitable for slurry atomisation as the sample was reported to "cone out" resulting in a reduction of sensitivity of the signal. The 3 mm injector tube was found to be the most suitable for slurry nebulisation. A 3 mm injector was also used in the work of Foulkes *et al.* (27). Jarvis and Williams (74) highlighted the importance of using a wide bore injector for slurry nebulisation into the ICP. The authors used a 3 mm diameter injector that resulted in a decrease in sample velocity through the injector aperture and hence a longer residence time in the plasma.

1.8 Calibration Techniques

1.8.1 Aqueous Calibration

For a slurry to be efficiently nebulised, vaporised and atomised, the particle size distribution, as previously mentioned, is critical. A narrow particle size distribution with a mean particle size of less than 2 μm will normally ensure sample transport and recoveries comparable to the equivalent solutions for most samples. If this is achieved then simple aqueous calibration may be

used successfully. This technique has been used by the majority of analysts who have achieved the desired mean particle size and stability of the slurry. For example, Totland *et al.* (77) used aqueous calibration standards in the analysis of geological samples by ICP-MS. Stock solutions (1000 μg ml^{-1}) of platinum group elements and gold were serially diluted to produce multielement standards in the required range with no need for matrix matching.

1.8.2 Use of an Internal Standard

Analytical accuracy and precision have also been markedly improved by employing an internal standard such as yttrium (63) and scandium (25) in ICP-AES. In ICP-MS aluminium has been used with success (75). Ebdon *et al.* (73) report the use of two internal standards in ICP-MS analyses, rhodium for a semiquantitative analysis and indium for a fully quantitative study. The internal standard may be used to compensate for reduced transport efficiencies, particularly in the analysis of refractory elements in geological samples. It is important that any internal standard used in aqueous solution is compatible with the selected dispersant.

1.8.3 Use of Standard Additions

It is possible with the slurry technique to calibrate by standard additions with aqueous solutions (50,60,71). However, this technique again assumes identical transport characteristics between solutions and slurries. Lobiński *et al.* (50) used the technique in the analysis of ZrO_2 by ICP-AES. Silicon nitride powder was analysed by Zàray *et al.* (60) using standard additions of a multielement (Al, Fe, Ca, Mg and Ti) stock solution.

1.8.4 Use of Empirical Correction Factors

Alternative calibration methods have been used when analysing slurries, again to improve analytical accuracy. Empirical correction factors have been

employed (20,36) where the intensity of an elemental line for a slurry analysis has been lower than that of an equivalent solution. Conventional internal standardisation will not suffice because of the differences in transportation and dissociation behaviour between the analytes present in the slurry particles and the internal standard. Thus a series of slurries may be analysed by dissolution as well as slurry nebulisation and correction values computed empirically which can later be applied to unknown slurries. Such a method relies on similar behaviour in all the slurries investigated.

1.8.5 Use of Intrinsic Internal Standardization

Variations in transport efficiency between aqueous standards and slurry samples may be overcome by using an intrinsic internal standard (21,28). An element in the slurry sample is selected to be monitored. The analyte line signals are then ratioed to the signal for the selected element. If the intrinsic internal standard element is present in a constant amount in all the samples, it can be used to correct for varying transport efficiency. Silicon has been used effectively in the analysis of kaolin by ICP-AES (28). The use of an intrinsic internal standard may, however, be invalidated if an acidic medium is used and partial digestion of the slurry occurs or if certain atomisation effects arise.

1.8.6 Use of Standard Slurries

Standard slurries have been used as an alternative to aqueous calibration in some analyses of solid samples (16,47,63). Standard reference materials are normally used as, for example, in the analysis of airborne particulate matter by ICP-AES (16). Standard suspensions were prepared by homogenising a known amount of the reference material. Fernandez *et al.* (47) used a reference slag in the determination of a range of elements. A range of geological standard reference materials has also been used (63). Standards were made from materials including SiO_2 rich granites, marine sediments and coals.

The use of standard slurries for calibration is problematical (56). The nature of the material being used for calibration must be identical to that of the unknown slurry sample. For heterogenous standard slurries (i.e. coal), elements will not be distributed uniformly and particle size distributions and densities of elements within the sample may not be comparable to the slurry being analysed.

1.9 Matrix Effects

There has been little work in the literature concerning liquid component matrix effects and associated interferences when slurry samples are analysed in plasmas. Laird *et al.* (40) measured the effect of matrix solution composition on matrix interferences for clay minerals using ICP-AES. The authors believed that matrix inferences are problematic due to the different forms of the aqueous standards and sample suspensions. Slurries were prepared in HNO_3 which acted partially to dissolve some of the clay particles in suspension. Cations were displaced from the clay framework by hydronium ions in the matrix solutions. Elements displaced and therefore in the matrix solution were transported to the plasma more readily and recoveries improved. The authors were able to rationalise in this way the differential elemental recoveries obtained. An experiment was also performed to ascertain whether the addition of 0.1 M NaCl to the matrix would effect elemental recoveries. It was suggested that the addition of 0.1 M NaCl aided dissociation and excitation of clay particles within the plasma and improved Al recoveries.

Jerrow and co-workers (86) analysed six soils and sediments by slurry nebulisation DCP-AES for seven elements. Recoveries for Ba, Sr, Ca and Al were found to be poor for three of the samples. The authors concluded that lithium or potassium salts added to the matrix to buffer EIE effects adversely affected recoveries due to cation exchange of the analyte element ion from the slurry particles into the solution phase.

Sparkes and Ebdon (85) found that for slurries, analysed by DCP-AES, containing lithium at a concentration of 5 g dm^{-3}, an increase in slurry concentration resulted in a decrease in the excitation temperature and electron number density. This was not observed if lithium was absent and the effect was attributed to an increase in the rate of radiative cooling of the plasma.

The effect of high salt matrices on analyte response for the analysis of milk powder by ICP-MS has been investigated (66). Na or Ca, 500 µg ml^{-1}, was added to a 10 ng ml^{-1} Pb solution and isotope ratio measurements performed. The precision in the presence of Na or Ca was lower than that obtained for a pure lead solution and this was attributed to transport effects either in the nebuliser or at the ICP-MS interface. Accuracy was not affected.

1.10 Fundamental Studies

1.10.1 Aerosol Formation, Transportation and Loss

Transportation of a slurry sample into a plasma is facilitated by the formation of an aerosol by the nebuliser and modified by the filtering action of the spray chamber. This physical process is critical to analytical accuracy and precision. If aqueous calibration standards are used then the transportation of slurries through the sample introduction system must mimic that of solutions. Fundamental investigations have examined the behaviour of slurries in terms of aerosol formation, transportation of the aerosol through the sample introduction system and any loss processes that occur.

Ebdon and co-workers (34) have made extensive comparative studies of solution and slurry behaviour in the ICP. Laser particle sizing, a non-intrusive technique, was employed to measure the slurry aerosol particle size distribution, between 1 and 40 µm, at various stages in the sample introduction system. It was found that the majority of particles emitted from an Ebdon v-groove nebuliser were below 20 µm in diameter and an increased

nebuliser gas flow rate resulted in the formation of finer particles. The particle size distribution was found to be modified by both double pass and single pass spray chambers indicating that ballistic, turbulent and recirculatory deposition processes occurred. The aerosol emitted from a 2 mm injector showed a reduction in the particle size distribution i.e. smaller particles were getting through whilst larger particles did not. A 3 mm injector allowed more of the larger particles to enter the plasma. Aerosols of 1 % m/v slurries did not behave differently from those of equivalent solutions under identical conditions and the authors concluded that aerosol formation, transportation and loss processes are the same for both systems.

Aerosol droplet size distributions of Al_2O_3 slurries (1% m/v) have been measured using a cascade impactor and collected above the injector (31). These authors found that a Babington nebuliser produced slurry aerosols equivalent to solution aerosols. It was noted that particles above 17 μm did not reach the ICP so sample homogeneity is important. An 'evaporation model' was developed to predict the analytical performance of slurry nebulisation into an ICP. The authors used the model to describe differences between solution and slurry evaporation and thus predict when aqueous calibration may be used.

Droplet size distributions have also been measured by Van Borm *et al.* (49) together with analyte transport efficiencies and analyte mass transport rates. The authors state that differences between solutions and slurries in terms of these three processes are dependent on the nebuliser gas flow, the characteristics of the instrument and most importantly on the type and state of the slurry.

Xhoffer and co-workers (53) measured exhaust aerosols, at the tip of the injector, of Al_2O_3, ZrO_2 and SiC ceramic suspensions using electron energy loss spectroscopy. The size, shape and surface characteristics of the slurry particle changed during the time spent in the sample introduction system and was found to be particularly dependent on the type of plasma gas used, the

type of slurry sample and the distance from the impactor part of the spray chamber to the torch.

The fundamental parameters of aerosol particle size were discussed in a paper by Goodall *et al.* (56). For efficient introduction into the plasma, the slurry particle size is known to be of major importance. The authors state that the particle size distribution of the slurry should not exceed a value determined by the density of the particle. A size occupancy diameter model was introduced which illustrates that for slurry nebulisation to be comparable to that of solutions, one slurry particle should be contained within a single aerosol droplet.

1.10.2 Temperature Measurements

Plasma processes may be investigated by using the excitation temperature (T_{exc}), the ionisation temperature (T_{ion}) and the electron number density (n_e) as diagnostic tools. Sparkes and Ebdon (85) used these parameters to explain slurry related phenomena in the DCP concerning matrix effects caused by the addition of easily ionised elements to the slurry matrix. Ebdon and Foulkes (67) have measured the rotational temperature of the ICP and employed vertical temperature mapping to investigate the processes occurring when a slurry particle enters a plasma. When solutions and slurries of up to 1 % m/v were introduced into the ICP no significant differences in the rotational temperature were observed. The presence of water from the aerosol appeared to raise the temperature in contrast to humidified argon. When slurries of fine particles (<2 μm) of compounds, which have melting points comparable to and boiling points in excess of the rotational temperature, were nebulised, excellent recoveries were observed. This confirmed that transport and atomisation efficiencies for solution and slurry introduction into the ICP are comparable under the conditions specified.

1.11 The Inductively Coupled Plasma as an Excitation Source

The inductively coupled argon plasma is currently the most widely used plasma technique employed in slurry sample analyses (13-80). This is due to many of the ideal requirements for elemental analysis being fulfilled by ICP based techniques (102). These requirements include the applicability of the technique to most elements; the ability to simultaneously determine major, minor, trace and ultratrace concentration levels; reduced interelement interference effects; the ability to analyse microgram sized samples; the ability to analyse solids with minimal preliminary sample preparation; and the attainment of acceptable precision and accuracy (102). Classical techniques involving flames, arcs and sparks have been less successful in achieving these capabilities. Flame like electrical discharges such as DCPs and MIPs do not possess annular channels for injecting the sample though the centre of the discharge, causing reduced plasma-sample interaction and resulting in reduced vaporisation, atomisation, ionisation and excitation. ICP discharges have unique properties when compared to these techniques in particular the robustness of the plasma, the high gas and electron temperature and the high electron number density. These characteristics result in relative freedom from matrix interferences and low detection limits. The number of papers published in the area of ICP spectroscopy reflects the attraction of the technique. In the field of atomic spectroscopy, approximately ten times more papers have been published since 1980 using ICP instrumentation compared to those exploiting the use of DCPs and MIPs (102).

1.12 The Use of Solid State Detectors in Analytical Spectroscopy

Traditionally, detection systems used in ICP-AES systems have employed scanning monochromators or polychromators with photomultiplier tubes (PMTs). Usually one emission line is selected for a particular analyte element for a quantitative determination. The thousands of emission lines available in plasma emission spectrometry for elemental determination cover the near infrared and vacuum ultraviolet region of the electromagnetic spectrum.

Making use of this wealth of information in the emission spectrum may result in improvements in sensitivity and precision. Measuring a number of lines simultaneously in an elemental determination enables diagnostic features to be monitored and multiple emission lines to be used in a quantitative analysis, along with their spectral backgrounds. Charge coupled device detectors (CCDs) are now in common use in atomic emission spectroscopy and are well documented in the literature (103-111). The CCD enables more than one line to be detected simultaneously and consists of a two dimensional pattern of CCD array segments. Each array segment is positioned on the detector so that a specific spectral region containing one or more emission lines may illuminate the segment (108). Each array segment may be addressed directly for information readout. The use of CCDs offers advantages over PMTs in terms of low noise characteristics, high UV quantum efficiency, wide dynamic range, rapid readout and charge antiblooming. By using CCDs as detectors the entire spectrum may be acquired over a specified wavelength range. For this reason, such detection technology may be used in qualitative and semi-quantitative analyses, where an immediate idea of the elemental composition of a sample is required (111).

1.13 Aims and Objectives of this work

The principal objective of this study was to investigate the fundamental mechanisms occurring from the process of slurry sample preparation through to excitation and atomisation of the species in the plasma. For simple aqueous calibration to be used in quantitative slurry sample analyses, it is necessary for the slurry to behave in an analogous way to that of a solution of equivalent concentration in terms of sample transport and atomisation processes.

To obtain ideal recoveries for a slurry analysis where analytical values are comparable to an equivalent solution, it is essential that several conditions are satisfied. It is first necessary to prepare a stable and homogenous dispersion

and ensure that the particle size distribution of the slurry is small enough so that sample transportation closely mimics an aqueous aerosol. The satisfactory attainment of such criteria formed a major part of this work. It is also essential that plasma operating conditions are optimised so that atomisation processes are ideal for the particular elemental slurry analysis. Such optimisation procedures were considered in detail and performed routinely.

Studies in the area of matrix effects, in particular those due to easily ionisable elements (EIEs) such as Li, Na, K and Cs, formed a large part of this project. The presence of such elements in the sample matrix is known to effect plasma emission for both ion and atom lines in a spatially dependent manner. The effect of EIEs on solutions and slurries was investigated in detail. Such matrix effects have been traditionally explained in terms of excitation, atomisation and ionisation phenomena. The effect of these concomitant elements on the sample mass transport efficiency of solutions and slurries has previously been ignored and is an important consideration if 'real' effects on emission are to be described and quantified. The introduction of simultaneous detectors in modern ICP instrumentation offers the analyst many unique capabilities for rationalising these phenomena. Such technology enables the measurement of more than one emission line to be commanded simultaneously. This may potentially be employed to overcome mass transport effects and to calculate physical markers, such as the plasma excitation temperature, which can, in turn, be used as an indicator of fundamental mechanisms occurring in the ICP. Computer controlled stepper motors may be employed to alter the viewing region of the plasma in modern spectrometers. In this way, spatial profiles may be constructed to provide a pictorial representation of the plasma. In this work, plasmas were viewed both axially ('end-on') and radially ('side-on').

The studies carried out in this project were performed on the Perkin-Elmer Optima 3000 series of instruments. Studies of the capabilities of the simultaneous detector were carried out for environmental slurry and solution

samples. In addition, the basic operation and programming of these instruments was extended to facilitate time resolved acquisition of data so that transient signals could be monitored for use in chromatographic and speciation studies.

Chapter 2 - Optimised Simultaneous Multi-Element Analysis Of Environmental Slurry Samples By ICP-AES

2.1 Introduction

In a recent paper (56) the fundamental relationships that limit transport efficiency of the slurry and ultimately the accuracy attainable by slurry nebulisation inductively coupled plasma atomic emission spectrometry were examined. The particle size distribution (PSD) of a slurry has long been recognised as the fundamental parameter that determines both the accuracy and precision of slurry nebulisation. Slurry transport processes may be considered to be most efficient where every aerosol droplet is occupied by a solid particle representative of the bulk, determined by the solid's density and aerosol size distribution. For example, a solid particle size of 2.9 μm for a material density 1 g cm^{-3}, falling to 1.5 μm for a material of density 7 g cm^{-3} are theoretical values for slurries passing through a Scott double pass spray chamber without desolvation. If this is achieved then matrix matched aqueous standards may be used for calibration of the instrument.

The degree of dispersion has often been ignored when a slurry is prepared and is an important oversight, considering its limiting effects in slurry nebulisation. Microflocculation through edge to centre attractive forces of very fine primary solid particles in, for example, clay and mineral suspensions leads to reduced analytical accuracy (24,38). This may be overcome by increasing the concentration of surfactant in the aqueous dispersant. However examination of the slurry using optical microscopy to identify any agglomeration of the particles should be a routine step in any slurry analysis.

An ICP-AE spectrometer employing the flexible, simultaneous, multielement data acquisition capabilities of the segmented-array charge-coupled-device detector may be used to determine elements of interest using both solution and slurry sample introduction. The latter technique, which involves sample introduction as an aqueous suspension of finely powdered material, offers a

rapid method for the analysis of matrices that are resistant to dissolution procedures or where sample preparation time greatly exceeds analysis time. Problems of safety, contamination and analyte losses are overcome when using this well established technique (23,24,28,30,38,72,73,112). Most previous studies of slurry analysis by ICP-AES have used sequential multi-element analysis whereas simultaneous multi-element analysis allows maximum advantage to be taken of the time saving capability of slurry analysis. In addition, correction using 'real-time' internal standardisation may be used to correct for instrument drift, transport efficiency differences, power fluctuations and gas flow variations throughout the duration of an analysis.

Optimization of operating variables is increasingly being used to enhance the analysis of slurries in plasmas. Some slurries may present difficulties in volatilisation and atomisation and the optimisation of plasma conditions may overcome or improve upon these problems.

Sparkes and Ebdon (85) used simplex optimisation to improve the determination of Mg in a kaolin slurry by DCP-AES. The signal to background ratio was used as the figure of merit. Seven parameters were optimised: horizontal and vertical viewing positions, nebuliser gas flow rate, plasma gas flow rate, concentration of ammonia dispersant, concentration of lithium buffer and the concentration of the slurry. A univariate search was carried out for all seven parameters after optimisation to illustrate the role of each of the parameters. A similar optimisation method was employed by Ebdon and Collier (28) for analysis of a 0.5 % m/v kaolin slurry but in this case the instrument used was an ICP spectrometer.

Ebdon and Wilkinson (23,24) used a variable step size simplex procedure to optimise for the analysis of Mn in coal slurries by ICP-AES. Plasma gas flow, auxiliary gas flow, nebuliser gas flow, RF power and the viewing height above the load coil were the variables investigated. Both an all argon plasma and an argon-nitrogen plasma were optimised and the signal to background ratio was used as the criterion of merit.

Gervais and Salin (45) optimised their procedure for the analysis of slurries by ICP-AES using a heated sample introduction system. Simplex optimisation was used in this case to optimise temperature and viewing height. The signal to blank ratio for six elements was employed as the criterion of merit and a variation of 5 % between the five best vertices was used as an indicator of the optimum being found. A simplex method was also used in the optimisation of ZrO_2 slurries for the analysis of Al (50). Forward power, sample uptake rate, nebuliser gas pressure, plasma gas flow rate and viewing height were the variables under investigation.

Zàray and co-workers (42) identified, using three dimensional plots, the optimum plasma operating conditions with respect to RF power (0.8 kW) and aerosol gas pressure (2 bar) for the determination of Al, Ca, Fe and Mg in silicon nitride powder. At the optimum conditions for the elemental analyses, 'atomisation efficiencies' ranged from 77 to 100%.

Fluctuations in the analytical signal originating in the ICP and the hardware used to make the measurement contribute to imprecision of the analytical signal. As the noise of a signal from different elements can be correlated as a function of time, the use of a spectrometer with simultaneous data acquisition capability would be a distinct advantage, and internal standards have been employed to significantly improve precision for solutions by this technique (113).

Although some analyses can be performed under standard conditions, line selection and evaluation of optimum conditions is essential to attain the required analytical performance in any analysis. A set of variables providing the optimum signal to background or signal to noise ratio can be defined by the response hypersurface created by the program; where a change in the value of any variable produces no appreciable improvement in the response. The spectrometer used for this work has two on-board algorithms which examine the interaction of various plasma parameters to facilitate optimisation. This allows a comparative evaluation of the potential of on-board

simultaneous multi-element slurry analysis to be made with alternative Simplex programmes. To date no work has been published on the optimisation of slurry analyses using the multi-element capabilities of the simultaneous charged coupled device detector.

2.2 Experimental

2.2.1 Instrumentation

All measurements were made on a Perkin-Elmer Optima 3000 echelle spectrometer (The Perkin-Elmer Corp) with a segmented-array charge-coupled-device detector (SCD). The design and evaluation of the echelle grating optical system and solid-state detector are discussed in the literature (108,114).

The range of instrument operating conditions used in this study are summed in Table 2.1. Default conditions enable the instrument to provide all the spectral data in any given measurement (including background signals) simultaneously. Thus, all the pixels on the detectors are commanded simultaneously to begin or end an exposure. Signals recorded on pixels within a subarray or between subarrays are acquired at the same time.

The emission lines of the analytes of interest used in these studies are given in Table 2.2.

2.2.2 Chemicals and Reagents

The following certified reference materials were used to prepare slurry suspensions for analysis:

Dolomite (British Chemical Standards 368-BAS, Middlesborough, Cleveland, UK)

MESS1 - Estuarine sediment (National Research Council of Canada, Ottawa, Canada)

RF Generator	
Frequency	40 MHz, free running
Power	900 - 1280W, computer controllable in 5W increments
Sample Introduction System	
Nebuliser	Ebdon V-Groove high solids
Torch	Demountable with 2.0 mm i.d. alumina injector and 4 mm observation slot.
Spray chamber	Perkin-Elmer (P.E.) Scott double pass or customised glass double pass
Peristaltic Pump	Gilson Minipuls 3, computer controlled
Sample Flow Rate	1.0 ml min^{-1}
Argon Flow Rate	
Plasma	15.0 l min^{-1}
Auxiliary	1.5 l min^{-1}
Nebuliser	Optimised on SBR (0.86-1.35 l min^{-1})
Spectrometer	
Polychromator	High energy echelle based
Resolution	Medium slit width (62 × 250 µm)
Viewing Height	Optimised on SBR (11-21 mm ALC)
Detector	Perkin-Elmer SCD mounted on Peltier cooler at -40°C

Table 2.1 - ICP-AES instrument parameters used for optimisation studies

ELEMENT	ANALYTICAL LINE (nm)
Aluminium	Al I 396.152
Arsenic	As I 193.696
Barium	Ba II 455.403
Cadmium	Cd I 228.802
Chromium	Cr II 267.716
Copper	Cu I 324.754
Iron	Fe II 259.940
Lanthanum	La I 408.672
Lead	Pb I 283.306
Manganese	Mn II 257.610
Molybdenum	Mo II 202.030
Nickel	Ni II 231.604
Strontium	Sr II 407.77
Vanadium	V II 310.230
Zinc	Zn I 213.856

Table 2.2 - Line selection of analytes of interest used in the slurry optimisation study

BCSS1 - Coastal Marine sediment (National Research Council of Canada, Ottawa, Canada)
BCR 145 - Sewage sludge (Community Bureau of Reference, Brussels, Belgium)
DR-N - Diorite rock (Geostandards, University Nancy, France)

All reagents used were of 'AnalaR' reagent grade (Merck Chemicals, Poole, Dorset, UK) and all solutions were prepared with doubly deionised water (Milli Q, Millipore, Harrow, Middlesex, UK) and stabilised using 2 % nitric acid.

Calibration standards were prepared by serial dilution of commercially available analytical standard solutions (1000 μg ml^{-1}, Merck).

2.2.3 Slurry Preparation

All slurries were prepared by the 'bottle and bead' method. Approximately 1.00g of sample was accurately weighed into a 30 cm^3 'Nalgene' bottle and vitrified zirconia beads (10g, 2 mm diameter, Glen Creston, Stanmore, UK) added. Aqueous dispersant was added so the beads were just covered and the bottle shaken for at least 10 hours, usually overnight for convenience, using a standard laboratory flask shaker at 800 oscillations/min. The resulting finely ground slurries were transferred quantitatively to a volumetric flask (100 cm^3) and made up to the mark with dispersant. Indium internal standard (10 μg ml^{-1}) was added to all slurries to correct for instrument drift and variations in atomisation efficiency.

The anionic dispersant used for Dolomite, MESS 1, BCSS 1 and DR-N was 0.5% *m/V* tetrasodium pyrophosphate (TSPP). For BCR 145, 0.5% *m/V* Aerosol OT and 1% *V/V* Triton X-100 were used.

Studies in sample charring were performed on BCR 145 sewage sludge as this multicomponent sample contained some fibrous material which proved resistant to being finely ground when the conventional slurry preparation

technique was used. A simple carbonisation or 'charring' procedure offers a potential solution to this problem and has been suggested for analysis of plant materials by XRF by Satake and Uehiro (115). In addition to improving the grinding of the slurry, this technique has the potential to significantly increase sample loading in the slurry.

2.2.4 Carbonisation Procedure

Approximately 0.5g of the sample was accurately weighed into a porcelain crucible, placed in a muffle furnace (Carbolite, Sheffield, UK), and the temperature raised to 250^0C. This temperature was chosen from preliminary studies which show poor recoveries due to incomplete carbonising of the organic fraction. Using such a procedure, the charring temperature must be closely regulated to avoid losses of volatile elements such as lead and cadmium from the sample matrix. The sample was left overnight for 12 hours and was then transferred to a 30 cm^3 'Nalgene' bottle and zirconia beads added. The sample was ground as described previously for four hours. TSPP 0.5% was used as the dispersant.

The particle size distribution of the slurries was determined using a Coulter Counter TA11 Multi-channel Counter (Coulter Electronics Ltd., Luton, UK). Isoton electrolyte (Coulter Electronics Ltd.) was used to suspend the samples which were sized using a sampling tube with a 140 μm orifice.

Efficiency of dispersion and general particle size range measurements were ascertained using optical microscopy.

2.2.5 Solution Preparation

As part of the direct comparison between a CRM as a slurry and one in solution, a dissolved sample of the reference material Dolomite was prepared by digesting 1.00 g in 20 ml of aqua regia (2:1 $HCl:HNO_3$) on a hot plate for 10 minutes. Indium internal standard (10 μg ml^{-1}) was added to all solutions.

2.2.6 Instrument Modifications and Sample Introduction

The existing instrumentation required minimum modification of the sample introduction system for slurry nebulisation. The gem tipped cross-flow nebuliser was changed to a V-groove nebuliser developed in this group (30,116) and the drain adapter was modified to prevent blocking by slurry particles. Slurries were maintained in homogenous suspension using a magnetic stirrer.

2.2.7 Optimisation Studies

Use was made of the two on-board algorithms for optimisation studies i) the directed search and ii) the exhaustive search programmes. These results were compared with those obtained from a variable step size Simplex programme in order to optimise plasma performance. The variable parameters were viewing height, nebuliser argon flow and RF generator power as solution studies have shown these to be the most critical. The boundary conditions were set as 5 - 25 mm above the load coil (ALC) for the viewing height, 0.60 - 1.50 l min^{-1} for the nebuliser gas flow and 800 - 1400 W for the RF power.

Optimum conditions were evaluated by measuring a 10 µg ml^{-1} aqueous standard, matrix matched to the anionic dispersant used. The signal to background ratio was used as the criterion of merit.

2.3 Results And Discussion

2.3.1 Optimisation

The Optima 3000 has, as stated, two on-board programmes which examine the interaction of three plasma parameters to facilitate optimisation. The first, an 'exhaustive search algorithm', uses the simplest of systems to find the optimum but to do so is required to examine all points over the hypersurface. The optimum can be located within plus or minus half of the interval of each

variable. However, to achieve 5% precision using 10 values for 3 variables, 1000 experiments are necessary. Despite being time consuming, the exhaustive search ensures a global optimum is found and provides detailed information about the response surface.

The second algorithm is known as the 'directed search algorithm' in that the location of each point depends on those that precede it. It is a gradient method developed by Fletcher and Powell (117). The second derivative of the response to each variable is calculated, then all values are changed to the values estimated to be the optimum by means of parabolic extrapolation (118). The process is then repeated to ensure that the optimum in the response surface has been reached. To optimise three variables in this way requires only 19 measurements making it one of the most efficient optimisation algorithms of its type, provided the response surface is smooth.

The results from these algorithms were then compared with those from a variable step size Simplex optimisation programme which has been used widely in the past to optimise ICPs (119, 120). A set of variables providing the best SBR is again defined on the response hypersurface where a change in the value of the variable produces no appreciable improvement in response.

Simplex is also a 'directed search' method which starts from a polygon of points on the response surface, which, in the case of 3 variables, is a tetrahedron. It proceeds by moving away from the worst of the points on a line that bisects the remaining points. A new point is evaluated and compared with the other two points to identify the point that is now the worst of the four. The process continues until convergence, i.e. the optimum is reached. To optimise a function of three variables and expect 5% precision, 15 - 25 experiments would be required.

All methods can locate an optimum but may require varying amounts of time depending on the efficiency of the search and the shape of the response surface. A variable step Simplex is the least prone to the identification of false

optima. Selection of an optimisation procedure is, therefore, usually made on the basis of its efficiency for a particular problem.

Initially, a range was specified for each variable using the DSA to give a rough indication of where the optimum values lie. A combination of individual values around the optimum given by the DSA was then used for the more comprehensive ESA so that the number of experiments normally needed for the ESA was reduced. It was found that there was little, or no difference in the optimum values calculated in each procedure. Optimisation was then carried out using the variable step size Simplex optimisation procedure and terminated when successive vertices brought no appreciable improvement in response.

The optimum operating conditions derived using the DSA/ESA combination and at the termination of the Simplex are given in Table 2.3 for various atom and ion lines. Simple aqueous standards were used in all initial optimisation studies.

Table 2.3 shows that the two optimisation methods give very similar optimum values for the variable parameters. To reinforce this, two diagnostic checks were carried out for each element. The background equivalent concentration (BEC) test is a useful indicator of the relative sensitivity of the instrument for a particular emission line and was measured using an aqueous solution of known concentration and both sets of values from each optimisation method. The same regime was used to calculate the limit of detection (LOD). For arsenic the BEC values were 1.62 mg l^{-1} and 1.53 mg l^{-1} from the DSA/ESA combination and Simplex respectively. The LOD values were calculated as 0.04 mg l^{-1} for both methods of optimisation.

The DSA/ESA combination and Simplex yield comparable results for the BEC test and the LOD for the arsenic 193.696 nm atom line. This was also found to be true for the Mn II 257.670 nm and Pb I 283.306 nm emission lines. Because very similar results were obtained for both procedures it was

	Mn II 257.670 nm		As I 193.696 nm		Pb I 283.306 nm	
VARIABLE	DSA/ESA OPTIMUM	SIMPLEX OPTIMUM	DSA/ESA OPTIMUM	SIMPLEX OPTIMUM	DSA/ESA OPTIMUM	SIMPLEX OPTIMUM
Viewing Height (mm)	19	18	14	14	18	19
Nebuliser Gas Flow (l/min)	1.10	0.90	0.89	0.95	1.08	1.10
RF Plasma Power (W)	1050	1150	1280	1300	980	1050
BEC (mg l^{-1})	0.08	0.12	1.62	1.53	2.78	3.43
LOD (mg l^{-1})	0.008	0.01	0.04	0.04	0.64	1.10

Table 2.3 - Comparison of DSA/ESA combination optimisation procedure with variable step size Simplex optimisation for determination of optimum operating conditions used in slurry nebulisation studies.

decided that for future optimisation single element studies, the DSA/ESA combination would be used. The convenience of the algorithm being stored and directly accessible on the on-board computer of the spectrometer together with the number of steps involved using the DSA/ESA combination were a distinct advantage. Table 2.4 lists the optimum conditions obtained using the DSA/ESA combination for a selection of elements.

The Optima 3000 measures all analytical lines simultaneously when carrying out a multielement analysis. Default conditions for each element set the viewing height to 15mm above the load coil (ALC), the RF Power to 1000 W and the nebuliser gas flow to 1.00 l min^{-1}. For a multielement analysis each element may be measured at its optimum viewing height, power and nebuliser argon flow but analysis of the elements is then rapid sequential rather than simultaneous; full optimum conditions only being valid when elements are measured individually. For simultaneous multi-element analysis all the elements must be measured under the same conditions. Any change to the source conditions (which includes the nebuliser gas flow and RF power level settings) will be common to all elements in a simultaneous multielement analysis. For example, if the nebuliser gas flow is set to 1.17 l min^{-1} which is the optimum for aluminium, this will not necessarily give the best SBR for zinc and compromise conditions must be used. These conditions can be obtained by employing Simplex optimisation with a multielement standard. Multielement optimisation requires the selection of a suitable objective function to represent the composite response from the group of elements of interest. Leary *et al.* (121) calculated this function using the general weighted average incorporating the reciprocal of the signal to background ratio $(SBR)^{-1}$:

$$F = n / \sum_{i=1}^{n} (SBR)_i^{-1}$$

where F is the objective function and n is the number of analyte elements. This equation, however, does not take sufficiently into consideration the fact that the SBR^{-1} function is very sensitive to a change in trace element

ANALYTICAL LINE (nm)	VIEWING HEIGHT (mm)	RF POWER (W)	NEBULISER GAS FLOW ($l\ min^{-1}$)
Al I 396.152	20	900	1.17
As I 193.696	14	1280	0.89
Ba II 455.403	15	1200	0.87
Cd I 228.802	13	1120	0.89
Cr II 267.716	21	1000	1.06
Cu I 324.754	20	920	1.13
Fe II 259.940	18	1000	0.86
La I 408.672	19	1120	1.12
Pb I 283.306	18	980	1.08
Mn II 257.610	19	1050	1.11
Mo II 202.030	11	980	1.02
Ni II 231.604	15	1000	1.00
Sr II 407.77	18	1000	1.35
V II 310.230	14	940	1.11
Zn I 213.856	14	1100	0.95

Table 2.4 - Optimum operating conditions determined using the DSA/ESA combination optimisation procedure

response but insensitive to a change in minor element response. Ebdon and Carpenter (122) incorporated a $SBR^{-0.7}$ function which responds with more appropriate sensitivity to both a minor element and a trace element change resulting in the following equation which is used throughout this work for multielement Simplex optimisation:

$$F = n / \sum_{i=1}^{n} (SBR)_i^{-0.7}$$

A 10 ppm multielement matrix matched standard of Cu, Mn, Pb and Zn was used during Simplex optimisation and optimum conditions evaluated. Univariate searches were carried out to support the results obtained using the Simplex optimisation. These optimum conditions found for the multielement analysis are shown in Table 2.5 together with the optimum conditions evaluated for a single element analysis using the DSA/ESA optimisation procedure. It should be noted that Simplex optimisation has resulted in the viewing height value being markedly different to optimum values obtained using the DSA/ESA optimisation procedure. The optimum Simplex conditions are, however, reproducible.

2.3.2 Analysis of Certified Reference Materials

To determine how the instrument performed using optimum operating conditions obtained using the DSA/ESA combination a range of certified reference materials were analysed using both solution and slurry sample introduction techniques with a 10 mg l^{-1} indium internal standard used to correct for variations in transport efficiencies between slurry samples and aqueous standards. The Optima 3000 manual background correction facility was utilised. Aqueous standards were used to calibrate the slurry analyses.

The first certified reference material to be analysed was Dolomite 368-BCS. The sample was prepared as both a solution and a slurry. The effect of

OPTIMISATION ANALYSIS	OPTIMUM VIEWING HEIGHT (mm)	OPTIMUM NEBULISER GAS FLOW (/min)	OPTIMUM RF POWER (W)
Lead (DSA/ESA)	18	1.08	980
Copper (DSA/ESA)	20	1.13	920
Zinc (DSA/ESA)	14	0.95	1100
Manganese (DSA/ESA)	19	1.11	1050
Compromise Conditions (Simplex)	12	0.94	1015

Table 2.5 - Compromise conditions for Pb, Cu, Zn, Mn multielement analysis obtained using Simplex optimisation compared to single element optimum conditions obtained using DSA/ESA optimisation using a P.E. spray chamber.

increased grinding time on recovery was also examined. Figure 2.1 shows the particle size distribution for dolomite and clearly demonstrates how increasing the grinding time of a slurry yields fewer particles of diameter in excess of 2.52 μm. This should result in a higher transport efficiency as described in the work of Goodall *et al.* (56). The density of dolomite is 2.84 g cm^{-3} and, according to the size occupancy diameter (SOD) model proposed by Goodall *et al.* (56), the ideal particle size of the slurry should be between 1.5 and 2.9 μm. As the number of particles satisfying the SOD model increases, so too does the relative transport efficiency of the slurry through the sample introduction system and the resultant analytical recovery.

Table 2.6 shows how the recoveries for aluminium, iron, chromium and manganese increase as the grinding time increases and that there is reasonable agreement between the observed and certified values. The recoveries increase with time, until after two hours there is no significant difference between the slurry results and the certified values. Grinding times above one hour appears to introduce contamination, particularly for Fe and Cr.

Two sediment reference materials were analysed as slurries; MESS1, an estuarine sediment and BCSS1, a coastal marine sediment. Figure. 2.2 shows the particle size distributions for the two sediments which were ground overnight. Both distributions show the mode to be at 2.52 μm, although there is a greater proportion of the larger particles in BCSS1. Table 2.7 shows the observed concentrations from slurry nebulisation compared with the certified values for the two sediments. It can be seen that for all elements there is close correlation between the two, an indication that grinding time is sufficient to obtain high recoveries of all elements analysed.

Diorite rock, DR-N, was ground for the same period of time as the previous two sediments and Fig 2.2 shows the particle size distribution. The mode, again is at 2.52 μm with the proportion of particles of this diameter being higher than the previous two sediment samples. Table 2.8 compares the

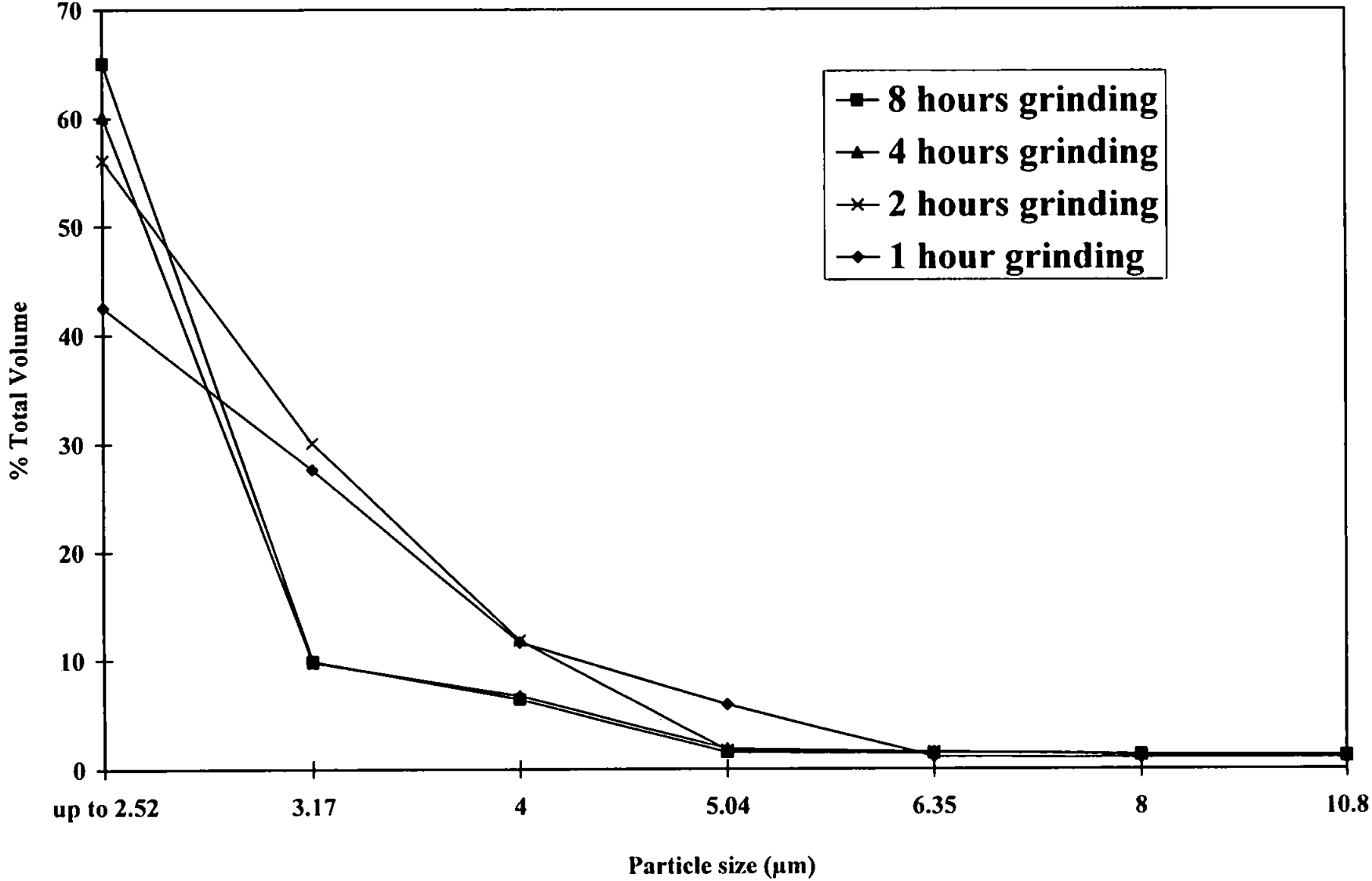

Figure 2.1 - Particle size distribution for dolomite as a function of grinding time

ELEMENT	OBSERVED CONCENTRATIONS FROM ANALYSIS (μg g^{-1})						CERT. CONC. (μg g^{-1})
	DIGEST 1	DIGEST 2	SLURRY (1hr)	SLURRY (2hrs)	SLURRY (4hrs)	SLURRY (8hrs)	
Al	829±58	841±51	787±61	799±58	823±50	827±63	901±45
Fe	1521±156	1556±139	1795±134	1814±172	1877±174	1894±92	1609±81
Cr	77±11	79±7	101±5	112±7	112±8	121±8	72±4
Mn	371±32	393±40	285±19	312±13	369±15	374±21	381±19

Table 2.6 - Determination of Al, Fe, Cr and Mn in Dolomite by ICP-AES

Uncertanties for the observed values are ± 3 s.d.

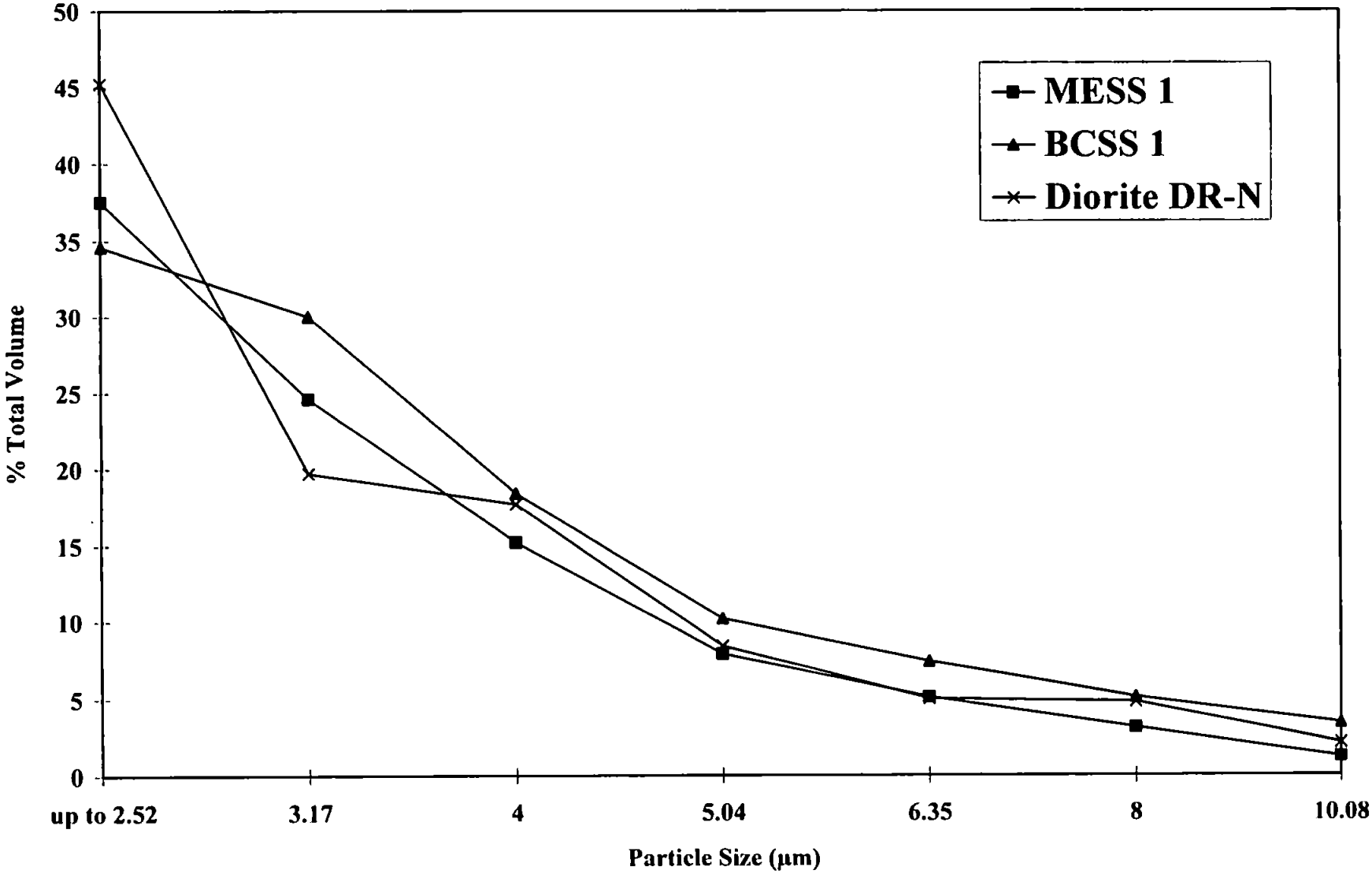

Figure 2.2 - Particle Size Distributions for MESS 1, BCSS 1 and Diorite DR-N Slurries

	MESS1		BCSS1	
ELEMENT	OBSERVED CONC. (μg g^{-1})†	CERTIFIED VALUE (μg g^{-1})†	OBSERVED CONC. (μg g^{-1})†	CERTIFIED VALUE (μg g^{-1})†
Al	5.3±0.2	5.8±0.2	6.0±0.6	6.2±0.2
As	11.31±1.34	10.61±1.23	10.45±1.31	11.12±1.48
Zn	171.2±24.0	191.3±17.0	112.4±19.9	119.1±12.0
Cr	121.4±53.6	71.3±11.1	144.9±23.9	123.8±14.7
Cu	24.52±1.93	25.12±3.86	18.02±1.50	18.56±2.79
Mn	438.9±17.5	513.8±25.0	215.1±40.4	229.2±15.4
Pb	40.53±2.62	34.27±6.16	20.54±3.78	22.76±3.41
V	88.16±7.17	72.49±17.00	104.01±13.97	93.45±4.92

Table 2.7 - Comparison of Observed Slurry Values vs. Certified Values for MESS1 and BCSS1

†Except Al where the result is % *m/V*

Uncertanties for the observed values are ± 3 s.d.

ELEMENT	OBSERVED CONCENTRATION ($\mu g\ g^{-1}$)†	CERTIFIED VALUE ($\mu g\ g^{-1}$)†
Al	18.5±1.4	17.5±1.7
Ba	279.1±108.6	385.2±86.6
Cd	0.08±0.01	0.09±0.01
Cr	39.3±5.33	42.1±10.0
Cu	50.02±4.67	50.11±7.33
Zn	132.6±20.9	145.2±16.3
Sr	281.1±84.8	400.7±49.4
Pb	53.7±13.3	55.2±10.6

Table 2.8 - Comparison of observed slurry values and certified concentrations for DR-N Diorite

†Except Al where the result is % *m/V*

Uncertanties for the observed values are ± 3 s.d.

observed and certified values for DR-N and shows that the two correlate closely indicating that grinding time is sufficient and that no agglomeration of particles is occurring within the slurry.

The particle size distribution for BCR-145 Sewage Sludge is shown in Fig. 2.3. It can be seen that the mode is at 4 μm with fewer particles of 2.52 μm and less. This distribution is reflected in the percentage recoveries shown in Table 2.9. Elements were measured individually using the DSA/ESA conditions given in Table 2.5. Recoveries for all elements are poor. Optical microscopy showed not only the larger particle size being present but also some agglomeration of the particles. While both the particle size and dispersion of the sample require attention if recoveries are to be improved under the conditions employed, the problem slurry allowed various parameters to be changed in order to study their effect on the slurry model.

It was observed that the existing double pass spray chamber had considerable dead volume and recoveries may be increased if this dead volume is reduced. A smaller customised glass double pass spray chamber was therefore made (Figure 2.4). Optimum conditions evaluated using the DSA/ESA combination and multielement Simplex optimisation procedure were then recalculated, previous values being no longer valid once modifications to the sample introduction system were made. Again, univariate searches were carried out to support the optimum values given by Simplex. Table 2.10 shows the single element optimum conditions obtained using the DSA/ESA optimisation and compromise conditions for Pb, Cu, Zn and Mn Simplex multielement analysis. Table 2.11 shows the LODs for the above elements measured for each set of optimum conditions.

Slurries of BCR-145 Sewage Sludge were analysed using the glass spray chamber to compare the recoveries obtained using the old spray chamber. Table 2.12 shows the concentration of lead, copper, zinc and manganese observed from slurries of BCR-145 compared with the certified values. The table summarises the results obtained from four separate experiments. Each

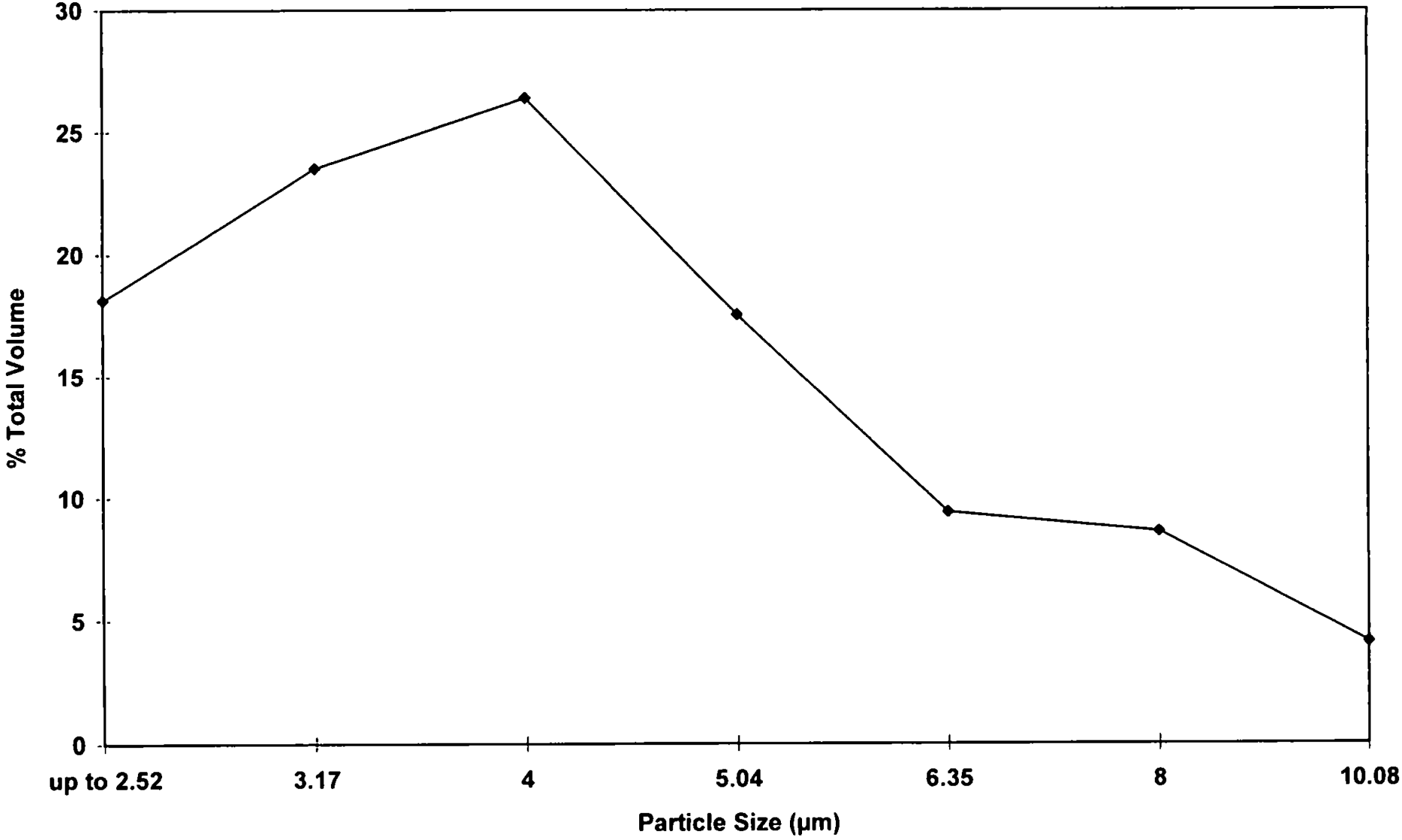

Figure 2.3 - Particle Size Distribution for BCR 145 Sewage Sludge

ELEMENT	OBSERVED CONCENTRATION ($\mu g\ g^{-1}$)	CERTIFIED VALUE ($\mu g\ g^{-1}$)	% RECOVERY
Cu	235.8±8.6	429.7±10.0	54.9
Mn	201.4±13.9	241.1±12.2	83.4
Pb	135.2±9.3	349.2±15.0	38.7
Zn	2635±218	2843.±64	92.7

Table 2.9 - Comparison of observed slurry values and certified concentrations for BCR-145 Sewage Sludge using a Perkin-Elmer Ryton Spray Chamber

Uncertanties for the observed values are ± 3 s.d.

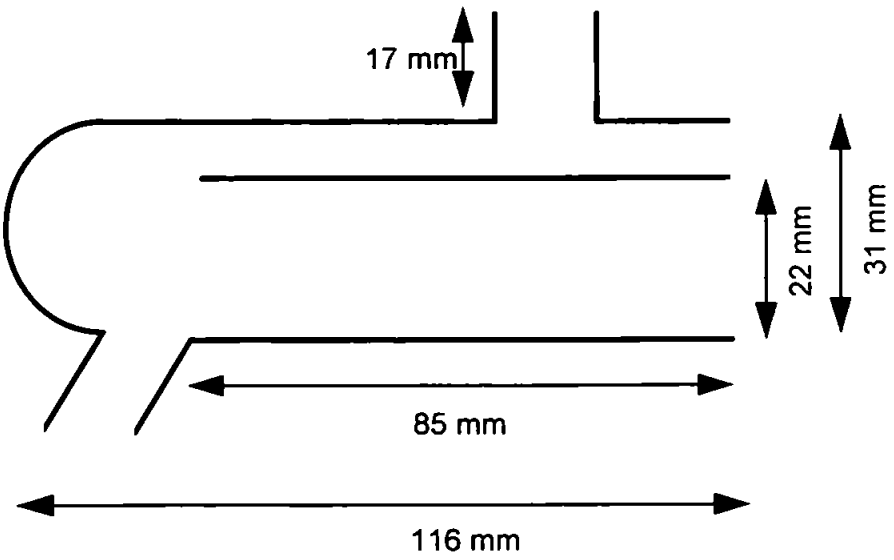

Customised Glass Double-Pass Spray Chamber

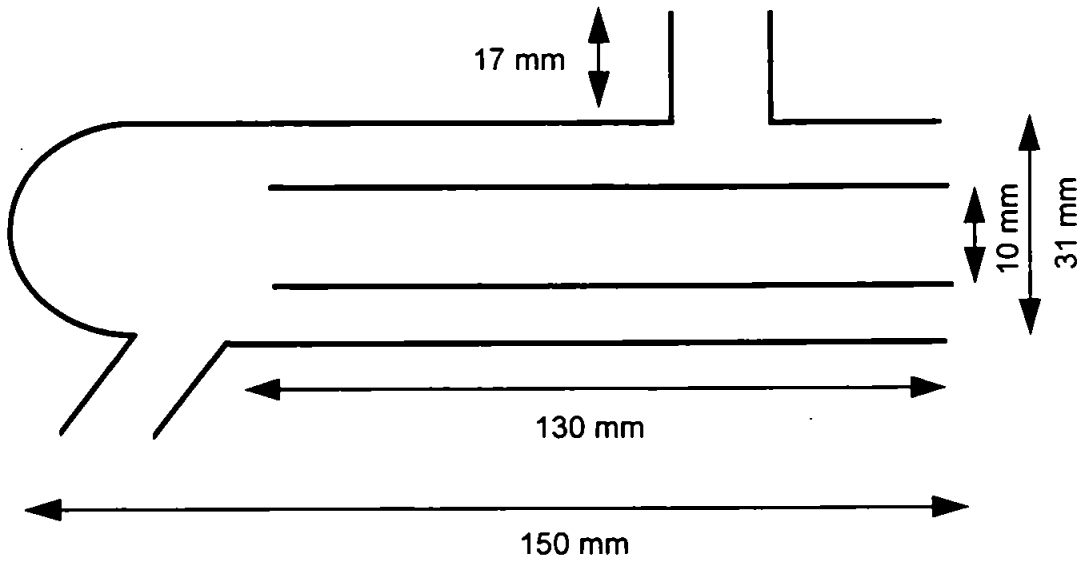

Perkin-Elmer 'Scott Type' Double-Pass Spray Chamber

Figure 2.4 - Comparison of customised glass and Perkin-Elmer spray chambers

OPTIMISATION ANALYSIS	OPTIMUM VIEWING HEIGHT (mm)	OPTIMUM NEBULISER GAS FLOW (l/min)	OPTIMUM RF POWER (W)
Lead (DSA/ESA)	13	0.88	1120
Copper (DSA/ESA)	23	1.15	860
Zinc (DSA/ESA)	10	0.91	1120
Manganese (DSA/ESA)	18	1.08	1000
Compromise Conditions (Simplex)	24	1.02	1195

Table 2.10 - Compromise conditions for Pb, Cu, Zn, Mn multielement analysis obtained using Simplex optimisation compared to single element optimum conditions obtained using DSA/ESA optimisation with a customised glass spray chamber

	LOD (mg l^{-1})	
ELEMENT	DSA/ESA OPTIMUM CONDITIONS	SIMPLEX OPTIMUM CONDITIONS
Pb	0.004	0.007
Cu	0.002	0.003
Zn	0.001	0.002
Mn	0.002	0.005

Table 2.11 - LODs measured for Pb, Cu, Zn and Mn using both DSA/ESA and Simplex optimum conditions and customised glass spray chamber

ELEMENT	P.E. SPRAY CHAMBER		CUSTOMISED GLASS SPRAY CHAMBER		
	OBSERVED CONC. ($\mu g\ g^{-1}$) DSA/ESA OPTIMA	OBSERVED CONC. ($\mu g\ g^{-1}$) SIMPLEX OPTIMUM	OBSERVED CONC. ($\mu g\ g^{-1}$) DSA/ESA OPTIMA	OBSERVED CONC. ($\mu g\ g^{-1}$) SIMPLEX OPTIMUM	CERTIFIED VALUE ($\mu g\ g^{-1}$)
Pb	135.2±9.3	134.5±49.3	241.1±41.2	215.8±47.0	349.2±15.0
Cu	235.8±8.6	211.8±29.3	339.7±23.3	320.4±112.6	429.7±10.0
Zn	1183±218	637±94	1490±142	1399±277	2843±64.
Mn	68.0±13.9	54.5±14.6	108.5±17.9	102.5±32.6	241.1±12.2

Table 2.12 - Comparison of observed slurry values with certified results for BCR-145 Sewage Sludge using different spray chambers and optimum conditions.

Uncertainties for the observed values are ± 3 s.d.

element was measured individually using the DSA/ESA combination optimum conditions for both the P.E and customised glass spray chambers. Concentrations of elements were also determined simultaneously using the Simplex multielement optimum conditions for each spray chamber.

It can be seen from Table 2.12 that the highest recoveries are achieved by measuring the elements individually using the DSA/ESA combination optimum values whilst employing the customised glass spray chamber. Recoveries are still not ideal even under these conditions. To determine whether agglomeration was also causing reduced recoveries, BCR-145 was prepared as two more slurries, one using 1% Aerosol OT and another using 1% Triton-X 100, a non-ionic surfactant. The customised glass spray chamber was used for all measurements and the results are given in Table 2.13 showing that the best recoveries for all four elements are given when Triton-X 100 is used as the dispersant. Optical microscopy results supported this finding. Less agglomeration of particles was observed when this surfactant was used to disperse the sewage sludge slurry, although recoveries are still not ideal, probably due to the poor slurry sample transport efficiency through the sample introduction system.

2.3.3 Carbonised Slurry Values

As the CRM sewage sludge was known to contain fibrous organic material, a sample of BCR 145 was carbonised before being prepared as a slurry. This procedure enables the carbon fibres to be ground more efficiently by the 'bottle and bead' process.

The particle size distributions for the two charred samples are shown in Figure 2.5 . It can be seen that the mode for each distribution is at 2.52 μm compared to 4μm for the uncharred sample (Figure 2.3). The analytical results obtained using the DSA/ESA combination optimisation parameters with this slurry are shown in Table 2.14.

ELEMENT	OBSERVED CONC. (μg g^{-1}) 0.5% AEROSOL-OT	OBSERVED CONC. (μg g^{-1}) 1% AEROSOL-OT	OBSERVED CONC. (μg g^{-1}) 1% TRITON-X 100	CERTIFIED CONC. (μg g^{-1})
Pb	215.7±47.9	186.4±12.0	236.3±5.9	349.2±15.0
Cu	320.4±112.6	153.9±5.9	340.4±3.9	429.7±10.0
Zn	1399±277	1173±5	1419±29	2843±64
Mn	102.5±32.6	91.2±2.6	107.8±3.9	241.1±12.2

Table 2.13 - Comparison of observed slurry values with certified values for various dispersants in the analysis of BCR-145, using a customised glass spray chamber.

Uncertainties for the observed values are ± 3 s.d.

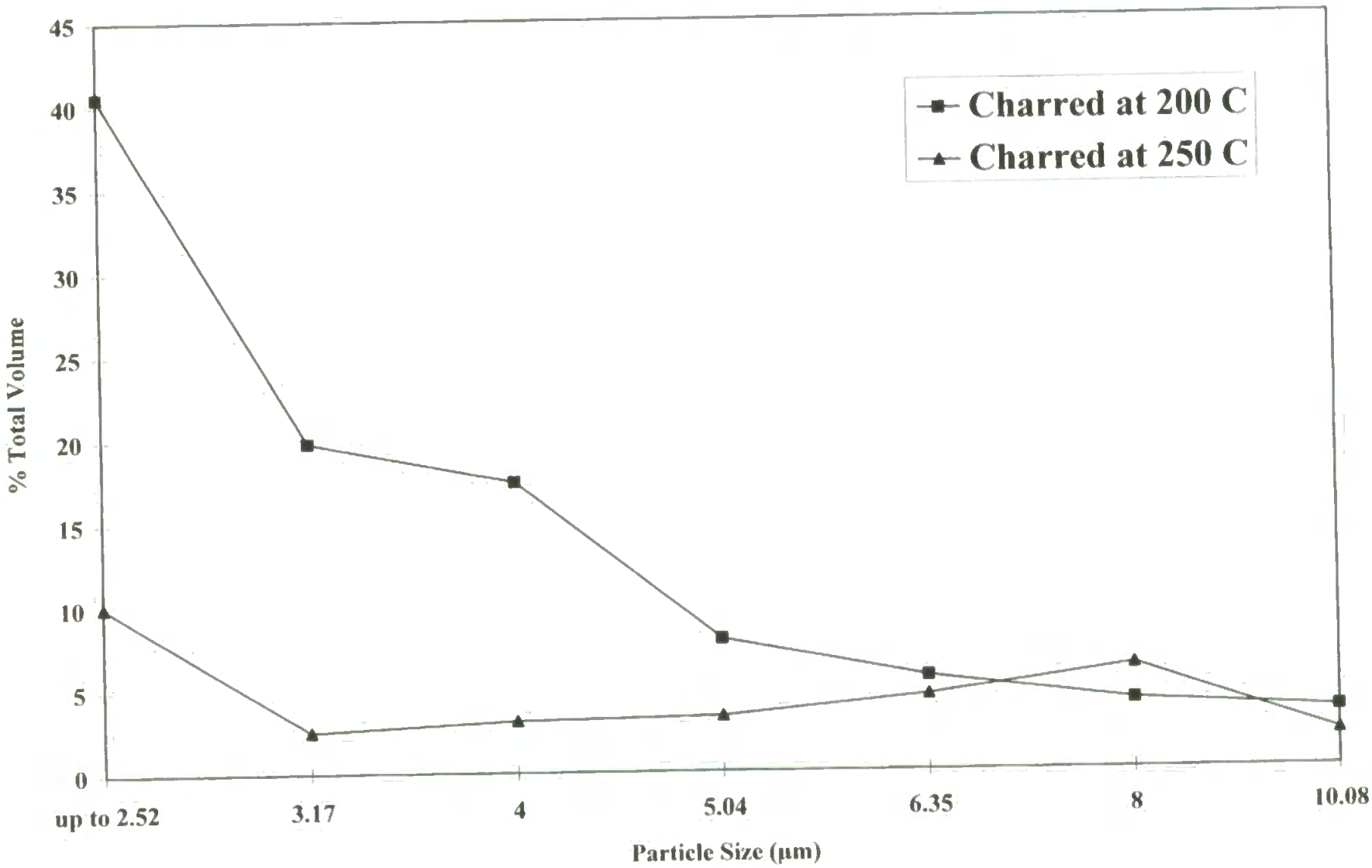

Figure 2.5 - Particle Size Distributions for BCR 145 Sewage Sludge after carbonisation procedure

ELEMENT	Observed Conc. ($\mu g\ g^{-1}$) Sample 1 Charred at 200°C	Observed Conc. ($\mu g\ g^{-1}$) Sample 2 Charred at 250°C	Certified Conc. ($\mu g\ g^{-1}$)
Pb	350.7±3.9	350.9±10.6	349.2±15.0
Cu	205.2±5.9	306.4±33.9	429.7±10.0
Zn	1581±40	2147±175	2843±64
Mn	123.3±0.6	173.0±18.6	241.1±12.2

Table 2.14 - Comparison of observed slurry values from charred BCR 145 - Sewage sludge with certified values

Uncertainties for the observed values are ± 3 s.d.

Although it may be expected that the recoveries for all elements may be improved after sample charring at 200 ^{0}C based on the evidence of the particle size distribution, Tables 2.13 and 2.14 show that, for copper, conventional slurry preparation without charring gives higher recoveries. Possible reasons for low Zn recoveries of this polydensitic, multicomponent sample are i) possible formation of volatile low melting point solids from the various elements present i.e. Zn and Cl to give $ZnCl_2$ which has an appreciable vapour pressure at the charring temperatures used, ii) that the element under investigation is associated with a larger particle size fraction due to a components measure of hardness (MOH) value causing reduced grinding efficiency and iii) that the element is associated with a denser fraction. It is not thought that volatilisation occurring during the carbonisation procedure is to blame for the low recoveries of copper (71.3 % after carbonisation). From Table 2.14 it can be seen that the recovery for lead is good. The recoveries for zinc and manganese improved from 49.9 % and 44.4 % for Zn and Mn respectively before carbonisation to 75.5 % and 71.8 % respectively when the sample was carbonised, although recoveries are still not ideal. If the element is found to be contained in the larger particle size range of the more dense fraction of the slurry, the particles may be lost in the sample introduction system resulting in poor recoveries as reported in the work of Ebdon *et al.*(38).

2.4 Conclusions

It has been demonstrated that it is possible to optimise a truly simultaneous multielement inductively coupled plasma emission spectrometer for both solution and slurry analysis using on-board optimisation algorithms. The results obtained are comparable with the established, rigorous optimisation technique of the variable step-size Simplex programme. The advantages of a simultaneous emission spectrometer incorporating a segmented array charge-coupled device detector have been demonstrated. In particular a range of certified reference materials have been analysed using multi-element compromise optimised conditions and both solution and slurry results were in

good agreement with certified values. Where full elemental recoveries were obtained it may be inferred that transport and atomisation efficiencies for slurries were comparable to those of solutions and that the SOD model was applicable. These recoveries were obtained using multielement optimised operating conditions for solution analysis illustrating that slurry behaviour in the ICP closely models that of solutions. The use of a customised, low dead-volume, double pass spray chamber and carbonisation prior to grinding improved recoveries for sewage sludge samples.

Chapter 3 - Applications Of Slurry Sample Nebulisation Into Inductively Coupled Plasmas

3.1 Introduction

Slurry nebulisation involves the introduction of a solid sample as an aqueous suspension of finely powdered dispersed material. The technique offers a rapid method for the analysis of matrices that are resistant to dissolution procedures or where sample preparation time greatly exceeds analysis time. The dissolution of samples may involve the use of hazardous chemicals, introduce errors from contamination and result in the loss of volatile analytes. For these reasons, slurry nebulisation is not only a viable but advantageous alternative to conventional wet digestion techniques (13-98).

The major applications of slurry sample introduction into plasmas are given in Table 3.1. These applications are listed alphabetically for sample type. The elements determined, analytical technique used and dispersant employed to stabilise the slurries are given. A broad range of applications is clearly evident showing that slurry nebulisation into plasmas is widely applicable throughout environmental, geological, biological, industrial and food analysis.

The studies summarised in Table 3.1 require that, for a slurry to give comparable analytical recoveries to that of a solution, the slurry must behave similarly in terms of sample transport through the sample introduction system and atomisation in the plasma. The particle size distribution of the slurry directly affects the sample transport and atomisation efficiency. Sample preparation is, therefore, the most critical step in an analysis employing slurry sample nebulisation. As previously stated, for efficient slurry transport and atomisation, each aerosol droplet must be occupied by a solid particle of mean diameter determined by the material density (the size occupancy diameter (SOD) model). As a guide, a slurry particle of 2.9 μm diameter and density 1 g cm^{-3} may yield satisfactory elemental recoveries, this value falling to 1.5 μm for higher (7 g cm^{-3}) density materials (56).

SAMPLE	ELEMENTS DETERMINED	PLASMA TECHNIQUE	DISPERSANT USED	COMMENTS	REFERENCE
Airborne particulate matter	Fe, Si, Al, Ti, Ca, Zn, Pb, Cu, Mn	ICP-AES	100 % xylene	Particulates collected on polystyrene fibre filters	17
Animal Tissue	Cu, Zn, Ca, P	DCP-AES	-	Babington slurry nebuliser used	81
Biological Materials	Mg, Ca, K, Na, Fe, Mn, Cu, Zn	ICP-AES	H_2SO_4	Carbonaceous slurries prepared	41
Biological Samples	Mg, Al, Mn, Fe, Co, Cu, Zn, As, Se, Br, Rb, Sr, Mo, Ag, Cd, Sb, Pb, U	ICP-MS	1% v/vTriton x-100	Detection limits range from 0.0001 $\mu g\ g^{-1}$ (U) to 0.52 $\mu g g^{-1}$ (Zn)	76
Botanical Samples	B, Cr, Ti, Mo	ETV-ICP-AES	-	Aqueous calibration used	91
Ceramic Powder	Fe, Mg	ICP-AES	-	Aqueous standards without matrix matching used for calibration	36
	Al, Ca, Si, Fe	ICP-AES	Various dispersants investigated	Effect of dispersant on slurry stability discussed	61

Table 3.1 - Applications of Slurry Nebulisation Into Plasmas

SAMPLE	ELEMENTS DETERMINED	PLASMA TECHNIQUE	DISPERSANT USED	COMMENTS	REFERENCE
	Al, B, Na, Mg, Ca, Ti, V, Cr, Mg, Mn, Fe, Co, Ni, Cu, Zn, Ga, Zr, Ba, La, Ce	ICP-AES and ICP-MS	-	Good agreement between two plasma techniques and with aqueous samples	70
Citrus and Tomato Leaves	Mn, Mg, Ca	ICP-AES	-	RSDs between 0.5 and 2.0%. Matrix matching avoided	44
Clays	Sc, Si, Ca, Fe, Al, Mn, Ti, Mg	ICP-AES	-	Grinding time and particle size controlled reliability of analytical calibration functions	25
	Si, Al, Ca, Mg, Fe	ICP-AES	0.1 M NaCl	Particle size effects and matrix solution composition on matrix interferences determined	40
	Al, Si, Ca, Fe, Mg, K	ICP-AES	1 M HNO_2 + 0.1 M NaCl	Aqueous calibration used	48
Coal	S	ICP-AES	0.5 % Triton X-100	Reduced nebuliser flow rate used with spray chamber geometry modification	22

Table 3.1 (continued) Applications of Slurry Nebulisation Into Plasmas

SAMPLE	ELEMENTS DETERMINED	PLASMA TECHNIQUE	DISPERSANT USED	COMMENTS	REFERENCE
	Mn	ICP-AES	0.5 % Triton X-100	Mixed gas plasmas and simplex optimisation used.	15
	Mn	ICP-AES	1 % Triton X-100	Optimum conditions established using simplex optimisation	23
	Cu, Fe, Mn, Ni	ICP-AES	1 % Triton X-100	Results compared to those obtained by ashing and digestion	24
	S, Al, Ca, Fe, Mg, Si, Ti, Mn	ICP-AES	40% glycerol and 2% Kodak photoflow	Various mixed gas plasmas used	39
	Al, Fe, Ca, Ti, Cr, Mn, Cu, Sr, V, Zn, Co, Ni Al, Ti, Fe, Be, Mg, Cr, Mn, Co, Ni, Cu, Ge, Rb, Ba, Ce, Sm, U	ICP-AES and ICP-MS	0.1 % Aerosol OT	Good agreement with certified values obtained using aqueous calibration	65

Table 3.1 (continued) Applications of Slurry Nebulisation Into Plasmas

SAMPLE	ELEMENTS DETERMINED	PLASMA TECHNIQUE	DISPERSANT USED	COMMENTS	REFERENCE
	Cr, Cu, Mg, Mn, Ni, Pb	DCP-AES	0.5 % Triton x-100	Near unity response factors observed	82
	Cu, Cr, Ni, Pb, Mn	ETV-ICP-MS	0.005% Triton X-100	Standard additions used	82
	V, Mn, Ni, Cu, Pb	ETV-ICP-MS	0.005 % Triton X-100	10 µg Pd added as a physical carrier with O_2 ashing	93
Firebrick	Ti, Fe, Al, Ca, Mg	ICP-AES	0.05 % $Na_4P_2O_7$	Hydrogen modified ICP used	51
	Ti, Fe, Al, Mg	ICP-AES	0.05 % $Na_4P_2O_7$	Freon 116 modified Ar ICP used	54
	Al, Ca, Fe, Mg, Ti	ICP-AES	0.5 % $Na_4P_2O_7$	Influence of particle size on analytical accuracy discussed	56
Foods	Mo	ETV-ICP-AES	-	Samples shaken for 15 - 20 minutes before analysis	89
Geological and Related Non-Conducting Materials	Ba, Ce, Co, Cr, Cu, Ni, Pb, Sr, V, Zn, Si, Fe, Al, Ca, Mg, Ti, Mn	ICP-AES	-	Yttrium added as an internal standard	63

Table 3.1 (continued) Applications of Slurry Nebulisation Into Plasmas

SAMPLE	ELEMENTS DETERMINED	PLASMA TECHNIQUE	DISPERSANT USED	COMMENTS	REFERENCE
Geological Materials	Si, Al, Fe, Ca, Ti, Na, P, S, Ba, Be, Ce, Co, Cr, Cu, Eu, La, Mn, Ni, Sr, V, Y, Yb, Zn	ICP-AES	-	Dispersants not added. Found that slurries <1.5 µm do not behave as solutions	55
	Be, B, Cr, Ge, As, Se, Nb, Mo, Ag, Cd, Sn, Sb, Te, Ta, W, Bi, Th, U	ICP-MS	0.05 % $Na_4P_2O_7$	13 reference materials analysed. Precision ± 5-10%	74
	Ru, Rh, Pd, Os, Ir, Pt, Au	ICP-MS	0.05 % $Na_4P_2O_7$	RSDs 2-30 % for most elements. Good agreement with certified values	77
Industrial Catalysts	Al, Si, Mg, Cu, Mn, Fe, V, Cr, Co, Ni	ICP-MS and ICP-AES	0.05 % $Na_4P_2O_7$	Solid deposition on sampling cone of ICP-MS gave low recoveries	72
Kaolin	Mg, Fe	ICP-AES	0.35% m/v ammonia solution	Effect of particle size, dispersants and viscosity discussed	28
	Fe, Mg, Ti, Si	ICP-AES	0.35% m/v ammonia solution	Various nebulisers, spray chambers and injector tubes employed	30

Table 3.1 (continued) Applications of Slurry Nebulisation Into Plasmas

SAMPLE	ELEMENTS DETERMINED	PLASMA TECHNIQUE	DISPERSANT USED	COMMENTS	REFERENCE
	Mg	DCP-AES	Aqueous ammonia solution	Simplex optimisation used	85
Lobster hepatopancreas	Co, Cr, Ni, Pb	ETV-ICP-MS	0.005% Triton X-100	Standard additions used	92, 93
	Cd, Cu, Fe, Zn	MIP-AES	10 % HNO_3	Good agreement with certified results	88
Milk Powder	Pb	ICP-MS	0.1 % Triton X-100	Lead isotope ratios measured for isotope dilution analysis	71
	P, Ca, Na, K, Mg, Cu, Fe, Zn, Mn	DCP-AES	0.01 % Triton X-100	Lithium enhancement buffer used	83
Ores and Flotation Feeds	Au, Pt, Pd, Ru, Rh	ICP-AES	-	Elements absorbed onto ion exchange resin then made into slurry	18
Oyster Tissue	V, Mn, Ni, Cu, Pb	ETV-ICP-MS	0.005% Triton X-100	Oxygen ashing employed. Pd added as a physical carrier	93
Pine Needles	Al, Cr, Mn, Fe, Co, Ni, Cu, As, Br, Rb, Sr, Cd, Sb, La, Ce, Eu, Pb, Th, U	ICP-MS	1% Triton X-100	Poor accuracy obtained due to fibrous nature of material	76

Table 3.1 (continued) Applications of Slurry Nebulisation Into Plasmas

SAMPLE	ELEMENTS DETERMINED	PLASMA TECHNIQUE	DISPERSANT USED	COMMENTS	REFERENCE
Plant Materials	Ca, Mg, Mn, P	ICP-AES	1 g dm^{-3} Aerosol OT	Sample ashed before grinding	56
	Cu, Mn, Pb, Zn	DCP-AES	0.01% Triton X-100	Carbonisation procedure used for fibrous material	83
Refractory Oxide Powders	Al, Cu, Fe, Mg, Nb, Si, Zr	ICP-AES	0.01% SHMP and monoisopropan-olamine	Slurry technique compared with direct insertion and electroerosion techniques	29
Refractory Samples	Cu, Zn, Pb, Sn, Ag, Fe, Mo, As, Zr	ICP-AES	0.1% Sodium hexametaphosphate	Fundamental studies carried out	38
Rice Flour	Mn, Fe, Co, Ni, Cu, Zn, As, Se, Br, Rb, Mo, Cd, Pb	ICP-MS	1% Triton X-100	Acceptable Accuracy and precision obtained	76
Rocks	Si, Ca, Mg, Fe, Al, Ti, Mn	ICP-AES	-	Grinding time and particle size effects investigated	25
	Al, K, Na, Si, Ba, Mn, Sr, Ti, Ca, Mg, Cu	ICP-AES and ICP-MS	0.1 % $Na_4P_2O_7$	Poor recoveries due to large particle size of slurry	66
Slags	Si, Ca, Mg, Al, Fe, Mn, Ti, Na, K	ICP-AES	0.35 % ammonia	Calibration performed using reference slag	47

Table 3.1 (continued) Applications of Slurry Nebulisation Into Plasmas

SAMPLE	ELEMENTS DETERMINED	PLASMA TECHNIQUE	DISPERSANT USED	COMMENTS	REFERENCE
Sulphide Ores	Cu, Zn, Pb, Sn, Ag, Fe, Mo, As, Zr	ICP-AES	0.1 % SHMP	Various instrument operating parameters used	27
Soils	Ca, Fe, Mg, Mn, Cu, V	ICP-AES	1% $Na_4P_2O_7$	Flow injection used	33
	Na, Ba, Sr, Ca, Mg, Al, Ti, Si	DCP-AES	0.1 % Triton x-100	EIE effects observed	72
Sediments	Al, Fe, Mg, Co, Cr, Cu, Mn, Ni, Pb, V, Zn	ICP-AES	0.01 % Triton X-100	Heated sample introduction system used	86
	Cu, Mn, Zn	ICP-AES	1 M HNO_3	Tandem source used	45
	V, Cr, Mn, Co, Ni, Cu, Zn, Sr, Ba, La, Pb	ICP-MS	Triton X-100	Desolvation device used to improve transport efficiency	52
	Na, Ba, Sr, Ca, Mg, Al, Ti, Si	DCP-AES	0.1% Triton X-100	EIE effects observed	78
	Cu, Zn	MIP-AES	10 % HNO_3	Good agreement with certified values	86
Silicate Rocks	La, Ce, Pr, Nd, Sm, Eu, Gd, Tb, Dy, Ho, Er, Tm, Yb, Lu	ICP-MS	0.1% Triton X-100	RSD = 0.8 - 6.3% for REEs contents of 0.13 - 38 µg ml-1	88

Table 3.1 (continued) Applications of Slurry Nebulisation Into Plasmas

SAMPLE	ELEMENTS DETERMINED	PLASMA TECHNIQUE	DISPERSANT USED	COMMENTS	REFERENCE
Silicon Carbide	Fe, Al, B, Cu, Ni, V, Na, Cr, Ca, Co, Ti	ICP-AES	0.1% Triton X-100	RSDs = 0.8 - 2.1%. Internal standard used	75
Silicon Nitride	C, Al, Ca, Fe, Mg	ICP-AES	-	Low power Ar ICP used	57
	Fe	ICP-AES	0.5% $Na_4P_2O_7$	Concluded that particle size should be <10 µm for good recoveries	35, 42
	Al, Fe, Ca, Mg, Ti	ICP-AES	1% HCl	Freon 12 halogenation agent added	60
Tea Leaves	Al, Ba, Mg, Mn	ICP-AES	0.05% Triton X-100	RSDs= 0.3 - 1.8%	59
	Cu, Cr, Ni, Pb	ETV-ICP-MS	0.005% Triton X-100	Standard additions used	92
	V, Mn, Ni, Cu, Pb	ETV-ICP-MS	0.005 % Triton X-100	Oxygen ashing employed.	93
Whole Plant	Cu	DCP-AES	0.5% Triton X-100	Alumina added to aid grinding	84
Zeolite	Zn, Pb, Cd, Mn, V, Cu, Ti, Ca	ETV-ICP-AES	1% HNO_3	Freon assisted graphite furnace vaporisation	90
Zirconium Oxide	Al, B, Ca, Cu, Fe, Mg, Mn, Na, Ti, V, Y	ICP-AES	-	Detection limits of 0.03 - 10 µg g^{-1} obtained. Results compare well to equivalent solutions	50

Table 3.1 (continued) Applications of Slurry Nebulisation Into Plasmas

Most of the samples shown in Table 3.1 require some degree of grinding so that the particle size distribution of the material satisfies the SOD model. Various grinding techniques have been used and are summarised in Table 1.1 for each of the samples given in Table 3.1. The atomisation efficiency and resultant accuracy of an analysis decreases with increasing particle size. This has been highlighted in the determination of various elements for selected samples given in Table 3.1 (22-25,28,38,44,47,48,65,66,70,91). It is known that for some polydensitic materials such as geological and refractory samples, preferential grinding of some of the material may occur (22,47). More uniformly ground slurries yield results with improved accuracy and precision (22). Particle size effects have been reduced using high temperature, *in situ* fluorination which aids volatilisation of refractory materials (60). In addition, materials which contain a degree of fibrous material, particularly biological samples, require charring before grinding to obtain the required particle size distribution (41,44,56,76,83,93).

The addition of dispersants to a slurry to maintain homogeneity has been used for the majority of samples prepared for slurry nebulisation (Table 3.1). The action of dispersants and the various types available have been previously discussed (Chapter 1.3.2 and Table 1.2). The use of acids as dispersants is common and, where high concentrations are used, improves analytical recoveries owing to partial dissolution of the slurry. This was the case when slurries of sediments were prepared using 10 % HNO_3 as a dispersant (78). In some instances, slurries have been prepared without the use of dispersants. Animal tissue (81), ceramics (36), biological materials (91,44), clays (25), foods (89), geological materials (25,55,63) and ores (18,57) have all been prepared as slurries without employing dispersants. Generally, recoveries were found to be poor, despite mean slurry particle size diameters being less than 5 μm in all cases. This is due to flocculation of the fine particles in the slurry which causes larger agglomerates to be formed. These larger particles are transported to and atomised less efficiently in the plasma.

It is generally accepted that, if the particle size distribution of the slurry is such that it models the behaviour of solutions in terms of atomisation and sample transport, aqueous calibration may be used successfully. Standard slurries have been used, however, in the analysis of geological materials (63) and slags (47). Recoveries were found to be low for some elements. The use of standard slurries for calibration has been criticised in the literature (56) as the sample transport and atomisation of the standard may not be identical to that of the unknown slurry, resulting in inaccurate results and low recoveries.

Optimisation of various instrument operating parameters has been performed in the analysis of clays (15,23,70,85). Other investigations where the influence of a single operating parameter on analytical recovery, such as the nebuliser gas flow rate and sample flow rate, was determined have also been investigated as the residence time of a slurry particle in the plasma is critical. It is generally accepted that for most materials, the slurry particle size distribution, the correct use of a dispersant and the nebuliser gas flow rate are the major factors influencing the analytical recoveries of slurries prepared from the samples listed in Table 3.1 (22-25,28,30,38,44,47,48,65,66,70).

A large variety of environmental samples were routinely analysed using slurry nebulisation throughout the duration of this project. Most of the samples that were analysed had, at some previous time, been prepared as slurries for introduction into plasmas. The grinding techniques and dispersants used for these samples were well documented in the literature. Some samples, where dissolution had proved unsuccessful, costly or time consuming, were presented to these laboratories for analysis by slurry nebulisation ICP-AES. This section describes how two such materials, carbon black and NIST SRM Total Diet, were analysed using slurry nebulisation ICP-AES, the first time these samples have been analysed using this method of solid sample introduction.

3.2 The Analysis of Sulphur in Carbon Black By Slurry Nebulisation ICP-AES

3.2.1 Introduction

Carbon black is a highly refractory graphite material that is notoriously tedious to bring into solution. Current techniques, used commercially to dissolve this sample, involve fusion and 'parr' bomb digestion methods, both of which are costly (as they require high purity reagents to reduce contamination) and labour intensive. Carbon black may be compared to coal in terms of its physical properties. Coal is a graphite containing material comprising several different minerals resulting in a polydensitic matrix. The analysis of coal by conventional aspiration of a solution of the material into plasmas has also been hindered in the past due to problems encountered during sample dissolution. As a result, the use of slurry nebulisation for the analysis of coal is well documented in the literature (15,22-24,39,65,73,82,93). The use of slurry nebulisation ICP-AES with aqueous calibration may therefore be extended for the analysis of carbon black. These samples are commercially available and the elimination of the dissolution step is desirable in industry as sample preparation time of the analysis would be greatly reduced.

For a slurry to be transported as efficiently as a solution, its particle size distribution (PSD) must lie within the aerosol size distribution (ASD) of the aerosol exiting the spray chamber (56). If this is achieved, then matrix matched aqueous standards may be used for calibration of the instrument. A radially viewed ICP-AE spectrometer with a nitrogen purged optical system was used to facilitate sulphur determination in this work. The analytical emission lines of interest for sulphur lie just within the vacuum ultraviolet region of the electromagnetic spectrum (167-375 nm). This requires additional purging of the sample introduction system with nitrogen to eliminate O_2 from air entrainment so that a decrease in sensitivity does not occur (air may absorb UV radiation resulting in a decrease in analyte emission intensity). McCurdy and Fry (22) prepared slurries of coal samples for the 'rapid' determination of sulphur using simple aqueous calibration and ICP-

AES. These authors monitored the background corrected 182.04 nm atomic emission line of sulphur in the analysis of two certified reference material coal samples. Accurate sulphur determinations were obtained using a small coal particle size (median particle diameter ≤ 6 μm), a reduced nebuliser gas flow rate (0.4 L min^{-1}) and a spray chamber free of obstructions such as baffles and impact beads. Slurry nebulisation was performed without wet or dry ashing, solvent extraction, matrix matching, standard additions or internal standardisation.

This study describes how four samples of carbon black were analysed using slurry nebulisation ICP-AES. Two certified coal reference materials were also analysed to enable method validation and instrument performance evaluation.

3.2.2 Experimental

3.2.2.1 Instrumentation

A Perkin-Elmer Optima 3000 radially viewed ICP-AE spectrometer (The Perkin-Elmer Corp. Norwalk, CT, USA) was used in this study. The instrument was equipped with a Perkin-Elmer radial demountable torch with 2.0 mm i.d. alumina injector, a Perkin-Elmer 'Scott-type' double pass spray chamber and an Ebdon v-groove high solids nebuliser (P.S. Analytical Ltd., Berkshire, UK) (30,116). The instrument operating conditions are given in Table 3.2. ICP emission measurements were performed using the 180.669 nm vacuum ultraviolet atomic sulphur emission line. The instrument was optimised for viewing height, nebuliser gas flow and RF power using the instrument on-board Directed Search Algorithm (117,118), described in detail in Chapter 2.3.1, using the signal to background ratio as the figure of merit and by aspirating an aqueous sulphur containing standard.

RF Generator	
Frequency	40 MHz, free running
Forward Power	1150 W (optimised using DSA algorithm)
Sample Introduction System	
Nebuliser	Ebdon v-groove high solids
Torch	Perkin-Elmer radial demountable with 2.0 mm i.d. alumina injector
Spray chamber	Perkin-Elmer 'Ryton' Scott double-pass
Sample Flow Rate	1.0 ml min^{-1}
Argon Gas Flow Rate	
Plasma	15 L min^{-1}
Auxiliary	1.0 L min^{-1}
Nebuliser	0.95 L min^{-1} (optimised using DSA algorithm)
Spectrometer	
Wavelength	S I 180.669 nm
Viewing Height	10 mm ALC (optimised using DSA algorithm)
Resolution	Medium (62 × 250 μm)

Table 3.2: Instrumental operating parameters used in the analysis of Carbon Black samples

3.2.2.2 Chemical and Reagents

All reagents used were of 'AnalaR' reagent grade (Merck, Poole, UK) and all solutions were prepared with double deionised water (Milli-Q, Millipore, Harrow, UK).

Calibration standards were prepared by serial dilution of commercially available analytical standard solutions (1000 μg ml^{-1}, Merck). Standards were matrix matched to the slurry samples by adding Triton X-100 (0.5 %) aqueous dispersant.

The following certified reference materials were used in the preparation of slurry suspensions for analysis: BCR 1632a, a bituminous coal and BCR 1635, a subbituminous coal (Community Bureau of Reference, Brussels, Belgium).

3.2.2.3 Slurry Preparation

Slurries were prepared in this study using the "bottle and bead" method. Approximately 0.1g of the coal and carbon black samples were weighed accurately into a 30 ml 'Nalgene' bottle. Vitrified zirconia beads (10.0 g, 2mm diameter, Glen Creston, Stanmore, UK) were added. Triton X-100 aqueous dispersant (0.5%) was prepared using double deionised water and was added to the bottle until the beads were just covered. The bottle was shaken for at least 8 hours (overnight for convenience) using a standard laboratory flask shaker. Up to 8 samples can be prepared in this manner and no attendance during the process is required. The resulting finely ground slurries were quantitatively transferred to a 100 ml volumetric flask and diluted to volume with dispersant.

Particle size analysis was carried out using a Coulter Counter (Coulter Electronics, Luton, Beds., UK). Samples were analysed using optical

microscopy immediately prior to aspiration into the sample introduction system to identify possible agglomeration of slurry particles.

3.2.3 Results and Discussion

3.2.3.1 Optical Microscopy Particle Size Analysis

The mean particle size for each sample, found using a calibrated optical microscope, is given in Table 3.3. It can be seen that the certified reference coal materials have a larger mean particle size than the carbon black samples. No agglomeration of the particles was apparent from microscopy studies and the slurry seemed to be well dispersed using the chosen Triton X-100 surfactant. Coal is a heterogeneous, polydensitic material and comprises a number of minerals of varying measures of hardness (MOH) values, grain sizes and friabilities. Grinding could therefore serve to reduce the particle size of some of the minerals more efficiently than others and larger particles may remain in the ground slurry. Longer grinding times or the use of a grinding material with greater MOH value may reduce the mean particle size of the coal sample further. Carbon black is, conversely, a monodensitic, homogenous graphite material which produces relatively uniform particle size distributions upon sample grinding.

3.2.3.2 Coulter Counter Analysis

The particle size distributions for the carbon black samples are shown in Figure 3.1. It can be seen that the majority of particles in the carbon black samples are of 2.52 μm in diameter or less. The particle size distribution shows little tailing towards the higher particle size ranges.

3.2.3.3 Concentration of Sulphur in Slurry Samples

The concentration of sulphur measured in the reference materials and carbon black samples, as % weight, is given in Table 3.4. Reported uncertainties are based on 3 standard deviations when n = 10 replicates. The results from the

SAMPLE	MEAN PARTICLE SIZE (μm)
BCR 1632a	2-3
BCR 1635	2
E6019	<1
E6020	<1
E6023	<1
E6024	<1

Table 3.3 - Optical Microscopy Analysis of Carbon Black and SRM Coal Samples

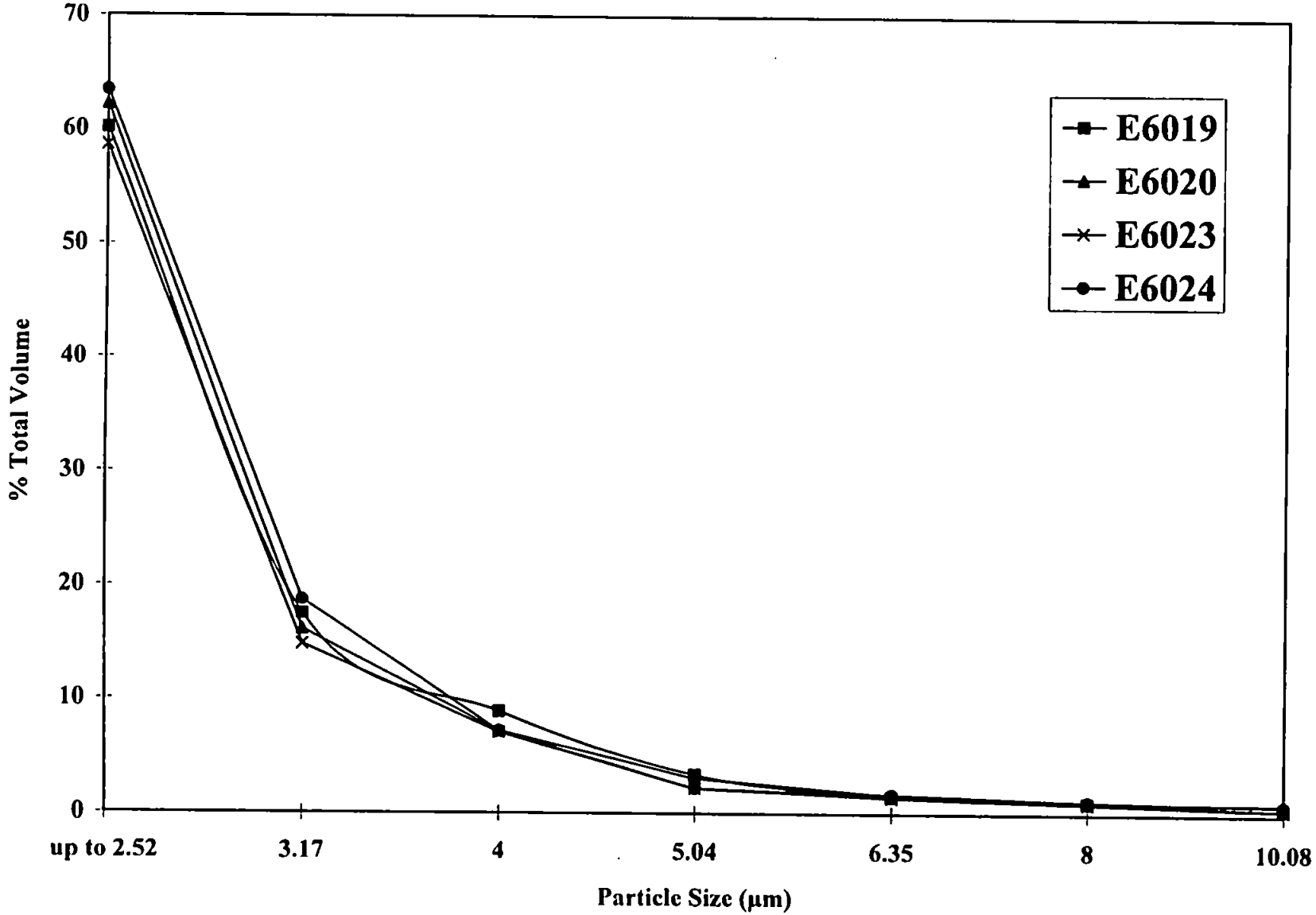

Figure 3.1 - Particle Size Distributions for Carbon Black Samples

CERTIFIED COALS	OBSERVED CONC. (wt %)	CERTIFIED CONC. (wt %)
BCR 1632a	1.51 ± 0.55	1.62 ±0.03
BCR 1635	0.27 ± 0.14	0.33 ±0.03
CARBON BLACK	**OBSERVED CONC. (wt. %)**	**CONC. IN DISSOLVED SAMPLE (wt %)**
Sample 1	0.60 ± 0.06	0.56*
Sample 2	0.49 ±0.03	0.48*
Sample 3	0.04 ± 0.01	0.04*
Sample 4	0.18 ± 0.03	0.17*

Table 3.4 - Concentration of Sulphur in Carbon Black and SRM Coal Samples

* No precision values available

SRM coal slurry samples lie within the measure of uncertainty for the certified values, however precision is extremely poor. This can be attributed to slurry sample inhomogeneity. There are three possible reasons as to why this may occur. When slurry particle size varies with sample composition, as in polydensitic coals, fractionation may occur in the sample introduction system (47). In addition, some mineral particles may be atomised in the plasma more efficiently. Materials with a low refractory mineral content are atomised more efficiently than materials with a high refractory content. The residence time of the analyte in the plasma also contributes an important role in analytical recovery, therefore the nebuliser gas flow and viewing height should be optimised for such inhomogenous materials.

The results from the slurry carbon black samples compare well with results obtained using a complex dissolution procedure carried out by an external laboratory. This may be attributed to the fact that the particle size distribution of the slurry samples was very fine (< 1 μm) and therefore obeyed the SOD model, where one aerosol droplet is occupied by a single particle. The choice of dispersant (Triton X-100) worked well to achieve a stable dispersion. This dispersant was chosen as i) it is non-ionic and gives good dispersion with carbonaceous materials and ii) the only other suitable dispersant was Aerosol OT (sodium sulphosuccinic acid) which contains sulphur and would therefore yield erroneous analytical results.

Although in this particular study only sulphur was determined it would have been possible to measure other elements simultaneously using the Optima 3000 by the slurry technique as it is known that the carbon black slurry models the behaviour of solutions in terms of transport through the sample introduction system and atomisation efficiency in the plasma.

3.3 The Analysis of NIST SRM 1548 Total Diet by Slurry Nebulisation ICP-AES

3.3.1 Introduction

Previous studies of slurries by ICP-AES have mostly used sequential multielement analysis on radially viewed instruments. Although relatively few analysts currently use an axially viewed ICP-AE spectrometer, due to instrument cost and availability, the use of such instruments may offer some advantages for slurry determinations. Viewing a plasma axially extends the source path length thereby increasing analyte emission intensity and potentially improving the sensitivity of aqueous analyses. This sensitivity enhancement results in an approximate 5 to 10 fold improvement in detection limits for many elements over radially viewed plasmas. Using this plasma configuration, elements may be determined at levels comparable to those obtained using GFAAS. A comparison of instrument manufacturers detection limits by different analytical techniques is presented in Table 3.5 (123). These detection limits were measured by calculating three times the standard deviation when ten replicates of the blank are measured. By using simultaneous detection in a multielement determination, maximum advantage may be taken of the time saving capabilities of slurry analysis.

This study describes how a National Institute of Standards and Technology (NIST, Gaithersburg, MD) Standard Reference Material (SRM) 1548 Total Diet, was prepared as a slurry and introduced into the plasma. Total diet is a mixture of typical foodstuffs which constitute an average human daily diet in the United States. The sample is, by definition, heterogeneous, and being of an organic basis, which is difficult to grind and break down, it is not surprising that this is the first time the material has been analysed using slurry nebulisation. The aim of this study was to investigate whether this method of solid sample introduction was suitable for measuring low elemental concentrations in such a sample without the need for sample dissolution, using an axially viewed plasma with simultaneous detection capability and simple aqueous standardisation.

Element	ICP		GFAAS
	Perkin-Elmer Optima 3000 (axial)	Perkin-Elmer Optima 3000 (radial)	Perkin-Elmer 5100 ZL
Ag	0.4	2	0.05
Al	2	5	0.3
As	2	20	0.5
Ba	0.07	0.1	0.9
Be	0.08	0.1	0.02
Cd	0.2	2	0.02
Co	0.4	3	0.4
Cr	0.2	3	0.08
Cu	0.5	1	0.25
Fe	0.3	3	0.3
Hg	0.5	50	1.50
K	2	70	0.02
Mn	0.1	0.4	0.09
Mo	0.7	5	0.2
Na	3	5	0.05
Ni	0.7	7	0.8
Pb	0.8	40	0.15
Sb	2	40	0.4
Se	2	50	0.7
Sr	0.1	0.06	0.06
Ti	0.2	0.5	0.9
Tl	2	50	0.4
V	0.4	3	0.3
Zn	0.1	3	0.3

Table 3.5: Detection Limits in $\mu g\ l^{-1}$ (ppb) obtained using various Perkin-Elmer analytical instruments.

3.3.2 Experimental

3.3.2.1 Instrumentation

All analyses were performed on a Perkin-Elmer Optima 3000 XL axially viewed ICP-AES instrument equipped with a demountable torch with 2.0 mm i.d. alumina injector, a Perkin-Elmer Scott double-pass spray chamber, and an Ebdon v-groove high solids nebuliser (P.S. Analytical Ltd.). The instrument operating conditions are given in Table 3.6. No attempt was made to optimise source conditions for specific analytes or to maximise sample throughput. In this way a direct comparison between solution and slurry performance could be made, under the normal plasma conditions used for aqueous calibration. The emission wavelengths and background correction points used in this multielement study are presented in Table 3.7.

3.3.2.2 Chemicals and Reagents

All reagents used were of 'AnalaR' reagent grade (Merck) unless otherwise stated. Matrix matched standards used in this study were prepared by serial dilution of commercially prepared standard solutions (The Perkin-Elmer Corp.) in deionised water.

3.3.2.3 Slurry Sample Preparation

Slurries were again prepared by the "bottle and bead" method. Approximately 2.0 g of the sample were weighed into a 30 ml polyethylene bottle and 10.0 g of zirconia beads (2 mm diameter) were added. Triton X-100 (0.5 %) was chosen as the dispersant for reasons previously stated (Chapter 3.2.3.3). The dispersant was found to be ideal for organic matrices. The only alternative dispersant, that produced stable slurries of Total Diet was Aerosol OT, an anionic surfactant. This dispersant could not be used as it contains Na (as sodium sulphosuccinic acid) which was one of the elements under investigation in this analysis. Triton X-100 was added until the beads were just covered and the bottle shaken overnight on a 'wrist-action' laboratory

RF Generator	
Frequency	40 MHz, free running
Forward Power	1300 W
Sample Introduction System	
Nebuliser	Ebdon v-groove high solids
Torch	Perkin-Elmer axial demountable with 2.0 mm i.d. alumina injector
Spray chamber	Perkin-Elmer 'Ryton' Scott double-pass
Sample Flow Rate	1.3 ml min^{-1}
Argon Gas Flow Rate	
Plasma	15 L min^{-1}
Auxiliary	0.50 L min^{-1}
Nebuliser	0.80 L min^{-1}
Spectrometer	
Resolution	Medium (62 × 250 μm)

Table 3.6 - Instrumental operating conditions used for the analysis of NIST SRM Total Diet

Element	Wavelength nm	Background Correction Points nm
Ca II	393.366	± 0.036
Cu I	324.766	± 0.030
Fe II	238.204	± 0.014
K I	766.511	± 0.093
Mg II	279.561	± 0.034
Mn II	257.610	± 0.016
Na I	588.995	± 0.018
Zn I	213.860	± 0.013

Table 3.7 - Wavelength selection and background correction points for the Optima 3000 XL used in the analysis of NIST SRM Total Diet

flask shaker. After grinding, slurries were transferred to a 100 ml volumetric flask and diluted to volume.

Particle size analysis was performed using optical microscopy immediately before analysis of the slurry samples.

3.3.3 Results and Discussion

A comparison of the experimental and certified concentrations for SRM Total Diet is given in Table 3.8. Reported uncertainties are based on 3 standard deviations where n = 10 replicates. It can be seen that all results obtained lie within the measure of uncertainty stated for the SRM. It can be seen that for some elements, precision is poor. This is due to sample inhomogeneity. As previously mentioned, the particle size of a slurry varies with sample composition. During the grinding procedure some of the Total Diet matrix would have been ground more efficiently. The more fibrous parts of the material would not have been ground effectively and thus the particle size will be larger. Fractionation in the sample introduction system may therefore have occurred along with incomplete atomisation in the plasma resulting in an ultimate decrease in precision. Carbonising the sample prior to grinding may improve the precision of the analysis as the fibrous material will be broken down. However, some of the more volatile elements may be lost during the charring process if excessively high temperatures are used. Although in this analysis, only the eight elements listed in Table 3.7 were determined, it would have been possible to measure other elements simultaneously using the Optima 3000 XL by the slurry technique.

3.4 Conclusions

The results of these studies illustrate that sample introduction by slurry nebulisation can be used successfully to analyse samples of carbon black and NIST SRM 'Total Diet' using both radially and axially viewed instruments; the first time slurry nebulisation has been reported for these materials. The

Element	Certified Value (µg/g)	Slurry Experimental Value (µg/g)
Na	6250 ± 260	6070 ± 50
K	6060 ± 280	5830 ± 130
Ca	1740 ± 70	1770 ± 10
Mg	556 ± 27	558 ±4.5
Fe	32.6 ± 3.6	35.5 ± 4.1
Zn	30.8 ±1.1	29.7 ± 5.9
Mn	5.2 ± 0.4	6.2 ± 0.4
Cu	2.6 ± 0.3	3.4 ± 0.7

Table 3.8: Comparison of Slurry Experimental and Certified Values for SRM 1548 Total Diet

particles in the slurries were well dispersed and displayed a small particle size with a narrow distribution making aspiration into the plasma efficient. This is reflected in the excellent correlation in results for NIST SRM Total Diet and in the agreement between solution and slurry results for carbon black samples. The need for time consuming digestion techniques using hazardous reagents and concentrated acids has been avoided by employing this method of solid sample introduction.

Chapter 4 - The Effect Of Easily Ionisable Elements On Solutions And Slurries In An Axially Viewed Inductively Coupled Plasma

4.1 Introduction

Some of the most important and significant unanswered questions in inductively coupled plasma atomic emission spectrometry (ICP-AES) lie in the area of matrix dependent interferences. It has been shown by many workers (124-135) that easily ionised elements (EIEs) such as lithium, sodium, potassium and caesium cause complex shifts in the spatial distribution of analyte emission and can cause erroneous analytical results.

The behaviour of slurries in the plasma, under certain conditions, has been shown to be different to that of solutions (38). This research (38) demonstrated that when the plasma is viewed 'radially' or 'side on' the emission signal versus viewing height profiles of particular slurries differ from those of solutions. Indeed, under certain plasma conditions and solid particle size distributions for some elements in slurries the emission signal at low viewing heights is greater than that for a solution of equivalent analyte concentration. Above the Normal Analytical Zone (NAZ) (128) the situation is reversed.

These effects have been attributed to such processes as i) simple transport phenomena, ii) simple time-dependent atomisation of the solid particles and iii) matrix enhancement and suppression from either the slurry-stabilising components (dispersants) or a change in the central channel's matrix composition as the solid particle breaks down. Confusion arises in correctly attributing the origin of these effects, to one or a combination of these processes, when the solutions used for calibration are not matrix matched to the slurries under investigation.

There has been limited comprehensive work in the literature concerning the effect of EIEs when looking at the plasma axially (136). No investigations into slurry behaviour have been documented for 'end on' viewing or for the use of axial viewing of EIE effects with ICP instrumentation having solid state detection. An axial ICP-AE spectrometer has been used to compare the effect of EIEs on atom and ion lines for solutions and slurries when the plasma is viewed 'end on'.

4.2 THEORY

Interpreting emission intensities directly gives no indication of the excitation and ionisation processes that may be occurring within the plasma. However, the ratio of emission intensity of an ion line, I_i ,to emission intensity of an atom line, I_a, has previously been used to measure and examine the energy characteristics of the ICP discharge (137,138).

The various species which constitute the plasma body such as neutral atoms, ions, molecules and electrons are distributed over many energy states. The states of the distribution are often defined by different temperatures that depend on the species used for the temperature measurements. Under the conditions of Local Thermodynamic Equilibrium (LTE) the ion/atom emission intensity ratio is related to the excitation temperature and the electron number density, which govern the population of the excited atom and ion levels, by the Saha equation via the Boltzmann function (139):

$$\frac{I_i}{I_a} = \left(\frac{4.83 \times 10^{21}}{n_e}\right)\left(\frac{g_i A_i \lambda_a}{g_a A_a \lambda_i}\right) T_e^{3/2} e\left(\frac{-E_{ion} - E_{exc}^{i} + E_{exc}^{a}}{kT_{exc}}\right) \quad (4.1)$$

where T_{exc} is the excitation temperature, T_e is the electron temperature, g is the statistical weight, A is the transition probability, λ is the wavelength (cm), n_e is the electron number density, E_{ion} is the ionisation energy, E_{exc} is the excitation energy (cm^{-1}) and k is the Boltzmann constant.

The experimentally measured ion/atom emission intensity ratio (I_i/I_a) can be related to those calculated from the LTE expression in terms of a non equilibrium parameter, b_r(140). This parameter is a measure of departure from LTE and is given by:

$$\left(\frac{I_i}{I_a}\right)_{exp} = b_r \left(\frac{I_i}{I_a}\right)_{LTE} \quad (4.2)$$

It is clear from the literature (141) that, on the whole, the ICP is not characterised by LTE ion-atom emission intensity ratios. However, the experimental values of I_i/I_a are usually within a factor of five from calculated LTE values. Consequently, any energy related values obtained using the experimentally obtained I_i/I_a ratio from the Saha equation, such as n_e and T values, will not be characteristic of a system in LTE.

To usefully employ ion/atom emission intensity ratios, it is generally accepted that the chosen atom and ion line wavelengths for a specific analyte be in close proximity and are free from spectral interferences. Various line pairs that have been measured for certain analytes of interest are given in a paper by Caughlin and Blades (141). For example magnesium has often been used (142) with the line selection Mg II 279.553nm (or Mg II 280.270 nm) and Mg I 285.213 nm. The excitation energies of the ionic and atomic lines are very close - 35,761 (35,669) and 35,051 cm^{-1} respectively. In addition, gA values are well documented for the element and to a relatively higher degree of accuracy (± 10%) compared with other species.

4.3 Experimental

4.3.1 Instrumentation

Axial profiles were obtained using a Perkin-Elmer Optima 3000 XL echelle spectrometer (The Perkin-Elmer Corp., Norwalk, CT, USA) with a segmented array charge-coupled device detector (SCD). The design and evaluation of the echelle grating optical system and solid state detector has been discussed previously (108,114). The operating conditions used in this study are given in Table 4.1.

For the axial profile studies, measurements were taken over the entire spatial surface in both the x and the y directions (Figure 4.1). The position of the optical mirror was altered using the computer controlled stepper motor in the spectrometer. In this way the spatial point where emission readings were taken could be changed and would be reproducible. A program was written using the instrument software to automate each analysis.

Emission intensity measurements were made using the Mg 279.553 nm ion and 285.213 nm atom lines. All measurements were background corrected.

RF Generator	
Frequency	40 MHz, free running
Forward Power	1200 W
Sample Introduction System	
Nebuliser	Ebdon V-Groove high solids
Torch	Demountable with 2.0 mm i.d. alumina injector
Spray Chamber	Perkin-Elmer Scott Double-pass
Peristaltic Pump	Gilson Minipuls 3, computer controlled
Uptake Rate	1.0 ml/min
Argon Flow Rate	
Plasma coolant	15 L/min
Auxiliary	1.5 L/min
Nebuliser	1.0 L/min
Spectrometer	
Polychromator	High energy, echelle based
Resolution	0.007 nm at 200 nm
Detector	Perkin-Elmer SCD

Table 4.1 - Plasma operating conditions used on the PE Optima 3000 XL ICP-AES

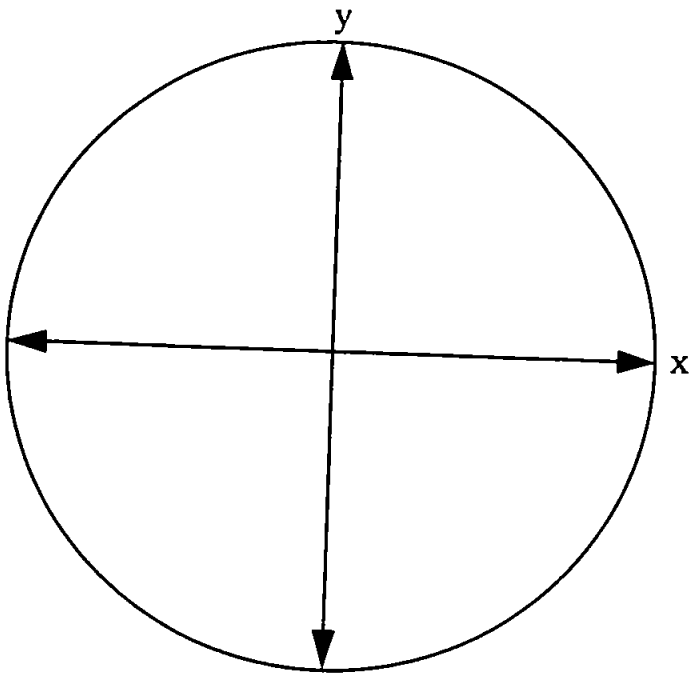

y = -6 to + 6 mm

x = -4 to + 4 mm

Figure 4.1 - The spatial surface of the axially viewed ICP

4.3.2 Chemicals and Reagents

All reagents were of 'AnalaR' reagent grade (Merck, Poole, UK) and all solutions were prepared with 18 megohm distilled, deionised water.

4.3.3 Solution and Slurry Preparation

Mg solutions, 10 μg ml^{-1} , were prepared by dilution of commercially prepared analytical standard solutions (1000 μg ml^{-1}, Merck). Slurries containing 10 μg ml^{-1} Mg, were prepared by grinding MgO using the bottle and bead method (30). Triton X-100 (0.5% *v/v*), a non-ionic dispersant, was used to prevent agglomeration of the particles. Particle size was monitored using both optical microscopy and a Coulter Counter (Coulter Electronics, Luton, Beds, UK). Solutions were matrix matched with the slurries by adding dispersant (Triton-X 100) to the same concentration.

Equimolar amounts (0.05 M) of Li, Na, K and Cs (as their respective chloride salts) were added to the Mg solutions and slurries. EIE interferences, as part of the solid slurry sample, were not investigated in this work. A 10 μg ml^{-1} Indium internal standard was added to all solutions and slurries to act as a drift normaliser. The In II 230.606 nm line was monitored simultaneously so that any instrument fluctuations could be monitored and corrected for. The Indium internal was chosen as it was found to be unaffected by the addition of EIEs under the experimental conditions used. This was verified prior to data acquisition and enhancement or suppression of the In signal was not observed when measurements were taken at numerous points over the plasma.

4.4 Results And Discussion

4.4.1 The Effect Of EIEs On Solutions

The ion/atom emission intensity ratio for a solution may be used to evaluate certain fundamental parameters such as b_r, temperatures and species densities at spatial positions in a plasma. The presence of a matrix element in the solution may significantly alter these parameter values. Complex shifts in the spatial distribution of analyte emission when EIEs are added to a solution, together with intensity changes, most clearly illustrate how the magnitude of these fundamental parameter values may be affected.

The experimentally measured ion/atom emission intensity ratio is an important indicator of how a system may change, once matrix elements are present, without the need to calculate absolute values of temperature and electron number densities. Comparing I_i/I_a for the same analyte in two systems can reveal discrete differences between the behaviour of the two separate solutions within the plasma discharge. If I_i/I_a from an analyte in one solution is compared to I_i/I_a from the same analyte of equivalent concentration but with an EIE matrix element added, any variation between the two must arise due to differences between excitation and/or ionisation and/or atomisation processes. It is known that increasing the mass concentration of concomitant matrix elements, such as EIEs, decreases the transport efficiency of an analyte of interest through the sample introduction system. This physical effect results from changes in the viscosity, surface tension and density of the solutions and hence changes in the nebulization efficiency, droplet size distribution and aerosol loss processes (143-145). This transport phenomenon is dependant upon the concomitant matrix (not on the analyte of interest) and must be corrected for in any measurements of intensity accompanying changes of EIEs.

The relationship between I_i/I_a for an analyte and I_i/I_a for the analyte with EIE added can be given in terms of the ratio D_{sol},

$$\frac{\left(\frac{I_i}{I_a}\right)_{solution+EIE}}{\left(\frac{I_i}{I_a}\right)_{solution}} = D_{sol} \qquad (4.3)$$

By calculating D_{sol}, transport effects are negated. While the presence of an EIE causes a decrease in sample throughput to the plasma (and hence a decrease in emission intensity) I_i/I_a values will be the same for the two systems (at a single spatial point) if excitation, ionisation and atomisation processes are comparable. For the axially viewed sample, for a 10 μg ml^{-1} Mg solution at a single spatial point, I_i may equal 10,000 counts/second while I_a may be 5,000 counts/sec. I_i/I_a is therefore 2. Similarly, at the same spatial position, for a solution with 0.05 M Li added I_i may be 8,000 counts/sec due to lower sample throughput and I_a may be 4,000 counts/sec. I_i/I_a for this second system will still be 2. The value for D_{sol} will be 1 illustrating that once the

sample analyte has entered the plasma it is behaving similarly in terms of ionisation, excitation and atomisation.

If the plasma processes involving the analyte of interest were to be the same in the presence or absence of an EIE then an axially viewed representation of the D_{SOI} values over the entire plasma would take the form shown in Figure 4.2. In practise, D_{sol} values usually deviate from 1. Figures 4.3a-d show D_{sol} values when a 10 μg ml^{-1} Mg solution alone is compared to a 10 μg ml^{-1} Mg solution containing 0.05 M Li, Na, K and Cs respectively. Values for D_{sol} have been calculated over the entire spatial surface of the plasma. The uncertainties of D_{sol} values at each spatial point were less than 2 % RSD in all cases.

When the D_{sol} profiles in Figures 4.3a-d are viewed in series it can be seen that there is increasing enhancement in the order Li<Na≤K<Cs. There are various ways in which this effect could be produced. i) Enhancement is caused by the atom line intensity decreasing and/or the ion line intensity increasing; ii) Enhancement is due to an increase in intensity of both atom and ion lines but where the ion line intensity is increased to a greater degree.

By taking the emission intensity of the Mg atom line from a solution with no EIE added as a reference point, the magnitude of the enhancement for atom emission with EIE added can be seen to be increasing in the order Li<Na≤K<Cs (Figure 4.4a-d) as represented by the ratio:

$$\frac{I_a solution + EIE}{I_a solution\_only} \qquad (4.4)$$

If there is no enhancement of the atom line on addition of an EIE then the ratio will be 1. This would also be the case for the ion line ratio:

$$\frac{I_i solution + EIE}{I_i solution\_only} \qquad (4.5)$$

In practice figures 4.4a-d show the enhancement effect follows the same order as before: Li<Na≤K<Cs. However the magnitude of the enhancement is

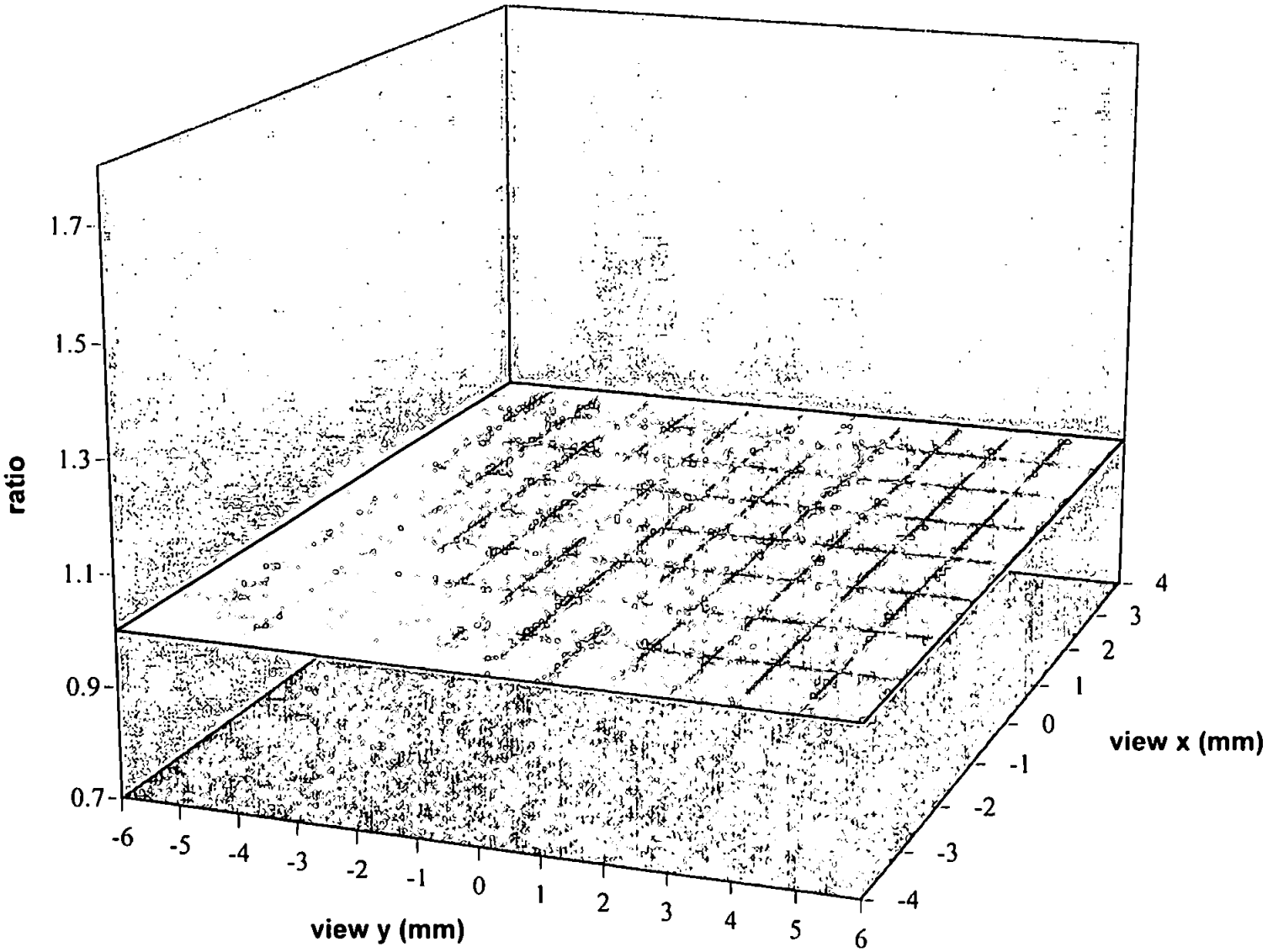

Figure 4.2 - Profile of the entire spatial surface when Dsol = 1 at all positions

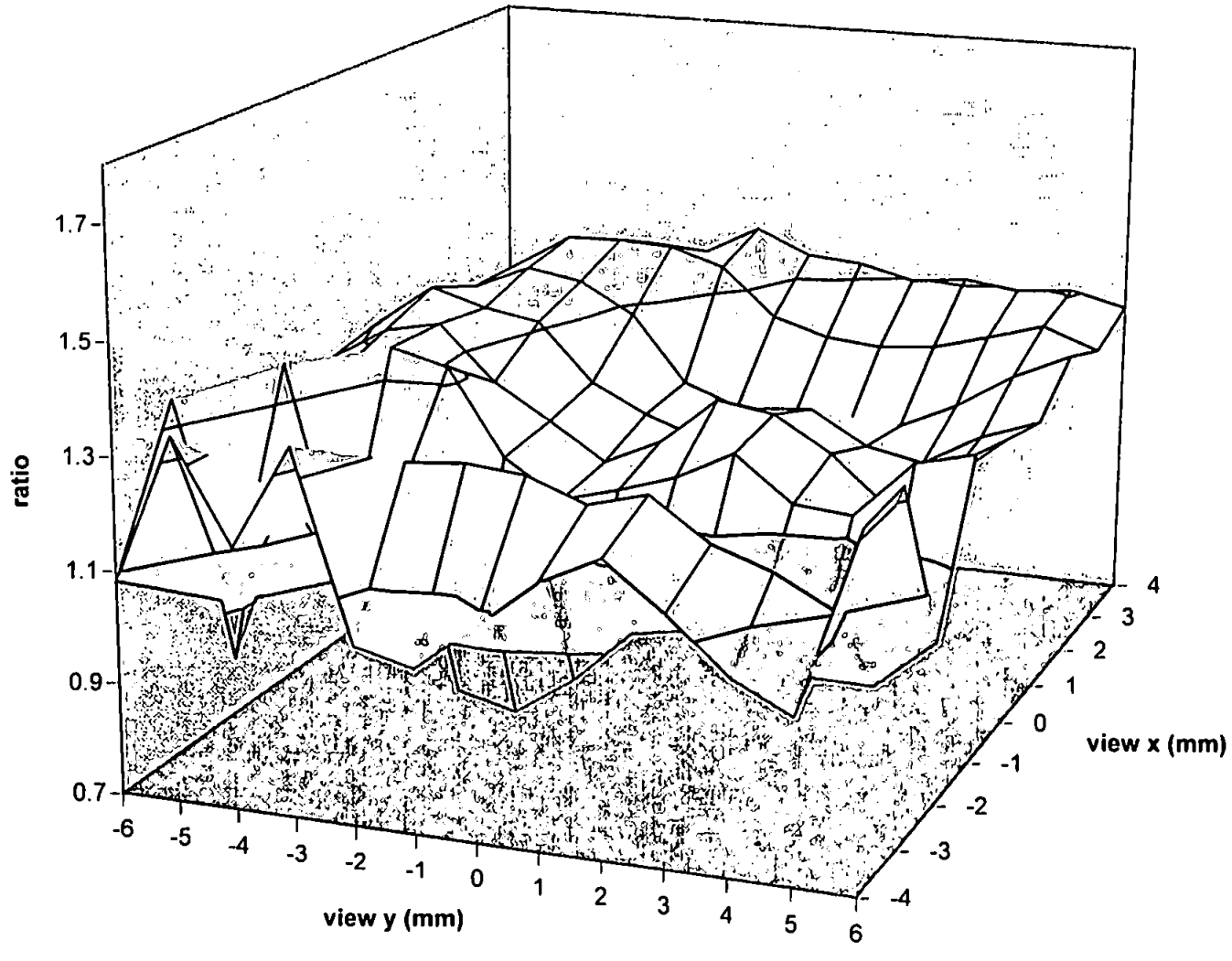

Figure 4.3a - Dsol values for a 10 µg ml-1 Mg solution containing 0.05 M Li

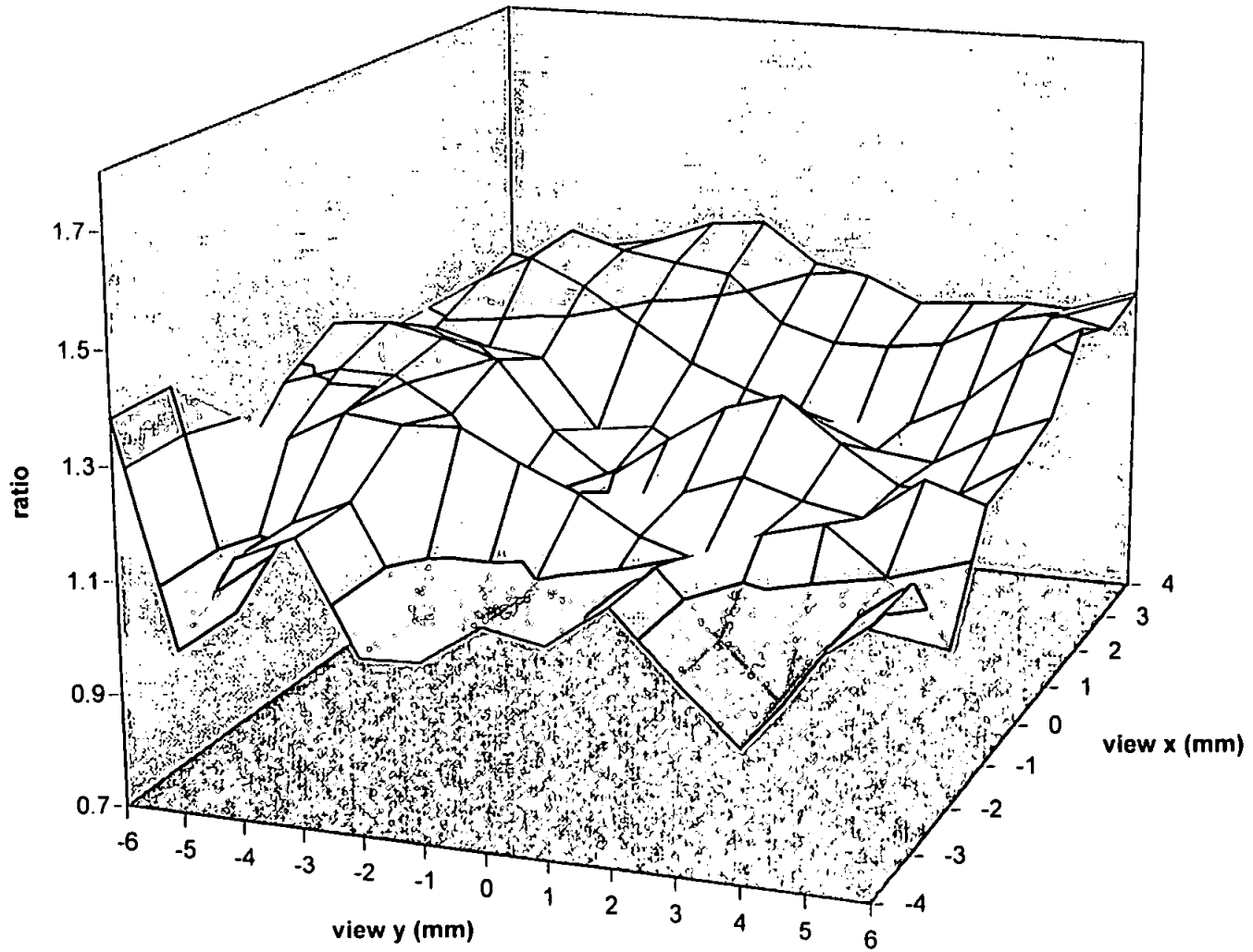

Figure 4.3b - Dsol values for a 10 µg ml-1 Mg solution containing 0.05 M Na

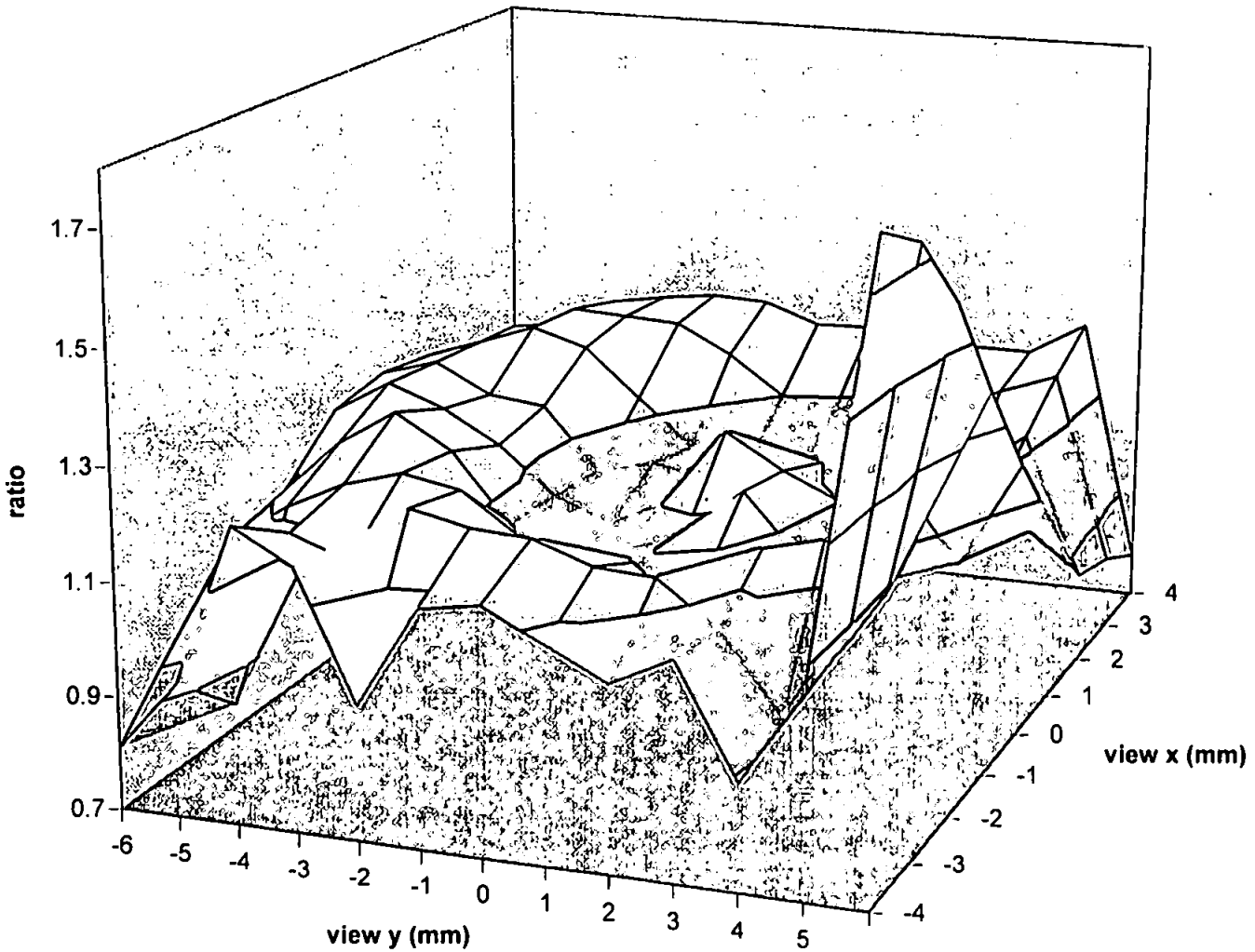

Figure 4.3c - Dsol values for a 10 µg ml-1 Mg solutoin containing 0.05 M K

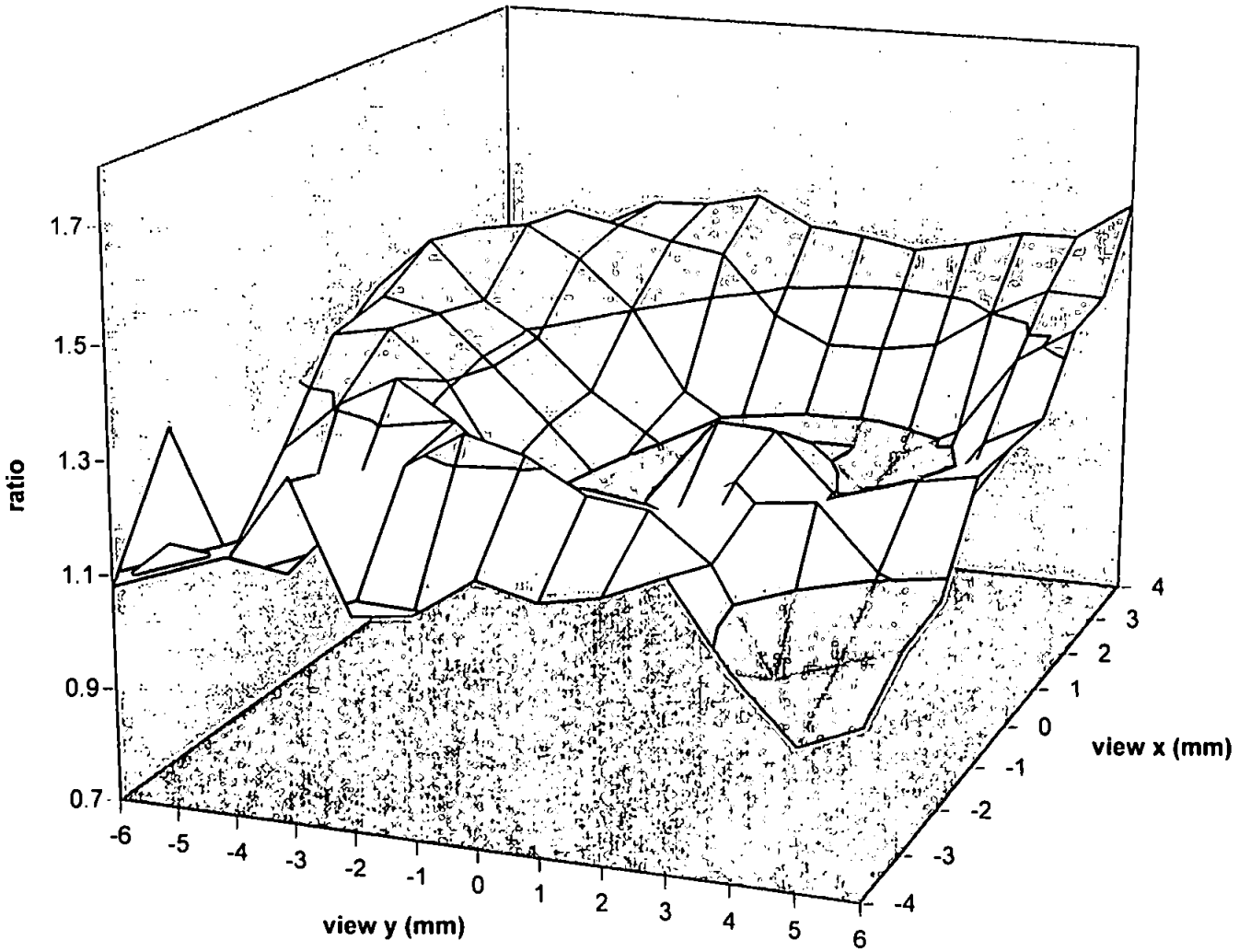

Figure 4.3d - Dsol values for a 10 µg ml-1 Mg solution containing 0.05 M Cs

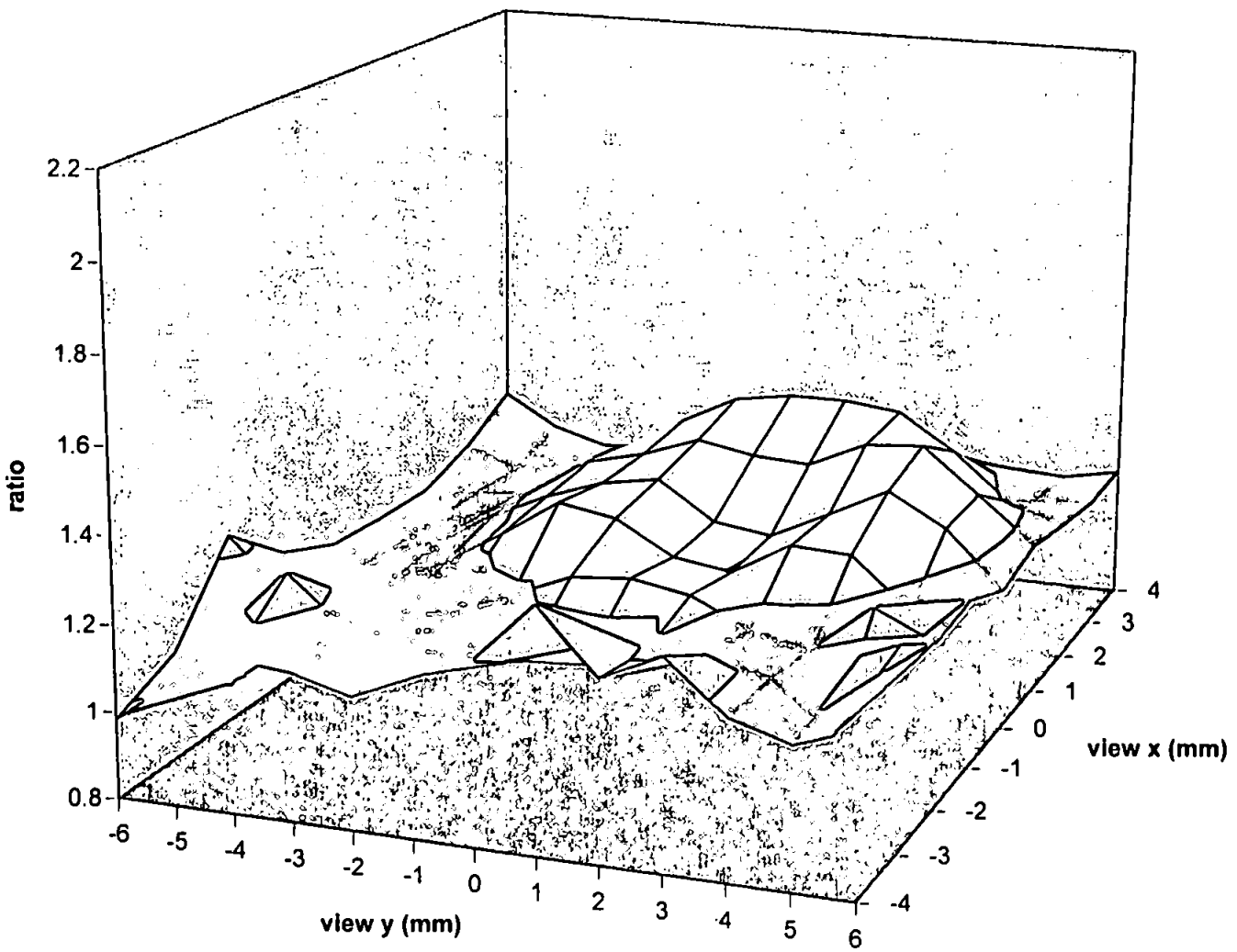

Figure 4.4a - Ratio of atom line emission (Mg solution + EIE / Mg solution only) for solutions containing 0.05 M Li

greater for the Mg ion line (Figure 4.5a-d) compared to that of the Mg atom line for a given EIE. This can be shown numerically in Table 4.2. The enhancement effect of Na, K and Cs is seen to be similar and more pronounced than that of Li. This may be due to the increased mass of the EIE resulting in reduced transport efficiency as compared to a solution with no EIE added. Because of this relative enhancement effect i.e.

$$\frac{I_i solution + EIE}{I_i solution\_only} > \frac{I_a solution + EIE}{I_a solution\_only} \qquad (4.6)$$

the profiles for D_{sol} (4.3a-d) show the order previously stated for the given EIE.

On inspection of Figures 4.4a-d and 4.5a-d, it can be seen that there are obvious differences between profiles obtained from atom and ion line ratios in terms of structure. While an ion line ratio profile is relatively flat across the whole field of view, there is definite structure to the atom line profile in all cases of EIE addition. The structure of the atom line ratio profile may be described in terms of a 'caldera'. The rim of the caldera is seen to be more pronounced as we descend the order Li, Na, K and Cs. Because these profiles are an atom line intensity ratio of solutions with EIEs/solutions without EIEs the rim effect reflects the change in atom emission intensity between the central analyte channel and that of the plasma body. It may be conjectured that the relative excited atom population is increased at this interface due to the presence of an EIE thereby indicating a change in energy exchange for this region. The structures seen in Figure 4.3a-d are a direct consequence of the ratio:

$$\frac{\left[\frac{I_i solution + EIE}{I_i solution\_only}\right]}{\left[\frac{I_a solution + EIE}{I_a solution\_only}\right]} \qquad (4.7)$$

which rearranges to give the ratio D_{sol}.

EIE UNDER STUDY	RANGE OF ATOM LINE RATIO VALUES	RANGE OF ION LINE RATIO VALUES	RANGE OF D_{sol} VALUES
0.05 M Li	1.00 - 1.30	1.40 - 1.60	0.80 - 1.30
0.05 M Na	1.30 - 1.60	1.70 - 2.00	1.00 - 1.35
0.05 M K	1.30 - 1.60	1.70 - 2.10	1.0 - 1.20
0.05 M Cs	1.40 - 1.73	1.80 - 2.20	1.10 - 1.45

Table 4.2 - Relative enhancement of atom line ratios, ion line ratios and D_{sol} values for a 10 µg ml^{-1} Mg solution in the presence of EIEs

It is interesting to note that the structured enhancement effects seen in D_{sol}, which were described in terms of a 'caldera' for the atom line intensity ratio, show a slightly different but definite structural enhancement on going from Li through Na and K to Cs, i.e. to that of a 'caldera' (possessing both a rim and an area of depression) but with an elevated 'island' at the centre. As this was not observed in the atom ratio profiles, this 'island' enhancement effect would seem to arise from changes in the excited ion population relative to that of the excited atom population in the presence of an EIE. This shows that there is also a change in the ion energy transfer processes near the centre of the analyte channel which accompany those between the analyte channel and the main plasma body when an EIE is added. The magnitude of the change for this 'island' effect increases in the same order as before for EIEs.

It should also be noted that the slight asymmetry shown in the atom 'caldera' profiles can be attributed to the perpendicular shear gas. This is used to 'cut' the tail flame of the plasma flat in preparation for axial viewing.

4.4.2 The Effect of EIEs on Slurries

As was demonstrated for solutions, the ion/atom emission intensity ratio for a slurry may also be used to calculate fundamental parameters. As the mass of a concomitant matrix element increases, the sample transport efficiency into the plasma discharge decreases accordingly.

The relationship between I_i/I_a for a slurry and I_i/I_a for a slurry with an EIE added can be given in terms of the parameter D_{slu}:

$$\frac{\left(\frac{I_i}{I_a}\right)_{slurry+EIE}}{\left(\frac{I_i}{I_a}\right)_{slurry}} = D_{slu} \qquad (4.8)$$

Transport effects are negated for the slurry systems using the same argument as that for a solution + EIE /solution only system.

When D_{slu} = 1, atomisation, excitation and ionisation effects for the two systems in the plasma discharge are equal. Figures 4.6a-d show D_{slu} values

when a 10 μg ml^{-1} Mg slurry is compared to a 10 μg ml^{-1} Mg slurry containing 0.05 M Li, Na, K and Cs respectively.

Using a Coulter Counter and optical microscopy, the mean particle size of the 10 μg ml^{-1} Mg (as MgO) slurry was measured to be below 2 μm but with the distribution tail extending up to 4 μm. Magnesium oxide is a refractory material possessing a high melting (2852 °C) and boiling point (3600 °C). With transport effects negated, any refractory particles up to 4 μm in diameter entering the plasma may allow the measurement of atomisation effects in the presence of EIEs compared with a slurry without any EIE.

When the D_{slu} profiles for the Mg slurries with equimolar amounts of different EIEs are viewed in series (Figures 4.6a-d) it can be seen that there is increasing enhancement in the order Li, Na, K, Cs. This is the same trend seen for D_{sol}. Again, by taking the intensity of a Mg atom emission line from a slurry with no EIE added as a reference point the magnitude of the enhancement for atom emission with EIE added can be seen to be in increasing order Li<Na<K<Cs. This is shown in Figures 4.7a-d and is represented by the ratio:

$$\frac{I_a slurry + EIE}{I_a slurry\_only} \qquad (4.9)$$

For the equivalent ion line intensity ratios, the enhancement effect again follows the order Li<Na<K<Cs. As was found in the case of the ion line intensity ratios for Mg solutions, the magnitude of the enhancement is greater for the Mg slurry ion line compared to that of the Mg atom line for the given EIE. This is represented by

$$\frac{I_i slurry + EIE}{I_i slurry\_only} \qquad (4.10)$$

and is shown in Figures 4.8a-d and in summary by Table 4.3.

Because of this relative enhancement effect i.e.

$$\frac{I_i slurry + EIE}{I_i slurry\_only} > \frac{I_a slurry + EIE}{I_a slurry\_only} \qquad (4.11)$$

EIE UNDER STUDY	RANGE OF ATOM LINE RATIO VALUES	RANGE OF ION LINE RATIO VALUES	RANGE OF D_{slu} VALUES
0.05 M Li	1.10 - 1.30	1.40 - 1.65	1.00 - 1.40
0.05 M Na	1.10 - 1.37	1.40 - 1.60	1.20 - 1.65
0.05 M K	1.10 - 1.34	1.35 - 1.50	1.20 - 1.65
0.05 M Cs	1.30 - 1.70	1.60 - 1.80	1.30 - 1.70

Table 4.3 - Relative enhancement of atom line ratios, ion line ratios and D_{slu} values of a 10 µg ml^{-1} Mg slurry in the presence of EIEs

the profiles for D_{slu} (Figure 4.6a-d) show the order previously stated for the given EIE.

The structures shown in figures 4.7a-d and 4.8a-d (atom line intensity ratios and ion line intensity ratios respectively) obtained from slurries, can be compared with the equivalent structures obtained from solutions (figures 4.4a-d and 4.5a-d). Similar energy transfer mechanisms are suggested for both. The presence of a 'caldera; with 'rim' enhancement for the atom line ratio when EIEs are added in the order Li<Na≤K<Cs and a relatively flat ion line ratio support this. The structures for D_{slu} shown in figure 4.6a-d are a consequence of the ratio:

$$\frac{\left[\frac{I_i slurry + EIE}{I_i slurry\_only}\right]}{\left[\frac{I_a slurry + EIE}{I_a slurry\_only}\right]} \qquad (4.12)$$

which rearranges to give D_{slu}. The similarities between energy processes of solutions and slurries may be extended when the structures for D_{slu} and D_{sol} with addition of different EIEs are included in the comparison (figures 4.3 a-d and 4.6a-d). The presence of both an increasing 'rim' and central 'island' in both sets of profiles is noted. This assumed spatial dependence of the energy transfer processes in the plasma does, however, appear to differ in magnitude between solutions and slurries and is considered in the next section.

4.4.3 Comparison of Solutions and Slurries

The ion/atom emission intensity ratio for an analyte in a slurry may be compared to that same intensity ratio from a solution of equivalent analyte concentration to see how the same fundamental parameters described previously may differ in magnitude for the two different sample introduction methods.

Comparing emission intensities for a single atomic or ionic line when aspirating solutions and slurries may yield discrepancies between the two

readings. The major cause of this phenomenon can be attributed in most cases to the lower sample transport efficiency of the slurry compared to that of a solution (56). For efficient nebulization and introduction into the injector via a spray chamber, the solid particle size distribution is critical. Larger particles 'settle out' within the sample introduction system and so sample throughput and therefore emission intensity for the analytical line in question decreases in turn.

By ratioing I_i/I_a for a solution and I_i/I_a for a slurry, transport effects can again be negated:

$$\frac{\left(\frac{I_i}{I_a}\right)_{solution}}{\left(\frac{I_i}{I_a}\right)_{slurry}} = D_R \qquad (4.13)$$

D_R values of the solution and slurry in the absence of EIEs are shown in Figure 4.9a. D_R can also be calculated for solutions and slurries containing the same EIE i.e.:

$$\frac{\left(\frac{I_i}{I_a}\right)_{solution+EIE}}{\left(\frac{I_i}{I_a}\right)_{slurry+EIE}} = D_R \qquad (4.14)$$

When D_R = 1, it may be assumed that, again, the atomisation, excitation and ionisation effects for the two systems in the plasma discharge are equal. Figure 4.9b-d shows D_R values when a 10 µg ml^{-1} Mg solution is compared to a 10 µg ml^{-1} Mg slurry with the addition of 0.05 M Li, Na, K and Cs respectively to both solution and slurry.

A definite structure to the D_R profile may reflect any spatial dependence differences in magnitude to the energy transfer processes between solution and slurry in a plasma. The D_R profiles do not show any well defined structure and, within limits, are relatively flat in cross section. Those mechanisms which bring about structure in the profiles may be considered very similar in

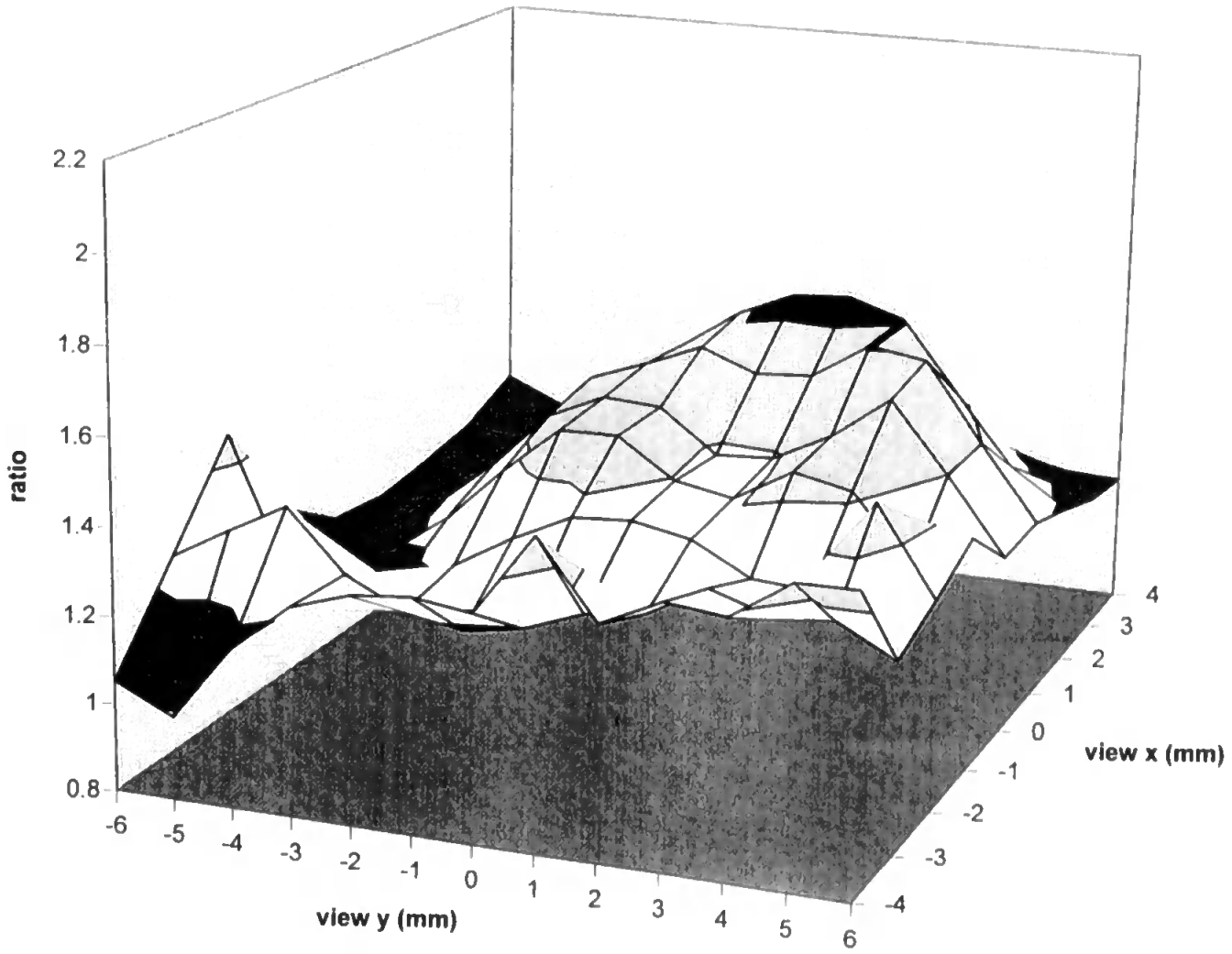

Figure 4.4b - Ratio of atom line emission (Mg solution + EIE / Mg solution only) for solutions containing 0.05 M Na

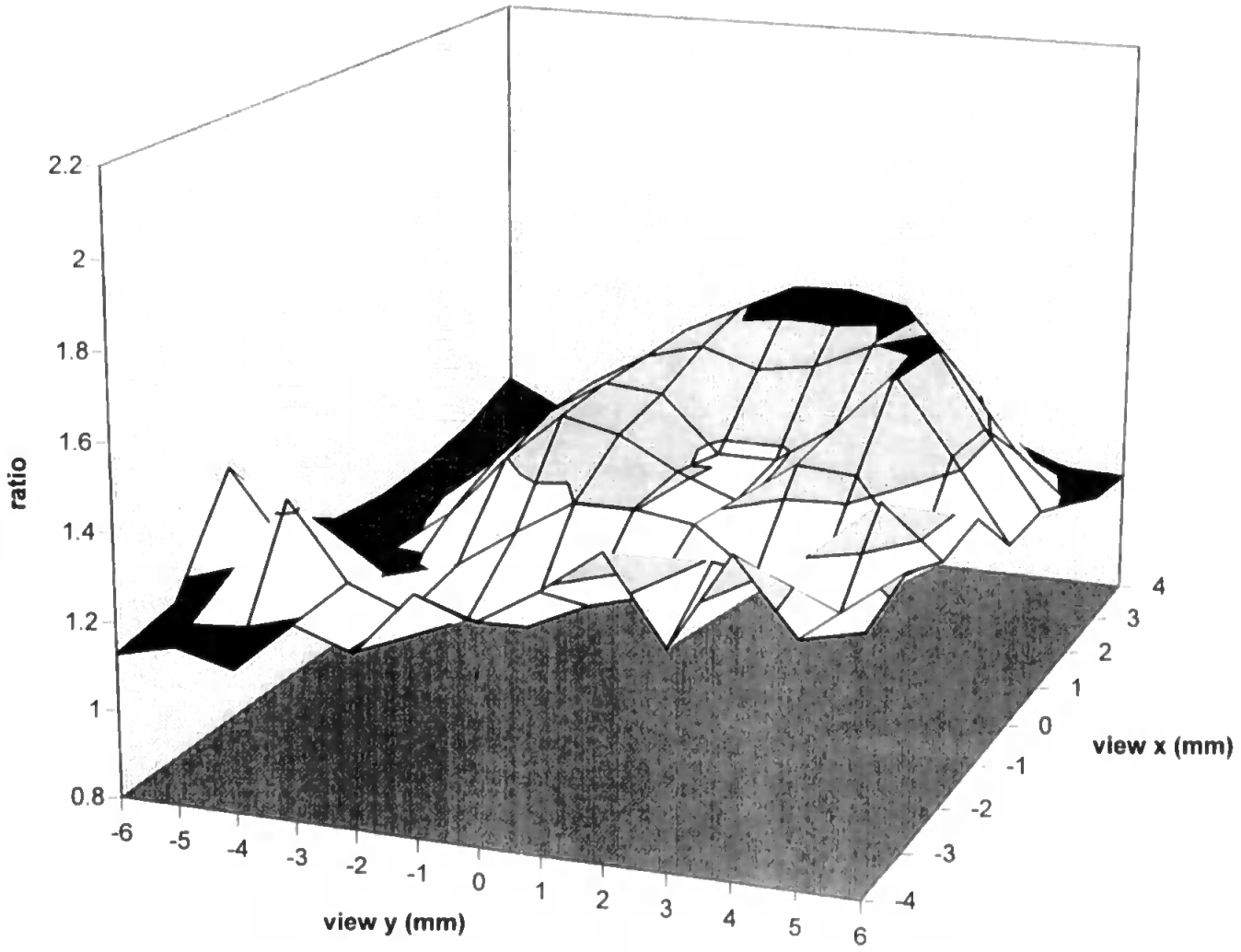

Figure 4.4c - Ratio of atom line emission (Mg solution + EIE / Mg solution only) for solutions containing 0.05 M K

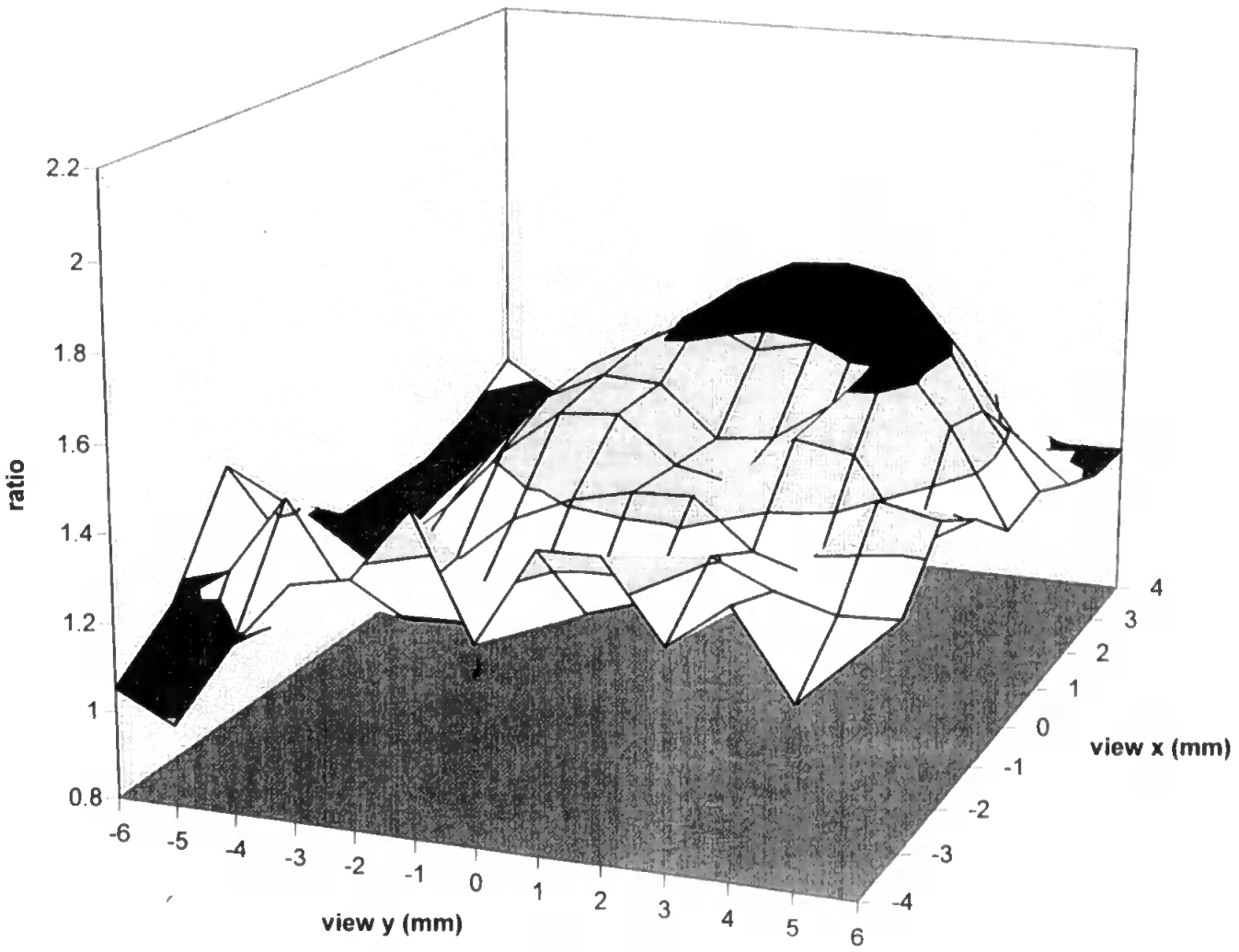

Figure 4.4d - Ratio of atom line emission (Mg solution + EIE / Mg solution only) for solutions containing 0.05 M Cs

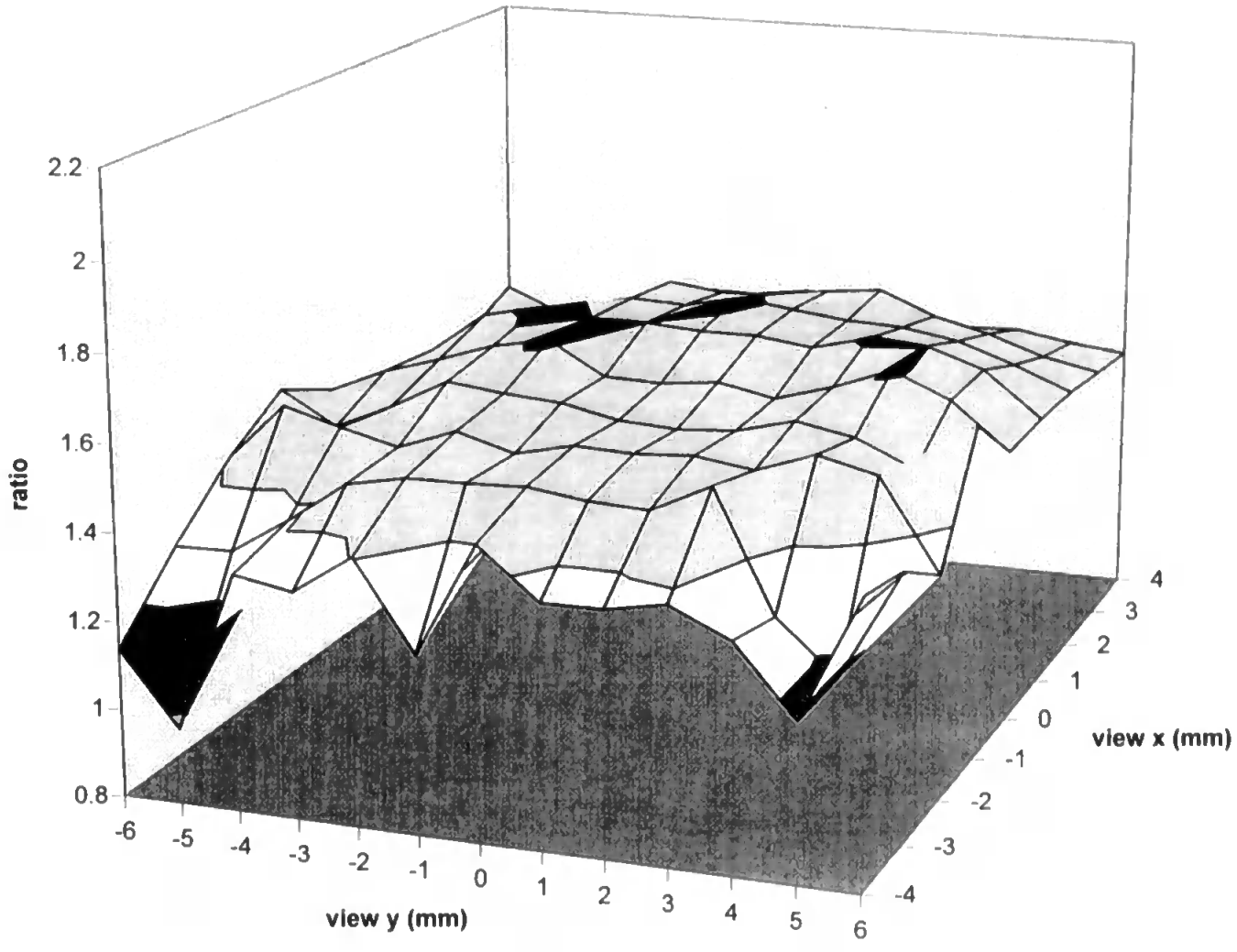

Figure 4.5a - Ratio of ion line emission (Mg solution + EIE / Mg solution only) for solutions containing 0.05 M Li

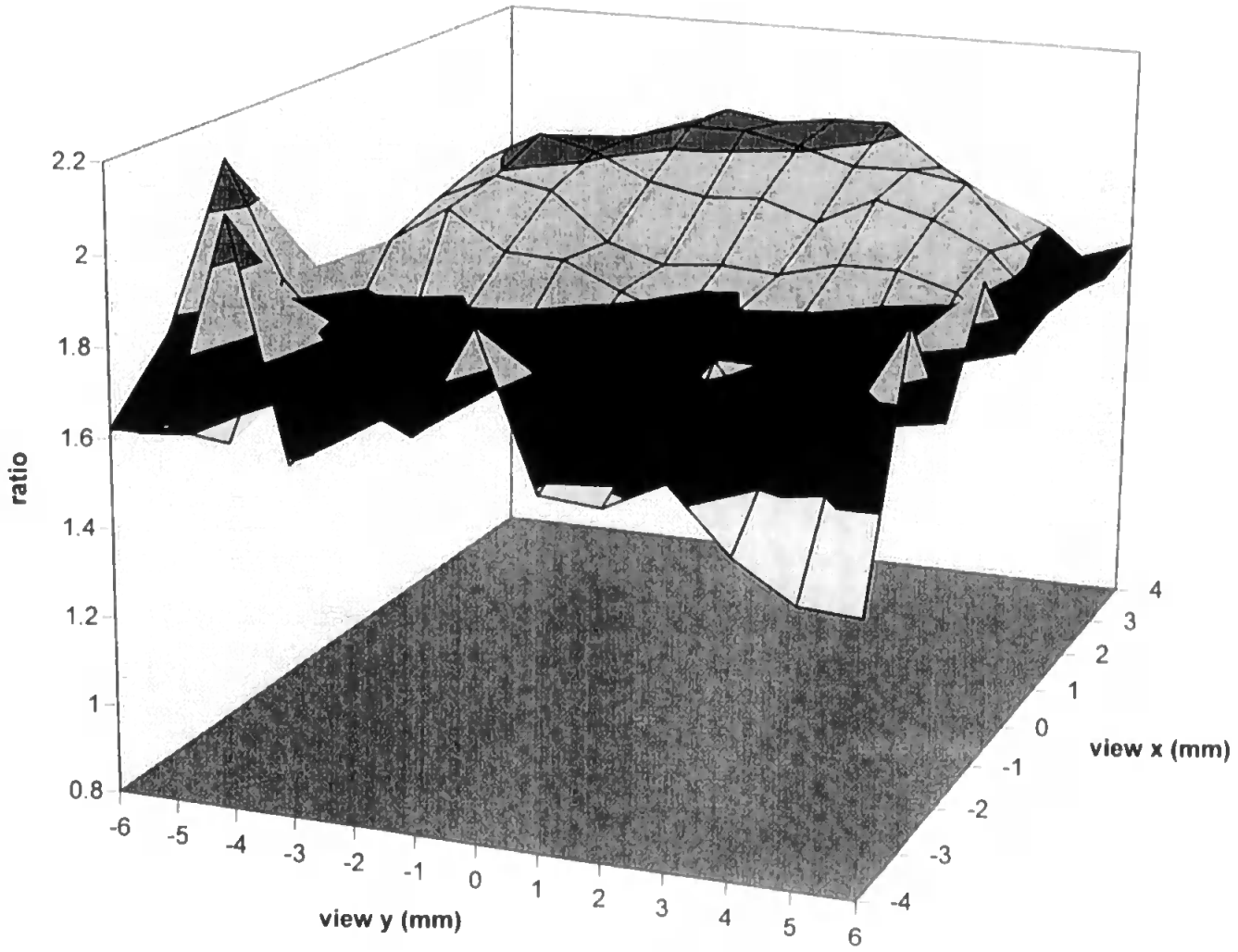

Figure 4.5b - Ratio of ion line emission (Mg solution + EIE / Mg solution only) for solutions containing 0.05 M Na

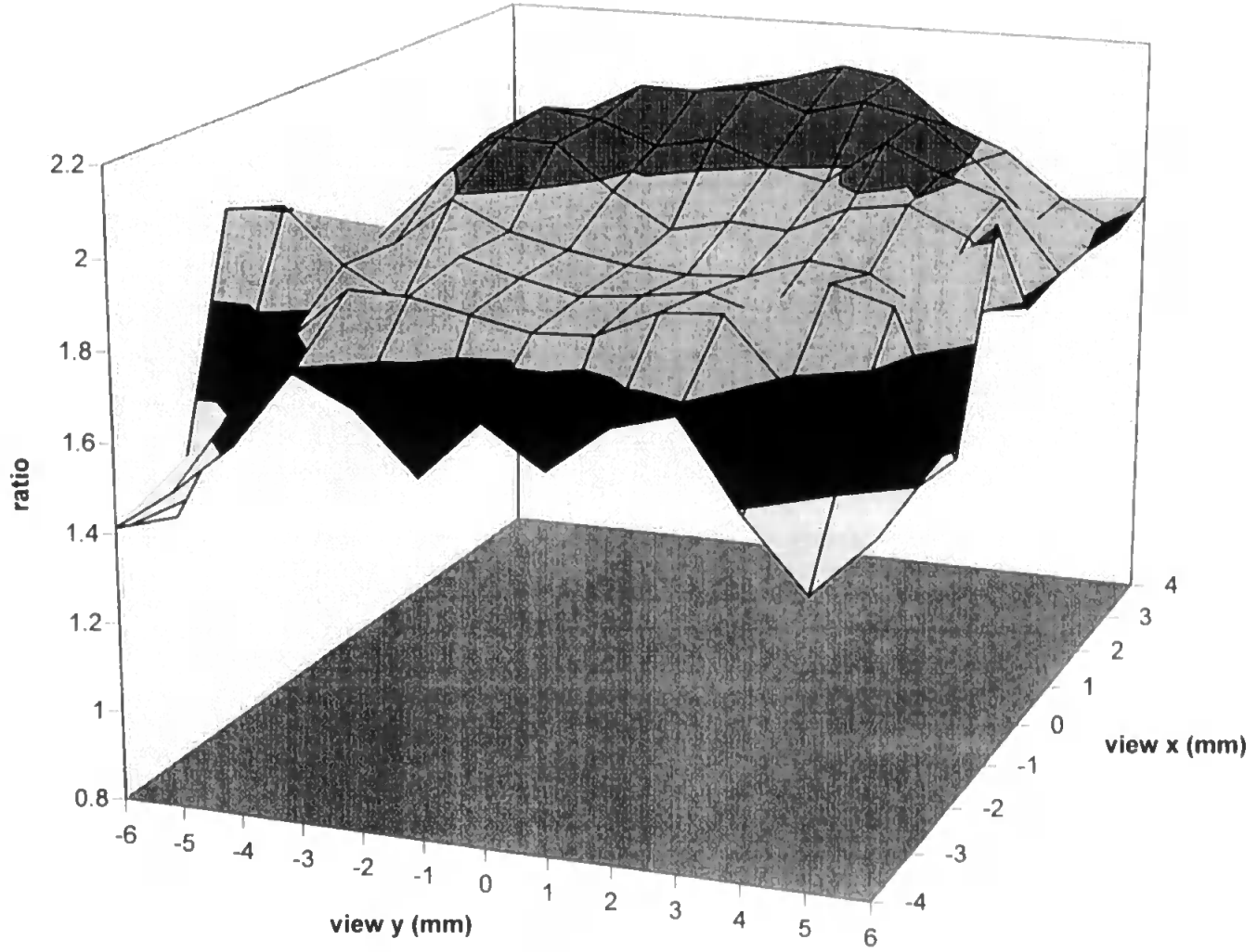

Figure 4.5c - Ratio of ion line emission (Mg solution + EIE / Mg solution only) for solutions containing 0.05 M K

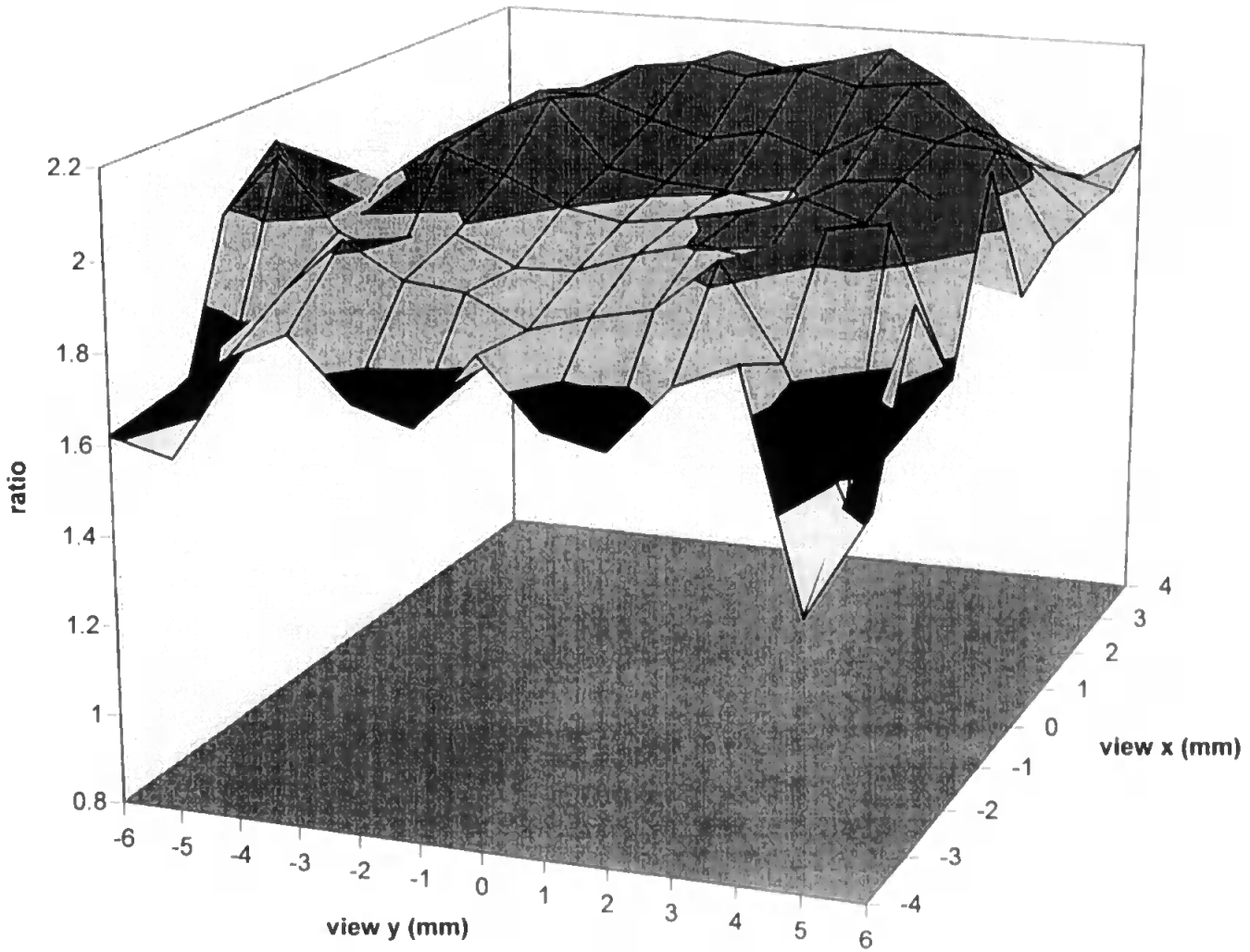

Figure 4.5d - Ratio of ion line emission (Mg solution + EIE / Mg solution only) for solutions containing 0.05 M Cs

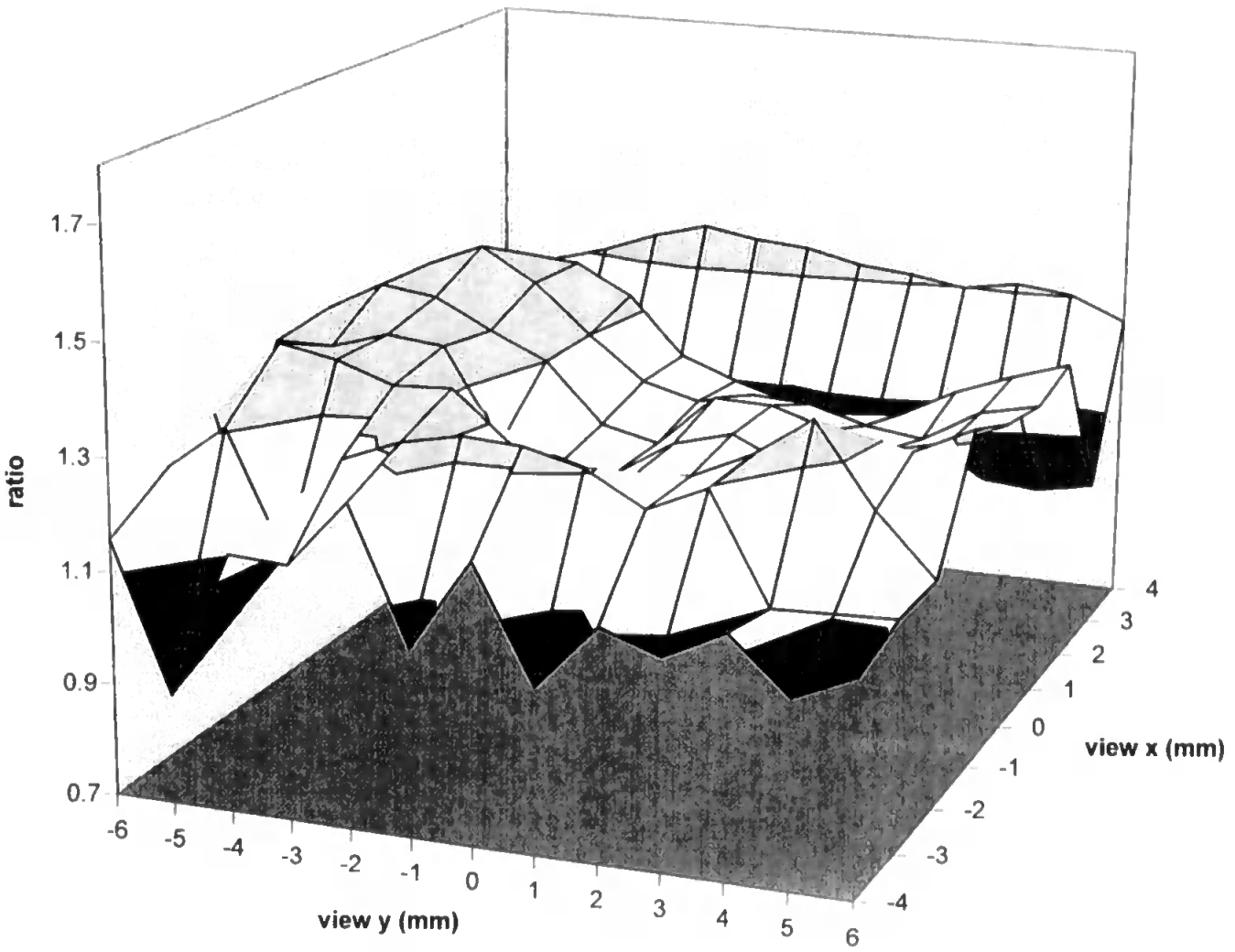

Figure 4.6a - Dslu values for a 10 µg ml-1 Mg slurry containing 0.05 M Li

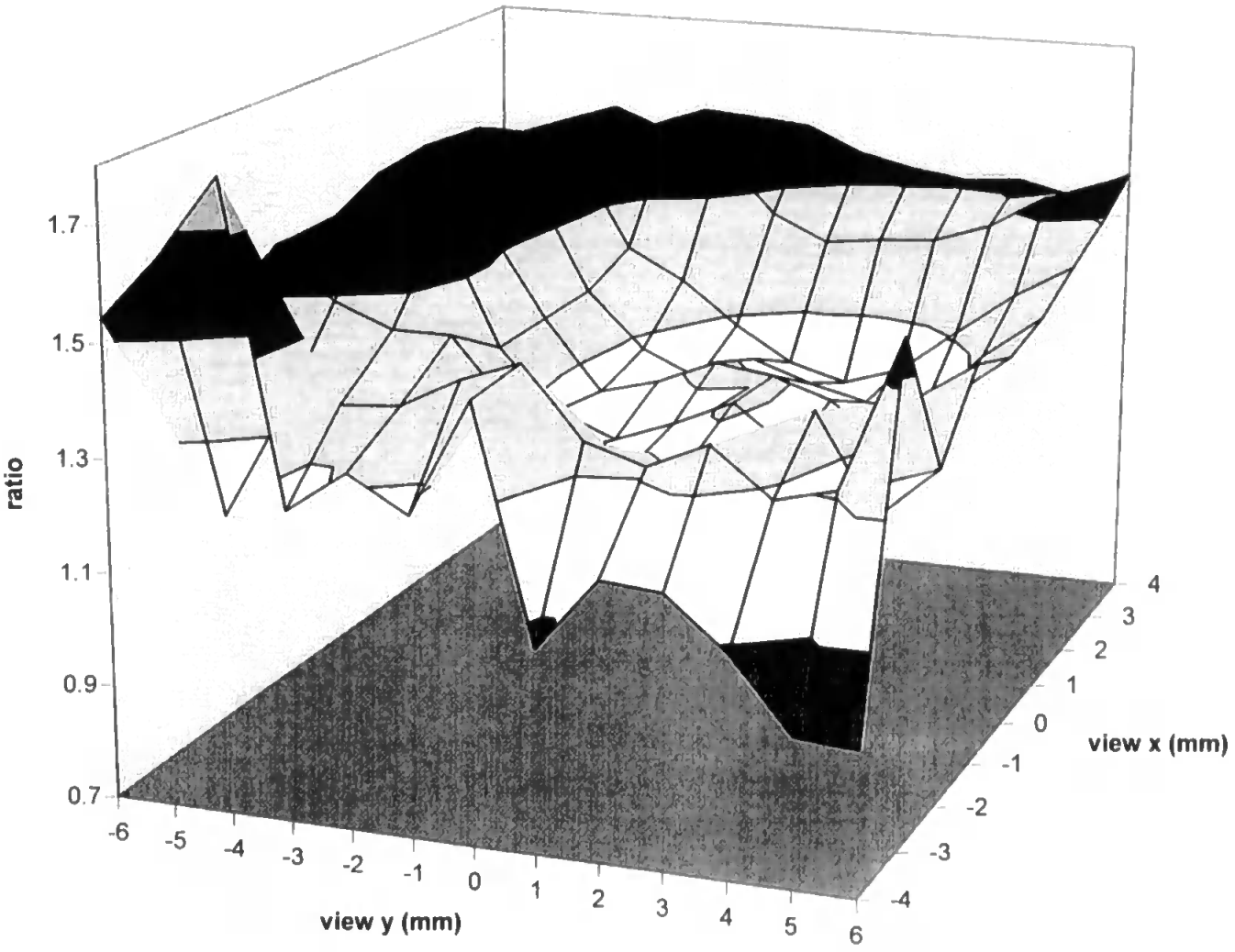

Figure 4.6b - Dslu values for a 10 µg ml-1 slurry containing 0.05 M Na

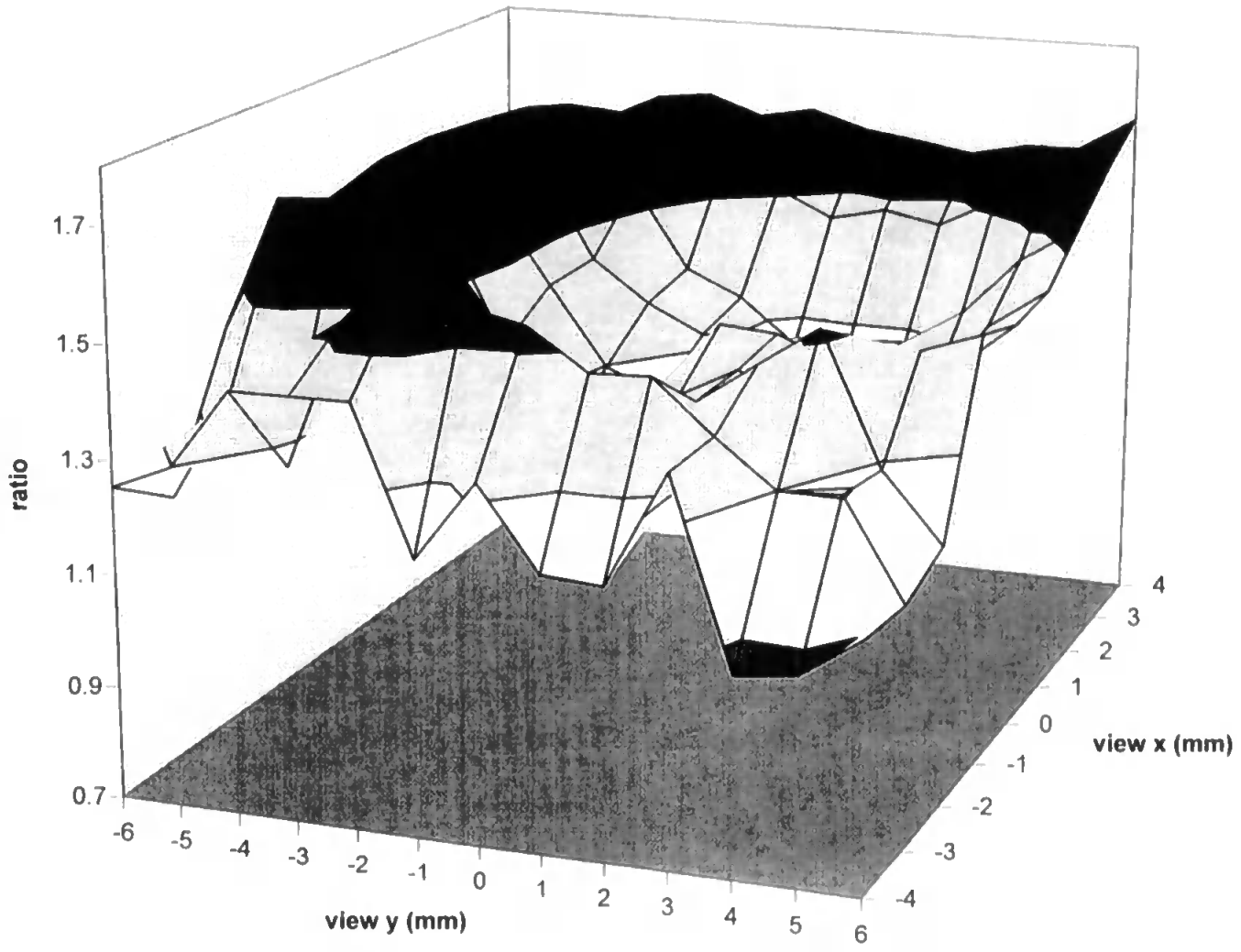

Figure 4.6c - Dslu values for a 10 µg ml-1 slurry containing 0.05 M K

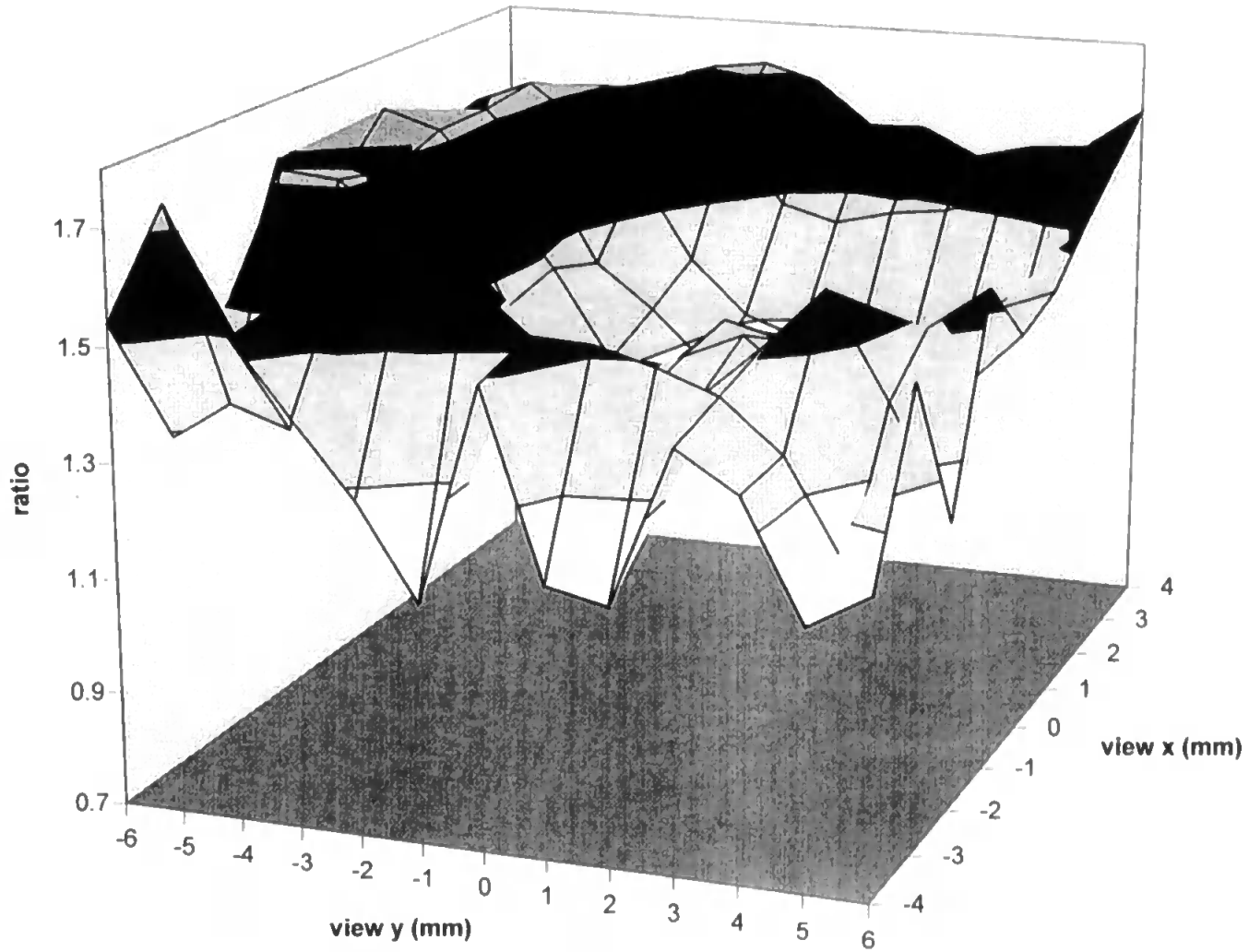

Figure 4.6d - Dslu values for a 10 µg ml-1 slurry containing 0.05 M Cs

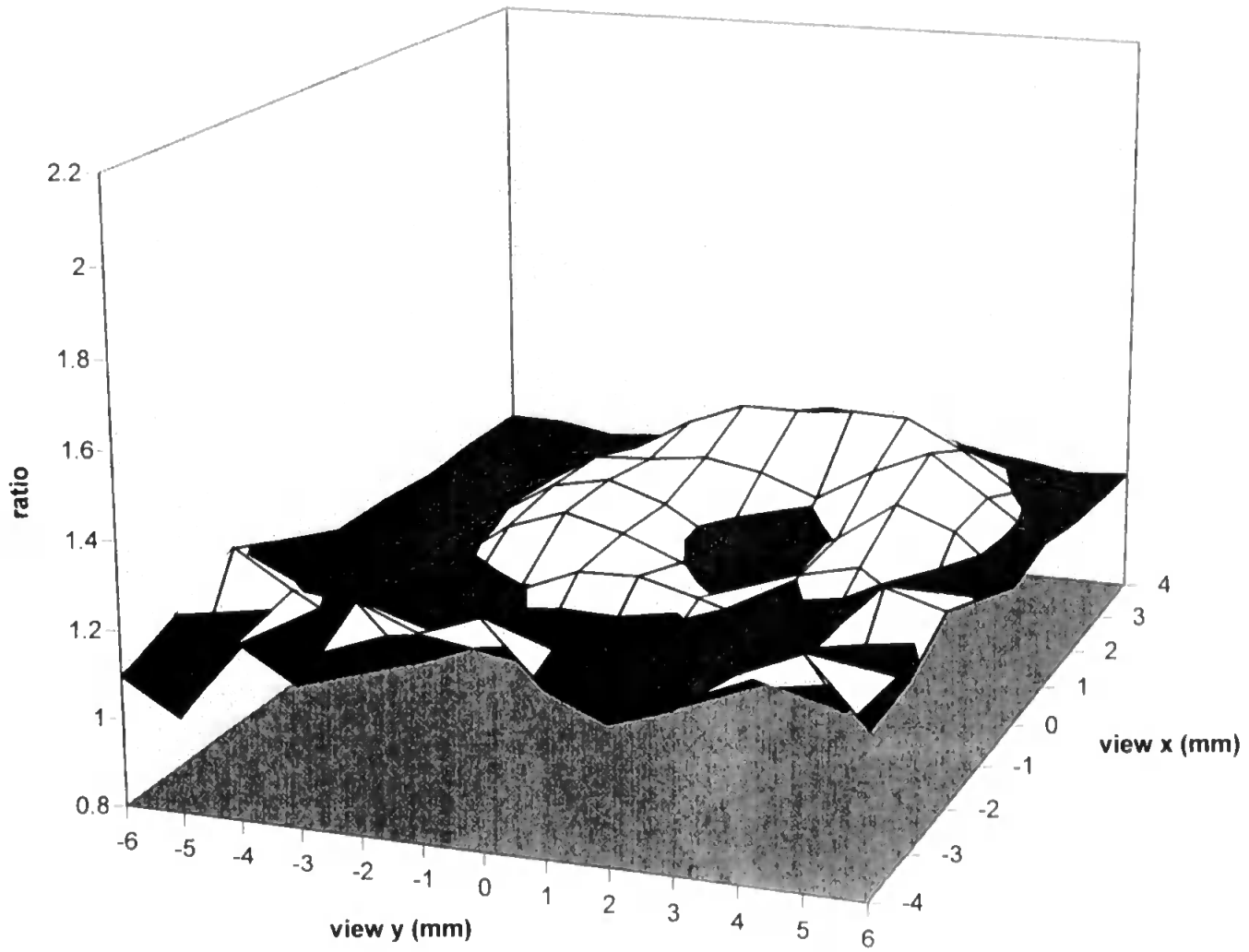

Figure 4.7a - Ratio of atom line emission (Mg slurry + EIE / Mg slurry only) for slurries containing 0.05 M Li

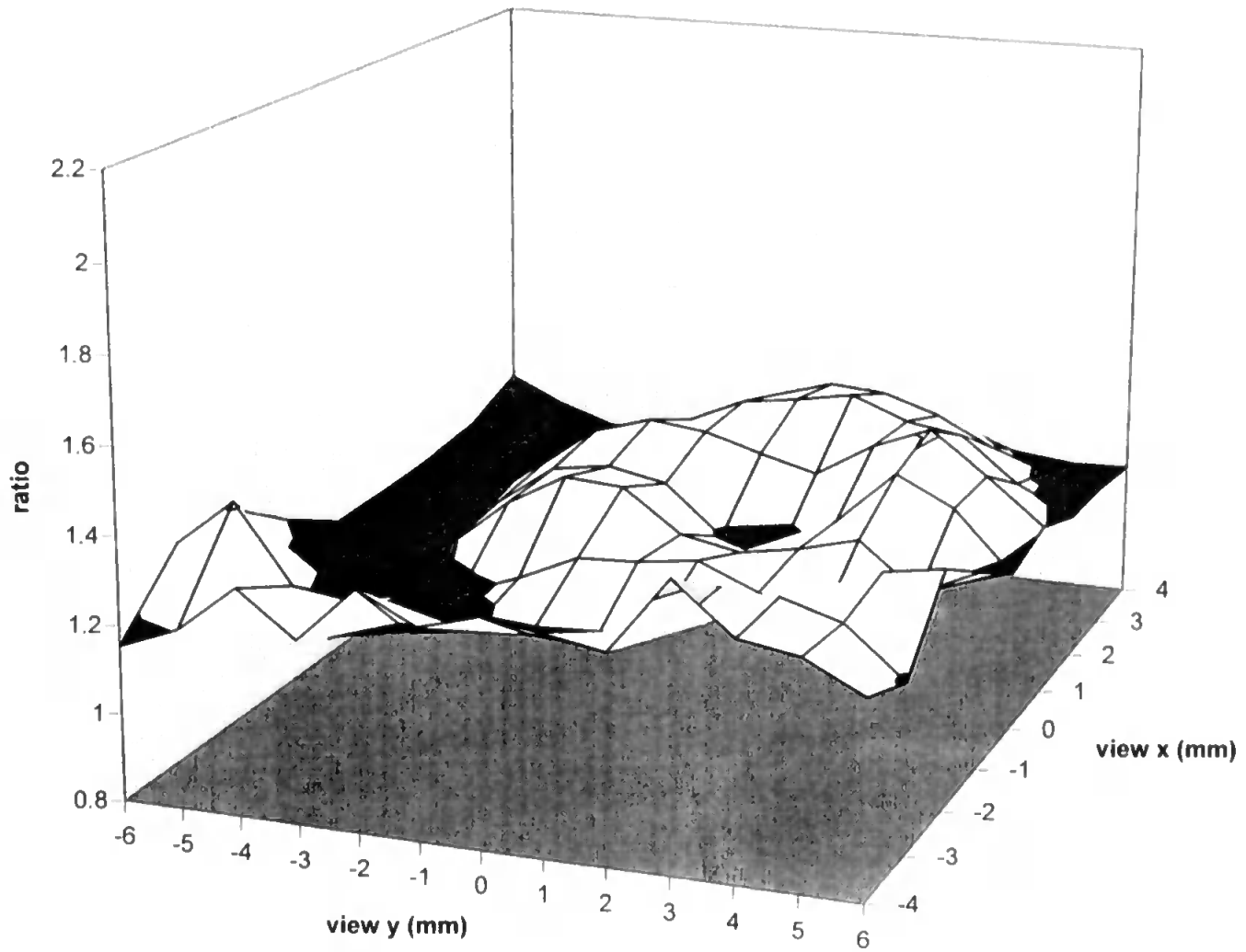

Figure 4.7b - Ratio of atom line emission (Mg slurry + EIE / Mg slurry only) for slurries containing 0.05 M Na

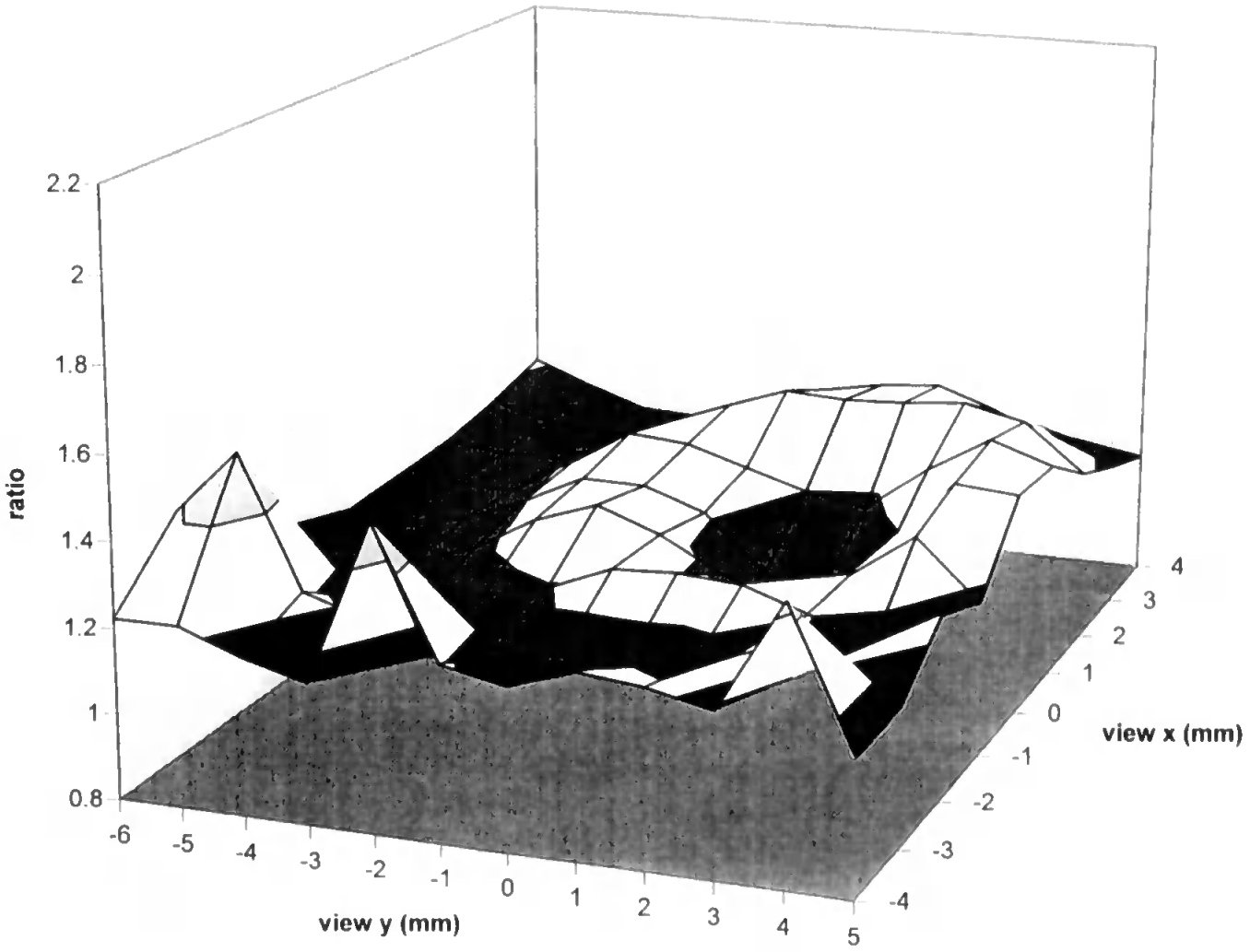

Figure 4.7c - Ratio of atom line emission (Mg slurry + EIE / Mg slurry only) for slurries containing 0.05 M K

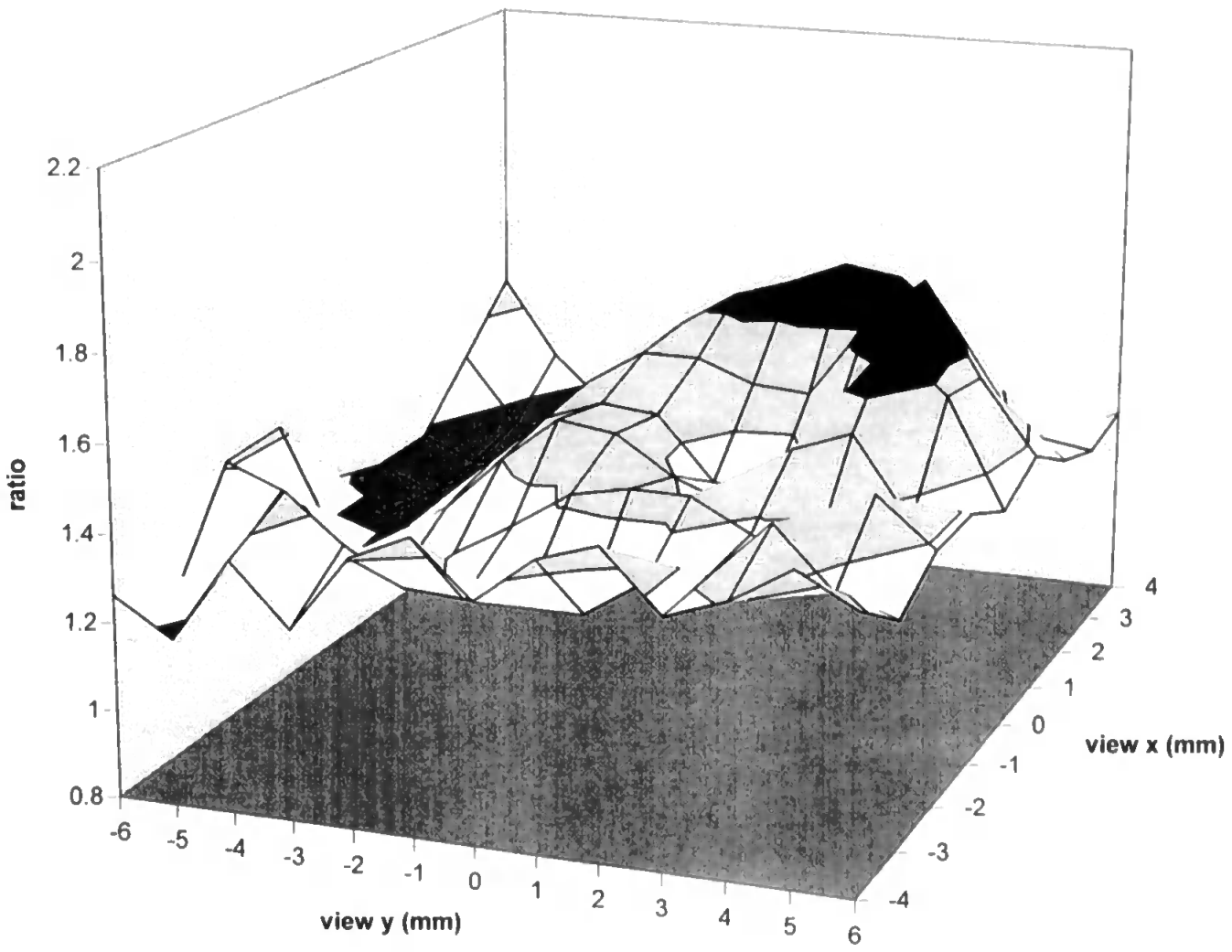

Figure 4.7d - Ratio of atom line emission (Mg slurry + EIE / Mg slurry only) for slurries containing 0.05 M Cs

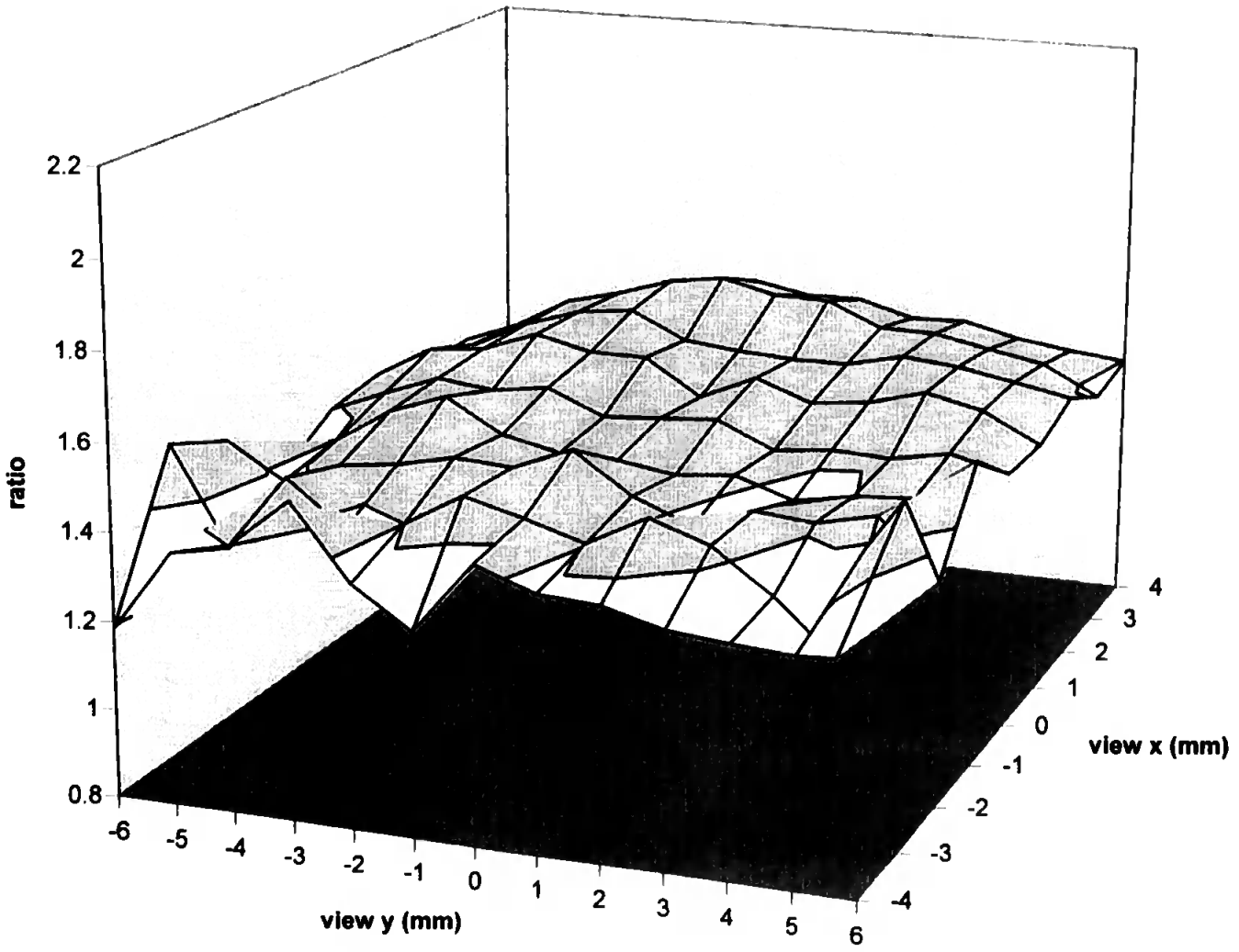

Figure 4.8a - Ratio of ion line emission (Mg slurry + EIE / Mg slurry only) for slurries containing 0.05 M Li

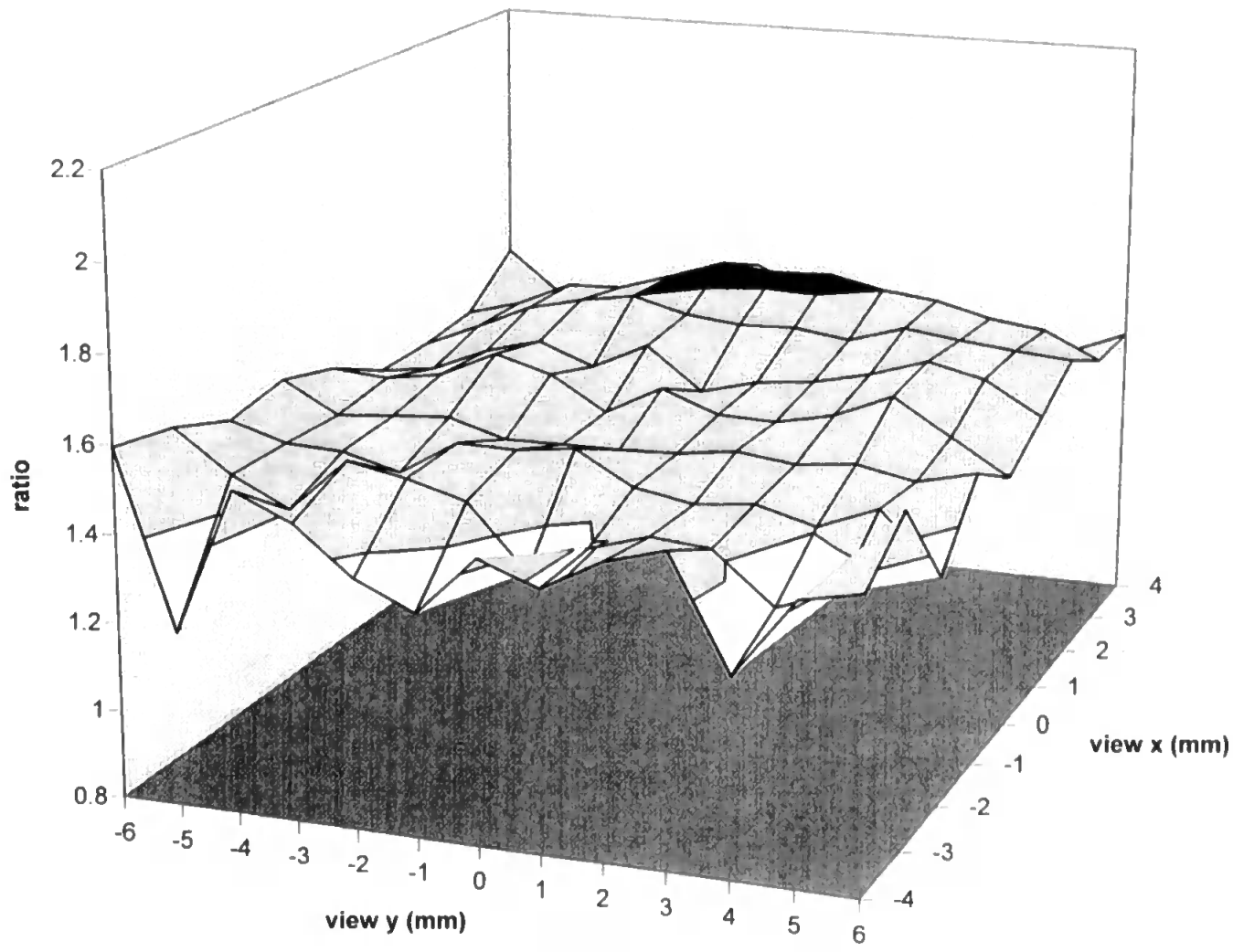

Figure 4.8b - Ratio of ion line emission (Mg slurry + EIE / Mg slurry only) for slurries containing 0.05 M Na

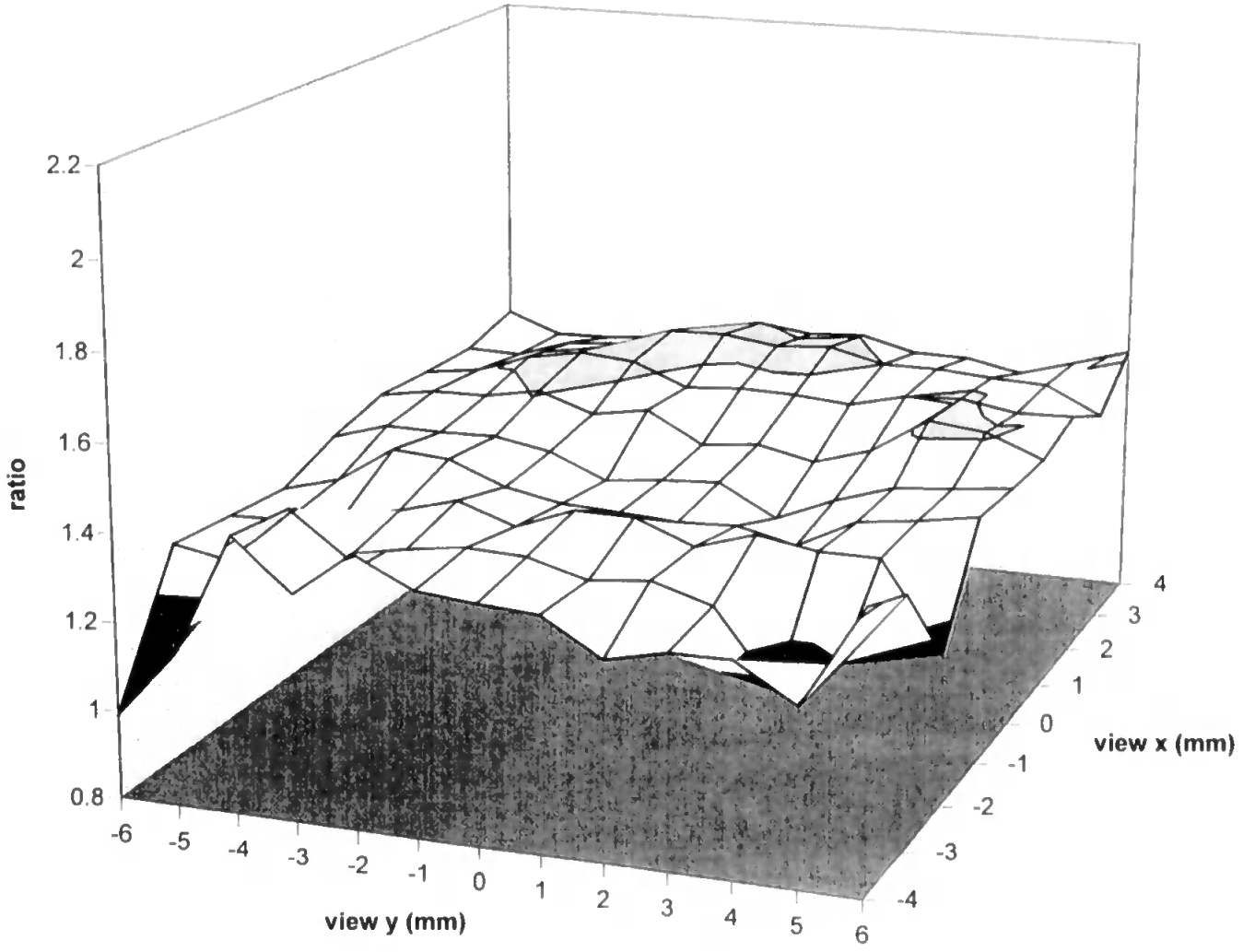

Figure 4.8c - Ratio of ion line emission (Mg slurry + EIE / Mg slurry only) for slurries containing 0.05 M K

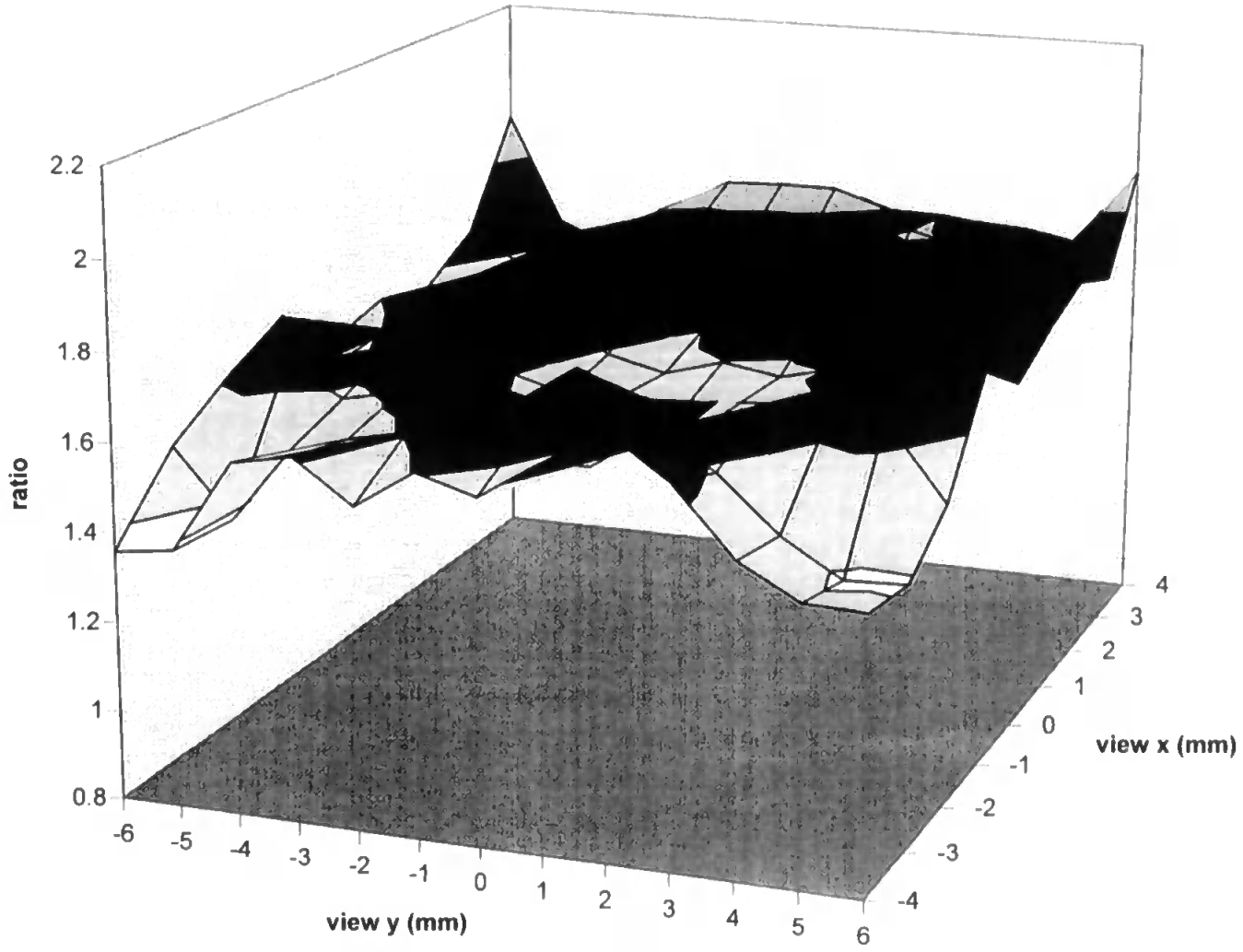

Figure 4.8d - Ratio of ion line emission (Mg slurry + EIE / Mg slurry only) for slurries containing 0.05 M Cs

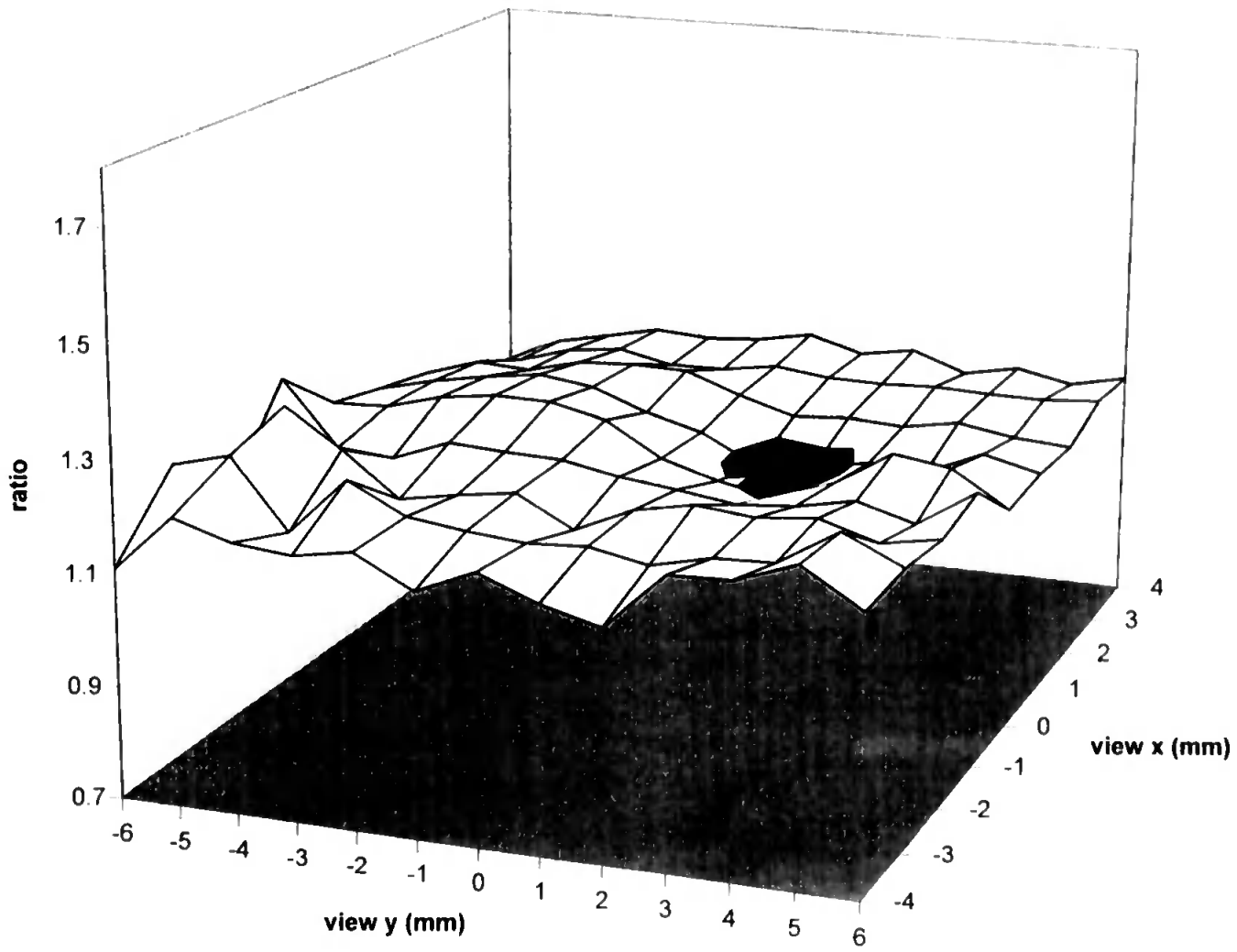

Figure 4.9a - DR values for Mg solutions and slurries containing no EIE

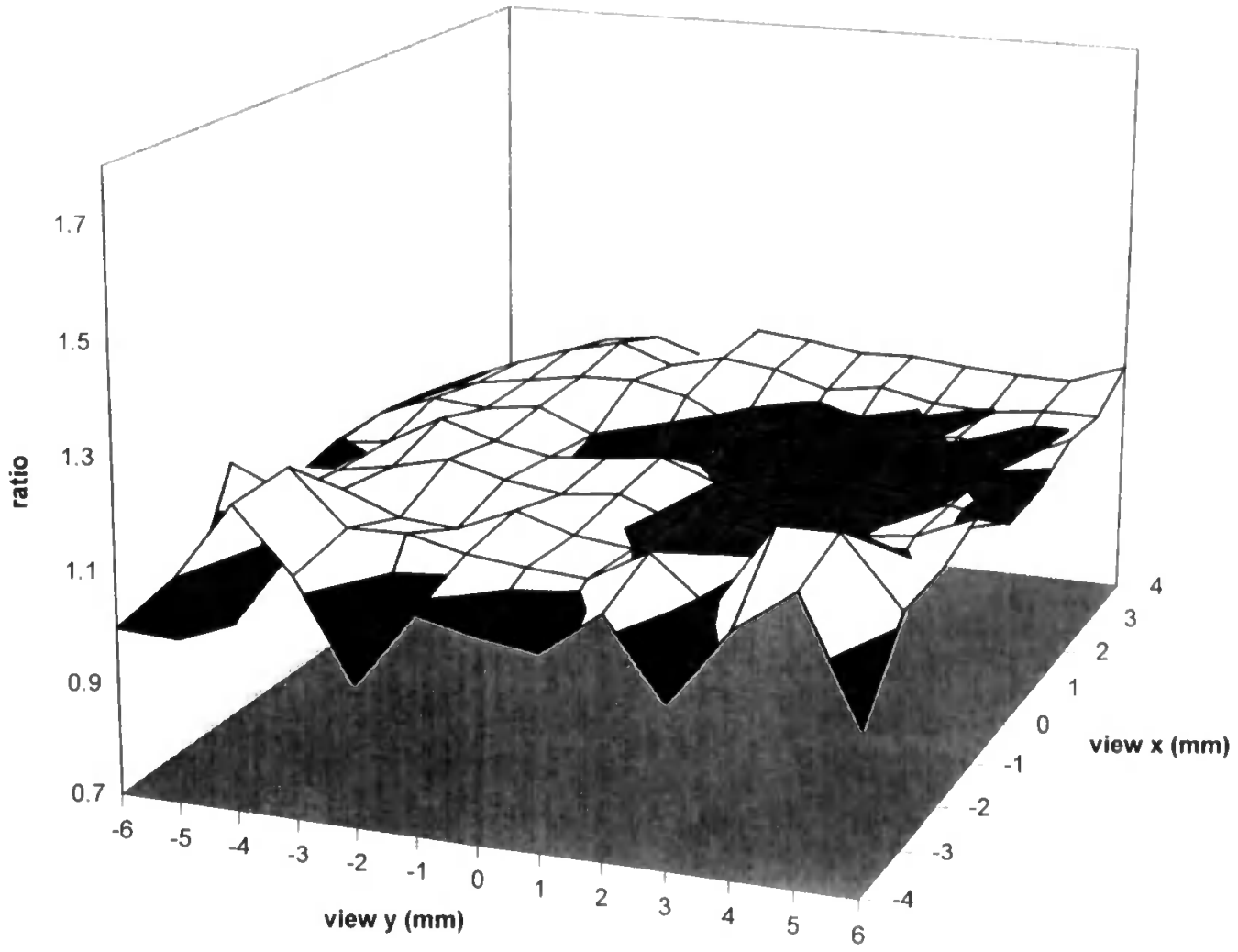

Figure 4.9b - DR values for Mg solutions and slurries containing 0.05 M Li

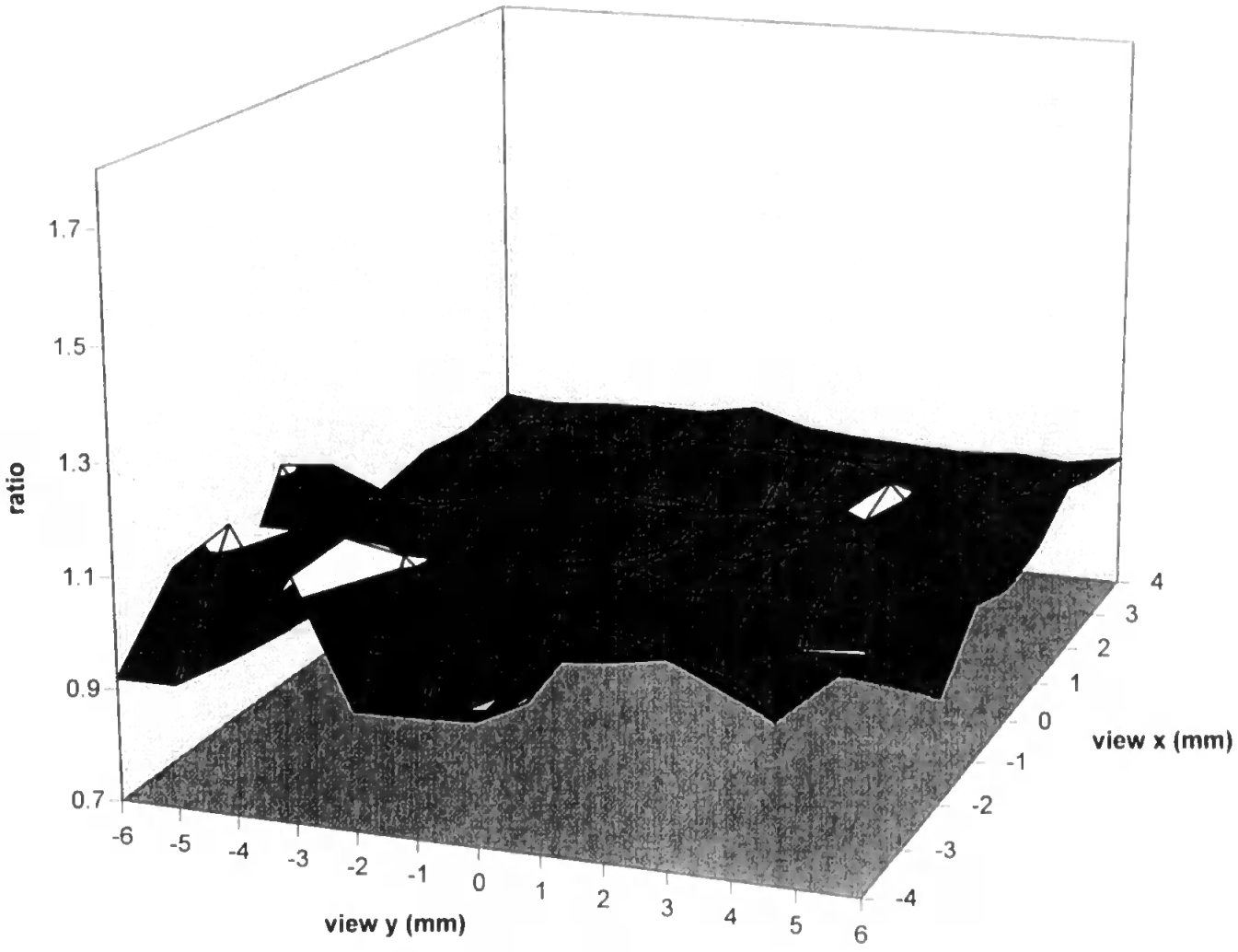

Figure 4.9c - DR values for Mg solutions and slurries containing 0.05 M Na

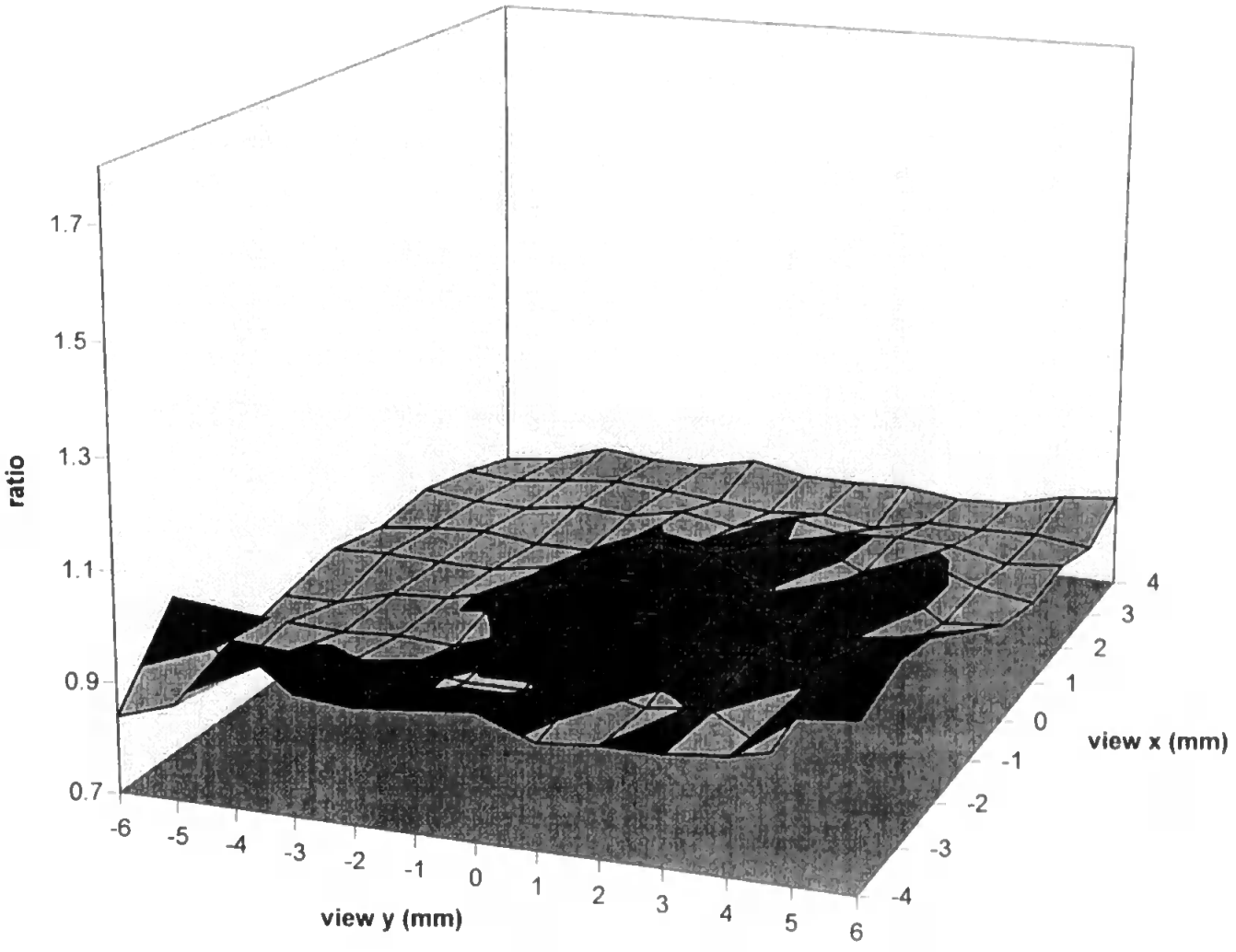

Figure 4.9d - DR values for Mg solutions and slurries containing 0.05 M K

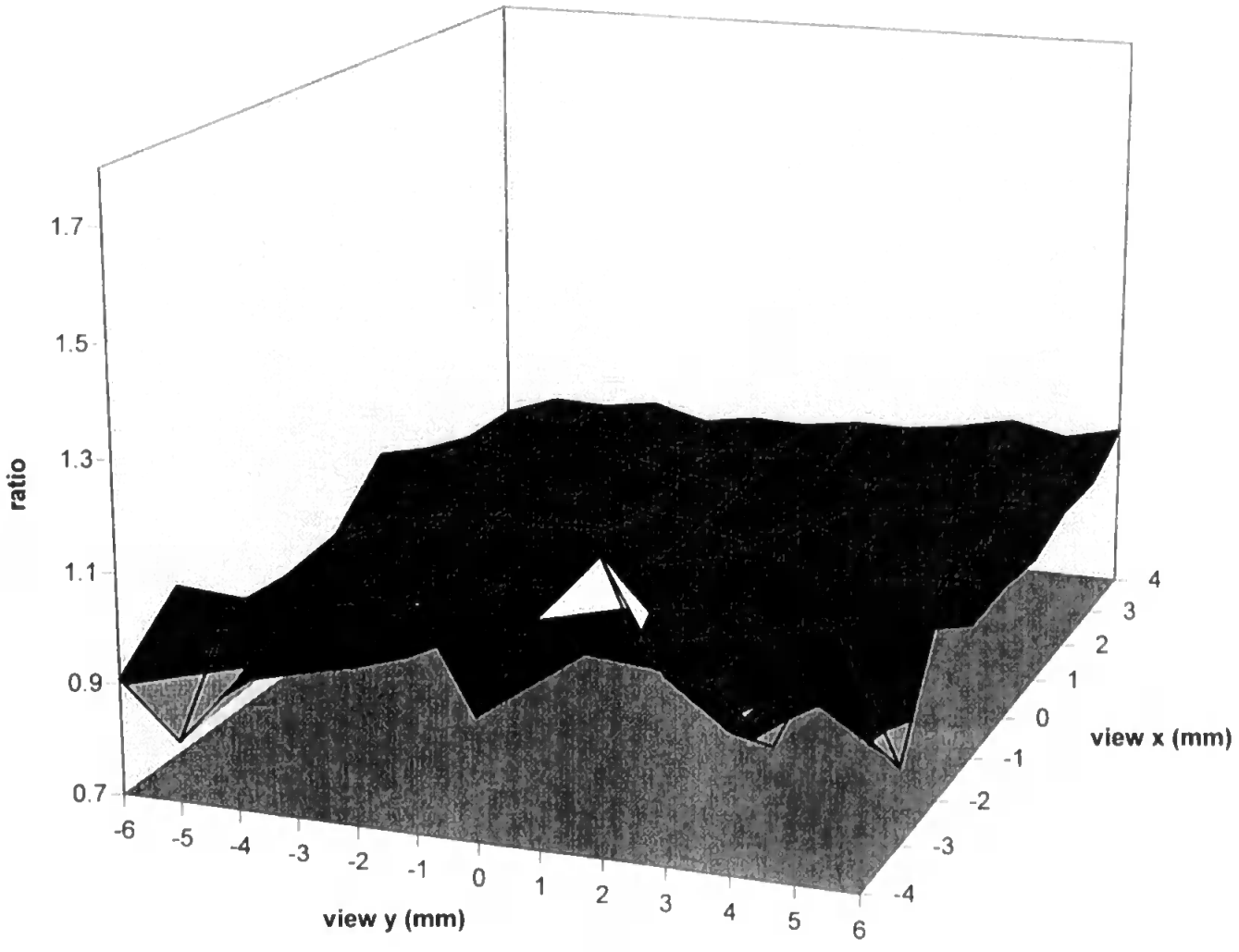

Figure 4.9e - DR values for Mg solutions and slurries containing 0.05 M Cs

solutions and slurries. Differences can therefore be described in terms of the 'flat' profile deviating from a D_R value of 1. The range of D_R values for each solution and slurry system are shown in Table 4.4. In the absence of an EIE D_R values up to 1.22 are seen. If the mechanisms and spatial dependence of energy transfer are the same for solution and slurry then one possible reason for the, as seen, flat deviation of the D_R value is atomisation efficiency. This would not be unexpected for a refractory oxide slurry containing particles up to 4 μm in diameter. The D_R value of 1.2 would suggest a relative atomisation efficiency of 80 to 85% and this is in accord with previous work (38).

In the presence of an EIE the D_R profiles still show a relatively flat cross section. However, the effect from adding EIEs in the order Li, Na, K, Cs, is to cause the flat D_R value to tend toward and finally reach 1.0. The magnitude of the difference between solution and slurry due to, for example, atomisation is greatly reduced.

4.5 General Discussion and Conclusions

Both solution and slurry intensity ratios show spatially dependent enhancement in the presence of EIEs. This effect is seen at the interface between the central channel of the carrier gas flow and the plasma main body. This implies that energy transfer processes which govern excitation in this annulus region are modified by EIEs, resulting in an increase in the excited atom population. While this would suggest that a further departure from LTE is produced by EIEs, this effect must not be considered in isolation. The ion intensity ratio change must also be taken into account in the presence of the same EIE of equivalent concentration. It is seen that this ratio is also increased but to a greater degree than the atom line ratios. The overall enhancement effect is that the ratios for both solutions and slurries show the following trend for a given EIE:

$$\frac{I_{i+EIE}}{I_i} > \frac{I_{a+EIE}}{I_a} \qquad (4.15)$$

SOLUTION/SLURRY SYSTEM	D_R VALUES
Mg only	1.15 - 1.22
Mg + 0.05 M Li	1.10 - 1.20
Mg + 0.05 M Na	1.00 - 1.10
Mg + 0.05 M K	0.90 - 0.97
Mg + 0.05 M Cs	0.90 - 1.00

Table 4.4 - The Effect Of The Addition Of An EIE On D_R Values

which does suggest that an increase in departure from LTE is produced by the addition of an EIE. Hence the intensity ratios from the Saha equation show this trend for both solutions and slurries:

$$\left(\frac{I_i}{I_a}\right)_{EIE} > \left(\frac{I_i}{I_a}\right) \qquad (4.16)$$

It is also noted from the Saha ratio profiles, D_{sol} and D_{slu}, that the energy transfer processes are also modified at the very centre of the analyte carrier channel. A scrutiny of the relative changes in the ion:ion and atom:atom intensity ratios, in the presence of an EIE, suggest that it is the 'ion' energy transfer processes that are implicated in this central channel 'island' enhancement.

While the energy transfer processes for solutions and slurries, with the addition of EIEs are very similar in their spatial dependence, the magnitude of the enhancement effects are different. Magnesium oxide is a high melting/boiling point refractory and the slurry produced from this solid contains a fraction of particles up to 4μm in diameter. Although simple aqueous transport effects are negated in the ratio method adopted, differences in the magnitude of enhancement for slurries may be attributed to relative particle atomisation efficiency. In the absence of an EIE the ratio method implies an atomisation efficiency of 80 to 85%. However in the presence of an EIE this efficiency, relative to a solution that is matrix matched, is increased in the order Li<Na≤K<Cs. D_R values suggest that from Na to Cs slurry atomisation efficiency approaches 100%.

Such a change in atomisation efficiency may be a 'real' atomisation effect i.e. that larger particles are broken down, or it may also be expressed in terms of subtle changes to the distribution of particles reaching the plasma. It has been shown that transport efficiency decreases with an increase in the matrix-matched loading for both solutions and slurries. If the particle loss processes within the sample introduction system are biased, the increased loading on going from 0.05 M Li to Cs may also reduce the larger solid particle fraction reaching the plasma. Therefore the smaller, easily atomised solid fraction

would increasingly contribute to the ratios measured. The overall effect would be to see an increase in the relative atomisation efficiency compared with the matrix matched solution. As EIEs may significantly modify the thermal conductivity of the plasma, any improvement seen for the slurries might be attributed to this effect.

Chapter 5 - The Effect of Easily Ionisable Elements on Solutions and Slurries in a Radially Viewed Inductively Coupled Plasma

5.1 The Effect of Easily Ionisable Elements on The Mass Transport Efficiency of Solutions and Slurries Used in Emission Spectrometry

5.1.1 Introduction

The effect of easily ionisable elements (EIEs) on the emission intensity of various analytes of interest from the ICP has been discussed in the literature (125-132,146-156). The addition of these EIEs has yielded both enhancement and depression of emission for various atom and ion lines and these effects have been shown to be dependent on various parameters such as the plasma power, argon gas flows and the spatial position of the point of observation in the ICP. The emission intensity of atom lines is known to be affected by EIEs low in the plasma in the initial radiation zone (126) while for ion lines these effects from EIEs are more marked higher up in the plasma in the normal analytical zone. This spatial dependence is also apparent when the plasma is viewed in a horizontal direction, with workers reporting off-axis enhancement for certain elements with EIEs added (125). In addition, 'cross over' effects have been observed for spatial profiles acquired in the vertical plane where peak emission intensity is shifted lower in the plasma for atom lines on addition of EIEs (129).

To date, however, these effects have purely been rationalised in terms of changes in atomisation and excitation phenomena and little work has been carried out to investigate the effect on sample transport efficiency through the sample introduction system that may arise when an EIE is added to the sample matrix (155). Skogerboe and Olsen (155) investigated aerosol transport effects for solutions in a MIP system when Na was added to a Pb analyte and a desolvation chamber was used in the sample introduction system. The amount of Pb reaching the plasma when Na was added to the matrix was found to be less than that for the aspiration of a solution with no EIE added. However, when no desolvation chamber was used, the mass

transport of the Pb solution was not dependent on the concentration of the Na matrix.

Depression effects observed for analyte emission upon addition of, for example, Cs may not be a 'true' depression of emission and, in fact, may be an enhancement effect that is overshadowed by the decrease in transport efficiency that arises upon addition of an EIE. A decrease in transport efficiency ultimately results in less of the sample analyte reaching the plasma and hence the analytical signal is decreased. Transport effects for solutions and slurries have been studied in detail and models for efficient slurry nebulisation proposed (34,56).

This work aims to quantify and clarify the effect that EIEs have on the transport efficiency and illustrate that the addition of a matrix element may significantly alter the transportation behaviour of an analyte in the sample introduction system of an ICP spectrometer.

5.1.2 Experimental

5.1.2.1 Apparatus

Solution and slurry mass transport efficiencies were measured using the apparatus shown in Figure 5.1.

A solution or slurry of known concentration was presented to the sample introduction system via a peristaltic pump at a liquid flow rate of 1 ml min^{-1}. The sample was nebulised using an Ebdon 'v-groove' nebuliser (P.S. Analytical, Sevenoaks, Kent, UK), at a carrier gas flow rate of 1 L min^{-1} , into a Perkin-Elmer 'Ryton' double pass spray chamber (Perkin-Elmer Ltd., Beaconsfield, UK). The aerosol sample then passed into a 2.0 mm i.d. bore alumina injector (part of the quartz demountable torch, Perkin-Elmer Ltd.) and was collected, via a flexible tube, in a polypropylene vessel containing 50 ml of water. The tube was positioned just below the water surface to provide a suitable back pressure similar to that experienced by an argon aerosol flow

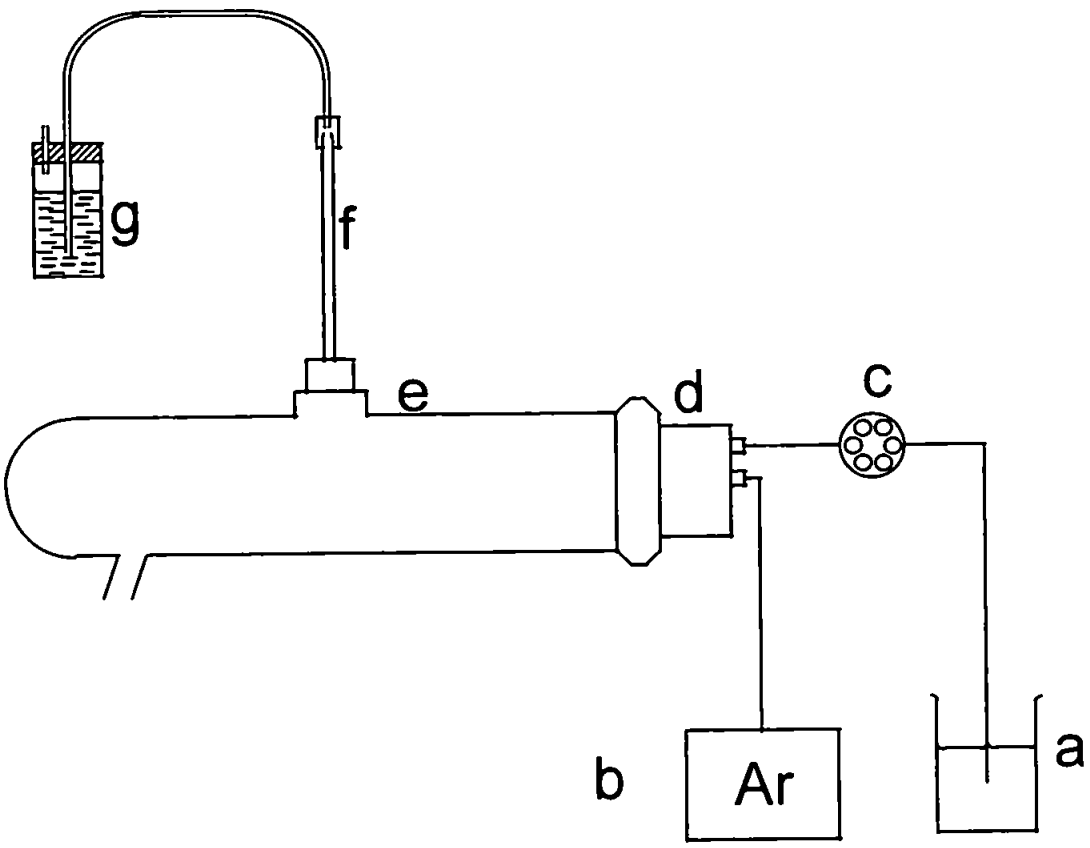

Figure 5.1- Schematic diagram of the sample introduction system used to measure the transport efficiency of solutions and slurries; a - sample presentation vessel (stirred for slurries), b - argon gas supply, c - peristaltic pump, d - Ebdon 'v-groove' nebuliser, e - Perkin-Elmer 'Ryton' Scott double pass spray chamber, f - alumina injector of 2.0 mm internal diameter, g - sample collection vessel.

punching the plasma. This back pressure is essential if the apparatus is to mimic the introduction of samples into an inductively coupled plasma.

A known amount of sample (250 ml) was introduced to the apparatus and the total amount was aspirated into the sample introduction system. The fraction of the sample exiting the alumina injector was quantified using titrimetric techniques to give measure of the transport efficiency of the sample for this particular sample introduction system.

5.1.2.2 Chemicals and Reagents

All reagents were of AnalaR reagent grade, unless otherwise stated.

5.1.2.3 Solution and Slurry Preparation

Solutions of $MnSO_4.2H_2O$ (1000 μg ml^{-1}, Mn^{2+}) were prepared by diluting the sample in doubly deionised water (MilliQ, Millipore, Harrow, Middlesex, UK). Slurries of MnO_2 (1000 μg ml^{-1}, as Mn) were prepared using the 'bottle and bead' method (30). Triton X-100 (0.5 % v/v), a non-ionic dispersant was used together with stirring in order to maintain stable and homogenous slurries for introduction to the apparatus.. The particle size distribution of the slurries was examined using a Coulter Counter (Coulter Electronics, Luton, Bedfordshire, UK) and by optical microscopy immediately prior to aspiration of the slurry. Equivalent concentrations of Triton X-100 were added to all solutions to achieve matrix matching.

The easily ionisable elements Li, Na, K and Cs (0.05 M, as their chloride salts) were added to all solutions and slurries in equimolar quantities.

5.1.2.4 Calculation of Solution Mass Transport

The concentration of Mn collected after exiting from the injector was evaluated by direct EDTA titration (157) using Eriochrome Black T as an

indicator. Hydroxylammonium chloride (0.25 g) was added to the solution to prevent oxidation and neutralised with dilute sodium hydroxide solution. Triethanolamine (3 cm^3) was added together with an ammonium nitrate buffer solution and several drops of Eriochrome Black T indicator. The subsequent mixture was warmed to 40°C and titrated using standardised EDTA solution, observing a red to blue change in colour. Manganese sulphate reacts with EDTA in a 1:1 reaction and thus the concentration of $MnSO_4$ can be calculated.

The mass transport efficiency of the solution, expressed as a fraction, may be calculated by dividing the mass of Mn^{2+} collected after the injector by the total mass aspirated into the sample introduction system (S.I.S.). To express this as a percentage, the equation takes the form:

$$\text{Mass Transport Efficiency} = \frac{\text{Mass of } Mn^{2+} \text{ collected after the injector}}{\text{Total mass of } Mn^{2+} \text{ aspirated into the S.I.S.}} \times 100\% \quad (5.1)$$

5.1.2.5 Calculation of Slurry Mass Transport

Before the amount of collected slurry could be analysed using a titrimetric technique, it was necessary to dissolve the MnO_2 particles. This was achieved using a method normally practised in the determination of manganese dioxide in pyrolusite (157) where the compound is treated with an excess of an acidified solution of a reducing agent. In this case sodium oxalate (0.1 M, 25 cm^3) was used with sulphuric acid (25 cm^3, 2 M) and the excess oxalate determined by titration with standard 0.1 M potassium permanganate (157). By calculating the amount of sodium oxalate oxidised in the dissolution reaction, the mass of MnO_2 can be evaluated.

The mass transport efficiency of the slurry, expressed as a fraction, was simply calculated by dividing the amount of MnO_2 collected after the injector

by the total amount of MnO_2 aspirated into the S.I.S. Again, in percentage terms this is expressed as:

$$\text{Mass Transport Efficiency} = \frac{\text{Mass } MnO_2 \text{ collected after the injector}}{\text{Total mass } MnO_2 \text{ aspirated into S.I.S.}} \times 100\ \% \quad (5.2)$$

5.1.3 Results And Discussion

The calculated mass transport efficiencies for the solutions and slurries with and without EIEs are given in Table 5.1.

It can be seen from Table 5.1 that the addition of an easily ionisable element results in a decrease in the mass transport efficiency for both solutions (1.33 - 0.60 %) and slurries (0.95 - 0.33 %). It can also be concluded that the transport efficiency of this particular slurry is measurably less than that of a solution of equivalent concentration. The addition of an EIE to a slurry results in a greater reduction of the mass transport efficiency compared with a solution of equivalent matrix loading.

The magnitude of the decrease in each case is dependent upon the total mass of the EIE matrix added to solutions and slurries. The higher molecular mass of the Cs salt (2.09 g/250 ml) results in a greater decrease in transport efficiency compared to the Li salt (0.53 g/250 ml) when both EIEs are present in equimolar proportions (0.05 M).

The aerosol formation and loss processes which occur within the sample introduction system depend upon a number of different parameters (100,101); the viscosity, surface tension and density of solutions are just three, which can be modified by the presence of a soluble EIE matrix (34,56).

It has been proposed that for efficient slurry nebulization into the inductively coupled plasma, a single slurry particle of the correct size range should be contained within a single aerosol droplet (the SOD model). If the overall distributions of the solution and slurry droplets are equal or very close

EIE Under Study	Matrix Loading of EIE (g/250 ml)	Mass transport efficiency for solution (%)	% Solution + EIE / % Solution only	Mass transport efficiency for slurry (%)	% Slurry + EIE / % Slurry only
Mn only	0	1.33±0.13	1.00	0.95±0.14	1.00
Mn + 0.05 M Li	0.53	1.20±0.08	0.90	0.60±0.13	0.63
Mn + 0.05 M Na	0.73	1.10±0.08	0.83	0.52±0.11	0.55
Mn + 0.05 M K	0.93	0.80±0.07	0.60	0.45±0.11	0.47
Mn + 0.05 M Cs	2.09	0.60±0.10	0.45	0.33±0.06	0.35

Table 5.1 - Calculated transport efficiencies for Mn solutions and slurries

then aqueous standards may be used to calibrate in a spectrometric analysis (56). The easily ionisable element salt will be present in the aqueous aerosol droplet containing the slurry particle. The total mass of any droplet travelling through the S.I.S. will therefore depend upon the mass of the matrix element salt in solution. The transport efficiency will, in turn, change according to the change in mass such that the mass transport efficiency of a slurry with Cs added, as the matrix element, will be less than that of a slurry with Li added to the dispersant matrix.

The particle size distribution of the slurry is not significantly affected by the addition of an EIE, as shown in Figure 5.2. The particle size distribution for a Mn only slurry is compared to that of an equivalent slurry with 0.05 M Cs added. The mode of the particle size distribution is at 2.52 μm. It can be seen that there is a 'tailing' to the distribution. These larger slurry particles (i.e. > 3 to 4 μm) explain the difference in transport efficiency between solution and slurry samples. The larger particle size fraction is not desired if the slurry sample is to pass efficiently through the sample introduction system in accordance with proposed models (56). These larger particles will 'settle out' in the spray chamber and it should be noted that a particle size of 10 μm diameter will be approximately 1000 times the mass of a particle of 1 μm diameter. It is therefore apparent that the loss of these larger particles in the sample introduction system will significantly reduce the mass fraction of slurry particles, being collected above the torch injector.

In the past, the change in mass transport efficiency upon addition of EIEs to solutions and slurries has not been considered in depth. This effect needs to be taken into consideration if 'true' emission enhancement and depression effects, from EIEs, on analyte intensity are to be quantified using plasma emission spectrometry.

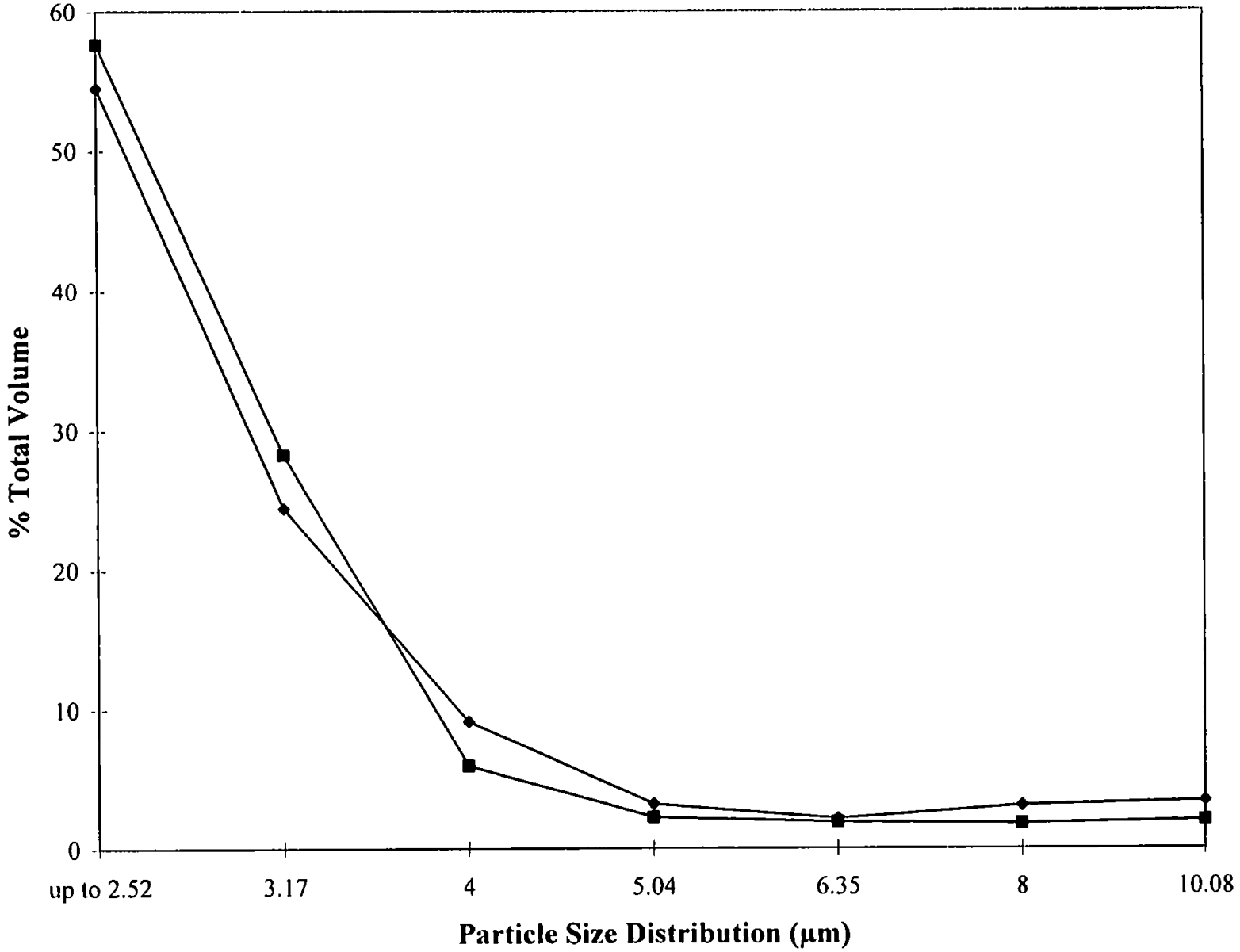

Figure 5.2 - Particle size distribution for MnO2 slurries. ◆ - MnO2 slurry with no EIE added, ■- MnO2 slurry with 0.05 M Cs added.

5.2 The Effect of Easily Ionisable Elements on The Emission Intensity of Solutions and Slurries

5.2.1 Introduction

It has been well established in the literature that the presence of certain elements in a sample matrix may considerably affect acquired spatial profiles and cause enhancement and/or depression effects (124-135). These elements are classified as easily ionisable elements (EIEs) and their behaviour in the inductively coupled plasma is not yet clearly understood.

Comparative studies between solutions and slurries in the ICP have shown that spatial characteristics for the two systems may be markedly different (38). Previous research has illustrated that under particular conditions, viewing height profiles for slurries, acquired using a radial or side on viewing mode, may be enhanced compared to the equivalent solutions low in the plasma in the area known as the Initial Radiation Zone (128).

Studies carried out and documented in Chapter 4 investigated the effect of EIEs on solutions and slurries in an axially viewed ICP. The effect was investigated upon Mg ion and atom line spatial profiles and certain inferences were made concerning energy transfer processes upon EIE addition to the sample matrix. A ratio method was introduced which eliminated the often forgotten transport effects caused by increased sample loading on the plasma when EIEs were added to the matrix.

In this study of the influence of EIEs upon solutions and slurries, Fe was chosen as the thermometric species of interest. Lines were selected that were free from spectral interferences and possessed transition probabilities with an acceptable degree of precision (167).

The lateral translation of a radially viewed ICP spectrometer with a solid state detector was used to acquire spatial information. In addition, lateral profiles were transformed using the Abel integral correction technique. Solutions and

slurries of Fe were aspirated into the plasma and the effect on emission intensity, due to the addition of EIEs to the sample matrices, was monitored. In order to explain observed phenomena, theoretical models have been proposed.

5.2.2 Theoretical Considerations

5.2.2.1 The Abel Inversion

An inductively coupled plasma is not an optically thin radiation source due to gradients of temperatures and emitting species from the central channel to the plasma body. The 'punched' plasma is a 'doughnut shaped' structure with circular symmetry and any lateral (side-on) measurements of the discharge will reflect this. Any emission intensity value obtained laterally will represent a value consisting of the sum of the emitting species through the plasma body at the point of observation. The Abel inversion is a mathematical integral technique used to obtain a corrected representation of the discharge. The technique has been described as a mathematical 'stripping' process (138) where the plasma is divided into sections equidistant along the radius of the discharge. The section at the outer edge of the discharge is subtracted from the next radial section to give a 'corrected' intensity value. These values are then fitted to a polynomial function and the first derivative integrated using equation 5.3 (138):

$$i(r) = -\frac{1}{\pi}\int_{r}^{R}\frac{dI(x)/dx}{\left(x^2 - r^2\right)^{1/2}}.dx \qquad (5.3)$$

where R is the radius of the plasma torch, I is the experimental intensity measured along a chord of distance x from the centre and r is the radial position along the radius R (138). The procedure used in this work and the program used is given in Appendix 1. The Abel inversion assumes circular symmetry and may be carried out for laterally viewed data measured by profiling the plasma in the horizontal plane.

5.2.2.2 Detector Efficiency Correction

The instrument used in this study employed an echelle grating which is used over many orders at a set blaze angle, where peak diffraction efficiency should occur. Any difference in optimum blaze angle with diffraction order of the wavelength in question will result in low optical throughput (114,169).

Echelle grating efficiency has been accounted for in this study so that emission line intensities could be adjusted for any influence arising from the set blaze angle. This is performed by calculating the blaze angle for the particular wavelength using equation 5.4:

$$\theta = \sin^{-1}\left(\frac{N\lambda}{2d\cos\phi}\right) \qquad (5.4)$$

where θ is the blaze angle, N is the grating order number, λ is the wavelength, d is the groove spacing and ϕ is the half angle in the horizontal plane between the incident and diffracted ray from the echelle grating. The blaze angle is then substituted into a polynomial expression to calculate the grating efficiency (108). In this way adjustments can be made when directly comparing two emission lines and the errors due to grating efficiency are minimised.

5.2.3 Experimental

5.2.3.1 Instrumentation

All spatial measurements of the inductively coupled plasma were carried out using a Perkin-Elmer Optima 3000 ICP spectrometer (The Perkin-Elmer Corp., Norwalk, CT., USA) with a radially orientated torch in the sample introduction system. The instrument is one of a series of spectrometers which employ solid-state detection and an echelle grating optical system, both of which are described in the literature (108,114).

Spatial profiles were obtained for consecutive lateral measurements in the horizontal plane. A computer controlled stepper motor was used to automatically adjust the position of a 2-axis mirror so that a discrete region in the plasma could be examined. All readings were automated by constructing a program within the instrument software. The instrumental operating parameters used in this series of experiments are listed in Table 5.2.

The traditional Optima 3000 demountable torch comprises a 4 mm viewing slot. A torch was designed with a 8 mm viewing slot so that a wider lateral profile could be measured and viewing through the quartz torch avoided. The wider slot was used with no observable affect upon plasma stability.

The instrument enables measurements to be carried out using either a high, medium or low resolution setting corresponding to three different slit widths. It is essential when making spatial observations that two consecutive viewing position zones do not overlap to avoid the contribution of emission from an adjacent position. The dimensions of the high resolution slit are 31 × 250 μm. Using this resolution setting it has been calculated that there is no overlap between lateral positions at the plasma image plane. In addition, the stepper motor which moves the first mirror of the transfer optics has a minimum stepping interval and is well matched to the image size in the lateral direction. The emission intensity of the Fe 385.991 nm and 382.043 nm atom lines were monitored. These lines were measured by accessing the U II 385.958 and Eu II 381.967 nm subarrays on the visible channel detector of the instrument and minor adjustments were made to ensure measurement of the correct wavelengths. Manual background correction points were used for all measurements.

5.2.3.2 Chemicals and Reagents

Reagents used in this work were of 'AnalaR' reagent grade (Merck, Poole, UK). Solutions were prepared using doubly deionised water.

RF Generator	
Frequency	40 MHz, free running
Forward Power	1100 W
Sample Introduction System	
Nebuliser	Ebdon v-groove high solids
Torch	Demountable, custom built with 8 mm wide observation slot and 2.0 mm i.d. alumina injector
Spray Chamber	Perkin-Elmer 'Ryton' Scott double -pass
Peristaltic Pump	Gilson Minipuls 3, computer controlled
Sample Flow Rate	1.0 ml min^{-1}
Argon Gas Flow Rate	
Plasma	14 L min^{-1}
Auxiliary	1.0 L min^{-1}
Nebuliser	0.8 L min^{-1}
Spectrometer	
Resolution	High resolution setting (31 × 250 µm)
Fe I wavelengths	382.043 nm 385.991 nm
Viewing Height	4 mm (ALC)

Table 5.2 - ICP operating parameters

5.2.3.3 Slurry and Solution Preparation

Slurries were prepared using the 'bottle and bead method' (30). A 10 000 µg ml^{-1} stock slurry was prepared by grinding Fe_2O_3 with 0.5 % Triton X-100 (non-ionic) dispersant to prevent coagulation and agglomeration of the particles. This dispersant was found to sustain stable slurries with mean particle size ranges of less than 1.5 µm in diameter. This is desirable if the analytical recovery of a slurry is to be comparable to that of an equivalent solution (56). The particle size of the slurry and true dispersion were verified using optical microscopy immediately prior to aspiration into the ICP.

$FeCl_2.4H_2O$ was used to prepare a stock 10 000 µg ml^{-1} Fe solution. Serial dilution of this solution was carried out to prepare 100 µg ml^{-1} solutions which were matrix matched for dispersant (0.5 % Triton X-100).

To all solutions and slurries, equimolar amounts (0.05 M) of EIEs were added. This procedure was identical to that described in Chapter 4.3.3 where the effect of easily ionisable elements was measured on Mg solutions and slurries. The EIEs added were Li, Na, K and Cs (as their respective nitrate salts.

5.2.4 Results and Discussion

5.2.4.1 The Effect of EIEs on the Emission Intensity of Solutions

Figure 5.3 shows the effect upon emission intensity of the Fe I 382.043 nm atom line when various equimolar amounts of EIEs are added to a 100 µg ml^{-1} Fe solution. The profile represents one half of the plasma as circular symmetry is assumed. The profiles were measured at a height of 4 mm above the load coil where the maximum atom emission intensity occurs (Figure 5.4). The Abel integral transformation was carried out for all profiles so that corrected radial comparisons could be made. It can be seen that the maximum emission intensity occurs at 0 mm in the central channel with emission intensity decreasing towards the edge of the plasma through the

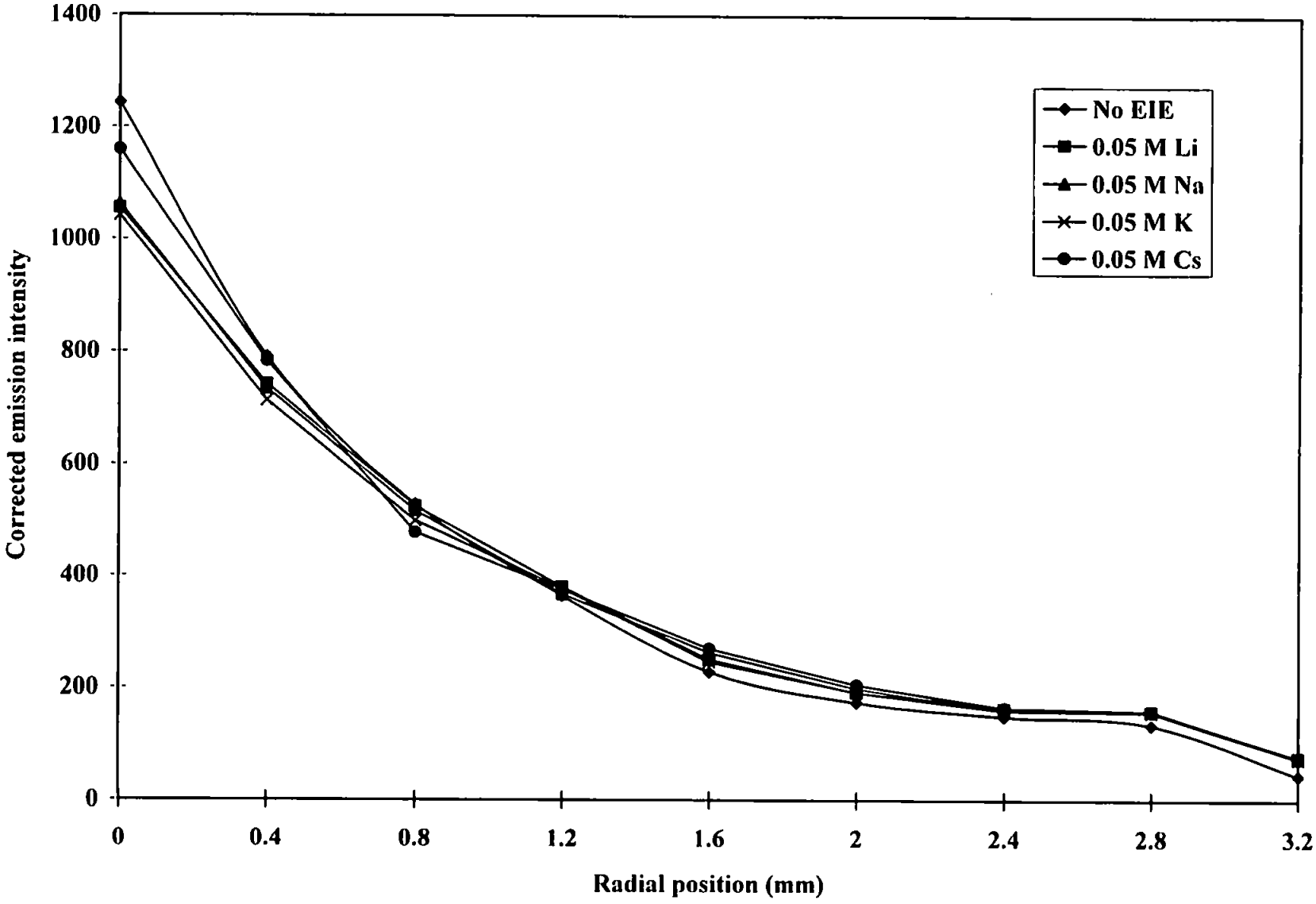

Figure 5.3 - Variation of emission intensity with radial position for a 100 µg ml-1 Fe solution measured at 382.043 nm with various EIEs added

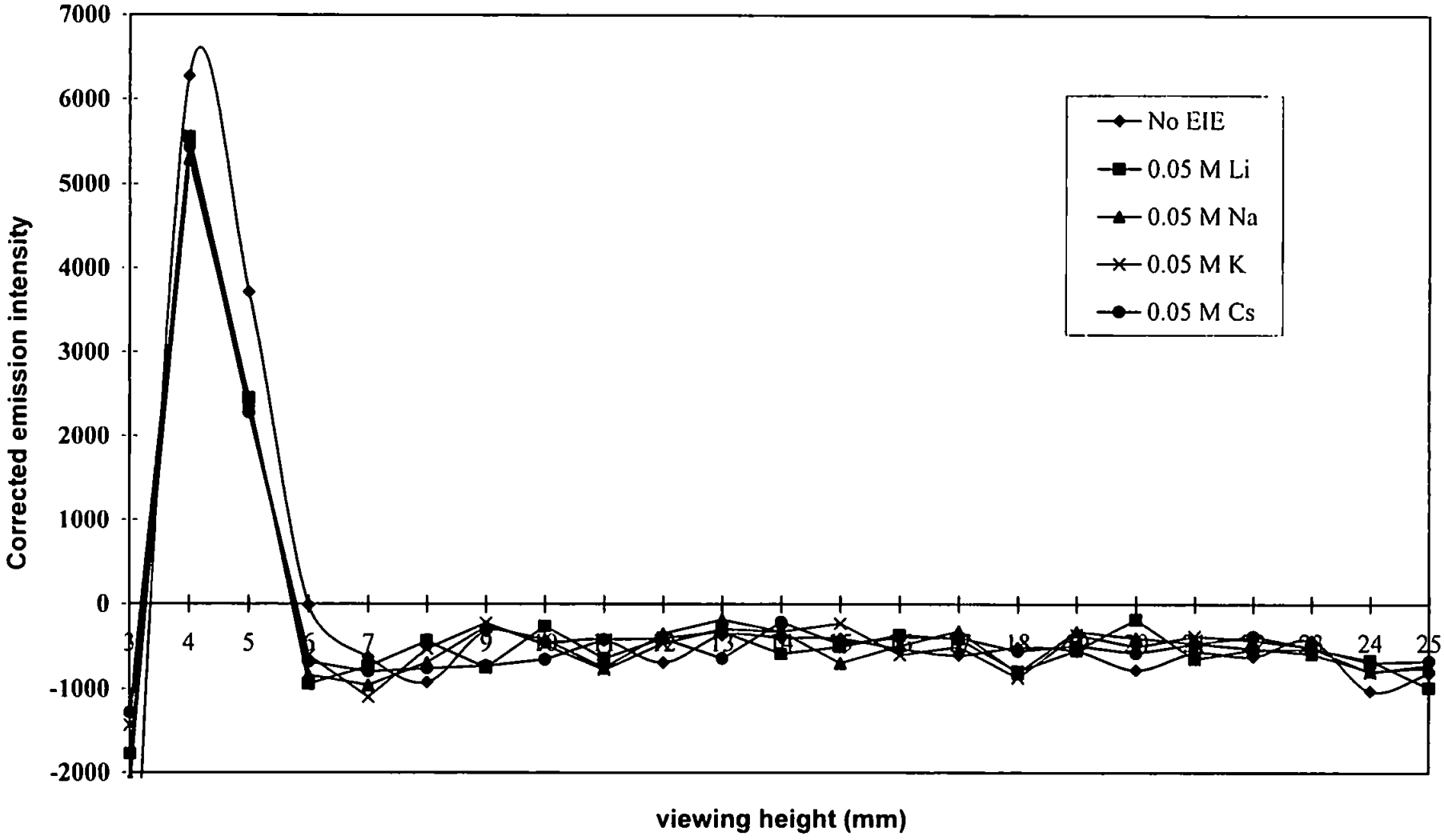

Figure 5.4 - Variation in emission intensity as a function of viewing height for a 100 µg ml-1 Fe solution measured at 382.043 nm

plasma body. No off axis enhancement was observed. A point of inflexion is observed at 2.4 - 2.8 mm in the Abel corrected profiles as, for example, in Figure 5.3. The corrected emission intensities show corruption at 3.6 - 4.0 mm, either side of the centre point. This is attributed to the edges of the torch slot and only data within these confines is considered. Uncertainties in emission intensity readings were less than 1.5 % at all spatial positions.

Addition of EIEs to the solution matrix can be seen to effect emission intensity around the central part of the plasma. All five profiles are similar towards the edge of the plasma. The addition of Li, Na, K and Cs to the sample matrix resulted in an apparent depression of the intensity of the atom line compared with the intensity of the atom line in the absence of an EIE. The magnitude is different for each EIE. This difference in depression for each matrix element is illustrated in percentage terms in Figure 5.5. Enhancement or depression effects may be expressed as a factor using equation 5.5:

$$\text{Net enhancement / depression} = \frac{\text{Emission intensity (solution + EIE)}}{\text{Emission intensity (solution only)}} \quad (5.5)$$

Figure 5.5 shows that lithium, sodium and potassium have the greatest 'apparent' depression effect and caesium the least. No simple relationship is observed between the magnitude of the depression effect and the molecular mass of the EIE added.

Figure 5.6 illustrates the effect upon the intensity of the Fe I 385.991 nm emission line for a 100 μg ml^{-1} Fe solution when the same EIEs are added in equivalent equimolar concentrations. These measurements were obtained simultaneously with measurements of the 382.043 nm atom line; an ability afforded by the CCD detector of the instrument. Again, the profiles have been Abel inverted. As for Figure 5.3, these represent the measured intensity at a viewing height position of 4 mm ALC. As previously discussed, only data to within the 0 to 3.6 mm lateral positions was considered for interpretation.

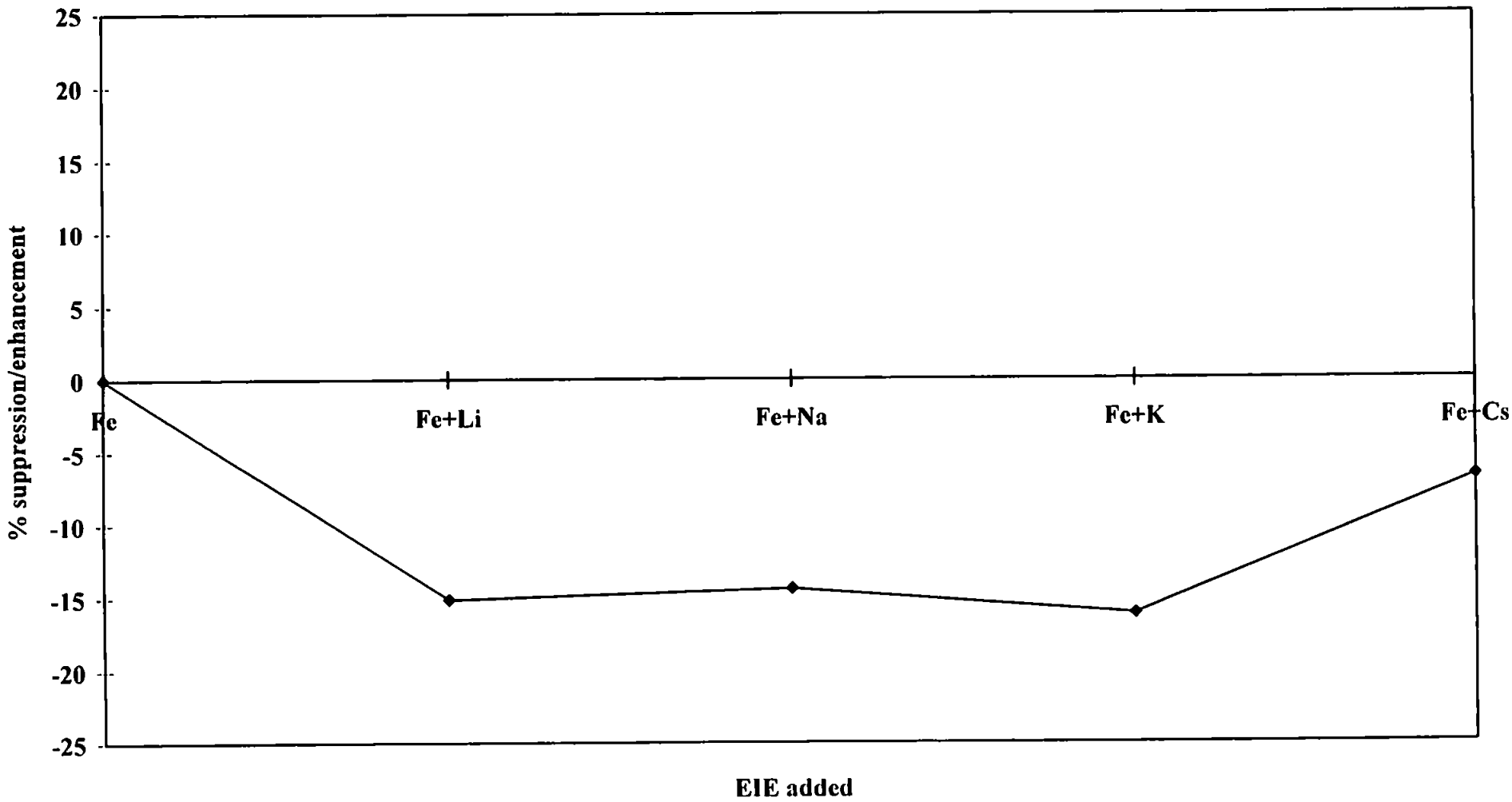

Figure 5.5 - Magnitude of the net suppression / enhancement effect at radial position 0 mm for a 100 µg ml-1 Fe solution measured at 382.043 nm

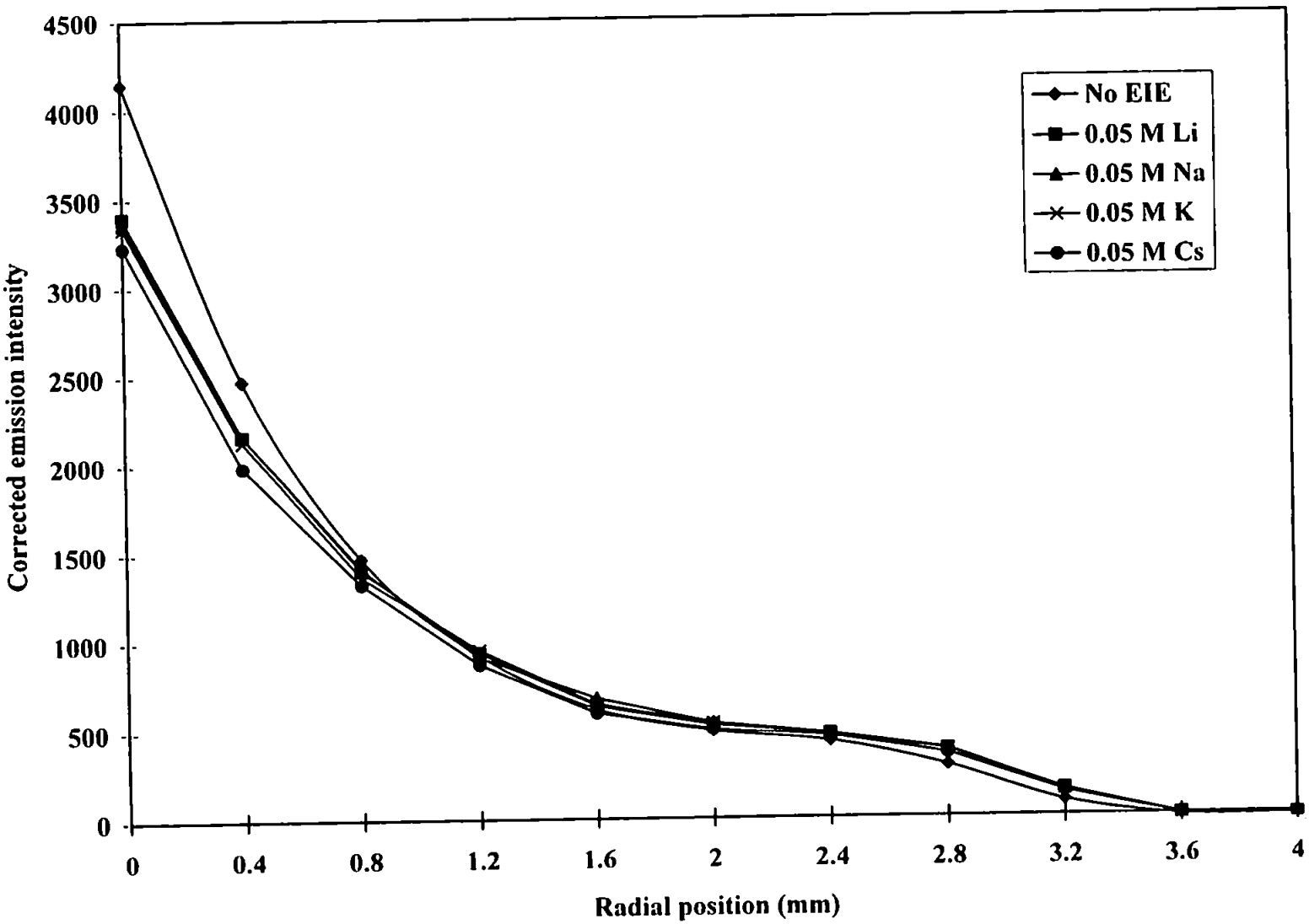

Figure 5.6 - Variation of emission intensity with radial position for a 100 µg ml-1 Fe solution measured at 385.991 nm with various EIEs added

Maximum emission intensity occurs at 0 mm i.e. at the centre of the plasma and again no off-axis enhancement is seen. Addition of an EIE causes an apparent significant depression for all elements added in this study. This 'depression' is most marked at the centre of the profile, becoming less towards the edge of the plasma. The magnitude of the depression varies according to the EIE added showing Cs to have the greatest depression and lithium the least. This effect is summarised in Figure 5.7. The magnitude of the depression effect observed for the Fe solution appears to be greater for the Fe I 385.991 nm line compared to that of the Fe I 382.043 nm line. The profiles shown in Figures 5.5 and 5.7 show obvious differences in shape. The former is almost symmetrical, with the least suppression shown for Cs. Conversely, Figure 5.7 shows a continual increase in suppression from Li to Cs. The *differences* between the two profiles may not be attributed to transport effects. Both wavelengths were monitored simultaneously, therefore any influence on emission intensity due to sample mass transport will be equivalent for the two emission lines.

Given the above, we may assume that differences in the structures of the two profiles are attributed to subtle changes in the excitation processes which populate the two excited states for the emission lines. An explanation for this difference may be obtained from examination of the Grotian diagram for Fe I. A simplified version is illustrated in Figure 5.8. It can be seen from the Grotian diagram that while both the 385 and 382 nm line emission is derived from an excited 4p orbital (i.e. ^5D state) the effective ground state for both is different. While the 385 nm line is the equivalent of a $3d^64s^14p^1$ to $3d^64s^2$ transition, i.e. $^5D_4$ (0 eV), that of the 382 nm line is the equivalent of a $3d^74p^1$ to $3d^74s^1$ (i.e. $^5F_5$ state) transition. The latter is approximately 0.8 eV above ground state $^5D^0$ and no transition to $^5D^0$ is allowed. Hence the two lines are independent and can be expected to display differences in enhancement or suppression. The magnitude of the population mechanism, if not the mechanism itself, may therefore be altered in the presence of an EIE.

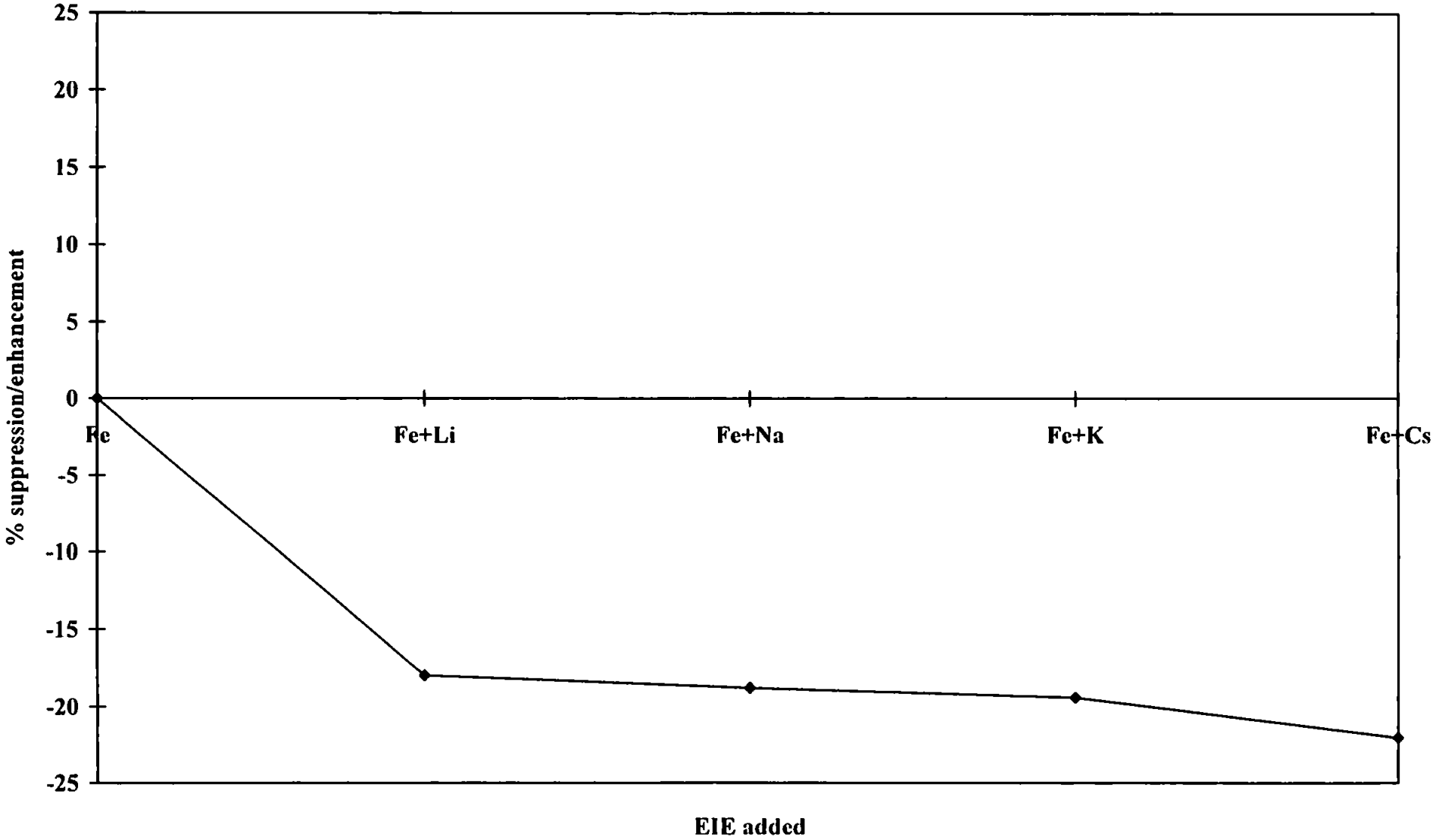

Figure 5.7 - Magnitude of the net suppression / enhancement effect at radial position 0 mm for a 100 µg ml-1 Fe solution measured at 385.991 nm

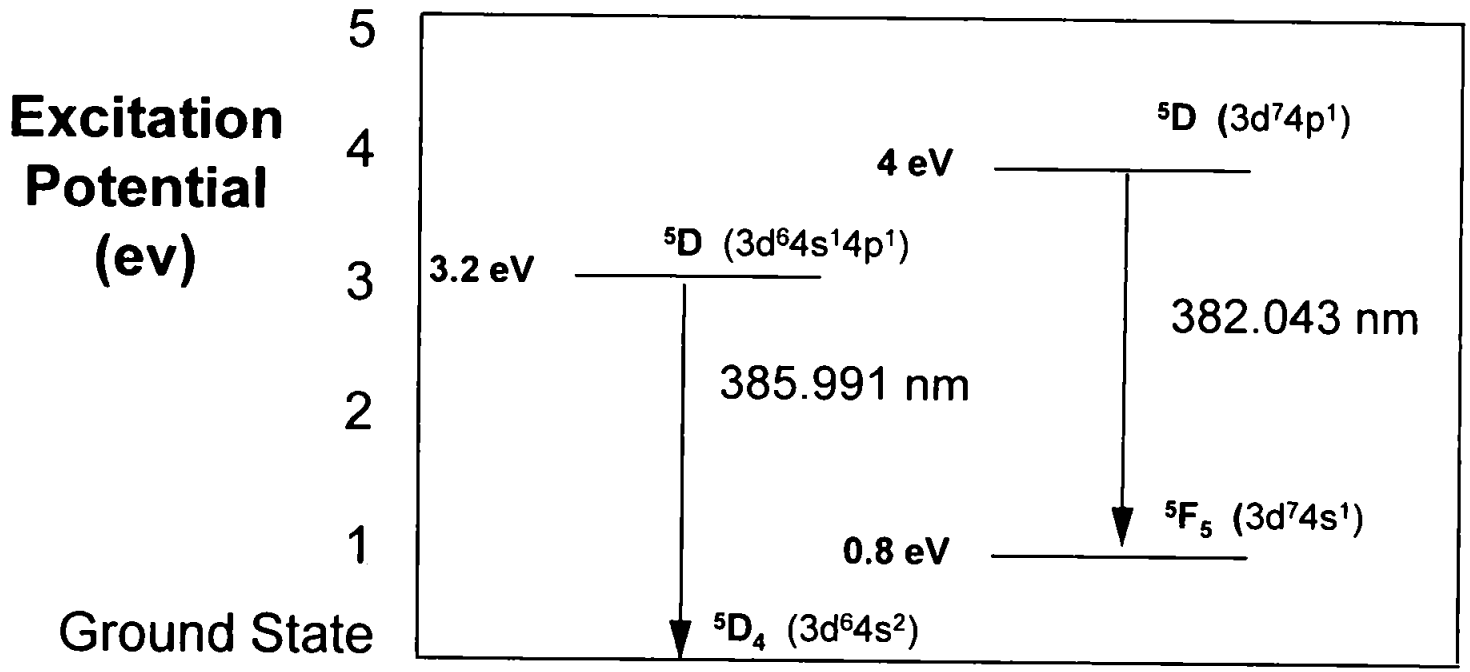

Figure 5.8 - Simplified Grotian Diagram for Fe I

The depression effects observed from any one emission line do not take into account differences in transport efficiency when an EIE is added to a solution. It is known from work in our laboratories (Chapter 5.1) that the addition of an EIE e.g. Cs, to the matrix can reduce the transport efficiency of a solution through the sample introduction system by up to 50 %. This results in a decrease in the observed emission intensity. The transport efficiency is dependent upon the constituent matrix element and decreases with the relative molecular mass of the matrix element. For example, the transport efficiency of a solution with Li added to the matrix will be greater than that of a solution with the higher molecular mass Cs added as a matrix element when added in equimolar proportions.

In Chapter 4 ion:atom emission intensity ratios were calculated to negate transport effects. If atom and ion lines are measured simultaneously for a solution, the emission intensity ratio can be compared to the emission intensity ratio when the same emission lines are measured for the equivalent sample with a matrix element added to give an overall ratio known as D_{sol}, i.e.

$$\frac{\left(\frac{I_i}{I_a}\right)solution + EIE}{\left(\frac{I_i}{I_a}\right)solution} = D_{sol} \qquad (5.6)$$

The presence of an EIE will reduce the transport efficiency of the solution through the sample introduction system which may 'mask' the real enhancement or depression effect caused by the EIE. Any variation of D_{sol} from unity will be a reflection of any change in the atomisation, ionisation and excitation processes occurring in the ICP.

Similarly, if two atom lines are used as in this study, for solutions, with and without EIEs, transport effects can be negated and differences in, for this case, excitation processes can be inferred. The relationship between the two solutions may be illustrated by calculating the ratio D_L:

$$\frac{\left(\frac{I_a^{\lambda_1}}{I_a^{\lambda_2}}\right)solution + EIE}{\left(\frac{I_a^{\lambda_1}}{I_a^{\lambda_2}}\right)solution} = D_L \qquad (5.7)$$

where I_a is the emission intensity of an atom line, λ_1 is 382.043 nm and λ_2 is 385.991 nm. Values of D_L have been calculated at the centre of the plasma profile where suppression effects upon Fe I emission are most apparent for various EIEs. The results are given in Table 5.3.

Any deviation of D_L values from 1 would reflect any changes in excitation processes between solutions with and without EIEs added for the two lines. For Li, Na and K, D_L values are similar and approximately equal to 1. This indicates that the addition of Li, Na and K affects the two lines to the same degree i.e. the mechanisms that populate these two states, if changed, are affected to the same degree. The addition of Cs to the solution, however, yields a D_L value of 1.20 at the centre of the plasma (4 mm ALC). It is apparent that excitation processes for the two lines are affected to different degrees by addition of this matrix element.

A value of D_L greater than 1 may be the result of one of at least three scenarios. Figure 5.9 schematically represents these three cases, when the presence of an EIE brings about a change in emission intensity for λ_1 (Fe I 382 nm) and λ_2 (Fe I 385 nm). It is noted that the emission intensity of λ_2 is always greater than that of λ_1.

Figure 5.9a displays the case where both lines are enhanced but the magnitude of enhancement from an EIE on λ_1 is greater than the enhancement from an EIE on λ_2. Figure 5.9b displays the case when both lines are suppressed but the magnitude of suppression from an EIE on λ_1 is

EIE UNDER STUDY	D_L (solution)
Li	1.04
Na	1.05
K	1.04
Cs	1.20

Table 5.3 - D_L values for a 100 µg ml^{-1} Fe solution in the presence of EIEs

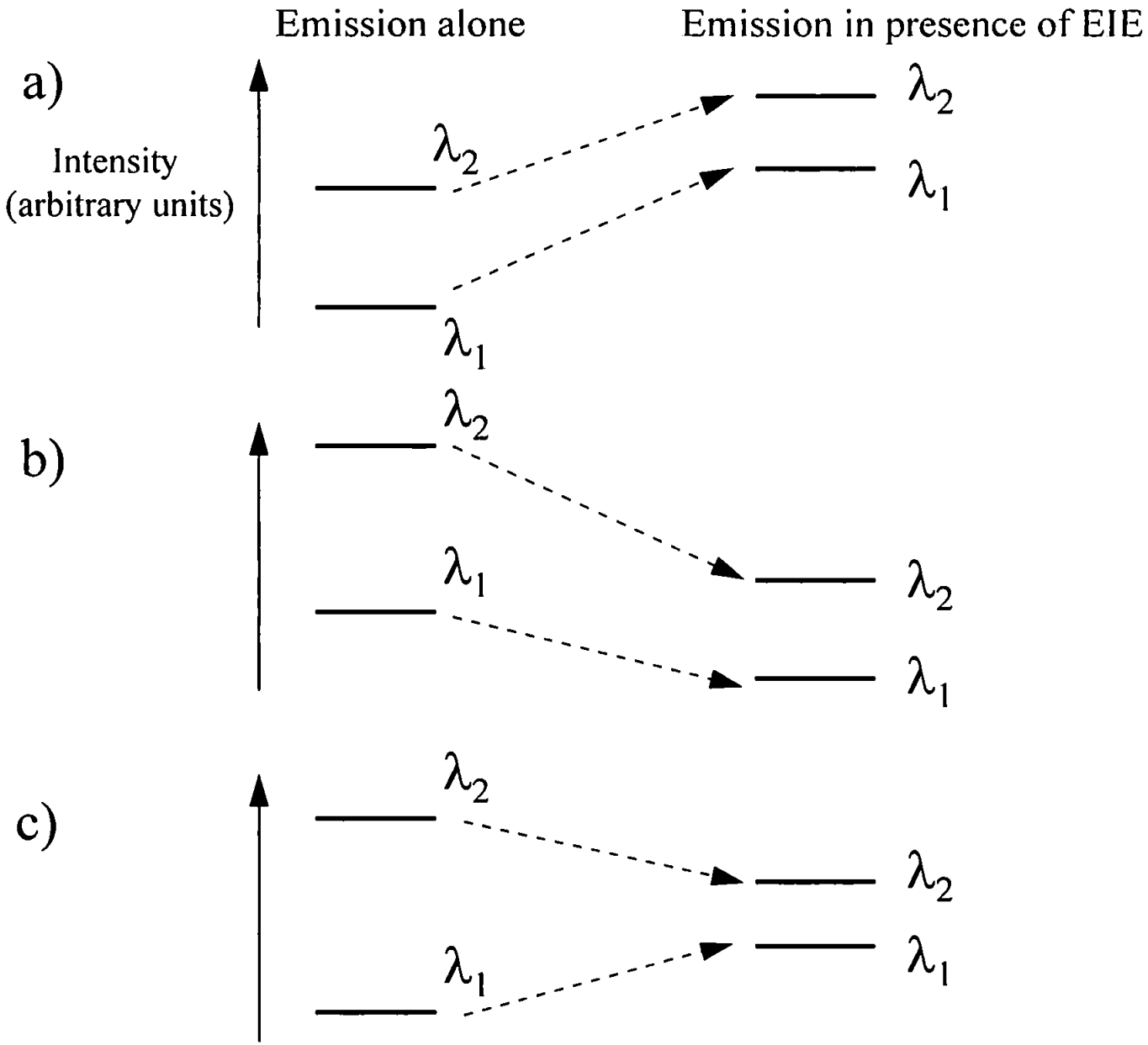

Figure 5.9 Three scenarios resulting in D_L values greater than unity

less than that suppression from an EIE on λ_2. Figure 5.9c is the obvious case where λ_1 is enhanced and λ_2 is suppressed.

As previously stated, suppression effects seen in Figures 5.5 and 5.7 do not individually take into account any transport effects that may arise upon addition of an EIE to a solution. The emission intensity from an analyte within a particular volume of plasma is proportional to the number of excited species passing through this volume. The number of species is itself a function of the transport efficiency and excitation parameters. If transport effects wholly govern intensity then summation of the intensities from an analyte within the given plasma volume should show a correlation with transport efficiency. Changes in transport efficiency would result in similar changes in summed intensities from the number of emitting species. If excitation effects become significant (e.g. enhancement or suppression of populations of excited species) then the correlation is lost. In the first part of this chapter (5.1) the transport efficiency of solutions with and without EIEs in equimolar proportions were measured. The overall change in this efficiency from adding Li, Na, K and Cs is expressed as a percentage. This can be compared with the ratio of the sum of the radial intensities from the analyte in the presence of the EIE to the sum of the radial intensities in the absence of the EIE, for each line, as shown in equation 5.8:

$$\sum_r = \frac{\sum I_{a\ EIE}^{\lambda_x}}{\sum I_a^{\lambda_x}} \times 100\% \qquad (5.8)$$

which, as stated, inherently includes transport effects. Table 5.4 shows the comparison for summed emission intensity ratios for solutions with and without EIEs for both the 382 and 385 nm Fe I lines with the change in transport efficiency with EIE.

It can be seen that transport effects do not govern the sum of the emission intensities and there is no correlation between percentage relative transport

EIE added	None	Li	Na	K	Cs
% RTE[1]	100	90	82	60	45
% $\Sigma_r \lambda_{382}$	100	96.8	96.8	94.6	100
% $\Sigma_r \lambda_{385}$	100	92.0	92.2	91.2	86.5
$\Sigma_r \lambda_{382}/\Sigma_r \lambda_{385}$	1	1.05	1.05	1.04	1.16
% $\Sigma_r \lambda_{382}$ - % RTE	0	6.8	14.8	34.6	55
% $\Sigma_r \lambda_{385}$ - % RTE	0	2	10.2	31.2	41.5

[1] Percentage Relative Transport Efficiency

Table 5.4 - Summed emission intensity ratios for solutions with and without EIEs for Fe I 382 nm and Fe I 385 nm, compared to percentage solution transport efficiency values.

efficiency (% RTE) and Σ_r for both emission lines. The higher values of the summation ratio show that transport effects severely 'mask' the real effect, that being an enhancement for both lines. Table 5.4 also shows how the relative effects of EIEs on each line confirms the D_L values obtained from equation 5.7. For each line, λ_1 and λ_2 , the addition of Li, Na and K appears to give approximately the same summation ratio, i.e. values of λ_1 (382 nm) are between 94.6 and 96.8 % and values for λ_2 are between 91.2 and 92.2 %. The ratio Σ_r (λ_1/λ_2) values for Li, Na and K are shown to be just above 1 (approximately equal to 1.05) in accordance with D_L values in Table 5.3. This suggests that for Li, Na and K the enhancement scenario shown in Figure 5.9a is operating but with approximately the same magnitude enhancement on the two lines. The ratio for Cs is shown to be 1.16 which is again comparable to the D_L value in Table 5.3 of 1.20. This also shows the scenario shown in Figure 5.9a to be the better model, where Cs is affecting the λ_1 382 nm emission line to a relatively greater extent than the λ_2 385 nm line. That the relative populations of these two excited states are changed by different degrees in the presence of different EIEs is displayed by the % $\Sigma_r\lambda_x$ - % RTE values in Table 5.4. This corrects for the transport phenomena and shows the relative enhancement effect on the two lines. The real enhancement of a line (corrected for transport) increases in the order Li < Na < K < Cs. This is in accordance with previous studies using EIEs (Chapter 4).

5.2.4.2 Radial D_L profiles for Solutions

Abel corrected radial D_L profiles can be used to visualise off-axis effects on the two lines due to the presence of EIEs. These are shown in Figure 5.10 at the peak viewing height of 4 mm ALC. With transport phenomena negated, the radial effect from the presence of an EIE on the two lines is similar giving values of approximately 1 for Li, Na, K out to 2.4 mm. Cs, however, again shows elevated values indicating that the λ_1 382 nm emission line is enhanced to a greater degree than the λ_2 385 nm line. The Cs values of D_L imply some spatial structure to this enhancement difference, i.e. high at 0 to 0.4 mm, low at 0.8 to 1.2 mm and high again at 1.6 to 2.0 mm. At this low

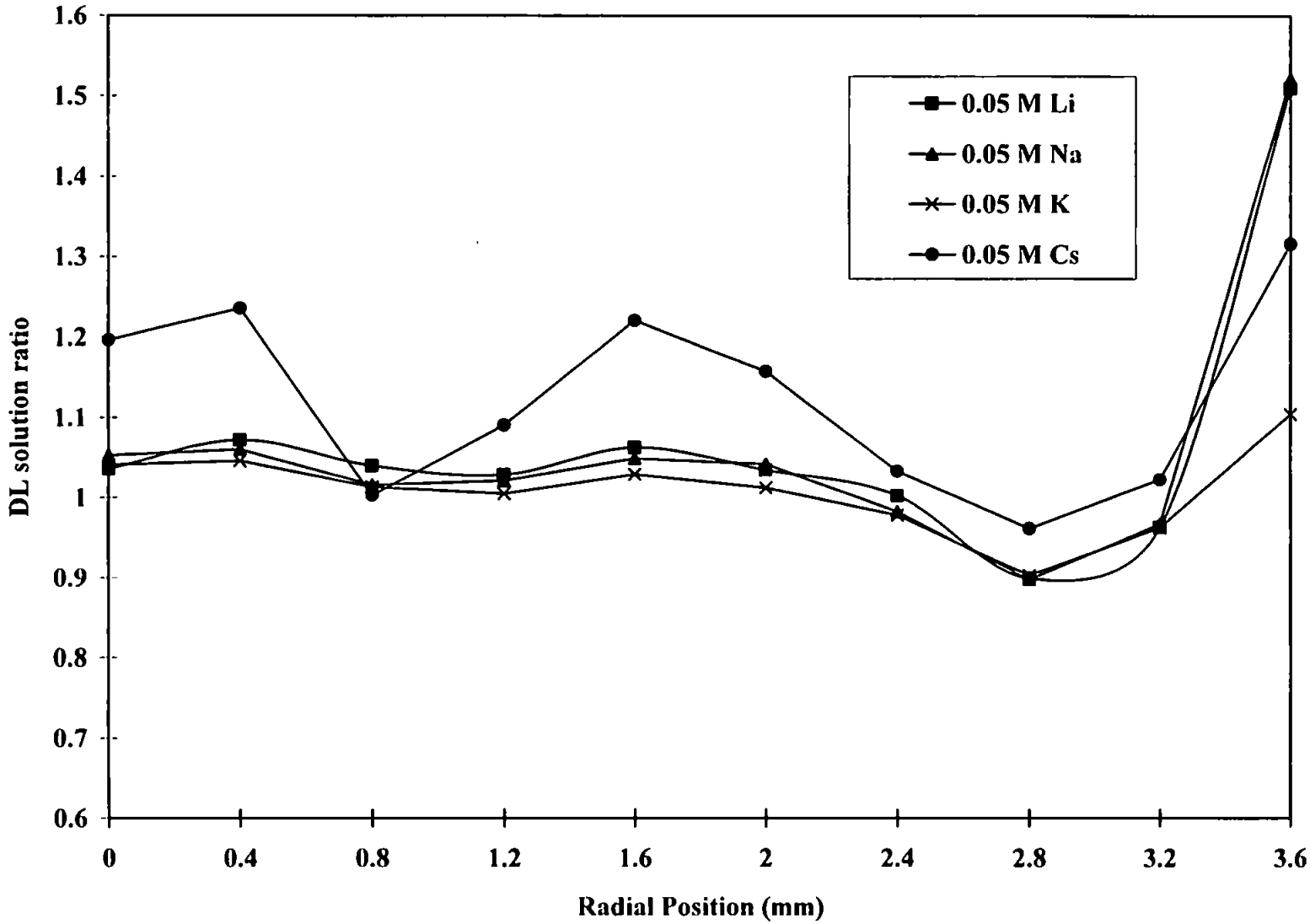

Figure 5.10 - DL solution ratio variation with radial position for a 100 µg ml-1 Fe solution with various EIEs added

viewing height the punched region where the central channel flows and plasma body meet is close to the second radial maximum. Spatial emission structure for atom lines and its dependence upon EIEs has been discussed in detail in Chapter 4.

5.2.4.3 The Effect of EIEs on the Emission Intensity of Slurries and Comparisons Between Solutions and Slurries

Figure 5.11 is the radial Abel inverted emission intensity profile, measured at 4 mm viewing height ALC for the Fe I 382.043 nm atom line, when 100 μgml^{-1} Fe slurries (with and without EIEs) are aspirated into the ICP. As in the previous profiles, only the emission intensities between 0 and 3.6 mm are considered. Uncertainties for the intensity readings are less than 1.5 % RSD.

As found for the equivalent solution intensity, peak emission again occurs at 0 mm, the centre of the plasma. The value of the peak emission intensity for the Fe slurry alone is lower (-15%) than that of the equivalent solution. This may in part be attributed to differences in the transport efficiencies for the two systems. The proportion of the Fe_2O_3 slurry particles below 1.5 µm was approximately 70 % which indicated that the slurry may not obey the single occupancy diameter model proposed by Goodall et al (56). The slurry recovery being 15 % lower than the equivalent solution suggests that some proportionally greater particle size loss processes are occurring within the sample introduction system. However atomisation effects cannot be discounted. The plasma is being observed in the relatively cool region just above the load coil (IRZ) and the 'real' atomisation efficiency for slurries may therefore be less than that of an equivalent solution.

As found with solutions, the addition of an EIE can also result in lower sample transport efficiency of a slurry through the sample introduction system. The EIE will be present in the aqueous layer droplet carrying the solid particle in a slurry dispersion and the mass of the EIE will affect the transport efficiency. As for solutions, the transport efficiency of a slurry with Li added to

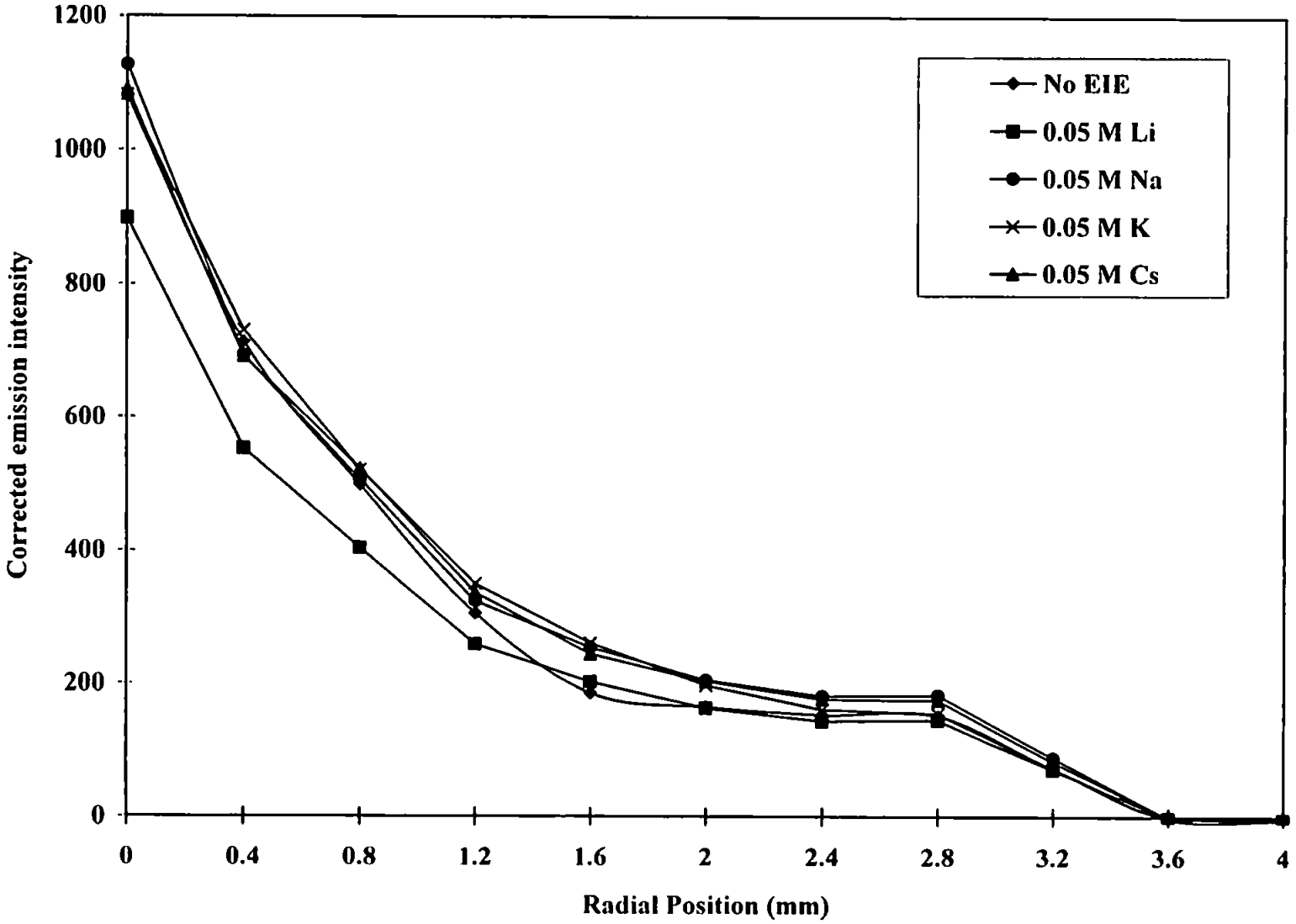

Figure 5.11 - Variation of emission intensity with radial position for a 100 µg ml-1 Fe slurry measured at 382.043 nm with various EIEs added.

the dispersant matrix will be higher than that of a slurry system with Cs added.

Figure 5.12 highlights that solutions and slurries can show subtle differences upon addition of the same EIEs when the identical analytical emission line is observed. For solutions, 'apparent' depression effects were observed for all matrix elements added (Figure 5.5). For the equivalent slurry, 'apparent' enhancement effects were observed at 382.043 nm when K and Cs were added to the dispersant matrix compared with the analyte in the absence of the EIE. The magnitude of the depression effects noted for Li and Na addition to the slurry (approximately -15 %) however, are similar to those of the equivalent solution for the 382.043 nm Fe I line.

Figure 5.13 shows the Abel inverted radial emission profiles, again at 4 mm ALC, for the Fe 385.991 nm line when 100 μg ml^{-1} Fe_2O_3 slurries, with and without EIEs, are aspirated into the ICP. Maximum emission intensity occurs at the 0 mm central point in the channel. This is the same as that found for the equivalent solution when the same atom line is measured. In contrast, the slurries measured at 385.991 nm showed no 'apparent' enhancement effects when EIEs were added to the slurry matrix compared with the analyte in the absence of the EIE. Depression effects are seen in all cases (Figure 5.14).

When the profiles for slurry emission, in the presence and absence of an EIE, for the two lines are compared (Figures 5.12 and 5.14) a difference in slope is noted. As these lines are measured simultaneously only a change in the relative population of excited species could bring this about as transport effects are the same, i.e. the two lines are affected to different degrees, dependent on the EIE added. This was manifest by the solution containing Cs under the same conditions (Figure 5.5 and 5.7) and it is again the presence of Cs in the slurry that shows the greatest relative change.

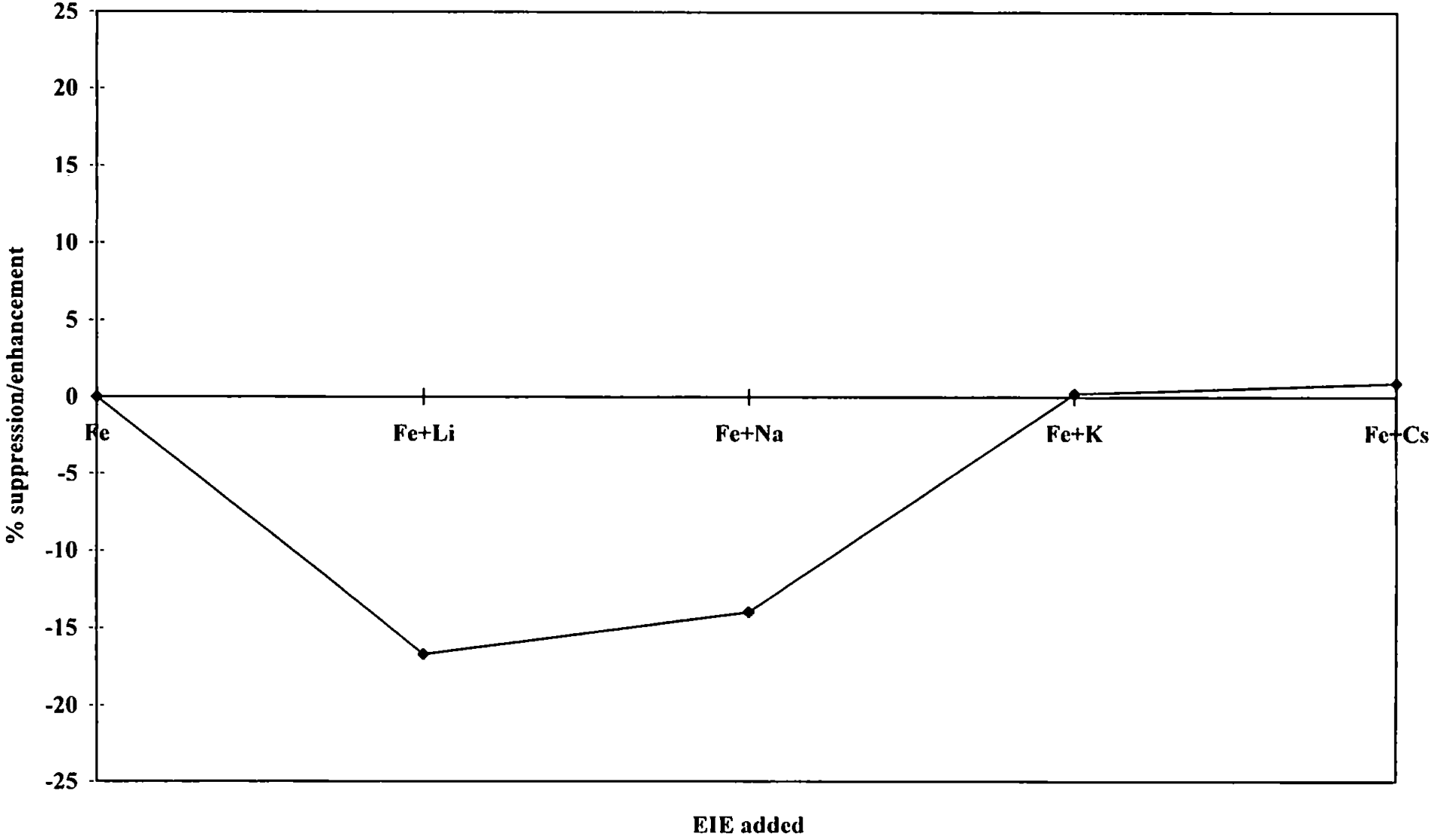

Figure 5.12 - Magnitude of the net suppression / enhancement effect at radial position 0 mm for a 100 µg ml-1 Fe slurry measured at 382.043 nm

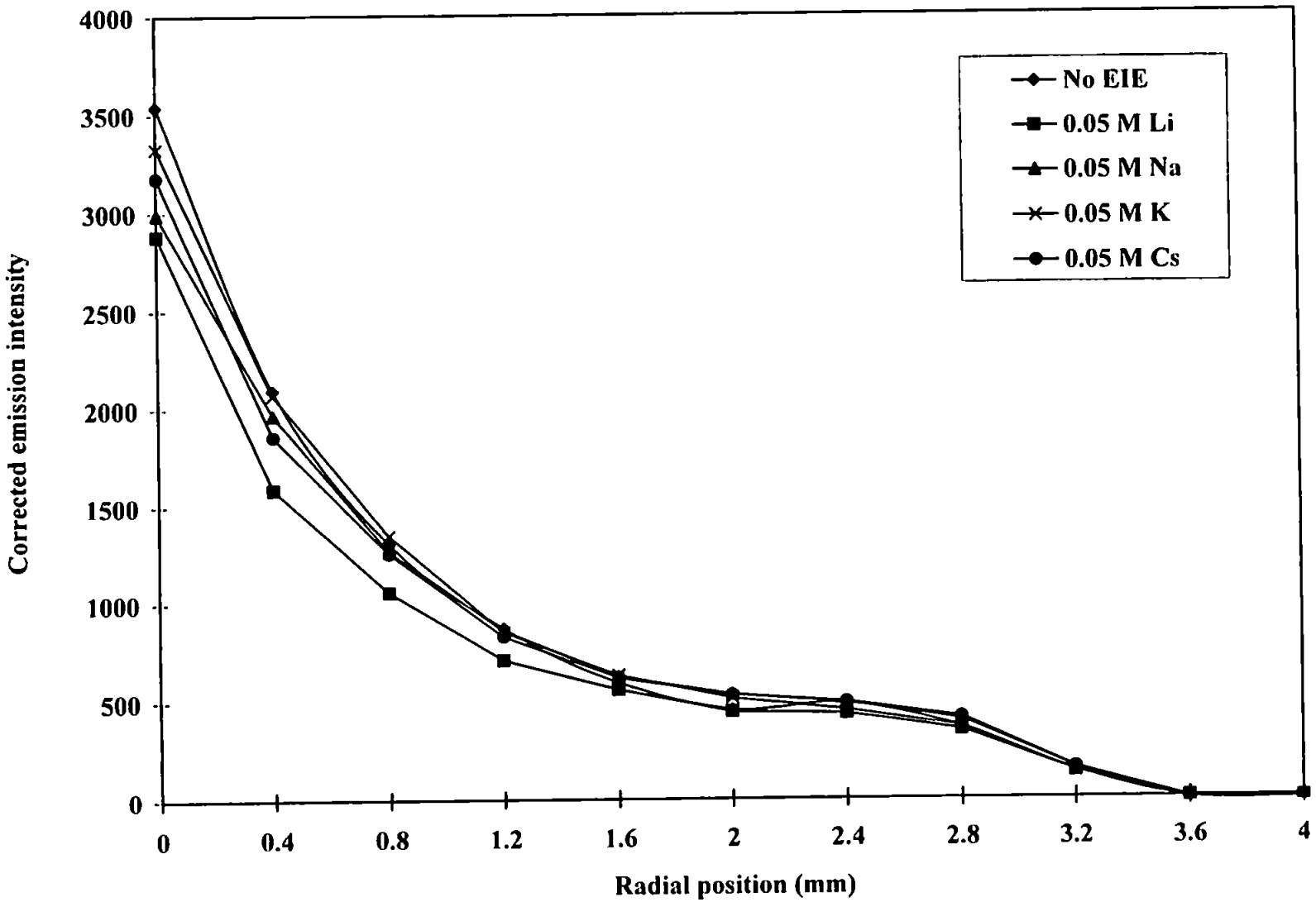

Figure 5.13 - Variation of emission intensity with radial position for a 100 µg ml-1 Fe slurry measured at 385.991 nm with various EIEs added.

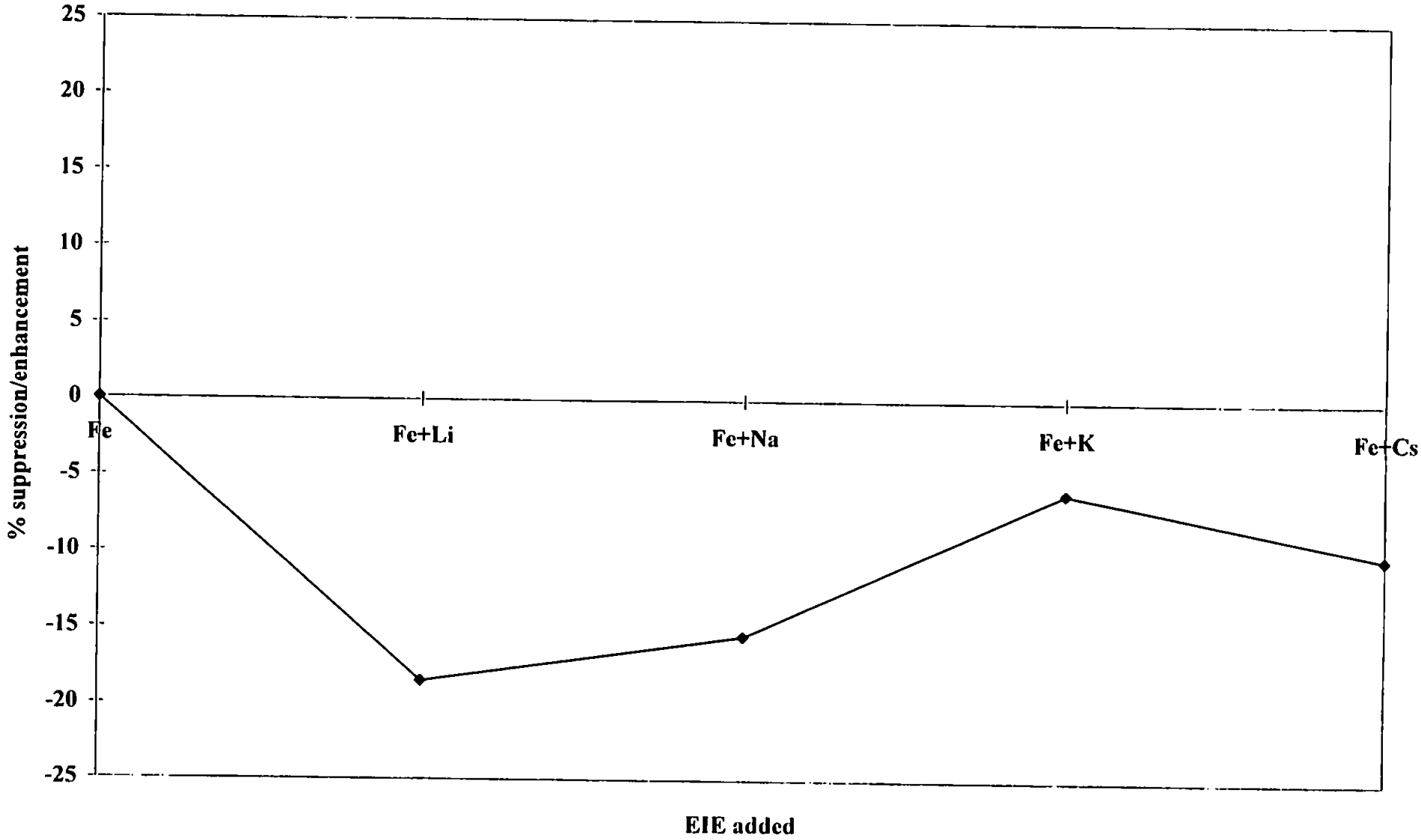

Figure 5.14 - Magnitude of the net suppression / enhancement effect at radial position 0 mm for a 100 µg ml-1 Fe slurry measured at 385.991 nm

Confirmation that the two lines are affected to different degrees for slurries in the presence of the same EIE, can be sought using slurry equivalent D_L values. Using equation 5.4, the transport negated D_L values for 100 μg ml^{-1} Fe_2O_3 slurries with various EIEs added were calculated and these are given in Table 5.5. Employing the same arguments as discussed in the solution section (a) the D_L values for Li and Na (1.02) are close to 1 showing that the two lines are affected to the same degree. The slightly elevated value for K (1.07) suggests an upward trend, in that the two lines are affected to slightly different degrees, but this value is similar to that of an equivalent solution containing K (1.05). The Cs value of 1.12 is, however, some 10 % greater than the Li and Na systems and shows the difference from its presence on the two lines to be quite marked. This is the same trend as seen in solutions when the Cs D_L value is some 15 % greater than the Li and Na counterparts.

When a slurry recovery is less than that of an equivalent solution under the same matrix and plasma conditions a problem arises in separating the effects of transport, atomisation and excitation. The effect from EIEs on transport of an analyte of interest in solutions may be considered constant for a given sample introduction system and given set of aerosol generating conditions (liquid and gas flow rates). This is not the case for different slurries whose particle size distributions are different and exceed given threshold values, i.e. do not model solutions efficiently. It is for this reason that slurries should not be used to calibrate for other slurry samples (56). In the solution section (5.2.4.1) previously discussed, the transport effects for solutions with and without EIEs were gauged using data obtained from Chapter 5.1, under the same conditions of sample introduction. The slurry data in Chapter 5.1 was for MnO_2 and is therefore different to the slurry employed in this study (Fe_2O_3). However, a scrutiny of the slurry profiles in Figures 5.12 and 5.14 compared with the solution profiles in Figure 5.5 and 5.7 together with the best scenario transport figures, given in Table 5.4, shows that again transport phenomena mask the enhancement effects for EIEs on slurry analyte emission. Again, enhancement is in the order Li<Na<K<Cs, which is comparable to solutions. While the effect from, in particular, Cs on the two

EIE UNDER STUDY	D_L (slurry)
Li	1.02
Na	1.02
K	1.07
Cs	1.12

Table 5.5 - D_L values for a 100 µg ml^{-1} Fe slurry in the presence of EIEs

lines for solutions and slurries is very similar (that shown in Figure 5.9a), the difference in magnitude of the enhancement from Cs (and possibly K) when comparing solutions and slurries can be attributed to one or a combination of two effects i) that the presence of an EIE produces a real enhancement of the relative atomisation efficiency of a slurry (to that of a solution) in the plasma and ii) the presence of an EIE when changing the transport efficiency of a slurry also increases the relative distribution of finer slurry particles entering the plasma giving an 'apparent' increase in relative atomisation efficiency. These effects were described in detail in Chapter 4.

5.2.4.4 Radial D_L profiles for slurries

D_L profiles for slurries, after Abel correction, are illustrated in Figure 5.15 and, as for solutions, can be used to demonstrate off-axis enhancement or suppression effects. The effect on the two emission lines from adding an EIE to the slurry dispersant matrix is similar for Li, Na and K from the centre of the plasma profile out to 2.4 mm. In an analogous way to solutions, Cs shows the highest D_L values, therefore illustrating that the λ_1 382 nm emission line is enhanced to a greater extent than the λ_2 385 nm line. This enhancement difference is reflected by variations in spatial structure of the profiles. The biggest difference is seen at 0 - 0.4 mm and 1.6 - 2.0 mm. The effect of EIEs on the spatial emission structure for atom lines has been previously described in Chapter 4.

5.3 General Discussion and Conclusions

The effect from adding equimolar quantities of easily ionised elements to solutions and slurries is to greatly modify the mass transport efficiency of a concomitant analyte of interest. The decrease in efficiency is proportional to the matrix loading and must be corrected for when EIE suppression/enhancement effects are determined directly from plasma emission.

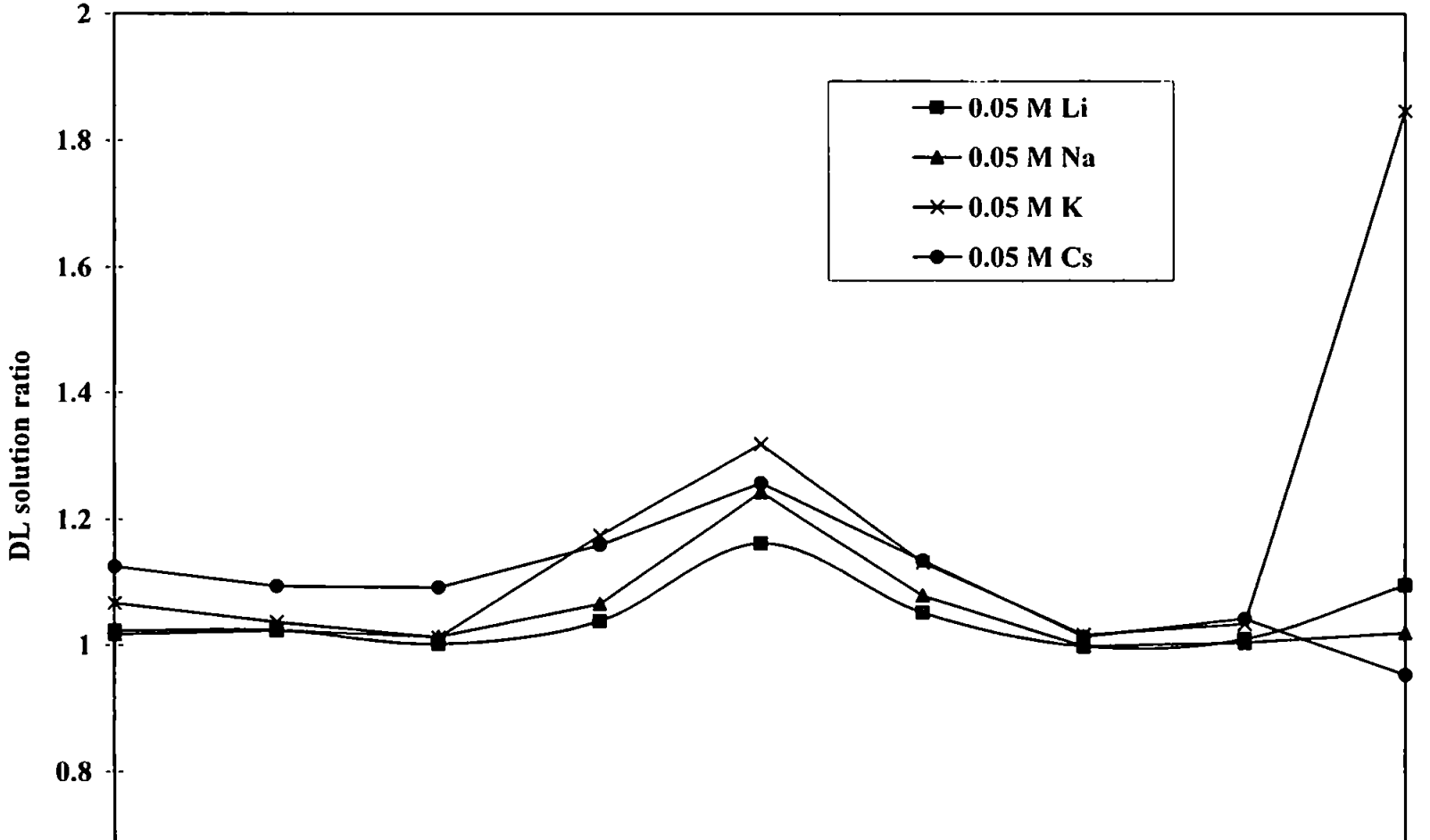

Figure 5.15 - DL slurry ratio variation with radial position for a 100 µg ml-1 Fe slurry with various EIEs added.

The addition of an EIE to a solution matrix affects the emission intensity of the analyte element most significantly at the centre of the plasma. For both Fe I 382.043 and 385.991 nm, an apparent depression effect is observed when a particular EIE is added. The magnitude of this depression for all EIEs is greater when the 385 nm line is measured, compared to the 382 nm line. This difference is shown to be caused by an effect other than sample transport, as both wavelengths were measured simultaneously. Differences in the radial plasma profile structures for solutions may be attributed to subtle changes in the excitation processes which populate the two excited states. These 'apparent' depression effects do not take into account differences in solution mass transport when an EIE is added to the matrix. Such transport effects have been negated by calculating D_L values. The addition of Li, Na, and K to solutions results in similar D_L values indicating that these EIEs effect the mechanisms which populate the excited states to the same degree. The addition of Cs causes the excitation processes for the two lines to be effected to different degrees.

The 'total' emission intensity within an observed plasma volume, given by the value from the sum Σ_r, can be considered directly proportional to the population of excited species within this volume. Changes in relative sample transport efficiency (% RTE) would be accompanied by a similar change in direction and magnitude for Σ_r if depression effects were to be attributed solely to mass transport. As there is no correlation between the two for solutions it may be concluded that transport effects severely 'mask' the real enhancement caused by the addition of EIEs to a solution. This real enhancement increases for both lines in the order Li<Na<K<Cs. D_L values for solutions indicate that the enhancement for the two emission lines is similar for Li, Na and K moving from the centre of the plasma towards the plasma body at 2.4 mm. An elevated D_L value for Cs indicates that the 382 nm line is enhanced more than the 385 nm line.

For slurries, peak emission also occurs at the centre of the plasma. While in many instances solutions and slurries are shown to have very similar trends,

i.e. slurries model solutions for a variety of phenomena, some subtle differences when EIEs are added to the sample matrix can be seen. 'Apparent' enhancement effects are observed when K and Cs are added and the 382 nm emission line is monitored. No such 'apparent' enhancement is observed for the 385 nm line. However, as found with solutions, apparent transport phenomena mask the 'real' enhancement effects for EIEs. This enhancement is in the order Li<Na<K<Cs for both lines which is comparable to that of solutions. D_L values for slurries with Li and Na added are close to 1 showing that both emission lines are enhanced to the same degree. A slightly higher value for K suggests an upwards trend, culminating with Cs which has the greatest difference in emission intensity values for the two wavelengths. The magnitude of this difference is similar for both solution and slurry systems.

Chapter 6 - The Effect of Easily Ionisable Elements on the Excitation Temperature of Solutions and Slurries in the Inductively Coupled Plasma

6.1 Introduction

The use of the plasma excitation temperature as a physical marker is a useful indicator of changes in fundamental processes that may be occurring within the ICP discharge. It has been stated by Raaijmakers *et al.* (158) that "In an atmospheric discharge in local thermodynamic equilibrium (LTE), the spatially resolved measurement of only one parameter, e.g. the electron density (n_e) or the electron temperature (T_e) is necessary and sufficient to characterise the discharge...". As the inductively coupled plasma is not in LTE, we must assume that any temperature measurements calculated will deviate from the LTE plasma at any spatial point (141).

In this study, the excitation temperature was used as a physical marker to establish direct comparisons and subsequent variation between solutions and slurries with and without the addition of EIEs. Various methods to calculate temperature in the plasma have been summarised in the literature (159). The excitation temperature may be used to draw inferences upon the population of atoms and ions in their respective excited states (160).

Again, Fe was chosen as the thermometric species of interest for this study. This element has been used by many workers to successfully perform general temperature calculations (161-166). Emission lines were selected according to freedom from spectral interferences and precision of transition probabilities (167).

Data has been acquired using the lateral translation of an ICP spectrometer with a solid state detector. The Abel inversion correction technique was used to transform lateral profiles measured when solutions and slurries of Fe with various EIEs added were aspirated into the plasma. In this study a radial ICP

spectrometer, where the plasma is viewed 'side-on', was used to acquire spatial emission profiles. This information was then used to determine the excitation temperature of the ICP at various spatial positions. Preliminary studies were undertaken to investigate the effect of EIEs on the excitation temperature obtained from an axially viewed plasma. These values of T_{exc} could then be compared with the radial values.

6.2 Theory

The ICP discharge may be defined as a partially ionised gas formed by electrical excitation. It is comprised of various species including neutral atoms, molecules, ions and electrons, all of which may be in an excited or ground state. The energy states at which the species exist may be described by the plasma temperature. In a gas where thermodynamic equilibrium exists, all species may be described by a single temperature. For an inductively coupled plasma, however, a single temperature is insufficient. The plasma may be described in terms of a number of temperatures such as the excitation temperature (T_{exc}), the ionisation temperature (T_{ion}), the rotational temperature (T_{rot}), the electron temperature (T_e) and the kinetic temperature (T_{kin}). These temperatures may be calculated using different energy levels for assorted thermometric species and, as a result, the values are often variable (163,137). For this reason, the plasma is said not to exist in LTE. Generally, T_{exc} increases with emission line energy increase. Because of this, if comparisons between literature values are to be made, it is important to ensure that similar temperature calculations are performed.

In this work, the relative line pair intensity ratio method was used to determine the excitation temperature. The ratio method was the only technique available to calculate temperatures based on the instrumental configuration available for use. As the plasma is known not to exist in LTE, it would be ideal to determine plasma temperature using a method independent of whether the plasma is in LTE. The obvious method of choice is to measure the Hß 486.1 nm line, calculate the electron number density, n_e, using the Stark effect on

the hydrogen line (168) and substitute this value into the Saha equation, along with experimentally measured ion/atom emission intensity ratios, to calculate T_{exc}. Other methods commonly used to acquire n_e for substitution include measuring the continuum intensity at 430 nm or the use of the Inglis-Teller method (168). While the configuration of the instrument data collection system does not allow these techniques to be employed, the line pair ratio method has been used successfully by many workers to acquire comparative data and subsequently pin point changes that can occur due to the presence of particular matrices.

The Line Pair Intensity Ratio method is derived from the Boltzmann equilibrium (137):

$$I = \left(\frac{hc}{4\pi\lambda}\right) g_k A \left(\frac{n_e}{Q(T_{exc})}\right) \exp\left(\frac{-E_k}{kT_{exc}}\right) \qquad (6.1)$$

where I is the intensity of an emitting species, h is Planks constant, c is the speed of light in a vacuum, λ is the wavelength of the emitting radiation (in metres), g_k is the statistical weight of the excited energy level, A is the transition probability for spontaneous emission, n_e is the electron population, Q is the internal partition function, E_k is the energy state (in wavenumbers, cm^{-1}) and k is the Boltzmann constant.

It can be seen that $\log(I\lambda/gA)$ is directly proportional to the excitation energy and a graph of $\log(I\lambda/gA)$ against T_{exc} should produce a straight line if several emission lines of the same element were to be measured under LTE conditions.

If two emission lines of the same element in the same ionisation state are measured, T_{exc} (the common excitation temperature) can be derived from equation 6.2 (168):

$$T_{exc} = \frac{0.625(E_1 - E_2)}{\log \frac{g_1 A_1 \lambda_2}{g_2 A_2 \lambda_1} - \log \frac{I_1}{I_2}} \qquad (6.2)$$

If this equation is to be used to produce valid temperature measurements it is important to measure two lines which have wavelengths existing in close proximity and which have a suitably large energy difference between them on the Grotian diagram of the corresponding element. Transition probabilities must be known to a relatively high (± 15%) degree of accuracy for precise temperature measurements to be made. It is known that the two line ratio method can yield results with good accuracy (137). It should be noted that, in the inductively coupled plasma, different line pairs produce variations in the excitation temperature measurements (160).

6.3 Experimental

6.3.1 Instrumentation - Radial ICP Spectrometer

Spatial measurements of the inductively coupled plasma were carried out using a Perkin-Elmer Optima 3000 ICP spectrometer (The Perkin-Elmer Corp., Norwalk, CT., USA) with a radially orientated torch in the sample introduction system. The instrument spectrometer employed solid-state detection and an echelle grating optical system, both of which are described in the literature (108,114).

Spatial profiles were obtained for consecutive lateral measurements in the horizontal plane. A computer controlled stepper motor in the spectrometer was used to automatically adjust the position of a 2-axis mirror so that a discrete region in the plasma could be examined. The mirror could be adjusted in both vertical and horizontal directions (Figure 6.1). All readings were automated using a custom written program within the instrument software. The operating parameters used in this series of experiments are listed in Table 6.1.

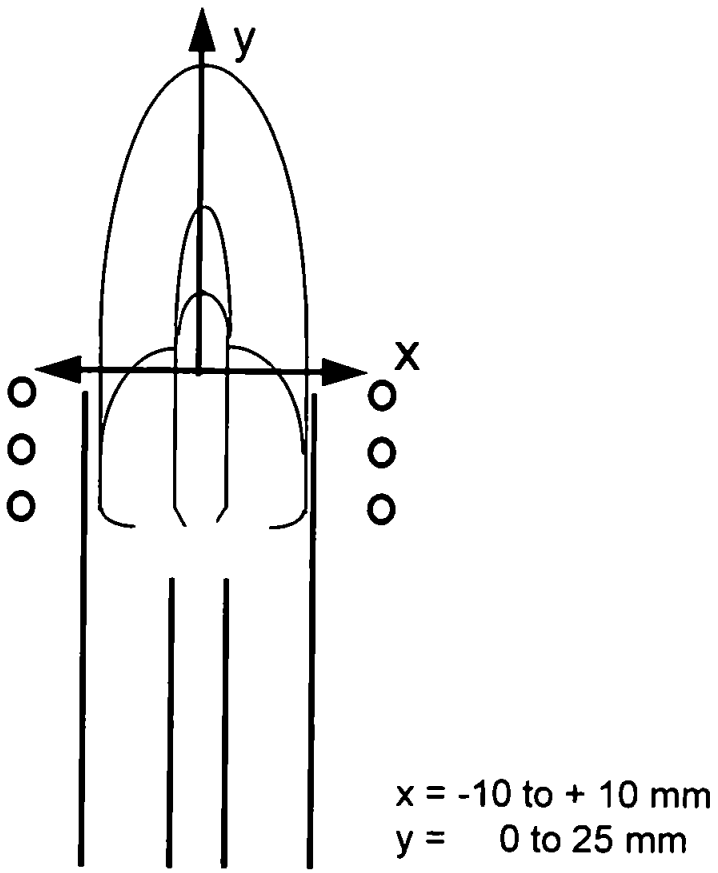

Figure 6.1 - Data Acquisition Using the Radially Viewed ICP

RF Generator	
Frequency	40 MHz, free running
Forward Power	1100 W
Sample Introduction System	
Nebuliser	Ebdon v-groove high solids
Torch	Demountable, custom built with 8 mm wide observation slot and 2.0 mm i.d. alumina injector
Spray Chamber	Perkin-Elmer 'Ryton' Scott double -pass
Peristaltic Pump	Gilson Minipuls 3, computer controlled
Sample Flow Rate	1.0 ml min^{-1}
Argon Gas Flow Rate	
Plasma	14 L min^{-1}
Auxiliary	1.0 L min^{-1}
Nebuliser	0.8 L min^{-1}
Spectrometer	
Resolution	High resolution setting (31 × 250 μm)
Fe I wavelengths	382.043 nm 385.991 nm
Viewing Height (ALC)	4 mm ALC

Table 6.1 - Radial ICP operating parameters

A torch with a 8 mm viewing slot , previously employed and described in Chapter 5.2.3.1, was used in this study. The wider slot had no observable affect upon plasma stability.

As discussed in Chapter 5 the instrument enables measurements to be made using either a high, medium or low resolution setting corresponding to three different slit widths. Two consecutive viewing position zones should not overlap so that the contribution of emission from an adjacent position is eliminated. The dimensions of the high resolution slit are 31 × 250 μm. This resolution setting was used in this study as no overlap between lateral positions at the plasma image plane occurs.

The emission intensity of the Fe 385.991 nm and 382.043 nm atom lines were monitored. These lines were measured by accessing the U II 385.958 and Eu II 381.967 nm subarrays on the visible channel detector of the instrument and minor adjustments were made to ensure measurement of the correct wavelengths. Manual background correction points were used for all measurements.

6.3.2 Instrumentation - Axial ICP Spectrometer

Axial profiles were acquired using a Perkin-Elmer Optima 3000 DV (dual view) echelle spectrometer (The Perkin-Elmer Corp., Norwalk, CT, USA). This instrument also employs a segmented array charged coupled device detector (SCD) and may be used in either radial or axial mode. The latter mode of viewing orientation was used in this part of the study. The operating conditions are given in Table 6.2.

Measurements were taken by viewing the plasma 'end-on' across the complete spatial surface, as described in Section 4.3.1 and represented by Figure 4.1. All readings were automated by constructing a program within the instrument software. No modifications to the torch were made.

RF Generator	
Frequency	40 MHz, free running
Forward Power	1100 W
Sample Introduction System	
Nebuliser	Ebdon v-groove high solids
Torch	Perkin-Elmer DV Demountable with 2.0 mm i.d. alumina injector
Spray Chamber	Perkin-Elmer 'Ryton' Scott double -pass
Peristaltic Pump	Gilson Minipuls 3, computer controlled
Sample Flow Rate	1.0 ml min^{-1}
Argon Gas Flow Rate	
Plasma	14 L min^{-1}
Auxiliary	1.0 L min^{-1}
Nebuliser	0.8 L min^{-1}
Spectrometer	
Resolution	High resolution setting (31 × 250 μm)
Fe I wavelengths	382.043 nm 385.991 nm

Table 6.2 - Axial ICP operating parameters

The high resolution setting of the spectrometer slit width was used to ensure that no overlap of consecutive viewing zones occurred. The dimensions of the high resolution slit are identical to those of the radial Optima 3000 instrument (31 × 250 μm).

The emission intensity of the Fe 385.991 nm and 382.043 nm atom lines were measured, again by accessing the U II 385.958 and Eu II 381.967 subarrays respectively on the visible channel detector. All emission intensity measurements were background corrected.

6.3.3 Chemicals and Reagents

Reagents used in this work were of 'AnalaR' reagent grade (Merck, Poole, UK). Solutions and slurries were prepared with doubly deionized water.

6.3.4 Slurry and Solution Preparation

Slurries were prepared using the 'bottle and bead method' (30). A 10 000 μg ml^{-1} stock slurry was prepared by grinding Fe_2O_3 with 0.5 % Triton X-100 (non-ionic) dispersant to prevent coagulation and agglomeration of the particles. This dispersant was found to sustain stable slurries with mean particle size ranges of less than 1.5 μm in diameter. This is desirable if the analytical recovery of a slurry is to be comparable to that of an equivalent solution (56). Serial dilution in 0.5 % Triton X-100 of the stock slurry was performed to obtain 100 μg ml^{-1} Fe containing slurries. The particle size of the slurry and true dispersion were verified using optical microscopy immediately prior to aspiration into the ICP.

$FeCl_2.4H_2O$ was used to prepare a stock 10 000 μg ml^{-1} Fe solution. Serial dilution of this solution was carried out to prepare 100 μg ml^{-1} solutions which were matrix matched for dispersant (0.5 % Triton X-100).

To all solutions and slurries, equimolar amounts (0.05 M) of EIEs were added. This procedure was similar to that described in Chapters 4 and 5 where the effect of easily ionisable elements on emission intensity was measured on Mg and Fe solutions and slurries. The EIEs added were Li, Na, K and Cs (as their respective nitrate salts). The effect of Cs upon excitation temperature was not investigated when the plasma was viewed axially.

6.4 Results And Discussion

6.4.1 The Effect Of EIEs on the Excitation Temperature When Viewing the Plasma Radially

Given that EIEs cause a 'real' enhancement of the emission intensity of an analyte for both solutions and slurries, as shown in Chapter 5, their effect upon the assumed LTE excitation temperature (T_{exc}) using the two line method was calculated. Relative intensities for the two lines (Fe I 382 and 385 nm) were measured simultaneously on a particular solution or slurry for a given EIE. As these intensities are employed as a ratio in calculating T_{exc} (equation 6.2) then transport effects are inherently eliminated. As stated, these particular emission lines were chosen for this work based upon the close proximity of the wavelengths, their significantly different energy states and the relatively high degree of accuracy of the gA values. Radial excitation temperatures were calculated using equation 6.2 and the physical parameters given in Table 6.3. Uncertainties for the temperature values are less than 2 % RSD at all spatial positions.

If the mechanism for population of the two states remains the same in the presence and absence of an EIE and if both states are changed to the same degree then the 'temperature' will not alter. If the above do not hold, a change in T_{exc} will be expected. Figures 6.2 and 6.3 show the radial profiles for excitation temperature at a viewing height of 4 mm ALC from the central position of the plasma out to 3.2 mm for solutions and slurries respectively. Values range from 3200 K at 0 mm up to 4000 K at 3.2 mm and the profiles are relatively flat out to 2.4 mm

Fe I Emission Line (nm)	Energy (eV)	Energy (cm^{-1})	gA ($\times 10^8 sec^{-1}$)	% error in gA values (ref. 160)
385.991	3.21	25 900	0.796	± 15%
382.043	4.10	33 096	6.16	± 10%

Table 6.3 - Physical constants used to calculate T_{exc}

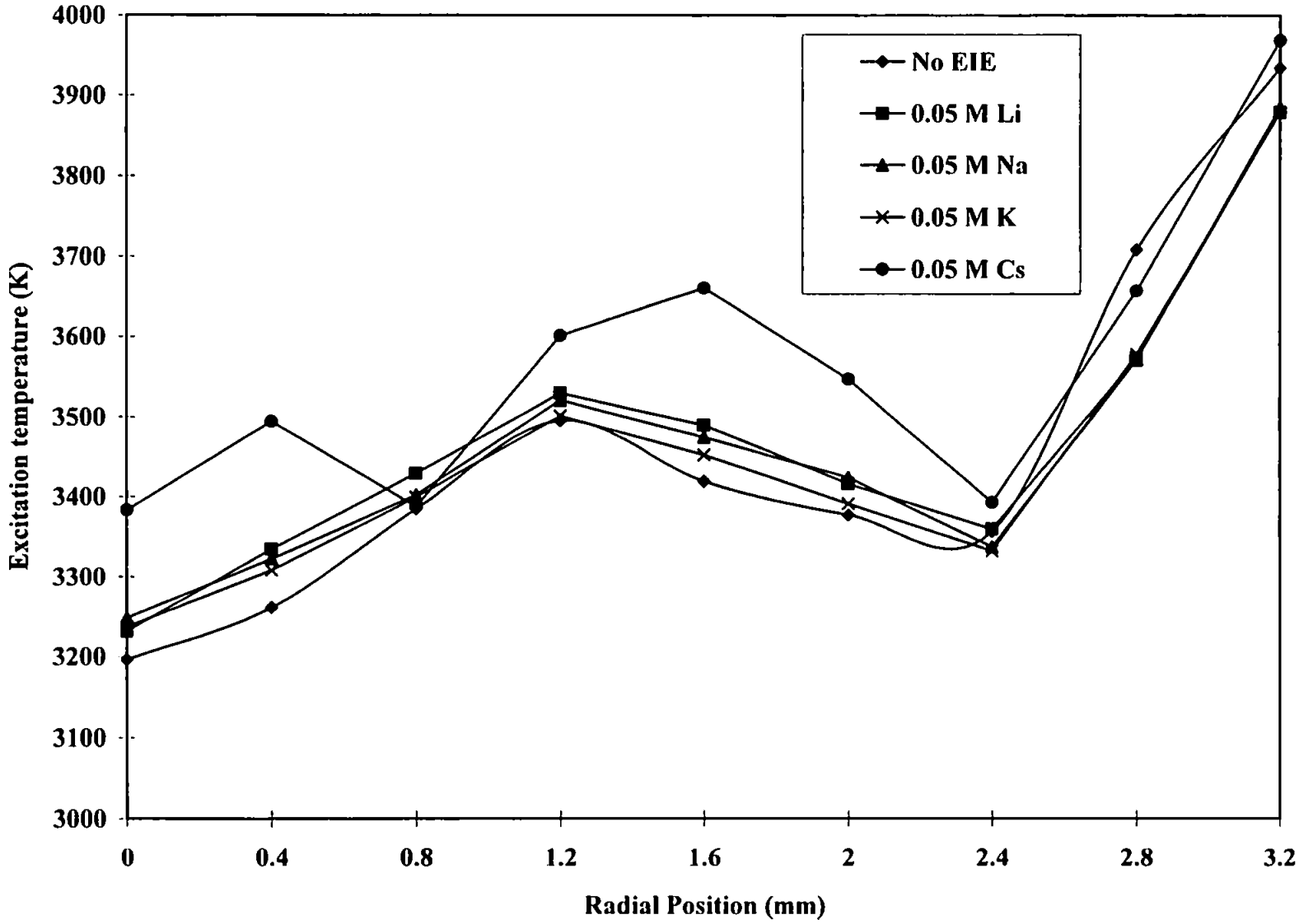

Figure 6.2 - Variation of Texc with radial position for solutions when various EIEs are added

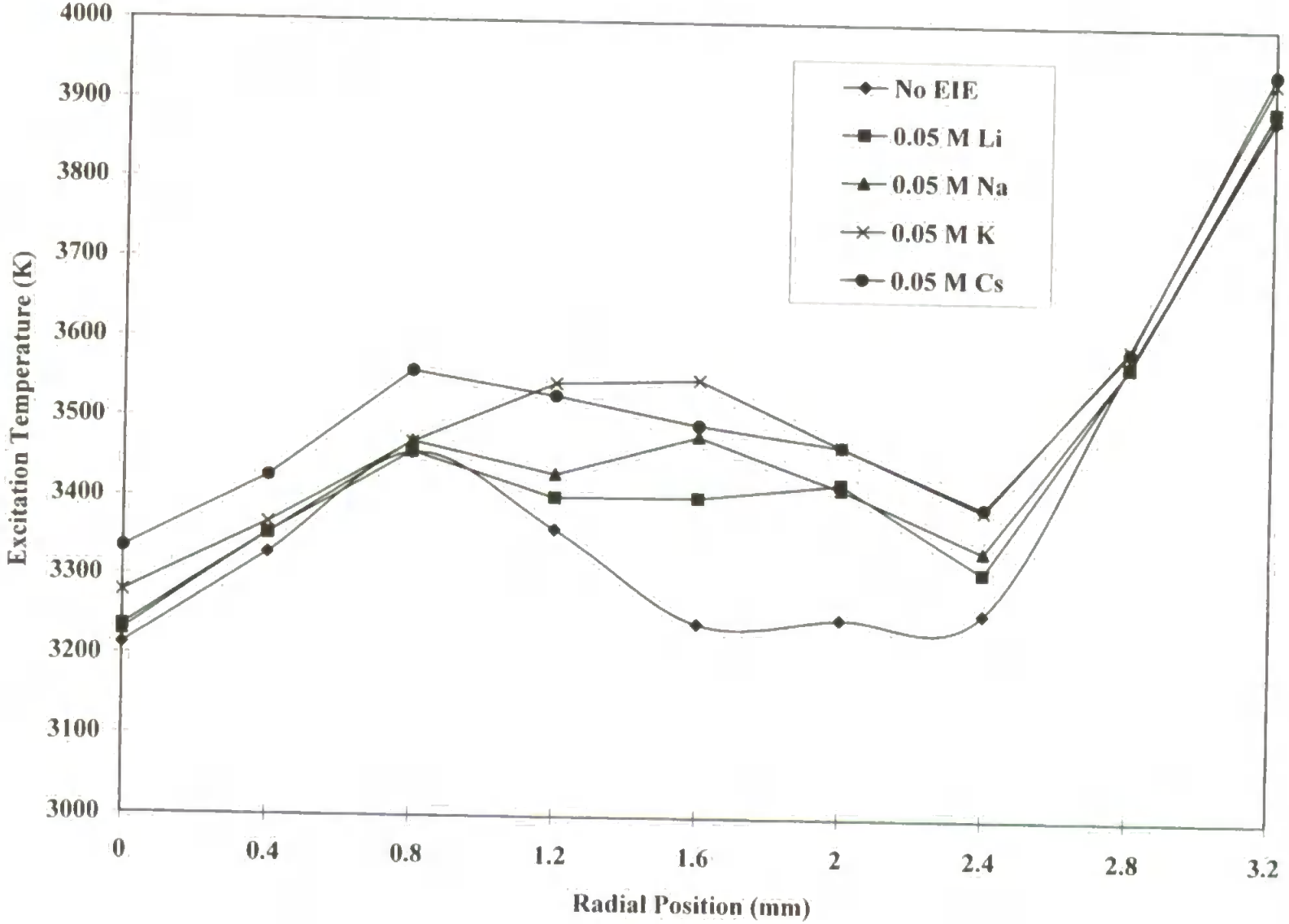

Figure 6.3 - Variation of Texc with radial position for slurries with various EIEs are added

for both solutions and slurries. However, some structure can be seen. The presence of Li, Na and K, together with the iron species show similar temperature trends in a solution system. Caesium shows a greater enhancement of the 'temperature' from iron at various points e.g. 0.4 and 1.6 mm. This effect is lost at 2.4 mm for Cs. The slurry radial temperature profiles while showing some similarities to solutions in structure appear broader in the presence of different EIEs. Values of T_{exc} beyond 2.4 mm begin to rise in both systems for all matrices, as expected, where the 'hotter' plasma body exerts its influence on entrained species.

While it has been shown that 'real' enhancement occurs in the presence of EIEs for both lines, the temperature values, based on the ratio $I_{\lambda 1}/I_{\lambda 2}$ manifest the 'differences' in enhancement for the two lines employed. Full Boltzmann plots show that the 'temperature' is dependant upon the thermometric species used and the analytical lines chosen. When these are held constant, in this case Fe I at 382 and 385 nm, the relative variation in temperature when modifying a particular parameter i.e. the presence and absence of EIEs, circumvent the need for absolute temperatures in order to study the effect from EIEs.. The values of T_{exc} shown in the radial profiles therefore present the relative change in magnitude of enhancement for the emission lines and hence the relative change in population of the two excited states.

If lateral diffusion effects are involved in the enhancement of these lines then at the centre of the plasma these effects would, most likely, be absent; both species Fe I and EIE entering together. The magnitude of the difference in enhancement would revert to the order Cs>K>Na>Li>No EIE and would be displayed as such by the temperature values. Table 6.4 shows the solution and slurry T_{exc} values for the central radial position 0 mm, at 4 mm viewing height. The trend in these values is similar to the order stated with, for solutions, Cs giving the highest value of approximately 3380 K, Na of 3250 K and 3200 K when no EIE is present. The slurry values are comparable. The relatively small change in temperature values with EIE must be considered in the 'light' of the form of the equation used to calculate them. The logarithmic

Solution	T_{exc} (K) *	Slurry	T_{exc} (K) *
Fe only	3196	Fe only	3212
Fe + 0.05 M Li	3231	Fe + 0.05 M Li	3234
Fe + 0.05 M Na	3247	Fe + 0.05 M Na	3229
Fe + 0.05 M K	3236	Fe + 0.05 M K	3277
Fe + 0.05 M Cs	3383	Fe + 0.05 M Cs	3333

Table 6.4 - T_{exc} values at radial position 0 mm for solutions and slurries

* Uncertainites less than 2 % RSD at all spatial positions

term log $I_{\lambda 1}/I_{\lambda 2}$ of equation 6.2 serves to compress the differences in intensities and hence the final value of T_{exc}. Values of T_{exc}, obtained using various other Fe I lines at comparable instrument settings are higher and the region of 5000-6000 K (161-166).

The relatively low value of T_{exc} between 0 mm and 2.4 mm, of around 3500 K, may in part be attributed to the particular lines chosen but may also be due to the region of the plasma where the spatial measurements are sampled. All radial profiles were obtained low in the plasma, at 4 mm ALC, in the region of the initial radiation zone. 'Temperatures' increase higher in the plasma towards the normal analytical zone from where emission measurements are normally taken. In addition, isocontour plots of electron number density, n_e (170) show that at the RF power level used in this work, n_e is relatively low in the centre of the plasma at a viewing height of 4 mm ALC. Low excitation temperatures are associated with lower values of n_e.

6.4.2 The Effect of EIEs on the Excitation Temperature When Viewing the Plasma Axially - Preliminary Studies

The effect of EIEs upon excitation temperature was also investigated using the axially viewed inductively coupled plasma. The same plasma conditions were employed as in the previous study which used the radial ICP. A direct comparison between the two modes of viewing could therefore be made with no influence upon T_{exc} arising due to variations in RF power or other source conditions. It is known from examination of isocontour plots of electron number density (170) that changes in the RF power of the plasma cause spatial variations in n_e. The electron number density is closely associated with the excitation temperature of a plasma according to the Saha equation (equation 4.2).

The two line method was again used to calculate T_{exc} by measuring the relative intensities of the Fe I 382.043 and 385.991 nm emission lines

simultaneously for a particular solution or slurry with various EIEs added. The excitation temperatures were calculated using equation 6.2 and the physical parameters used for the radial study (Table 6.3).

Figure 6.4 shows the spatial profile for T_{exc} when the plasma is viewed axially for a 100 μg ml^{-1} Fe solution. Values of T_{exc} range from approximately 3800 K at the centre of the profile to 6000 K towards the edge of the profile. As mentioned in the previous section (6.4.1) the increase in temperature may be attributed to the plasma body region being relatively 'hotter' than that of the central channel, therefore influencing excitation to a greater degree. Some spatial structure may be observed in Figure 6.4. The profile shows approximate circular symmetry and the excitation temperature is seen to increase gradually towards the edge of the profile.

The addition of Li to the solution matrix causes this spatial structure to be lost (Figure 6.5). The profile has no circular symmetry and appears to be 'jagged' with various 'peaks and 'troughs'. Values of T_{exc} range from 3800 to 6000 K, illustrating that the addition of this EIE to the solution matrix does not appear to cause an increase in T_{exc}. Previous studies of an axially viewed plasma (Chapter 4) illustrated that solution emission intensity ratios for Mg atom and ion lines showed enhancement upon the addition of EIEs to the analyte matrix. Studies carried out in Chapter 5 also showed enhancement from 'corrected' atom emission intensities when the plasma is viewed radially in the presence of such matrix elements. Large differences in T_{exc} radial profile values upon addition of various EIEs were not observed.

The addition of Na and K to a 100 μg ml^{-1} Fe solution gives similar axial profiles to that obtained for Li and show complex spatial structure. The range of values obtained axially for T_{exc} when EIEs are added to such a solution are given in Table 6.5. No increase in excitation temperature is observed when EIEs of different mass are added and no trends are apparent.

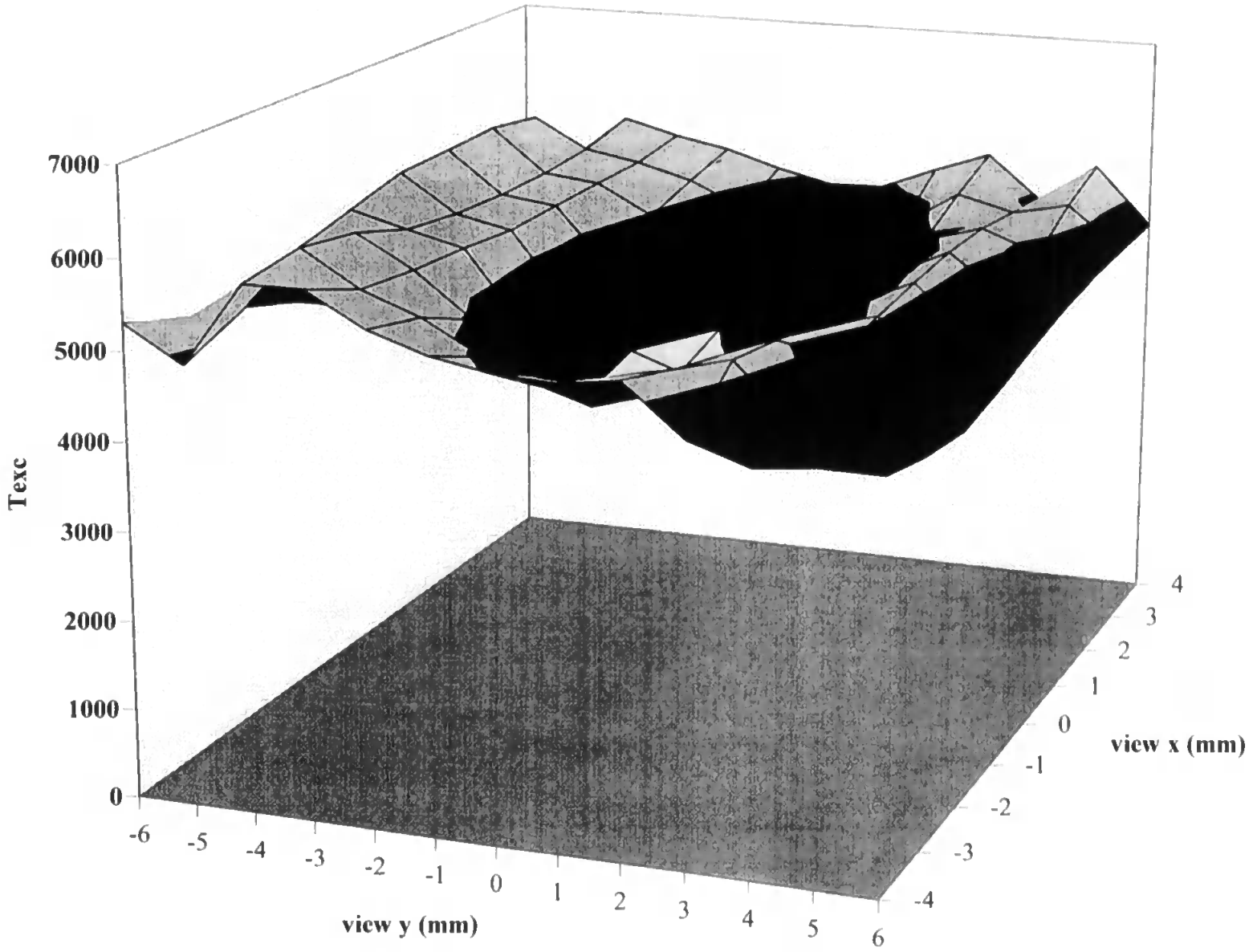

Figure 6.4 - Excitation temperature spatial profile for a 100 µg ml-1 Fe solution with no EIE added

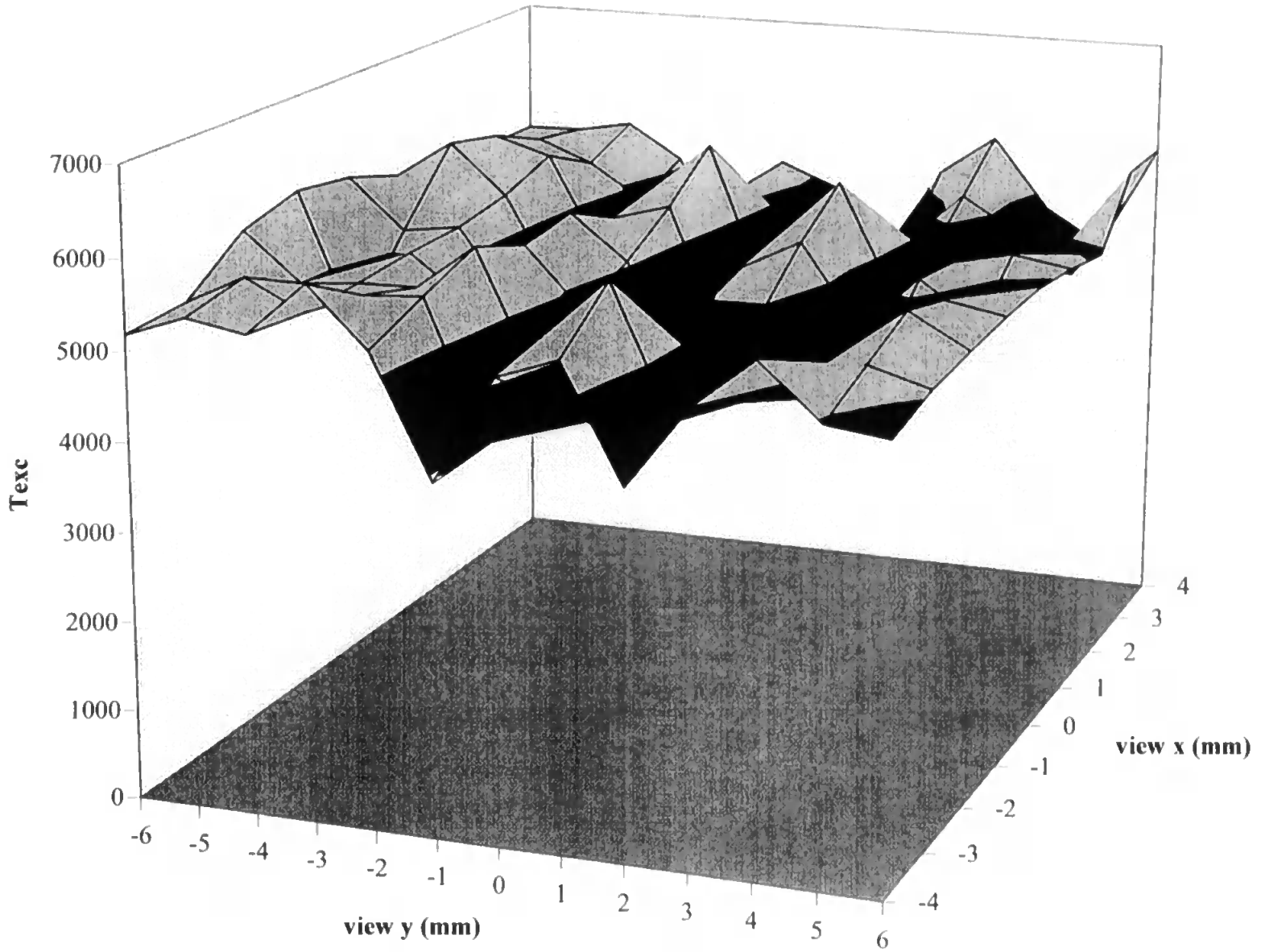

Figure 6.5 - Excitation temperature spatial profile for a 100 µg ml-1 Fe solution with 0.05 M Li added

Solution	T_{exc} range (K)*	Average value of T_{exc}*	T_{exc} at centre of profile*	Slurry	T_{exc} range (K)*	Average value of T_{exc}*	T_{exc} at centre of profile*
Fe only	3800 - 6000	4869	3793	Fe only	4250 - 6500	5419	4251
0.05 M Li	3800 - 6000	4886	3797	0.05 M Li	4200 - 6500	5368	4190
0.05 M Na	3800 - 5900	4915	3786	0.05 M Na	4150 - 6500	5347	4149
0.05 M K	3800 - 6000	4872	3790	0.05 M K	4180 - 6500	5236	4143

Table 6.5 - T_{exc} values for solutions and slurries in an axially viewed ICP

* Uncertainty values are less than 2 % RSD at all spatial positions.

Figure 6.6 is the spatial T_{exc} profile for a 100 μg ml^{-1} Fe slurry when the plasma is viewed axially. Again, it can be seen that complex spatial structure is observed and the profile is very similar to that obtained when an EIE is added to a solution. The addition of EIEs to slurries results in similar T_{exc} spatial profiles, as observed for EIE addition to solutions. The range of T_{exc} values for slurries are also given in Table 6.5. It can be seen that these T_{exc} ranges for slurries are very similar and show no apparent differences for the three EIEs studies in this work. No significant trends are seen upon EIE addition as were found when the plasma was viewed radially. It can be seen that the T_{exc} range of values for slurries are slightly higher (by approximately 400 - 500 K) than those obtained for solutions. The average excitation temperature across the axially viewed plasma was calculated for solutions and slurries and these results are given in Table 6.5. The average excitation temperature is not significantly affected upon addition of EIEs to either solutions or slurries and is in the region of 4900 K for solutions and 5400 K for slurries. Average values of T_{exc} across the plasma for slurries are therefore approximately 500 K higher than for solutions. Also given in Table 6.5 are the excitation temperatures calculated at the centre of the axial plasma profile. For the solutions analysed, this temperature is approximately 3800 K and is unaffected by the addition of EIEs. The values of T_{exc} in the centre of the profile are, therefore, lower than the mean excitation temperature, indicating that T_{exc} is lower in the central channel of the plasma and higher towards the plasma body. For slurries, T_{exc} at the plasma profile centre is approximately 4200 K which, again is significantly lower than the mean value of T_{exc} for each of the slurries.

The addition of EIEs to the solution and slurry matrices does not seem to effect the values of T_{exc} when the plasma is viewed axially. However, this does not mean that the two Fe I emission lines, used to calculate T_{exc} according to equation 6.2, are unaffected by the matrix elements. Enhancement or depression of the two lines may occur when an EIE is added but if no apparent effect is observed on T_{exc}, the enhancement or depression for both emission lines must be very similar in magnitude, as described by the

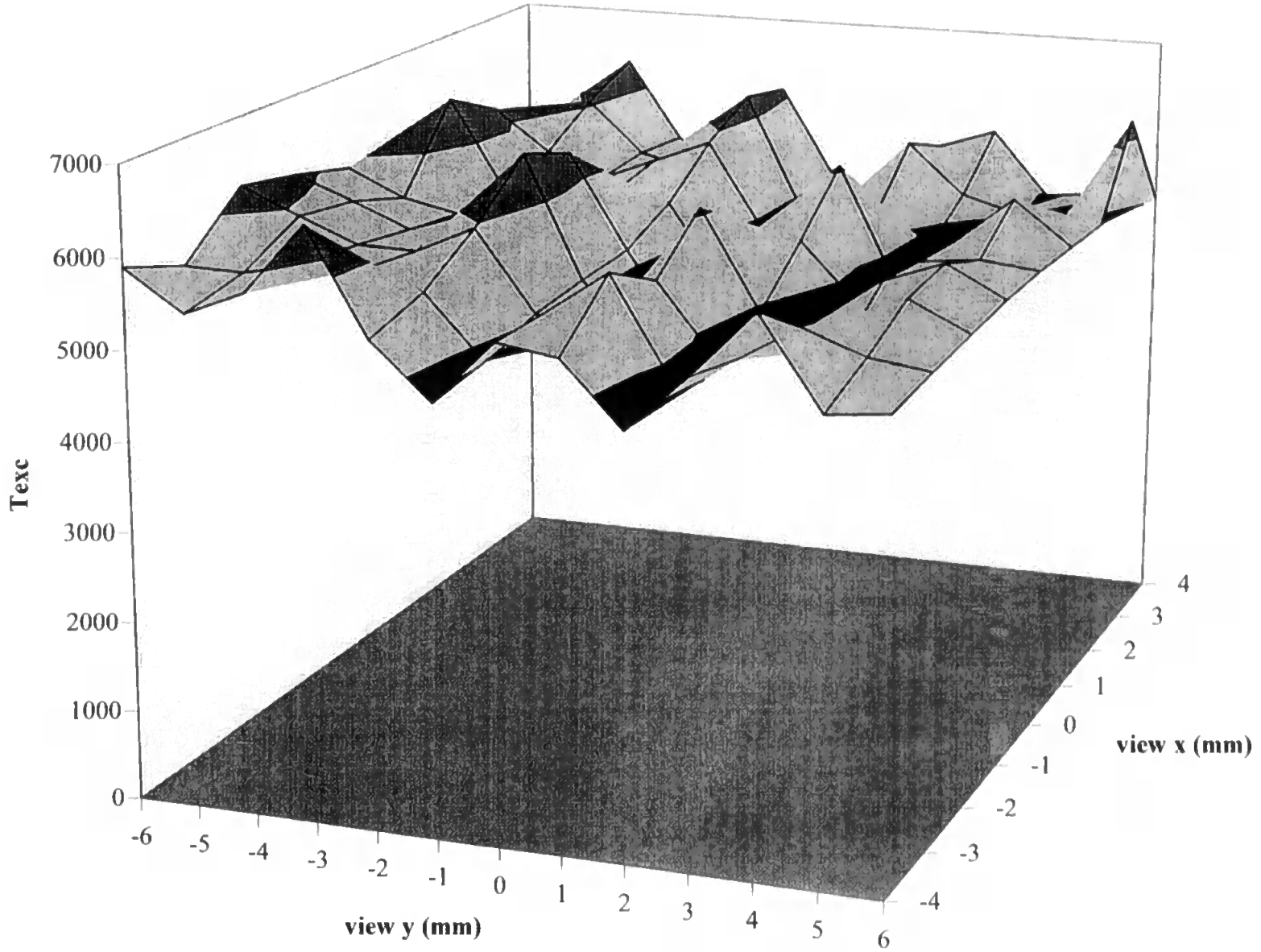

Figure 6.6 - Excitation temperature spatial profile for a 100 µg ml-1 Fe slurry with no EIE added

scenarios illustrated in Figure 5.9a and b.. In summary, for no observable effect on T_{exc} upon EIE addition:

$$\log \frac{I^1_{\lambda 382}}{I^1_{\lambda 385}} = \log \frac{I^2_{\lambda 382}}{I^2_{385}}$$

where I^1_λ is the emission intensity when no EIE is added and I^2_λ is the emission intensity upon EIE addition.

Values of T_{exc} obtained using a radially viewed plasma for the same thermometric species were in the region of 3200 - 3800 K. For the axially viewed plasma, higher values of T_{exc} are obtained. When the plasma is viewed axially, the emission of the analyte is observed through the entire optical depth of the plasma and the contribution from all emitting species, giving rise to a 'collective' intensity at a particular spatial position, are considered in calculations based on emission intensity. In a radially viewed plasma, radial profiles of excitation temperature are based on emission intensity readings at a particular viewing height. For the atom lines used in this study, the viewing height where emission intensity observations were made was low in the plasma where the plasma is relatively cooler. In an axially viewed plasma, 'hotter' regions of the plasma are taken into consideration when calculations of T_{exc} are performed, therefore T_{exc} values are higher and are comparable to values of T_{exc} quoted in the literature (161-166) when Fe is used as the thermometric species and plasma operating parameters are comparable. Alder *et al.* (163) and Houk *et al.* (166) calculated T_{exc} to be approximately 6000 K at a viewing height of 4 mm ALC and using Fe I emission lines.

6.5 General Discussion and Conclusions

The effect of EIEs upon excitation temperature has been measured using a two line ratio method derived from the Boltzmann equilibrium. Both emission lines were measured simultaneously, therefore transport effects were

eliminated when comparisons between excitation temperature values for various systems were made. It was found that the addition of an EIE to a solution or slurry caused T_{exc} to range from 3200 to 4000 K across the radial plasma profile (0 to 3.2 mm). 'Temperatures' increase to 3500/3700 K at 1.6/2.0 mm and show a peak consistent with the position of the carrier flow - plasma body interface. Beyond 2.4 mm (just into the plasma body) the values of T_{exc} rise to 4000 K (from entrainment of species). Values of T_{exc} shown by the radial profiles reflect the relative change in magnitude of enhancement for the emission lines used and therefore indicate changes in population of the excited states. Values of T_{exc} for solutions and slurries, measured at the centre of the plasma profile, show Cs to give the highest T_{exc} values and the solution or slurry system with no EIE added, the least. Although the variation in T_{exc} upon the addition of an EIE is small, the trends observed are similar to the trends in enhancement obtained when various EIEs are added to solution and slurry systems. The relatively low values of T_{exc} may be attributed to both the low viewing height ALC where measurements were taken and/or the particular analytical emission lines chosen.

Preliminary studies using an axially viewed ICP show that the addition of EIEs to both solutions and slurries does not significantly effect values of T_{exc}. Mechanisms populating the Fe atom lines used to calculate T_{exc} may not be effected upon EIE addition or ,conversely, both lines may be effected to the same degree which results in no observable enhancement or depression of temperature. Preliminary studies indicate that the addition of an EIE to a solution or slurry matrix gives complex axial spatial temperature profiles which are not easily interpreted. Values of T_{exc} measured axially are comparable to literature values obtained using similar plasma operating conditions. This is because measuring T_{exc} using an axially viewed plasma takes into consideration all emission from the central channel of the plasma, including the 'hotter' regions. In contrast, radially obtained values of T_{exc} were lower than those documented in the literature due to only a selected, cooler region of the plasma being employed for temperature measurements (the IRZ).

Chapter 7 - Silicon Speciation Using High Performance Liquid Chromatography - Inductively Coupled Plasma Atomic Emission Spectrometry

7.1 Introduction

High performance liquid chromatography (HPLC) coupled with inductively coupled plasma atomic emission spectrometry (ICP-AES) is now a well established technique used where knowledge of the chemical form of an element and quantitative information is required. The separation ability of reversed phase HPLC coupled with the sensitivity offered by ICP-AES is attractive for characterising compounds in areas such as clinical chemistry, environmental chemistry, food science, forensic science and toxicology.

Silicon is the second most abundant element on the surface of the earth and constitutes about 28 % by weight (oxygen is the most common at 47 %). It may exist in the elemental form silicon, found in human hair, bones, epidermis and dental enamel (171); as the oxidised form silica, SiO_2, a significant constituent of concretes, ceramics and other building materials (172); as silicates, used in analgesics and antacids and excreted in the urine within hours of exposure (173) ; or in the organosilicon form known commonly as silicones.

Among the organosilicon compounds, polydimethylsiloxanes (PDMS) represent the most important class because of the quantity produced (ca 700,000 tons in 1990) (174). Biomedical applications of PDMS are numerous (175). They are used to formulate replacement joints, in intravenous tubing, in retinal surgery, as antiflatulence products and, most commonly, in plastic and reconstructive surgery. During the last 30 years, PDMS gel filled implants have been used extensively in reconstructive mammaplasty, primarily because PDMS was considered to be nonbiodegradable and chemically, immunologically and physiologically inert (176) and thus to have no ill effects in humans (177). However, a number of reports made in recent years have

highlighted the hazards of low molecular weight migratable degradation products in breast implants, summarised in a review by Talcott (178).

Breast implants have been associated with human adjuvant disease (179,180) and silicone lymphadenopathy (181). In addition concerns about problems associated with breast implants have recently expanded to include physical, biochemical and immunological responses to PDMS (182). Questions concerning an increased cancer risk to women with these implants have been raised. However, a detailed review of the literature by Edelman *et al.* yielded no evidence to support this association (183).

An estimated 1 - 2 million women in the US have used silicone breast implants. Indications from the breast implant global settlement response and new litigation on face or body cosmetic implants suggest that we are now in the midst of an epidemic with thousands of women and children ill from silicon related disease (178). Exposure of children to implant related disease by migration through placental walls or by breast feeding has been documented (184-187).

PDMS polymers, which form the silicone gel in breast implants are manufactured from elemental silicon. The silicone rubber implant shell is also made of PDMS with fumed, amorphous silica added as a 'strengthening' filler (188). It has been shown (189) that the implant gel filling can 'bleed' through the implant wall over time. In addition, the implant may frequently deteriorate due to the absorption of body fluids (190, 191) and the formation of cracks that result in implant rupture.

The migration of organosilicon compounds from implants to local and distant sites through a lymphatic or hematogenous pathway has been reported (192). After injection in high concentration in mice, silicone oil was found in vacuoles in adipose tissue (193,194), lymph nodes (193,194), liver (193,194), kidney (193), spleen (193, 194), pancreas (193) and ovary (193). These studies only revealed total silicon levels and did not reveal the chemical form of the

compound(s) that may have been present. This means that no information about the body's response to organosilicon compounds could be obtained.

It is known that PDMS is not chemically inert, but undergoes chemical degradation (195-197). This degradation involves siloxane bond redistribution and hydrolysis, ultimately resulting in the formation of low molecular weight organosilicon compounds. Many of the resulting hydroxy-functional hydrolysis products are water soluble and the cyclic compounds, such as octamethylcyclotetrasiloxane, and trimethylsiloxyl end blocked oligomers are volatile. It is important that these species are identified so that information about the end products of silicone metabolism and the intermediate metabolic products can be gleaned.

Silicone compounds may be separated according to polarity, solubility and size, generally by liquid chromatographic techniques (198). It has been shown (198) that inductively coupled plasma atomic emission spectrometry as a means of detection is a very sensitive method to determine the very low levels of organosilicon species that may be present in environmental samples when using an organic mobile phase. Whilst ICP-MS has been used for numerous trace element speciation studies, silicon suffers from severe interferences for the N_2^+ ion obtained from air, whilst ICP-AES does not suffer from such interferences.

Size exclusion chromatography (SEC) has been used to successfully separate high molecular mass organosilicon compounds (198,199) and ICP-AES has been employed as a detector in these studies. Hausler and Taylor (200,201) used SEC in the analysis of coal to separate organically bound metals from the matrix. Toluene was used as the mobile phase prior to introduction into the ICP. Reversed phase HPLC with ICP detection of silicon and a methanol-water gradient has been used to separate interferences from various silicon complexes (202).

Direct aspiration of organic solvents into the ICP has traditionally posed difficulties (203,204). In the past, use of a modified chromatograph-to-sample introduction system interface or modification of the spray chamber and nebuliser have been required. Boorn and Browner (205) evaluated the performance of a low power ICP for thirty organic solvents using the lack of carbon deposition on the injector of the torch as a guide to plasma tolerance. To date, however, no investigation has been reported into the effect of organic solvents when viewing the plasma axially. Although the attainment of lower limits of detection has been well documented for 'end on' viewing with aqueous systems, an investigation into the performance of axial instruments with organic sample nebulisation is required to evaluate whether or not any detection limit improvements can be made.

Given the abundance of silicon in the environment and human body, studies of the impact of organosilicon compounds in the human body requires sensitive methodology to discriminate between the various forms of silicon which may be present in clinical samples (206). The aim of this work was to identify, separate and quantify a range of PDMS breakdown compounds for such studies. The use of the HPLC-ICP system is presented for both reversed-phase and SEC modes. In addition, a direct comparison of detection limits and precision values obtained using both axially and radially viewed ICP-AES instruments for various species of silicon containing compounds has been made.

7.2 Reversed Phase Separation of Polar Organosilicon Compounds

7.2.1 Experimental

The separation of three polar silicon containing compounds (inorganic silicon, hexamethyldisiloxane and 1-3, tetramethylsilane-diol) using reversed phase chromatography was implemented using a Phenomenex ODS C_{18} capped column, 250 × 2 mm i.d. (Phenomenex, Macclesfield, UK). The column was maintained at room temperature throughout the study and samples eluted with an isocratic mobile phase consisting of 30 % methanol in filtered, de-

ionised water (Milli-Q, Millipore, Harrow, UK). The liquid flow rate was 1.0 ml min^{-1}.

Two liquid chromatograph-spectrometer configurations were used in this study so that comparisons could be made between the analytical performance of radially and axially orientated inductively coupled plasma instrumentation.

7.2.1.1 Instrumentation - Radial Viewing of the ICP

The first chromatographic system to be implemented employed a Perkin-Elmer 410 LC pump (Perkin-Elmer Ltd., Beaconsfield, UK) coupled with a radially viewed Perkin-Elmer Optima 3000 ICP atomic emission spectrometer. The Optima 3000 is equipped with a segmented array charged coupled device detector and echelle monochromator and permits the simultaneous monitoring of more than one wavelength. The ICP was operated under the conditions listed in Table 7.1.

The use of organic solvents in the plasma generally requires more robust operating conditions than those employed for conventional aqueous samples. An increase in RF power and coolant gas flow produces a stable plasma discharge that can be operated for an appreciable length of time without carbon deposition on the alumina injector of the quartz torch. In addition, the velocity of the sample in the ICP may be increased by increasing the nebuliser gas flow. A disadvantage of this however may be lower analytical signal readings due to the lower residence time of the analyte in the ICP.

The introduction of organic solvents into the ICP results in a green plasma plume, characteristic of C_2 emission. Plasma resistance to organic solvents is manifested by an increase in reflected power of the instrument. The free running generator of the Optima 3000 series of instruments brings about adjustment of the variable capacitors via a matching circuit. If the reflected power increases dramatically a safety mechanism operates that extinguishes the plasma to prevent damage to the RF generator. For this reason, the

PARAMETER	RP-HPLC-ICP-AES
Frequency (MHz)	40
Forward Power (W)	1150
Plasma Gas Flow Rate ($l\ min^{-1}$)	15
Auxiliary Gas Flow Rate ($l\ min^{-1}$)	1.0
Nebuliser Gas Flow Rate ($l\ min^{-1}$)	0.8
Solvent	MeOH/H_2O (30:70 %)
Solvent Flow Rate ($ml\ min^{-1}$)	1.0
Silicon Wavelength (nm)	251.611
Nebuliser	P.E. 'Gem Tip' cross flow
Spray Chamber	P.E. Scott Double Pass

Table 7.1 - Operating conditions for the radially viewed ICP - Reversed Phase HPLC System

introduction of an organic solvent into the ICP must be brought about gradually so that the matching circuits in the RF generator may adjust in small increments to compensate for the mismatching of the plasma impedance.

7.2.1.2 Data Acquisition for the Radially Viewed ICP-Chromatographic System

A macro program was written within the Optima 3000 Unix software that enabled up to 300 replicates of a sample to be performed sequentially. The peak area of the background corrected spectra was calculated by integrating 3 pixel widths on the corresponding subarray of the solid state detector. An emission intensity reading was recorded every 10 seconds which was the minimum time interval for consecutive sample readings. The ICP emission signal information was stored on a database and converted via a conversion program to DOS format. The converted files were then suitable for importing into a Perkin-Elmer Turbochrom 4 chromatographic data system, providing integrated chromatographic peak areas.

7.2.1.3 Instrumentation - Axial Viewing of the ICP

The chromatograph consisted of a Perkin-Elmer series 200 LC pump coupled to a Perkin-Elmer Optima 3000 DV ICP emission spectrometer (The Perkin-Elmer Corp., Norwalk, CT).

Optimum power and nebuliser gas flow were found using on-board directed search and exhaustive search algorithms in the Perkin-Elmer Optima 3000 ICP Unix software using the signal to background ratio as the figure of merit. Plasma operating conditions are given in Table 7.2. For a direct comparison between axial and radial instruments, plasma source conditions were optimised for each viewing orientation. As previously mentioned, the introduction of organic solvents into the ICP results in a characteristic green plasma plume. The Optima 3000 DV employs a shear gas which cleaves the

PARAMETER	RP-HPLC-ICP-AES
Frequency (MHz)	40
Forward Power (W)	1450
Plasma Gas Flow Rate ($l\ min^{-1}$)	15
Auxiliary Gas Flow Rate ($l\ min^{-1}$)	1.0
Nebuliser Gas Flow Rate ($l\ min^{-1}$)	0.8
Solvent	MeOH/H_2O (30:70 %)
Solvent Flow Rate ($ml\ min^{-1}$)	1.0
Silicon Wavelength (nm)	251.611
Nebuliser	P.E. 'Gem Tip' cross flow
Spray Chamber	P.E. Scott Double Pass

Table 7.2 - Operating conditions for the axially viewed ICP - Reversed Phase HPLC System

plasma plume to prevent self absorption in this region so most C_2 emission can be seen in the central channel of the plasma.

7.2.1.4 Data Acquisition for the Axially Viewed ICP-Chromatographic System

A novel data acquisition system for the construction of chromatograms was developed for this work. Using Perkin-Elmer ICP "Winlab' software (The Perkin-Elmer Corp., Norwalk, USA) it was possible to measure transient signals by manipulation of the sample integration time and number of sample replicates measured. The peak area of the background corrected spectra was calculated by integrating 3 pixel widths on the corresponding subarray of the solid state detector. All data was stored to a database in Winlab. Chromatograms were then constructed by plotting net emission intensity values as a function of time using Microsoft Excel 5 and Microsoft Query programs. Integrated chromatographic peaks can be easily calculated in Excel 5. By using this method of data manipulation, data density may be improved by a factor of 5 when compared to data acquisition using Perkin-Elmer Unix software due to the increase in the number of data points.

7.2.1.5 Sample Introduction System

Injections of standards and samples into the mobile phase carrier stream were made using a Rheodyne (Cotati, CA, USA) switching valve with a 100 µl sample loop attached.

A Perkin-Elmer Scott Double-Pass spray chamber made from 'Ryton' plastic was used. A Perkin-Elmer 'Gem-Tip' cross flow nebuliser was used for aspiration of the HPLC mobile phase into the spray chamber.

7.2.1.6 Silicon Standards

The silicon standards used in the reversed phase work were i) hexamethyldisiloxane (Fluka, Gillingham, UK), ii) a 1000 μg ml^{-1} commercially prepared inorganic silicon standard (BDH, Poole, UK) and iii) 1,3-tetramethylsilanediol which was synthesised in -house (207) for use as a silanol standard. The structures of the compounds are shown in Figure 7.1. Standards were kept refrigerated until immediately before use due to their ability to undergo rapid polymerisation at room temperature.

It is an important practical consideration to avoid all glassware when dealing with these compounds due to their surface active characteristics. The use of glass flasks and bottles may lead ultimately to erroneous results. In addition, any PDMS lubricants should be eliminated from the sample introduction system and torch assembly.

Reagent grade chemicals were used throughout except where otherwise indicated. All solutions were degassed with helium prior to use.

7.2.2 Results and Discussion - Reversed Phase Separation of Polar Compounds

Low molecular weight polar and volatile organosilicon species of similar polarity were separated by reversed phase HPLC followed by element specific detection. Previous studies (198) have indicated that silanols may interact too strongly with silica based packing materials making these columns unsuitable for this study. However, a stability study over several days with a 30 % capped ODS column did not indicate performance degradation. Typical background levels with a standard C_{18} ODS column (uncapped) gave high background levels of Si that showed marked daily variation. Sensitivity and LOD values for Si degraded with time. Reproducibility from day to day was poor, typically around 20%. Limits of detection were more than an order of magnitude higher than those attained using the C_{18}

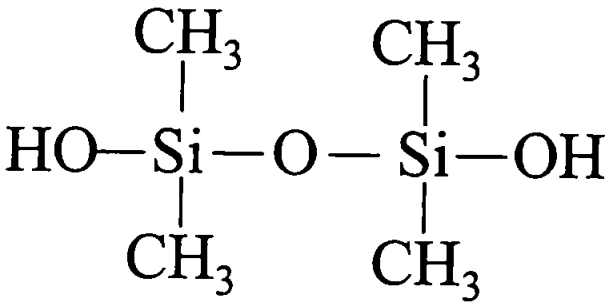

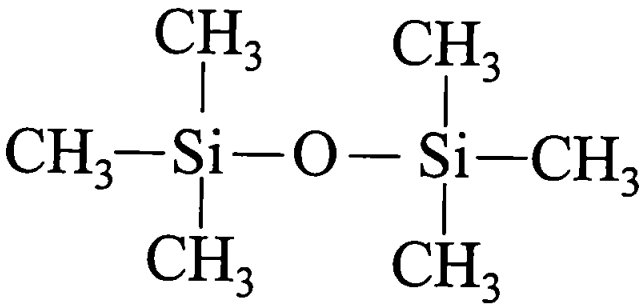

Figure 7.1 - Structures of compounds used in reversed phase HPLC: above, 1,3-tetramethylsilanediol and below, hexamethyldisiloxane.

ODS 30% capped column. The capped column resolved the compounds of interest and permitted the separation of soluble inorganic silicon species.

A typical separation of 20 μg ml^{-1} inorganic silicate (as Si), 20 μg ml^{-1} 1,3-tetramethylsilanediol (as Si) and 20 μg ml^{-1} hexamethyldisiloxane (as Si), using the radially viewed ICP chromatographic system is shown in Figure 7.2. The retention time for inorganic silicon was 3.8 minutes, 5.9 minutes for tetramethylsilanediol and 32.1 minutes for hexamethyldisiloxane. The overall reproducibility of the system for each compound was 3.2%, 5.4% and 2.3% for inorganic silicon, tetramethylsilanediol and hexamethyldisiloxane respectively.

Using this radially viewed system, calibration graphs were linear to 100 $\mu g ml^{-1}$ Si for the three compounds of interest. Comparison of the three calibration graphs prepared for the values of silicon concentration is shown in Figure 7.3. The response, or sensitivity, of the column for each compound differs significantly. The sensitivity was calculated to be 2601 peak area units/μg ml^{-1} Si for inorganic silicon, 2250 area units/μg ml^{-1} Si for tetramethylsilanediol and 1373 area units/μg ml^{-1} Si for hexamethyldisiloxane where n = 10 replicate injections. The difference in sensitivity was not a result of the ODS capped column. By removing the column and simply flow injecting the samples into the plasma a similar difference in sensitivity was observed for the three compounds. One explanation may attribute this phenomena to the different sample transport efficiency for each compound through the sample introduction system. The higher molecular weight compounds may be transported less efficiently into the plasma resulting in lower emission readings for Si and therefore a decrease in sensitivity.

The detection limits obtained were 0.1 μg ml^{-1} Si for inorganic silicon, 0.4 μg ml^{-1} Si for tetramethylsilanediol and 0.5 μg ml^{-1} Si for hexamethyldisiloxane.

A separation of 10 μg ml^{-1} inorganic silicon (as Si), 10 μg ml^{-1} 1,3-tetramethylsilanediol (as Si) and 10 μg ml^{-1} hexamethyldisiloxane (as Si)

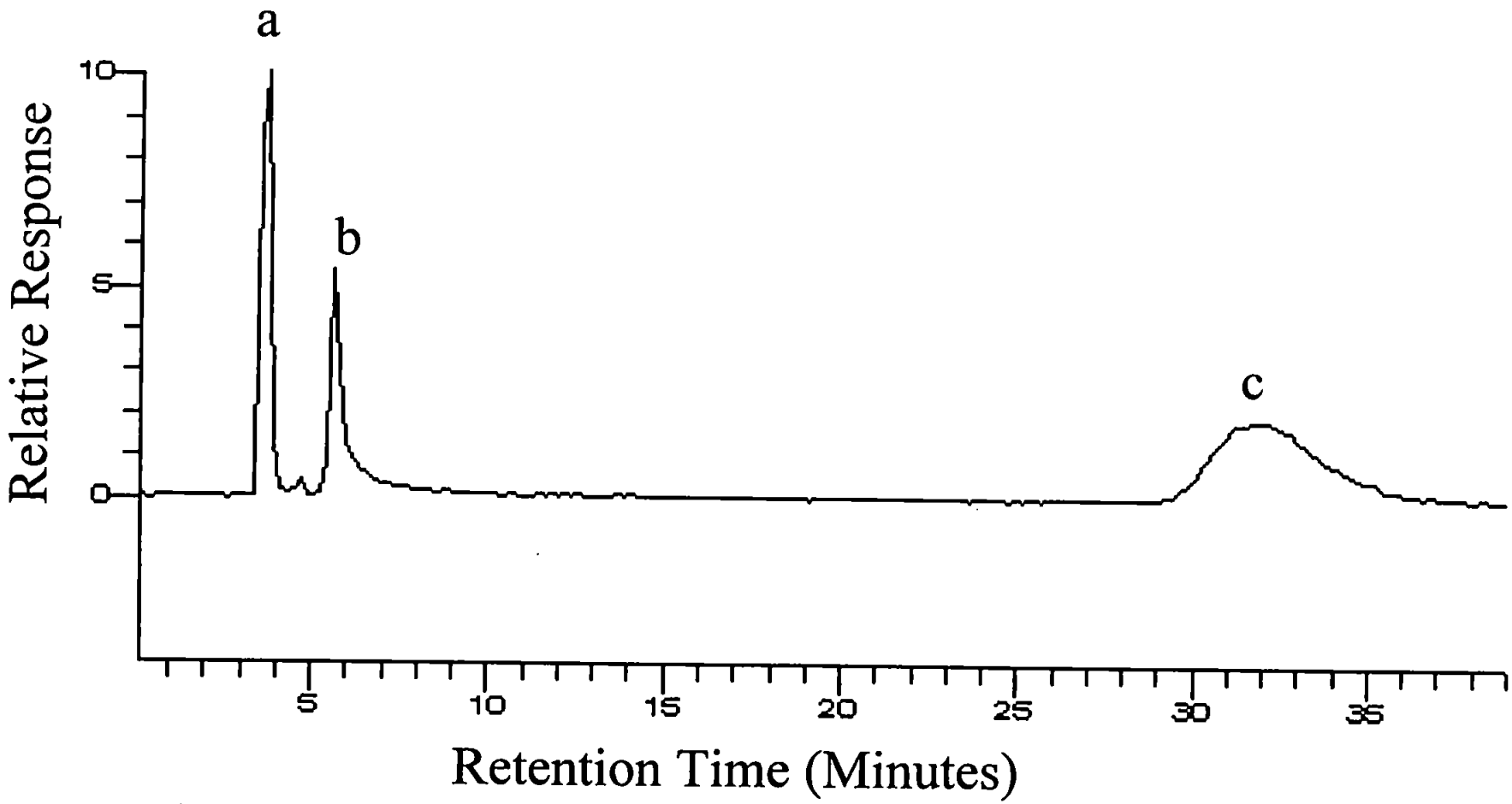

Figure 7.2 - Separation of a) inorganic silicon, b) 1,3-tetramethyldisilanediol and c) hexamethyldisiloxane by reversed phase HPLC-ICP-AES. All compounds present at 20 µg ml^{-1} Si.

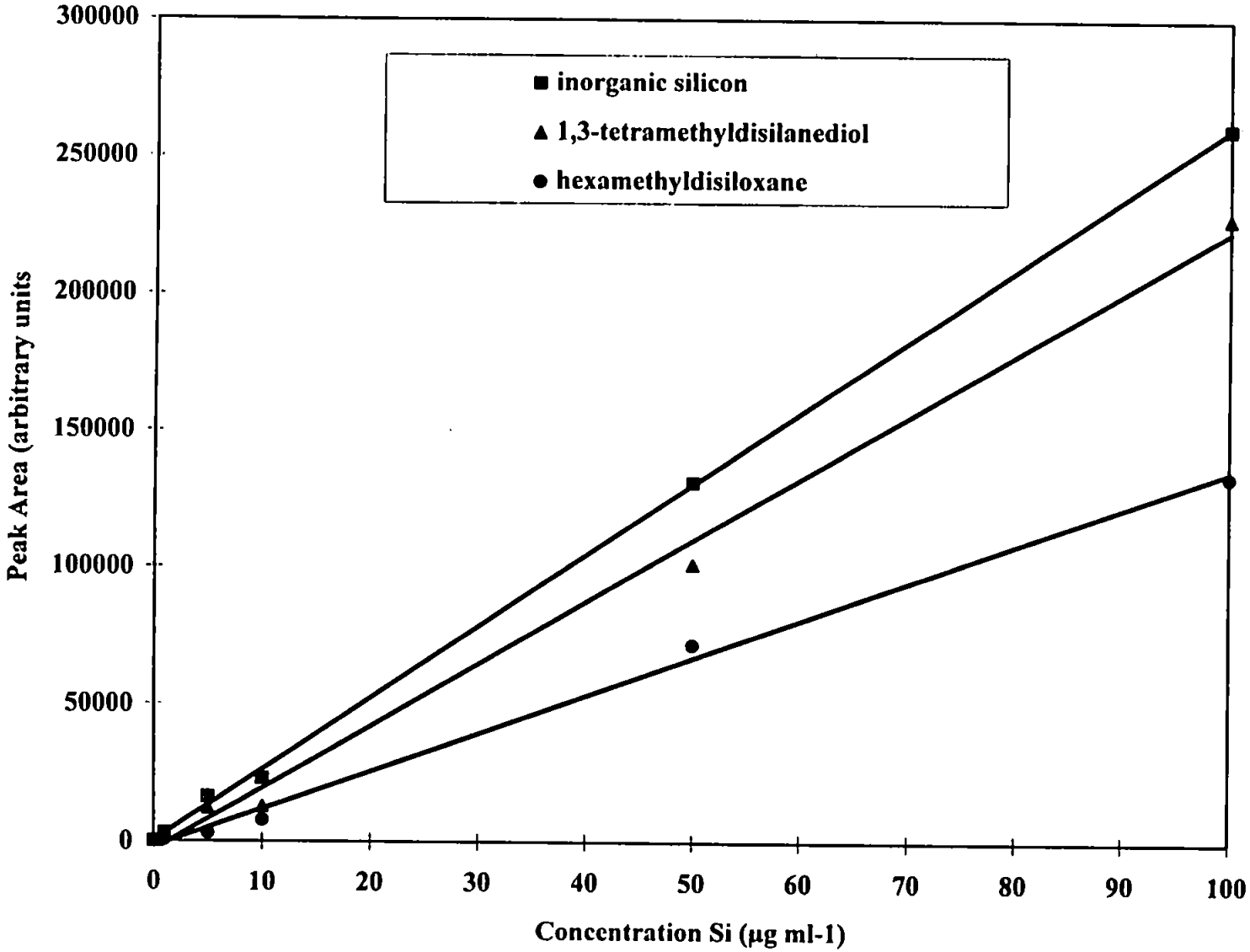

Figure 7.3 - Calibration graphs for compounds used in reversed phase HPLC-ICP-AES.

performed using the axially viewed system is shown in Figure 7.4. Retention times for the various species are 2.5 minutes for inorganic silicon, 4.5 minutes for tetramethylsilanediol and 27.9 minutes for hexamethyldisiloxane. The reproducibility of the system for each compound was 5.3%, 5.7% and 5.9% for inorganic silicon, 1,3-tetramethylsilanediol and hexamethyldisiloxane respectively, found by measuring the peak area where n = 5 replicates.

The calculated detection limits using the axially viewed ICP were 0.18 μg ml^{-1} Si for inorganic silicon, 0.30 μg ml^{-1} Si for tetramethylsilanediol and 0.48 μg ml^{-1} Si for hexamethyldisiloxane.

The use of the radial Optima 3000 ICP as a detector for these compounds indicated similar detection limits and better reproducibility, as shown in Table 7.3. It should be noted that the integration time of one second, for the data acquired using the radial Optima was the same as that used for the axial system.

It is well known that detection limits can be improved dramatically when viewing an inductively coupled plasma axially compared to radial viewing (208). A general improvement in detection limits of about a factor of five may be observed when aspirating aqueous samples into the axially viewed ICP. This is attributed to viewing the plasma along an increased path length therefore achieving a higher optical throughput. However, it has been demonstrated (208) that for samples with high levels of matrix constituents, detection limit improvement is markedly reduced. It has been shown by Boorn and Browner (205) that the introduction of organic species into a radially viewed ICP may result in poorer limits of detection for a wide range of elements. However, Evans and Ebdon (209) illustrated that the use of a water cooled spray chamber may offer potential improvements in limits of detection when organic solvents are aspirated.

Separation of silicon containing compounds using a radially viewed ICP indicates better reproducibility of this hyphenated HPLC-ICP system for

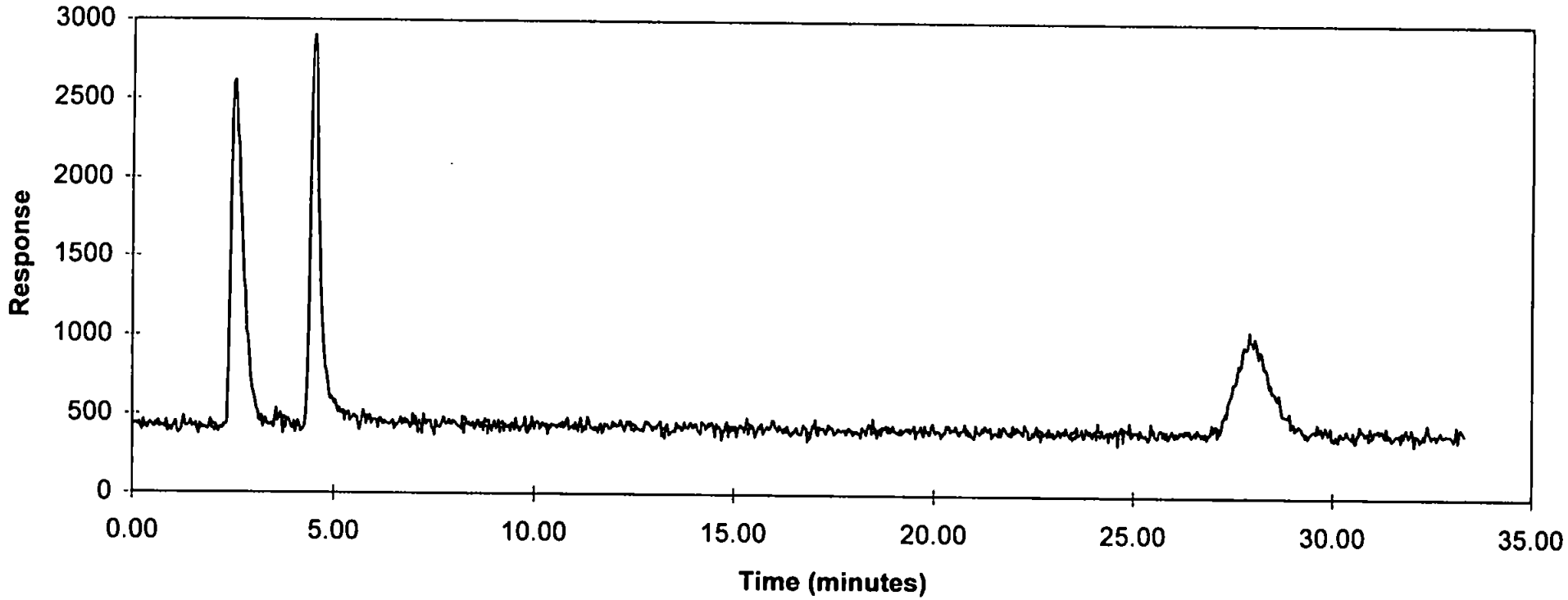

Figure 7.4 - Separation of a) inorganic silicon, b) 1,3-tetramethylsilanediol and c) hexamethyldisiloxane by reversed phase HPLC and axially viewed ICP-AES. All compounds present at 10 µg ml-1

Compound	LOD - radial ($\mu g\ ml^{-1}$)	LOD - axial ($\mu g\ ml^{-1}$)	Reproducibility - radial (%) (using 20 $\mu g\ ml^{-1}$ solution)	Reproducibility - axial (%) (using 10 $\mu g\ ml^{-1}$ solution)
Inorganic Si	0.10	0.18	3.2	5.3
Tetramethyl-silanediol	0.40	0.30	5.4	5.7
Hexamethyl-disiloxane	0.50	0.48	2.3	5.9

Table 7.3 - Comparison of detection limits and reproducibility data for axial and radial HPLC-ICP-AES systems

obtaining chromatographic peaks. Table 7.4 shows a comparison of the background equivalent concentration (BEC) and the relative standard deviation of the background (RSDB) for 10 μg ml^{-1} inorganic silicon where n = 5 replicates. The BEC determines the concentration of the analyte which is equivalent to the background at the analyte wavelength and is therefore a measure of the sensitivity of the instrument. It can be seen that the BEC values for the two modes of viewing are similar. However, the RSDB is significantly better when the analytical signal is acquired using the radial mode. The RSDB is the reciprocal of the Signal to Noise Ratio (SNR) where the "signal" in this case is the equivalent of the background signal. An increase in RSDB when viewing in the axial mode indicates an increase in the background noise. This may be attributed to the fact that the optimum viewing height can be found using a radial system where plasma noise, due to nebulisation of the organic solvent, is at a minimum. When viewing in axial mode this component of noise cannot be eliminated therefore the reproducibility of results is less precise and RSDB values are worse.

7.3 Size Exclusion Chromatographic Separations of Polydimethylsiloxane Compounds

7.3.1 Experimental

7.3.1.1 Instrumentation

Size Exclusion Chromatographic (SEC) separations were carried out using an LKB Bromma 2150 HPLC pump (Bromma, Sweden) operated in isocratic mode coupled with the radially viewed Perkin-Elmer Optima 3000. Operating conditions for the ICP for the size exclusion chromatography are shown in Table 7.5. Again, the Perkin-Elmer Scott Double Pass spray chamber and 'Gem-Tip nebuliser were used and injections made through a Rheodyne switching valve with a 100 μl sample loop. Chromatographic separations for SEC-ICP were carried out on a Phenogel 5 M3 size exclusion column 300 × 7.8 mm i.d. (5 μm) (Phenomenex) at a flow rate of 1.0 ml min^{-1} xylene. A Phenogel 5 guard column 50 × 7.80 mm (5 μm) was used in front of the column. Ambient temperature conditions were used.

Mode of Plasma observation	BEC ($\mu g\ ml^{-1}$)	RSDB (%)
Axial	0.96	6.2
Radial	0.88	3.8

Table 7.4 - Comparison of BEC and RSDB values for radial and axial systems for inorganic Si with a 30% MeOH/H_2O mobile phase

PARAMETER	SEC-ICP-AES
Frequency (MHz)	40
Forward Power (W)	1200
Plasma Gas Flow Rate ($l\ min^{-1}$)	15
Auxiliary Gas Flow Rate ($l\ min^{-1}$)	1.0
Nebuliser Gas Flow Rate ($l\ min^{-1}$)	0.6
Solvent	Xylene
Solvent Flow Rate ($ml\ min^{-1}$)	1.0
Silicon Wavelength (nm)	251.611
Nebuliser	P.E. 'Gem Tip' cross flow
Spray Chamber	P.E. Scott Double Pass

Table 7.5 - Operating conditions for the radially viewed ICP - SEC HPLC System

7.3.1.2 Data Acquisition

Chromatograms were acquired using the same methodology employed for the construction of chromatograms for the reversed phase HPLC system coupled with the radially viewed ICP spectrometer. A macro was written within the Optima 3000 Unix software that enabled up to 300 replicates of a sample to be performed sequentially. Again, the peak area of the background corrected spectra was calculated by integrating 3 pixel widths on the corresponding subarray of the solid state detector. Emission intensity readings were acquired every 10 seconds. The ICP emission signal information was stored to a database and converted via a conversion program to DOS format. The converted files were then imported into the Perkin-Elmer Turbochrom 4 chromatographic data system which enabled integration of peak areas to be calculated with ease.

7.3.1.3 Silicon Standards

Three PDMS fluids of different viscosity (measured in centiStokes) were used as standards for the SEC studies, 200/1000 cS, 200/20 cS and 200/0.65 cS (BDH). The molecular weight attributed to each standard, related to viscosity, is given in Table 7.6.

For the determination of PDMS by SEC, stock standard solutions were prepared from these standards and stored in amber coloured bottles at room temperature. Calibration graphs were constructed by plotting the area of the peak for each standard versus the PDMS concentration.

Glassware was used for all polymer work as the high molecular weight compounds do not have any significant surface active characteristics and do not silanize the glass surfaces of flasks and containers.

PDMS FLUID	MOLECULAR WEIGHT
200/1000 cS	162
200/20 cS	1500
200/0.65 cS	16500

Table 7.6 - Relationship between molecular weight and viscosity of PDMS compounds

7.3.1.4 Results and Discussion - Size Exclusion Chromatographic Separations of Polydimethylsiloxane Compounds

Size exclusion chromatographic separations of three PDMS polymers (molecular weight range 162 - 165,000) were carried out in xylene. This solvent dissolved the PDMS polymers of interest. At a liquid flow rate of 1.0 ml min^{-1} and nebuliser gas flow rate of 0.6 l min^{-1} a stable plasma was obtained. Typical chromatograms for this system are shown in Figures 7.5 and 7.6. Figure 7.5 shows the separation between the two highest molecular weight species both at 20 µg ml^{-1}. The retention time for 200/1000 cS PDMS was 7.0 minutes and 9.5 minutes for 200/20 cS PDMS. It should be noted that the two peaks were not fully resolved. Some success for improvements in resolution was indicated when the mobile phase polarity was changed by mixing xylene with a more polar organic solvent such as 10 % propanol. However, the addition of propanol caused instability of the plasma discharge which resulted in the plasma extinguishing during chromatographic separations.

Figure 7.6 shows the separation of the three PDMS polymers using 100 % xylene as the mobile phase. The retention times for 200/1000 cS, 200/20 cS and 200/0.65 cS PDMS were 7.0, 9.5 and 12.3 minutes respectively. The reproducibility of the system for each compound was 4.5 %, 2.7 % and 4.4 % for 200/ 1000 cS, 200/20 cS and 200/0.65 cS PDMS respectively. Each species was present at a concentration of 20 µg ml^{-1} Si. It can be seen that the response for each of the PDMS compounds was different. The sensitivity was calculated to be 29000, 24000 and 25000 peak area units/ µg ml^{-1} Si for 200/0.65 cS, 200/20 cS and 200/1000 cS respectively. Again, this may be due to less efficient transport efficiency of the compound through the sample introduction system and/or incomplete decomposition in the plasma.

Calibration graphs (Figure 7.7) were linear to 100 µg ml^{-1} Si for the lowest molecular weight PDMS (200/0.65 cS) and from 5 - 100 µg ml^{-1} Si for the higher molecular weight oligomers (200/20cS and 200/1000cS). Detection

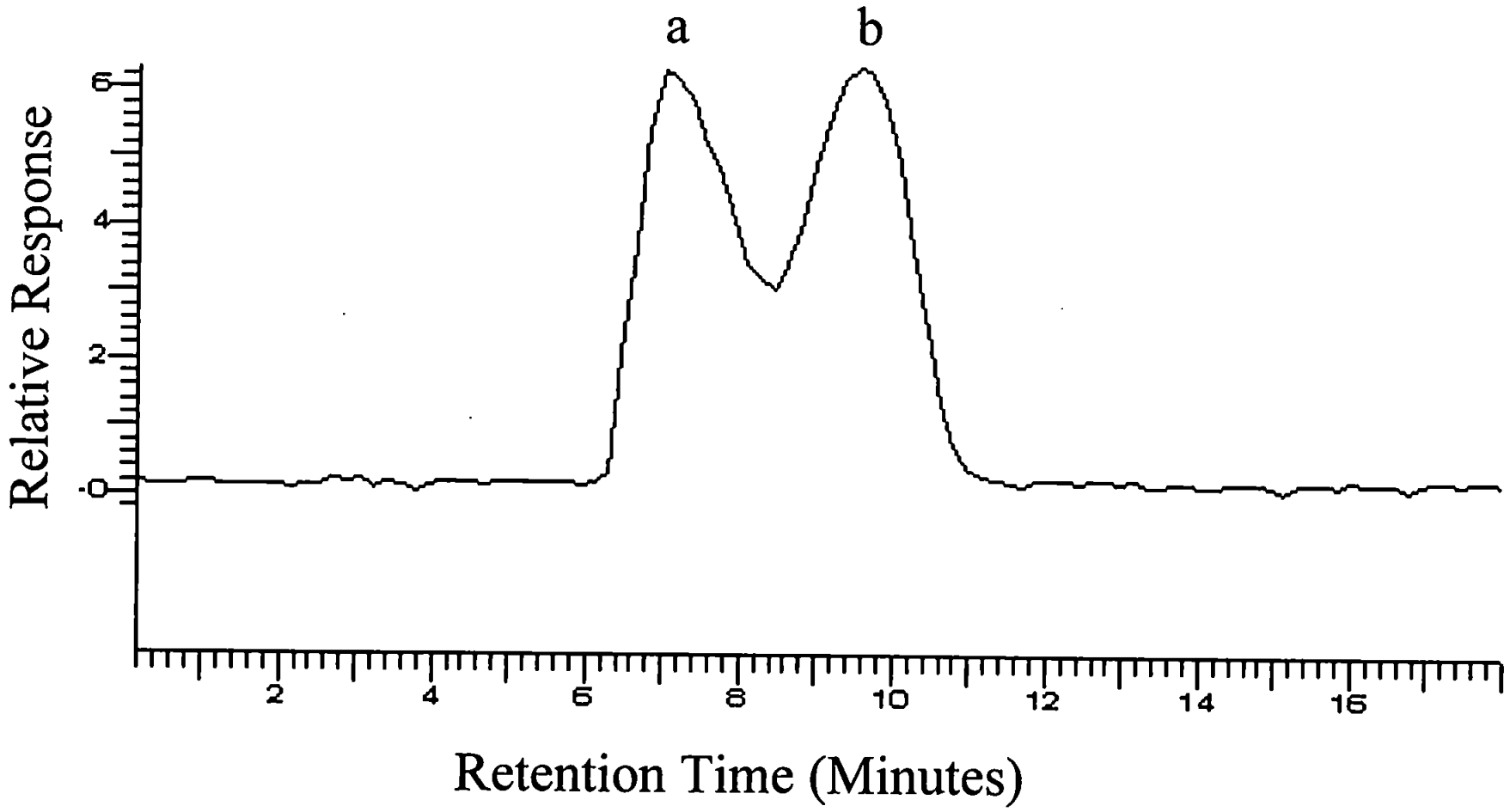

Figure 7.5 - SEC Separation of a) 200/1000 cS and b) 200/20 cS PDMS compounds. Both compounds present at 20 µg ml^{-1} Si

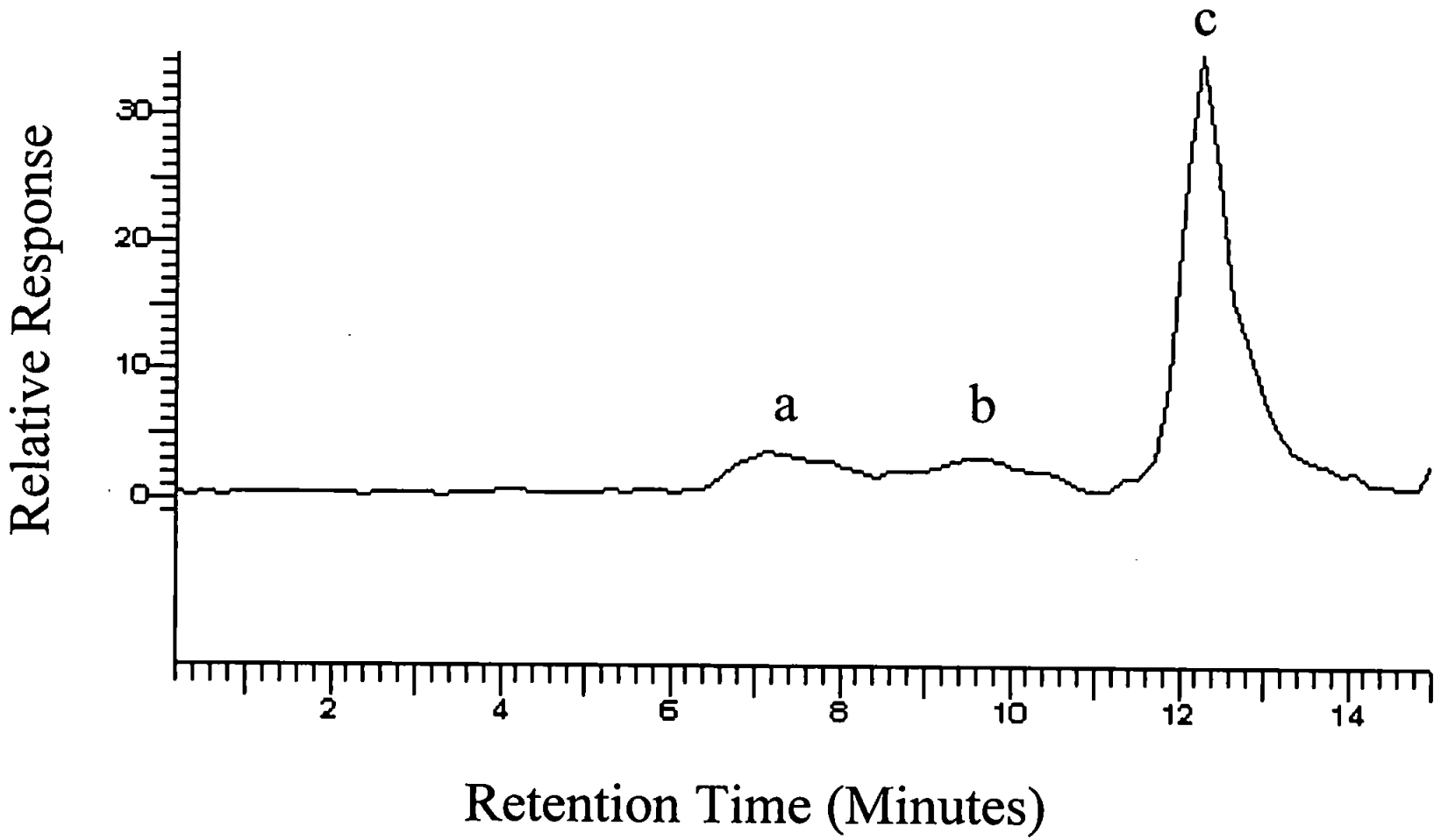

Figure 7.6 - SEC separation of a) 200/1000 cS, b) 200/20 cS and c) 200/0.65 cS PDMS compounds. All compounds present at 20 µg ml^{-1} Si

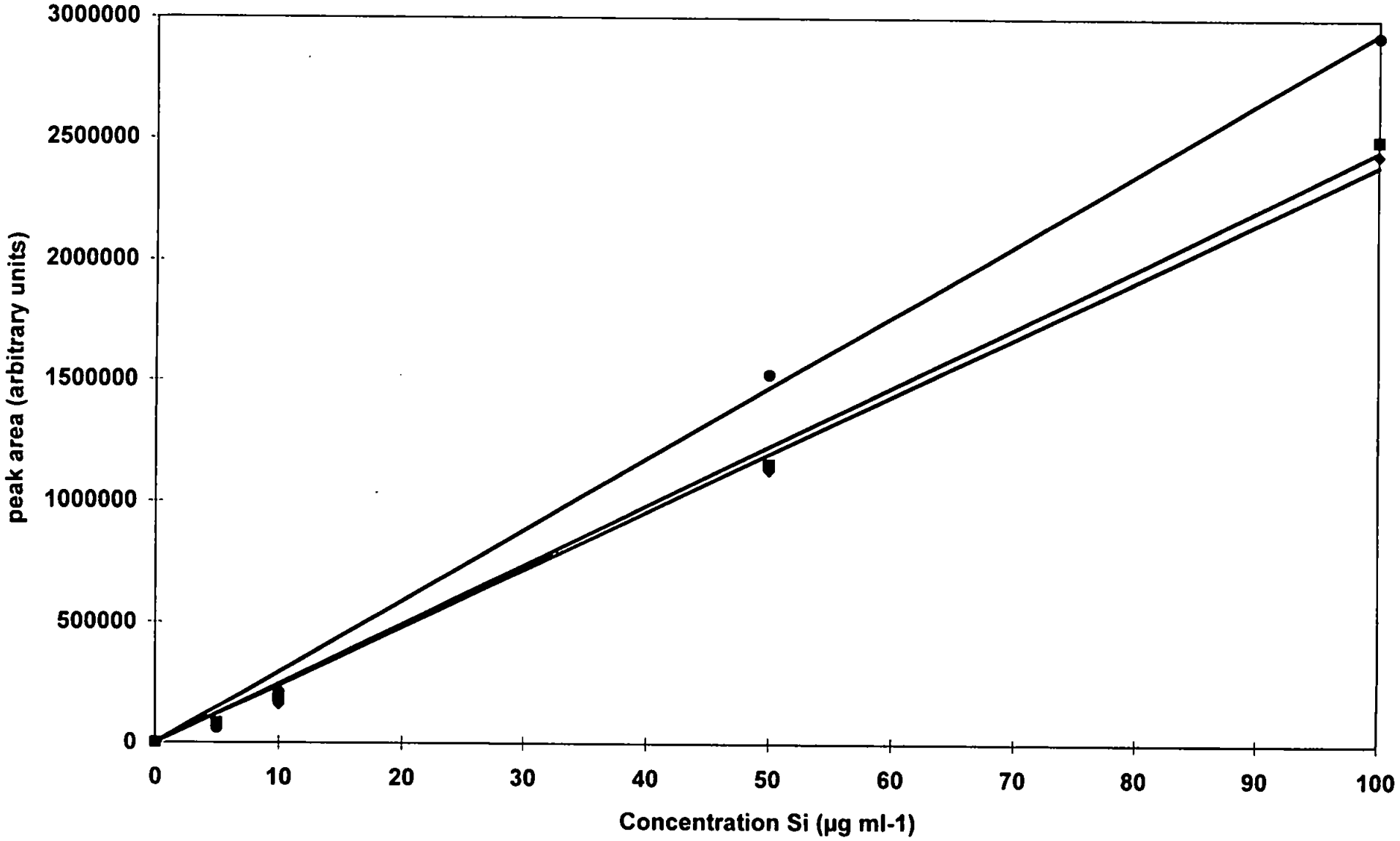

Figure 7.7 - Calibration graphs for compounds used in SEC-ICP-AES: ■ 200/1000 cS, ◆ 200/20 cS and ● 200/0.65 cS PDMS

limits were 0.5 μg ml^{-1} Si for 200/0.65 cS and 5 μg ml^{-1} Si for the PDMS compounds of higher molecular weight.

It must be noted that the size exclusion column was not calibrated. To enable the identification of various molecular weight PDMS compounds in unknown samples, molecular mass calibration of the column using polystyrene standards must be performed.

7.4 Conclusions

This work has demonstrated the feasibility of using reverse phase HPLC-ICP-AES to determine polar silicon compounds and the use of SEC-ICP-AES to determine organosilicon polymers. Given the presence of silicon in many analytical samples, speciation of silicon would seem to be of particular value and the use of ICP-AES clearly eliminates the problems often reported for the measurement of silicon by ICP-MS. While the detection limits obtained, 0.1 to 5 μg ml^{-1}, may need to be improved for some environmental and biological samples, the capability to preface the chromatography with automated preconcentration techniques is readily available. It has also been demonstrated that the software approach taken is a valuable way of obtaining transient signal data from an array based spectrometer.

It has been demonstrated that the use of reversed phase HPLC-ICP-AES when viewing the plasma in axial mode offers no significant improvement in detection limits over viewing the plasma radially. Although viewing the plasma axially when introducing aqueous samples into the ICP offers a five to ten fold increase in detection limits, no such advantage is seen for samples with a high organic content. Although BEC values are similar, the reproducibility of results is less and RSDB values poorer when viewing the plasma axially compared to viewing radially. This is attributed to the fact that the measured analytical signal contains an element of noise that is not as severe when observing the plasma 'side on'.

Chapter 8 - Conclusions and Suggestions for Future Work

8.1 Conclusions

The work presented in this thesis has described the use of inductively coupled plasma atomic emission spectrometry for slurry and solution analysis. The versatility of simultaneous detectors has been illustrated and applied to the multielement analysis of slurry and solution samples. The importance of the use of optimisation algorithms in the analysis of these samples has been addressed. In addition, matrix effects have been studied for solutions and slurries, in particular those due to easily ionisable elements, using two plasma orientations. Time resolved chromatographic studies were also performed for the speciation of silicon containing compounds.

The preparation of slurry samples has been shown to be an important step for ICP analysis using slurry nebulisation. Both grinding and dispersion of the slurry are essential prerequisites for efficient transport through the sample introduction system and atomisation in the plasma. Additional improvements in elemental recoveries and precision may be obtained using optimisation algorithms. This study has shown that it is possible to optimise a simultaneous multielement analysis for slurry samples using a solid state segmented array charged coupled device (SCD) detector and on-board instrument optimisation programmes. Analytical recoveries obtained using the well established variable step-size simplex programme were compared to results obtained using on-board algorithms. The results obtained for the two optimisation procedures were in good agreement and, in some instances, the quicker on-board algorithms excelled the rigorous simplex technique. A range of certified materials were analysed as slurries using multielement compromise conditions obtained using the on-board optimisation algorithm. Results were in good agreement with certified values. Full recoveries were obtained for a number of elements using aqueous calibration illustrating that slurries closely model solutions in terms of transport and atomisation efficiencies. Optimum operating parameters were obtained by aspirating

solutions. These conditions were found to be applicable for slurry analyses which again reinforces the statement that slurry behaviour in the ICP closely models that of solutions. Where analytical recoveries were less than ideal for sewage sludge samples, the use of a customised glass spray chamber and carbonising procedures improved accuracy and precision.

Sample introduction by slurry nebulisation has been applied to carbon black and NIST SRM 'Total Diet' samples, the first time these particular samples have been analysed using this method of solid sample introduction. Both slurries were prepared using the well established 'bottle and bead' method with Triton X-100 as a dispersant. The dispersant was found to produce stable and reproducible slurries, with satisfactory particle size distributions, for both samples. A radial ICP instrument with optimised operating parameters was used for the analysis of sulphur in carbon black samples. Results were comparable to those obtained using a complex dissolution technique, therefore highlighting a potential alternative method for the analysis of this sample without the need for hazardous, costly and time consuming sample dissolution. In contrast, an axially viewed ICP spectrometer was used in the analysis of Total Diet. This sensitive mode of viewing the plasma eliminated the need for operating parameter optimisation. Elemental recoveries were found to be comparable to certified values.

The effect of easily ionisable elements (EIEs) on solutions and slurries in an inductively coupled plasma with axial viewing also formed part of this study. Ion/atom emission intensity ratios are directly related to plasma excitation temperature and electron number density according to the Saha equation. They may be used as an indicator of how a system may be affected upon the addition of matrix elements, such as EIEs. By comparing I_i/I_a for the same analyte element in a solution or slurry with and without EIE addition, differences between the behaviour of the two systems may be highlighted. Any variation between the two systems must arise due to differences between excitation and/or ionisation and/or atomisation processes.

It has been shown that increasing the mass of concomitant matrix elements in solutions and slurries greatly modifies the mass transport efficiency of the analyte of interest. In solutions and slurries this transport phenomenon is dependant on the matrix element and not on the analyte of interest. The decrease in transport efficiency is directly proportional to the mass of the EIE added and must be corrected for when EIE suppression and enhancement effects are obtained from emission intensity data.

Axially obtained solution and slurry intensity ratios illustrate enhancement in the presence of EIEs. This enhancement has been shown to be spatially dependant and is seen at the interface between the central channel of the carrier gas flow and the plasma main body. It is concluded that energy transfer processes governing excitation are modified by EIEs. The result is an increase in the excited atomic population. Although this may appear to be a departure from LTE, the effect must be considered along with ion line intensity ratio changes for the same EIE of equivalent concentration. The ion line intensity ratio is seen to increase to a greater degree than the atom line ratios upon EIE addition. By considering both profiles, an increase in departure from LTE is produced by the addition of an EIE.

Structural changes in the D_{sol} and D_{slu} profiles may also be observed when EIEs are added to solutions and slurries. The energy transfer processes are modified at the centre of the plasma profile in the region of the analyte carrier channel. The ion line emission ratios for both methods of sample introduction are implicated in this central channel enhancement.

The magnitude of the enhancement effects for solutions and slurries are seen to be different when the plasma is viewed axially. These differences may be attributed to variations in atomisation efficiency in the plasma for solution and slurry particles. Magnesium oxide was used to prepare the slurry samples in this particular study. The material is highly refractory and, compared to an equimolar solution, the atomisation efficiency of the slurry is less than that of a solution (approximately 80 to 85 %). This slurry atomisation efficiency

increases, however, upon EIE addition in the order Li<Na≤K<Cs. From D_R values it can be seen that from Na to Cs the slurry atomisation efficiency tends towards 100 %.

The addition of the EIE may cause a 'real' atomisation effect where large particles are broken down more efficiently or subtle changes to the distribution of particles reaching the plasma may be occurring. It was found that increased mass loading from 0.05 M Li to Cs can reduce the sample transport efficiency and therefore the larger solid particle fraction reaching the plasma. Smaller particles would therefore contribute more to the ratios for Cs than those for Li. The overall effect would be an increase in the relative atomisation efficiency compared to solutions.

A radially viewed inductively coupled plasma with solid state detector was also used to monitor the effect of EIEs on solutions and slurries. Lateral profiles were transformed using the Abel integral correction technique. Solutions and slurries of Fe were employed and spatial information again acquired using the lateral translation of the instrument optics in the horizontal plane. The emission intensity of two atomic lines were monitored.

Radial profiles show that the addition of an EIE to a solution effects the emission intensity of the analyte element most significantly at the centre of the plasma. For both Fe I 382.043 and 385.991 nm emission lines, an apparent depression effect is observed when EIEs are added. This depression is greater for the 385 nm line. Differences in depression for the two lines is not caused by sample transport, as the two lines were measured simultaneously, but instead is due to differences in the mechanisms of excited state population. Depression effects observed for analyte emission upon EIE addition may not be a 'true' depression of emission and, in fact, may be an enhancement effect which is overshadowed by the decrease in transport efficiency that arises upon EIE addition. A decrease in transport efficiency results in less of the sample analyte reaching the plasma and hence the analytical signal decreases.

Such transport effects have been negated by calculating D_L values. The addition of Li, Na and K to solutions results in similar D_L values indicating that these EIEs effect excited state population mechanisms to the same degree. The addition of Cs causes the excitation processes for the two atomic emission lines to be effected to different degrees.

Within an observed plasma volume, the total emission intensity is directly proportional to the population of excited species within this volume. Any change in the sample transport efficiency upon EIE addition would be accompanied by a similar change in the total emission intensity in terms of magnitude and direction. No correlation between the two was found, therefore it may be concluded that transport effects severely 'mask' the enhancement caused by EIE addition. The 'actual' enhancement occurs in the order Li<Na<K<Cs. D_L solution values indicate that the magnitude of enhancement for both atomic emission lines is similar to Li, Na and K from the plasma centre towards the plasma body at 2.4 mm. The D_L value for Cs is higher suggesting that the 382 nm line is enhanced more than the 385 nm line.

Some subtle differences between solutions and slurries are observed when EIEs are added to the sample matrix. Apparent enhancement effects are seen for K and Cs when the 382 nm line is monitored. This is not seen for the 385 nm line. Again, transport phenomena mask the 'real' enhancement effect caused by EIE addition to the sample matrix and enhancement is in the order Li<Na<K<Cs for both lines. Calculated D_L values for Li and Na addition to slurries are approximately equal to 1 indicating that the same degree of enhancement is occurring for both atom lines. This value is slightly higher for K and even greater for Cs which has the greatest difference in emission intensity for the two wavelengths.

The plasma excitation temperature (T_{exc}) was used as a physical marker to establish direct comparisons and subsequent variation between solutions and slurries with and without EIE addition. Iron was used as the thermometric

species of interest. Both radial and axial ICPs were used to acquire spatial emission profiles. The Boltzmann two line method was used to calculate T_{exc}. As the two lines are measured simultaneously, transport effects are eliminated when comparisons between excitation temperature values upon EIE addition for solutions and slurries are made. Values of T_{exc}, illustrated by radial profiles, reflect the relative change in magnitude of enhancement for the emission lines used and therefore indicate changes in population of the excited states. Cs was found to give the highest T_{exc} values for solutions and slurries at the centre of the plasma profile. The solution and slurry systems with no EIEs added gave the lowest values of T_{exc}. The variation in T_{exc} upon the addition of EIEs is small but the trends showing increase in T_{exc} are similar to the trends in enhancement obtained when EIEs are added to solution and slurry systems. Values of T_{exc} obtained radially are relatively low compared to literature values.

Preliminary profiles of T_{exc} using an axially viewed ICP show that the addition of EIEs to both solutions and slurries does not significantly effect values of T_{exc}. The addition of an EIE to a solution or slurry matrix yields complex axial spatial temperature profiles which may not be interpreted easily. Values of T_{exc} obtained axially are comparable to literature values measured using similar plasma operating conditions. Axial measurements of T_{exc} using an axially viewed plasma take into consideration the total emission along the central channel of the plasma including the hotter regions of the normal analytical zone. Radially obtained values of T_{exc} were obtained lower in the plasma in the cooler initial radiation zone and so are lower than literature values.

The final part of this study demonstrated the feasibility of using reverse phase HPLC-ICP-AES for the determination of low molecular weight, polar, silicon compounds and the use of SEC-ICP-AES for the analysis and separation of long chain, high molecular weight organosilicon polymers. The use of ICP-AES as a detector for Si in these speciation studies eliminated the interference problems encountered using ICP-MS for the determination of Si.

The detection limits obtained using a radially viewed plasma for the two chromatographic configurations ranged from 0.1 to 5 μg ml^{-1}. In addition, it has been demonstrated that transient signal data may be obtained from an array based spectrometer.

Viewing the plasma in axial mode offered no significant improvements in detection limits over radial viewing when analysing samples with a high organic content. Reproducibility of results and RSDB values are worse for axial viewing owing to the element of noise that is measured. This noise is not as severe when the plasma is viewed 'side-on' and the optimum viewing height is selected.

8.2 Further Work

As sample preparation is such a critical step in the analysis of slurries, additional improvements regarding the efficiency of the grinding techniques could be made. The reduction of the maximum particle size of the slurry to below 2 μm, with minimum grinding time and contamination, is essential if slurry nebulisation is to challenge conventional solution nebulisation for the majority of materials. The use of harder grinding media in the preliminary stages of sample preparation, such as tungsten carbide in a ball mill, may achieve a reduction in both particle size and sample preparation time. In addition, investigations into the use of alternative dispersants may be carried out in an attempt to improve dispersion and minimise agglomeration.

The application of slurry sample nebulisation to carbon black samples proved to be very successful but highlighted the need for efficient grinding and dispersion of heterogeneous, polydensitic materials, such as coal. The analysis of coal using alternative grinding methods and dispersants is an area for additional study. Analysis of materials with fibrous matrices, such as 'Total Diet' may also be improved by employing sample charring prior to grinding and dispersion. Further studies are required in this area to determine optimum temperatures for ideal elemental recoveries.

It has been shown that a truly simultaneous analysis of a slurry sample may be performed using compromise conditions determined using simplex optimisation. The work in this thesis described compromise conditions for the simultaneous analysis of only four elements. It would therefore be advantageous to carry out further studies so that compromise conditions may be found for a larger number of elements with analytical recoveries comparable to an analysis where elements are determined individually.

Further modifications to the sample introduction system of the Perkin-Elmer Optima 3000 series of instruments may also improve analytical recoveries of a simultaneous multielement analysis. In particular, it is necessary to modify the customised glass small volume spray chamber and other designs of spray chamber to help improve slurry transport behaviour

Fundamental studies of easily ionisable elements (EIEs) as concomitant matrix elements may be more clearly understood if further axial excitation temperature measurements (T_{exc}) and electron number density (n_e) calculations are made. Values of n_e may yield information regarding departures from LTE when EIEs are added to solutions and slurries, and differences between the behaviour of various EIEs in the plasma. By comparing values of T_{exc} and n_e a more complete picture of the mechanisms producing enhancement and suppression effects may be obtained. Values of n_e may be calculated by measuring the Stark broadening of the Hβ emission line at 486.1 nm, a technique which does not assume LTE. These values of n_e may then be used to calculate T_{ion} via the Saha equation. T_{ion} and T_{exc} values could be compared at the same spatial position and any differences between the two may highlight departures from LTE when EIEs are added to solutions and slurries. An alternative analytical instrument to the Optima 3000 is required if these measurements are to be performed as the solid state CCD detector cannot accommodate the broad band of emission from the Hβ line.

Experiments to investigate whether EIEs actually modify the particle size distribution of the slurry may also offer potential explanations regarding the effect of EIEs on sample mass transport. Experiments to distinguish atomisation effects alone, using well defined, monodispersed particles, may be useful to explain the effect of EIEs upon aspiration into the plasma.

Preliminary studies involving the speciation of silicon containing compounds have been presented. The separation of a wider variety of compounds, the use of gradient elution and the attainment of lower limits of detection are requirements if the technique is to be applied to 'real' biological and environmental samples. Biological samples may be analysed to yield information regarding the breakdown mechanisms of organosilicon compounds in the human body via the hematogenous system. Little is known about the decomposition of PDMS compounds to water soluble, low molecular weight compounds in the human body. It is suggested that a clinical trial be set up in the future to monitor the concentration of various water soluble organosilicon compounds in urine and serum samples from patients with silicone breast and penile implants. The ultimate goal would be to isolate and measure those compounds that cause silicon related diseases in humans, so that preventative measures may be taken when implants start to bleed or rupture. In addition, it may be possible to suggest alternatives to the implant materials currently used in plastic and reconstructive surgery.

REFERENCES

1) Browner, R.F. and Boorn, A.W., Anal. Chem., 1984, 56, 786A

2) Hoare, H.C. and Mostyn, R.A., Anal. Chem., 1967, 39, 1153

3) De Silva, K.N. and Guevremont, R., Spectrochim. Acta, 1990, 45B, 997

4) Salin, E.D. and Horlick, G., Anal. Chem., 1979, 51, 2284

5) Sommer, D. and Ohls, K., Fresenius Z. Anal. Chem. 1980, 304, 97

6) Li-Xing, Z., Kirkbright, G.F., Cope, M.J. and Walton, J.M., Appl. Spectrosc., 1983, 37, 250

7) Scott, R.H., Spectrochim. Acta, 1978, 33B, 123

8) Keilsohn, J.P., Deutsch, R.D. and Hieftje, G.M., Appl. Spectrosc., 1983, 37, 101

9) Aziz, A., Broekaert, J.A.C., Lagua, K and Leis, F., Spectrochim. Acta, 1984, 39B, 1091

10) Lagua, K., in "Analytical Laser Spectroscopy", Ch 2, p. 47, Wiley, New York, 1979

11) Thompson, M., Goulter, J.E. and Sieper, F., Analyst, 1981, 106, 32

12) Denoyer, E.R., Fredeen, K.J. and Hager, J.W., Anal. Chem., 1991, 63, 445A

13) Fuller, C.W., Hutton, R.C. and Preston, B., Analyst, 1981, 106, 913

14) Saba, C.S., Rhine, W.E. and Eisentraut, K.J., Anal Chem., 1981, 53, 1099

15) Wilkinson, J.R., Ebdon, L. and Jackson, K.W., Anal. Proc., 1982, 19, 305

16) Sugimae, A. and Mizoguchi, T., Anal. Chim. Acta., 1982, 144, 205

17) Spiers, G.A., Dudas, M.J. and Hodgins, L.W., Clays Clay Miner, 1983, 31, 397

18) Watson, A.E. and Moore, G.L., S. Afr. J. Chem., 1984, 37, 81

19) Algeo, J.D., Heine, D.R., Phillips, H.A., Hoek, F.B.G., Schneider, M.R., Freelin, J.M. and Denton, M.B., Spectrochim. Acta, 1985, 40B, 1447

20) Page, J.R. and Jewel, K.E., Soil Sci., 1985, 139, 211

21) Mackey, J.R. and Murphy, W.J., Zeolites, 1985, 5, 233

22) McCurdy, D.L. and Fry, R.C., Anal. Chem., 1986, 58, 3126

23) Ebdon, L. and Wilkinson, J.R., J. Anal. At. Spectrosc., 1987, 2, 39

24) Ebdon, L. and Wilkinson, J.R., J. Anal. At. Spectrosc., 1987, 2, 325

25) Halicz, L. and Brenner, I.B., Spectrochim. Acta, 1987, 42B, 207

26) Brenner, I.B., Lang, Y., Le Marchand, A. and Grosdaillon, P., Amer. Lab., 1987, 19, 17

27) Foulkes, M.E., Ebdon, L. and Hill, S., Anal. Proc., 1988, 25, 92

28) Ebdon, L. and Collier, A.R., J. Anal. At. Spectrom., 1988, 3, 557

29) Broekaert, J.A.C., Leis, F., Raeymaekers, B. and Zàray, G., Spectrochim. Acta, 1988, 43B,339

30) Ebdon, L. and Collier, A.R., Spectrochim. Acta, 1988, 43B, 355

31) Raeymaekers, B., Graule, T., Broekaert, J.A.C., Adams, F. and Tschöpel, P., Spectrochim. Acta, 1988, 43B, 923

32) Verbeek, A and Brenner, I.B., J. Anal. At. Spectrom., 1989, 4, 23

33) Ambrose, A.J., Ebdon, L., Foulkes, M.E. and Jones, P., J. Anal. At. Spectrom., 1989, 4, 219

34) Ebdon, L., Foulkes, M.E. and Hill, S., Microchem. J., 1989, 40, 30

35) Varga, I., Záray, G., Szèpvolgyi, J. and Kònya, G., Mikrochim. Acta, 1989, 3, 381

36) Min, H. and Xi-En, S., Spectrochim. Acta, 1989, 44B, 957

37) Van Borm, W.A. and Broekaert, J.A.C., Anal. Chem., 1990, 62, 2527

38) Ebdon, L., Foulkes, M.E. and Hill, S. and J. Anal. At. Spectrom., 1990, 5, 67

39) Long, G.L. and Brenner, I.B., J. Anal. At. Spectrom., 1990, 5, 495

40) Laird, D.A., Dowdy, R.H. and Munter, R.C., J. Anal. At. Spectrom., 1990, 5, 515

41) Fagioli, F., Landi, L., Lacatelli, G., Righini, F. and Settimo, R., J. Anal. At. Spectrom., 1990, 5, 519

42) Zàray, G., Farkas, A. and Varga, I., Acta, Chim. Hungarica, 1991, 128, 489

43) Isozaki, A., Ogawa, M., Shibagaki, M. and Morita, Y., Anal. Sci., 1991, 71, 1249

44) Carrión, N., Fernández, A., Eljuri, E.J., Murillo, M. and Franceschetto, M., At. Spectrosc., 1991, 12, 162

45) Gervais, L.S. and Salin, E.D., J. Anal. At. Spectrom., 1991, 6, 41

46) Rademeyer, C.J., Collins, C.S. and Butler, L.R.P., J. Anal. At. Spectrom., 1991, 6, 329

47) Fernandez, M.L., Fairman, B. and Sanz-Medel, A., J.Anal. At. Spectrom., 1991, 6, 397

48) Laird, D.A., Dowdy, R.H. and Munter, R.C., Soil Sci. Soc. Amer. J., 1991, 55, 274

49) Van Borm, W.A.H., Broekaert, J.A.C., Klockenkämper, R., Tschöpel, P. and Adams, F.C., Spectrochim. Acta, 1991, 46B, 1033

50) Lobiński, R., Van Borm, W., Broekaert, J.A.C., Tschöpel, P. and Tölg, G., Fresenius J. Anal. Chem., 1992, 342, 563

51) Ebdon, L. and Goodall, P., J. Anal. At. Spectrom., 1992, 7, 1111

52) Karanassios, V, Usypchuck, L., Moss, P. and Salin, E.D., J. Anal. At. Spectrom., 1992, 7, 1243

53) Xhoffer, C., Lathen, C., Van Borm, W, Broekaert, J.A.C., Jacob, W. and Van Grieken, R., Spectrochim. Acta, 1992, 47B, 155

54) Ebdon, L. and Goodall, P., Spectrochim. Acta, 1992, 47B, 1247

55) Halicz, L., Brenner, I.B. and Yoffe, O., J. Anal. At. Spectrom., 1993, 8, 475

56) Goodall, P., Foulkes, M.E. and Ebdon, L., Spectrochim. Acta, 1993, 48B, 1563

57) Goulter, J., Tiz. Int. Powder Bulk Mag., 1992, 116, 41

58) Chen, C. and McCreary, T.W., Appl. Spectrosc., 1994, 48, 410

59) Manickum, C.K. and Verbeek, A.A., J. Anal. At. Spectrom., 1994, 9, 227

60) Záray, G., Varga, I. and Kántor, T., J. Anal. At. Spectrom., 1994, 9, 707

61) Fariñas, J.C., Moreno, R. and Mermet, J.M., J. Anal. At. Spectrom., 1994, 9, 841

62) Garten, R.P.H., J. Chin. Chem. Soc., 1994, 41, 259

63) Brenner, I.B., Zander, A., Kim., S. and Henderson, A. Spectrosc. Europe, 1995, 7, 24

64) Ebdon, L. and Evans, E.H., Euro. Spectrosc. News, 1988, 79, 9

65) Parry, H.G.M. and Ebdon, L., Anal. Proc., 1988, 25, 69

66) Darke, S.A., Long, S.E., Pickford, C.J. and Tyson, J.F., Fresenius J. Anal. Chem., 1990, 337, 284

67) Ebdon, L. and Foulkes, M.E., Chemia Analityczna, 1990, 35, 109
68) De Silva, K.N. and Guevremont, R., Spectrochim. Acta, 1990, 45B, 933
69) Jarvis, K.E., Chem. Geol., 1992, 95, 73
70) Broekaert, J.A.C., Lathen, C., Brandt, R., Pilger, C., Pollman, D., Tschöpel, P. and Tölg, G., Fresenius, J. Anal. Chem., 1994, 349, 20
71) Dean, J.R., Ebdon,L. and Massey, R., J. Anal. At. Spectrom., 1987, 2, 369
72) Williams, J.G., Gray, A.L., Norman, P. and Ebdon, L., J. Anal. At. Spectrom., 1987, 2, 469
73) Ebdon, L., Foulkes, M.E., Parry, H.G.M. and Tye, C.T., J. Anal. At. Spectrom., 1988, 3, 753
74) Jarvis, K.E. and Williams, J.G., Chem. Geol., 1989, 77, 53
75) Mochizuki, T., Sakashita, A., Iwata, H., Ishibashi, Y. and Gunji, N., Anal. Sci., 1989, 5, 311
76) Mochizuki, T., Sakashita, A., Iwata, H., Ishibashi, Y. and Gunji, N., Fresenius J. Anal. Chem. 1991, 339, 889
77) Totland, M., Jarvis, I. and Jarvis, K.E., Chem. Geol., 1993, 104, 175
78) Hartley, J.H.D., Hill, S.J. and Ebdon, L., Spectrochim. Acta, 1993, 48B, 1421
79) Pollman, D., Pilger, C., Hergenröder, R., Leis, F., Tschöpel, P. and Broekaert, J.A.C., Spectrochim. Acta, 1994, 49B, 683
80) Balaram, V., Current Science, 1995, 69, 640
81) Mohamed, N., Brown, R.M. and Fry, R.C., Appl. Spec., 1981, 35, 153
82) McCurdy, D.L., Wichman, M.D. and Fry, R.C., Appl. Spec., 1985, 39, 984
83) Sparkes, S. and Ebdon, L. Anal. Proc., 1986, 23, 410
84) Vien, S.H. and Fry, R.C., Appl. Spec., 1988, 42, 381
85) Sparkes, S.T. and Ebdon, L., J. Anal. At. Spectrom., 1988, 3, 563
86) Jerrow, M., Marr, I. and Cresser, M., Anal. Proc., 1992, 29, 45
87) Jerrow, M., Marr, I. and Cresser, M., J.Anal. At. Spectrom., 1992, 7, 1117
88) Matusiewicz, H. and Sturgeon, R.E., Spectrochim. Acta, 1993, 48B, 723
89) Bin, H., Zucheng, J. and Yune, Z., J. Anal. At. Spectrom., 1991, 6, 623

90) Alary, J.F., Hernandez, G. and Salin, E.D., Appl. Spec., 1995, 49, 1796

91) Yongchao, Q., Zucheng, J., Yune, Z. and Bin, H., J. Anal. At. Spectrom., 1995, 10, 455

92) Grégoire, D.C., Miller-Ihli, N.J. and Sturgeon, R.E., J. Anal. At. Spectrom., 1994, 9, 605

93) Fonseca, R.W. and Miller-Ihli, N.J., Appl. Spec., 1995, 49, 1403

94) Bauman, H., Fresenius J. Anal. Chem., 1992, 342, 907

95) Darke, S.A. and Tyson, J.F., Microchem. J., 1994, 50, 310

96) De Benzo, Z.A., Velosa, M., Ceccarelli, C., de la Guardia, M. and Salvador, A., Fresenius J. Anal. Chem., 1991, 339, 235

97) Parfitt, G.D., 'Dispersion of Powders in Liquids, 3rd Ed., Applied Science Publishers, London, 1981

98) Allen, T., 'Dispersion of Powders' in 'Particle Size Measurement',3rd Ed., Chapman and Hall, London, 1981

99) Foulkes, M.E., PhD Thesis, University of Plymouth, 1988

100) Sharp, B.L., J. Anal. At. Spectrom., 1988, 3, 613

101) Sharp, B.L., J. Anal. At. Spectrom., 1988, 3, 939

102) Montaser, A. and Golightly, D.W., 'Inductively Coupled Plasmas in Anaytical Atomic Spectrometry', 2nd Ed., VCH Publishers, Inc, New York, 1992

103) Mork, B.J. and Scheeline A., Appl. Spectrosc., 1988, 42, 1332

104) Epperson, P.M. and Denton, M.B., Anal. Chem., 1989, 61, 1513

105) Schmidt, K.P., Becker-Ross, H. and Florek, S., Spectrochim. Acta, 1990, 45B, 1203

106) Bilhorn, R.B., Proc. Spie, Int: Soc. Opt. Eng., 1991, 74, 1448

107) Hartnett, M., Diamond, D., Kiernan, L. and Costello, J., Anal. Proc., 1992, 29, 52

108) Barnard, T.W., Crockett, M.I., Ivaldi, J.C., Lundberg, P.L., Yates, D. A., Levine, P.A. and Saver, D.J., Anal Chem, 1993, 65, 1231

109) Mermet, J.M. and Ivaldi, J.C., J. Anal. At. Spectrom., 1993, 8, 795

110) Falkin, D. and Vosloo, M., Spectrosc. Europe, 1993, 5, 16

111) Soulder, L. and Mermet, J.M., Appl. Spectrosc., 1995, 49, 1478

112) Ebdon, L. and Parry, H.G. M., J. Anal. At. Spectrom., 1988, 3, 131

113) Mermet, J.M. and Ivaldi, J., J. Anal. At. Spectrom., 1993, 8, 795

114) Barnard, T.W., Crockett, M.I., Ivaldi, J.C. and Lundberg, P.L., Anal. Chem., 1993, 65, 1225

115) Satake, K. and Uehiro, T., Analyst, 1985, 110, 1165

116) Ebdon, L. and Cave, M.R., Analyst, 1982, 107, 172

117) Fletcher, R. and Powell, M. J. D., Computer Journal, 1963, 6, 163

118) Thomas, R. J. and Collins, J. B., Spectroscopy, 1989, 5, 1144

119) Ebdon, L., Cave, M.R. and Mowthorpe, D.J., Anal. Chim. Acta., 1980, 115, 179

120) Ebdon, L. and Norman, P., Anal. Proc., 1986, 23, 420

121) Leary, J. J., Brookes, A. E., Dorrzapf, A. F. and Golightly, D. W., Appl. Spectrosc., 1982, 36, 37

122) Ebdon, L. and Carpenter, R. C., Anal. Chim. Acta, 1987, 200, 551

123) The Guide to Techniques and Applications of Atomic Spectroscopy, The Perkin-Elmer Corporation, Norwalk, CT, 1993, 5.

124) Kawaguchi, H., Ito,T., Ota, K. and Mizuike, A., Spectrochim. Acta, 1980, 35B, 199

125) Blades, M.W. and Horlick, G., Spectrochim. Acta, 1981, 36B, 881

126) Koirtyohann, S.R., Jones, J.S., Jester, C.P. and Yates, D.A., Spectrochim. Acta, 1981, 36B, 49

127) Gunter, W.H., Visser, K. and Zeeman, P.B., Spectrochim. Acta, 1982, 37B, 571

128) Rybarczyk, J.P., Jester, C.P., Yates, D.A. and Koirtyohann, S.R., Anal. Chem. 1982, 54, 2162

129) Faires, L.M., Apel, C.T. and Niemczyk, T.M., Appl. Spec., 1983, 37, 558

130) Gillson, G. and Horlick, G., Spectrochim. Acta, 1986, 41B, 619

131) Olesik, J.W. and Williamsen, E.J., Appl. Spec. 1989, 43, 1223

132) Wu, M. and Hieftje, G.M., Spectrochim. Acta, 1994, 49B, 149

133) Galley, P.J., Glick, M. and Hieftje, G.M., Spectrochim. Acta, 1993, 48B, 769.

134) Hanselman, D.S., Sesi, N.N., Huang, M. and Hieftje, G.M., Spectrochim. Acta, 1994, 49B, 495

135) Galley, P.J. and Hieftje, G.M., Spectrochim. Acta, 1994, 49B, 703

136) Faires, L.M., Bieniewski, T.M., Apel, C.T. and Niemczyk, T.M., Appl. Spec. 1985, 39, 5

137) Furuta, N. and Horlick, G., Spectrochim. Acta, 1982, 37B, 53

138) Boumans, P.W.J.M. and de Boer, F.J., Spectrochim. Acta, 1977, 32B, 365

139) Boumans, P.W.J.M., Theory of Spectrochemical Excitation, Hilger and Watts, London, 1966

140) Caughlin, B.L. and Blades, M.W., Spectrochim. Acta, 1984, 39B, 1583

141) Caughlin, B.L. and Blades, M.W., Spectrochim. Acta, 1985, 40B, 1539

142) Mermet, J.M., Anal. Chim. Acta, 1991, 250, 85

143) Skogerboe, R.K. and Freeland, S.J., Appl. Spec., 1985, 39, 916

144) Skogerboe, R.K. and Freeland, S.J., Appl. Spec., 1985, 39, 920

145) Skogerboe, R.K. and Freeland, S.J., Appl. Spec., 1985, 39, 925

146) Veillon, C. and Margoshes, M., Spectrochim. Acta, 1968, 23B, 503

147) Kirkbright, G.F., Ward, A.F. and West, T.S., Anal. Chim. Acta, 1972, 62, 241

148) Kirkbright, G.F., Ward, A.F. and West, T.S., Anal. Chim. Acta, 1973, 64, 353

149) Larson, G.F., Fassel, V.A., Scott, R.H. and Kniseley, R.N., Anal. Chem., 1975, 47, 238

150) Boumans, P.W.J.M. and de Boer, F.J., Spectrochim. Acta, 1975, 30B, 309

151) Abdallah, M.T., Mermet, J.M. and Trassy, C., Anal. Chim. Acta, 1976, 87, 329

152) Boumans, P.W.J.M. and deBoer, F.J., Spectrochim. Acta, 1976, 31B, 355

153) Kornblum, G.R. and de Galan, L., Spectrochim. Acta, 1977, 32B, 455

154) Kalnicky, D.J., Fassel, V.A. and Knisely, R.N., Appl. Spectrosc., 1977, 31, 139

155) Skogerboe, R.K. and Olsen, K.W., Appl. Spectrosc., 1978, 32, 181

156) Gunter, W.H., Visser, K. and Zeeman, H.B.B., Spectrochim. Acta, 1982, 36B, 881

157) Vogel's Textbook of Quantitative Inorganic Analysis, 4th ed., Basset, J., Denney, R.C., Jeffery, G.H. and Mendham, J., Longham, London, 1978

158) Raaijmakers, I.J.M.M. and Boumans, P.W.J.M., Spectrochim. Acta, 1983, 38B, 697

159) Kornblum, G.R. and de Galan, L., Spectrochim. Acta, 1977, 32B, 71

160) Houk, R.S. and Olivares, J.A., Spectrochim. Acta, 1984, 39B, 575

161) Kalnicky, D.J., Knisely, R.N. and Fassel, V.A., Appl. Spec. 1977, 31, 137

162) Kalnicky, D.J., Knisely, R.N. and Fassel, V.A., Spectrochim. Acta, 1975, 30B, 511

163) Alder, J.F., Bombelka, R.M. and Kirkbright, G.F., Spectrochim. Acta, 1980, 35B, 163

164) Mermet, J.M., Spectrochim. Acta, 1975, 30B, 383

165) Jarosz, J., Mermet, J.M. and Robin, J.P., Spectrochim. Acta, 1978, 33B, 55

166) Houk, R.S., Schoer, J.K. and Crain, J.S., Spectrochim. Acta, 1987, 42B, 841

167) Wiese, W.L., Spectrochim. Acta, 1991, 46B, 831

168) Mermet, J.M., in 'Spectroscopic Diagnostics' in Basic Concepts in ICP Emission Spectroscopy Part 2: Applications and Fundamentals. Boumans, P.W.J.M. ed. Wiley-Interscience, 1987

169) Ivaldi, J.C., Personal Communication, June 1996.

170) Caughlin, B.L. and Blades, M.W., Spectrochim. Acta, 1985, 40B, 987

171) Carlisle, E.M., in: Biochemistry of the Essential Ultratrace Elements. Frieden, E., ed., Plenure Press, New York, 1984, pp 257 - 291.

172) Le View, R.R., Harrison, M.C., Cook, R.R. and Lane, T.H., Plast. Reconstr. Surg., 1993, 92, 163

173) Dobbie, J.W. and Smith, M.J.B. in "Silicon Biochemistry Ciba Foundation Symposium 121", Evered, D. ed., J. Wiley, New York, 1986, pp 194-213

174) Stroh, A., in 'Frontiers of Organosilicon Chemistry' Bassingdale, A.R. and Gaspar, P.P. ed. Royal Society of Chemistry, Cambridge, 1991, pp 81-85

175) Arkles, B. and Redinger, P., in: 'Biocompatible Polymers, Metals and Composites', Szycher, M. ed., Technomic Publishing, Lancaster, PA, 1983, pp. 749 - 768

176) Van Noort, R. and Blank, M.M. in Biocompatibility of Clinical Implant Materials, Williams, D.F. ed, vol 2, pp 79-98, CRC Press Inc., Boca Raton, FL, USA, 1981 vol 2, pp 79-98

177) McGrath, M.H. and Burckhardt, B.R., Plast. Reconst. Surg., 1984, 74, 550

178) Talcott, T.D., Int. J. Occ. Med. Toxicol., 1995, 4, 113

179) Kumagai, Y., Shiokawa, Y., Medsger, T.S. and Rodnan, G.P., Arthritis Rheum., 1984, 27, 1

180) Sergott, T.J., Linoli, J.P., Balswin, C.M. and Laub, D.R., Plast. Reconst. Surg., 1986, 78, 104

181) Truong, L.D., Cartwright, J., Goodman, M.D. and Woznicki, D., Am. J. Surg. Pathol., 1988, 12, 484

182) Picha, G.J. and Goldstein, J.A., Plast. Reconst. Surg. 1991, 87, 490

183) Edelman, D.A., Grant, S. and van Os, W.A.A., Int. J. Fert. Menopaus. Studies, 1995, 40, 274

184) Brautbar, N., Vojadami, A and Campbell, A., Arch. Environ. Health, 1994, 49, 151

185) Kessler, D., Merkatz, R.B. and Schapiro, R., N. Engl. J. Med., 1992, 326, 2607

186) Levine, J.J. and Llowite, N.T., J. Am. Med. Assoc., 1994, 271, 213

187) Teuber, S.S. and Gershwin, M.E., Intl. Arch. Allergy. Immunol., 1994, 103, 105

188) LeVier, R.R., Harrison, R.R. and Lane, T.H., Plast. Reconstr. Surg., 1993, 92, 163

189) Barker, D.E., Retsky, M.I. and Schultz, S., Plast. Reconstr. Surg. 1978, 61, 836

190) Carmen, R. and Kahn, P., J. Biomed. Mater. Res., 1968, 2, 457

191) Allwork, S.P. and Norton, R., Thorax, 1976, 31, 742

192) Weiner, S.R. and Paulus, H.R., Plast. Reconst. Surg. 1986, 77, 185

193) Rees, T.D., Ballantyne, D.L., Seidman, I. and Hawthorne, G.A., Plast. Reconst. Surg., 1967, 39, 402

194) Nosanchuk, J.S., Plast. Reconst. Surg., 1968, 42, 562

195) Garrido, L., Pfleidener, B., Papisov, M. and Ackerman, J.L., Magn. Reson. Med., 1992, 29, 839

196) Pfleidener, B., Ackerman, J.L. and Garrido, L. Magn. Reson. Med., 1993, 30, 534

197) Garrido, L., Pfleidener, B., Jenkins, B.G., Hulkes, C.A. and Kopans, D.B., Magn. Reson. Med., 1994, 31, 328

198) Dorn, S.B. and Skelly Frame, E.M., Analyst, 1994, 119, 1687

199) Smith, A.L. and Parker, R.D., in "The Analytical Chemistry of Silicones", ed. Smith A.L., J. Wiley, New York, 1991, pp 71 - 95

200) Hausler, D.W. and Taylor, L.T. Anal. Chem., 1981, 53, 1223

201) Hausler, D.W. and Taylor, L.T. Anal. Chem., 1981, 53, 1227

202) Heine, D.R., Denton, M.B. and Schlabach, T.D., J. Chromatogr. Sci., 1985, 23, 454

203) Uden, P.C., Quimby, B.D., Barnes, R.M. and Elhot, W.G., Anal. Chim. Acta, 1978, 101, 99

204) Boorn, A.W., Cresser, M.S. and Browner, R.F., Spectrochim. Acta, 1980, 35B, 823

205) Boorn, A.W. and Browner, R.F., Anal. Chem., 1982, 54, 1402

206) Cavic-Vlasak, B.A., Thompson, M. and Smith, D.C., Analyst, 1996, 121, 53R

207) Carpenter, J.C. and Cella, J.A., J. Organomet. Chem., 1994, 480, 23

208) Ivaldi, J.C. and Tyson, J.F., Spectrochim. Acta, 1995, 50B, 1207

209) Ebdon. L., Evans, E.H. and Barnett, N.W., J. Anal. At. Spectrosc., 1989, 4, 505

Papers Published as a Result of This Study

"Optimised Simultaneous Multi-Element Analysis of Environmental Slurry Samples by Inductively Coupled Plasma Atomic Emission Spectrometry Using a Segmented Array Charge-Coupled Device Detector"; Ebdon, L., Foulkes, M.E. and O'Hanlon, K., Anal. Chim. Acta, 1995, 311, 123.

ICP Application Study No. 81, "The Analysis of NIST SRM Total Diet by Slurry Nebulization ICP-OES", O'Hanlon, K. and Barnes, K.W., The Perkin-Elmer Corp., Norwalk, CT, USA, 1995.

"The Effect of Easily Ionisable Elements on Solutions and Slurries in an Axially Viewed Inductively Coupled Plasma"; O'Hanlon, K., Ebdon, L. and Foulkes, M.E., J. Anal. At. Spectrom., 1996, 11,427.

ICP Application Study No. 83, "The Analysis of Sulphur in Carbon Black by Slurry Nebulization ICP-OES", O'Hanlon, K. and Barnes, KW., The Perkin-Elmer Corp.,Norwalk, CT, USA, 1996.

"Slurry Nebulization Into Plasmas - A Review", O'Hanlon, K., Ebdon, L. and Foulkes, M.E., J. Anal. At. Spectrom., 1996 (in press).

"The Effect of Easily Ionisable Elements on the Mass Transport Efficiency of Solutions and Slurries", O'Hanlon, K., Ebdon, L. and Foulkes, M.E., J. Anal. At. Spectrom., 1996 (in press).

"The Effect of Easily Ionisable Elements on Emission Intensity and Excitation Temperature for Solutions and Slurries in a Radially Viewed Inductively Coupled Plasma with Simultaneous Detection Capability"., O'Hanlon, K., Ebdon, L. and Foulkes, M.E., J. Anal. At. Spectrom., 1996 (in press).

Meetings and Conferences Attended

Perkin-Elmer Environmental Symposium, London, UK, April 1994.

R and D Topics in Analytical Chemistry Meeting, University of Hertfordshire, UK, July 1994.

7th BNASS, University of Hull, UK, July 1994.

European Winter Conference on Plasma Spectrochemistry, Cambridge, UK, January 1995.

R and D Topics in Analytical Chemistry Meeting, University of Hull, UK, July 1995.

SAC 95, University of Hull, UK, July 1995.

European Winter Conference on Plasma Spectrochemistry, Ft. Lauderdale, Florida, USA, January, 1996.

8th BNASS, University of East Anglia, Norwich, UK, July, 1996.

Also attended, during the course of this study from 1993-96, were invited Royal Society of Chemistry Lectures, invited postgraduate lectures in analytical and environmental chemistry, departmental colloquia and weekly research group seminars at the University of Plymouth

Presentations

Oral presentation, Perkin-Elmer Environmental Symposium, London, UK, April 1994.

Departmental research lecture, University of Plymouth, UK, May 1994.

Poster presentation, R and D Topics in Analytical Chemistry Meeting, University of Hertfordshire, UK, July 1994.

Poster presentation, 7th BNASS, University of Hull, UK, July 1994.

Poster presentation, European Winter Conference on Plasma Spectrochemistry, Cambridge, UK, January 1995.

Oral presentation, The Perkin-Elmer Corp., Norwalk, USA, June 1995.

Poster presentation, R and D Topics in Analytical Chemistry Meeting, University of Hull, UK, July 1995.

Poster and oral presentations, SAC 95, University of Hull, UK, July 1995.

Departmental research lecture, University of Plymouth, UK, November 1995.

Oral presentation, European Winter Conference on Plasma Spectrochemistry, Ft. Lauderdale, Florida, USA, January, 1996.

Participant in panel discussion entitled "Solid Sample Introduction", European Winter Conference on Plasma Spectrochemistry, Ft. Lauderdale, Florida, USA, January, 1996.

Oral presentation, 8th BNASS, University of East Anglia, Norwich, UK, July, 1996.

Appendix 1

Abel Inversion Programme to calculate radial profiles from lateral data

Written by Dr. Izumi Ishii, The George Washington University, USA, October 1987

```
10 REM ***** RADIAL DISTRIBUTION FOR TEMPERATURE *****
30 REM WRITEN BY IZUMI ISHII   *****  OCT 1987
70 REM PART-1: By using the NESTOR-OLSON ABEL INVERSION method
the lateral data
80 REM are spatially resolved.see refs. 2 & 3.
90 REM PART-2: By using the SLOPE METHOD, the EXCITATION
TEMPERATURE at
100 REM different radius is calculated. For SLOPE-METHOD.
140 DIM QA(10, 10), BS(10), JC(10), IR(10), JO(10), VY(10), AA(10), BB(10),
CC(10), DD(10), EE(10), FF(10), GG(10)
150 DIM XI(51), A(51, 51), B(51, 51), TRI(51), T(51), J(10, 51), xs(10, 10)
160 DIM G(10), RTP(10), w(10), E(10), Y(10)
170 DIM SX#(12), SY#(12), SY(12), VA(10), DX(51), DY(51), VARIANCE(10)
180 DIM XX(200), YY(200), XP(200)
200 INPUT "The number of lines :", eline
1900 REM       EXCITATION TEMPERATURE MEASUREMENT (SLOPE
METHOD)
1920 nN = eline
1930 FOR eline = 1 TO nN
   PRINT "SPECTRAL LINE #", eline
   INPUT "INPUT DATAFILE :", FILE$
   OPEN "I", 1, FILE$
   INPUT #1, NPTS
   NR = NPTS
   FOR I = 1 TO NPTS
   INPUT #1, XX(I), YY(I): J(eline, I) = YY(I): NEXT I: CLOSE #1
1940 INPUT "DEXCITATION ENERGY (eV)<Ha=1.89,Hb=2.55>  "; w(eline)
1950 INPUT "EXCITATION ENERGY  (eV)<Ha=12.09,Hb=12.75>"; E(eline)
1960 INPUT "gf VALUES          <Ha=0.696,Hb=0.122>"; RTP(eline)
   PRINT "  "
1970 NEXT eline
1980 REM
1990 REM CALCULATE LOG(G.RTP.W^3/J(line,radius))
2000 REM       assuming G is RTP already includes G factor
   REM calculate log(rtp*W^3/j(line,radius))
2010 FOR RADIUS = 1 TO NR
2020 FOR eline = 1 TO nN
   IF J(eline, RADIUS) = 0! THEN Y(eline) = 0!: GOTO 2040
2030 Y(eline) = RTP(eline) * w(eline) ^ 3 / J(eline, RADIUS)
2040 NEXT eline
2050 REM
```

```
2060 REM CALCULATE SLOPE FOR LOG(G.RTP.V/J(LINE<RADIUS))
VERSUS E
2070 REM USING LINEAR LEAST SQUARE FIT, Y=M*X+B  (log(y)=M*e+B
M=1/(8.614e-5*T(K))
2080 REM
        REM    if nn>2 then goto 2090
        REM    if y(1)<=0 then yy(radius)=0:goto 2250
        REM    if y(2)<=0 then yy(radius)=0:goto 2250
        REM    m=(log(y(2))-log(y(1)))/(e(2)-e(1))
        REM    goto 2245
2090 XYSUM = 0: XSUM = 0: YSUM = 0: X2SUM = 0: Y2SUM = O: N = 0
2100 FOR J = 1 TO eline
   IF Y(J) <= 0 THEN GOTO 2160
   N = N + 1
   Y(J) = LOG(Y(J))
2110 XYSUM = XYSUM + (E(J) * Y(J))
2120 XSUM = XSUM + E(J)
2130 YSUM = YSUM + Y(J)
2140 X2SUM = X2SUM + (E(J) ^ 2)
2150 Y2SUM = Y2SUM + (Y(J) ^ 2)
2160 NEXT J
   IF N <= 1 THEN YY(RADIUS) = 0: GOTO 2250
2170 m = (N * XYSUM - XSUM * YSUM) / (N * X2SUM - XSUM ^ 2)
2180 REM B=YSUM/N-M*XSUM/N
2190 REM CC=(N*XYSUM-XSUM*YSUM)/SQR((N*X2SUM-
XSUM^2)*(N*Y2SUM-YSUM^2))
   REM if cc=0 then xp(radius)=0 else cc=1/cc/8.614e-5:xp(radius)=cc
2230 REM PRINT "CORRELATION COEFICIENT";CC
2240 REM PRINT "RADIUS";RADIUS;"EXCITATION TEMP.";T(RADIUS)
2245 YY(RADIUS) = 1 / m: YY(RADIUS) = YY(RADIUS) / 8.614E-05
2250 PRINT RADIUS; YY(RADIUS): NEXT RADIUS
   GOSUB 3000
   INPUT "OUTPUT FILENAME(T)=", FILE$
   OPEN "O", 3, FILE$
   PRINT #3, NR
   FOR I = 1 TO NR
   PRINT #3, XX(I), YY(I): NEXT I: CLOSE #3
2260 END
2270 RETURN
2280 REM ************************************************************************
2290 PRINT "       SIMULTANEOUS LINEAR EQUATIONS(SLE)"
2300 FL% = 0
2310 DT = 1: MZ% = N: IF FL% >= 0 THEN MZ% = N + 1
2320 EP = 1E-12
2330 FOR K = 1 TO N
2340 PV# = 0
2350 FOR I = 1 TO N
2360 FOR J = 1 TO N
2370 IF K = 1 THEN 2430
```

```
2375 REM Kazzer, I've changed varible IS to ZS, due to logical operator
overlap
2380 FOR ZS = 1 TO K - 1
2390 FOR JS = 1 TO K - 1
2400 IF I = IR(ZS) THEN 2450
2410 IF J = JC(JS) THEN 2450
2420 NEXT JS, ZS
2430 IF ABS(QA(I, J)) <= ABS(PV#) THEN 2450
2440 PV# = QA(I, J): IR(K) = I: JC(K) = J
2450 NEXT J, I
2460 IF ABS(PV#) < EP THEN DT = 0: PRINT "DETERMINANT ZERO":
RETURN
2470 DT = DT * PV#
2480 FOR J = 1 TO MZ%: QA(IR(K), J) = QA(IR(K), J) / PV#: NEXT J
2490 QA(IR(K), JC(K)) = 1 / PV#
2500 FOR I = 1 TO N
2510 QA = QA(I, JC(K))
2520 IF I = IR(K) THEN 2570
2530 QA(I, JC(K)) = -QA / PV#
2540 FOR J = 1 TO MZ%
2550 IF J <> JC(K) THEN QA(I, J) = QA(I, J) - QA * QA(IR(K), J)
2560 NEXT J
2570 NEXT I, K
2580 FOR I = 1 TO N: JO(IR(I)) = JC(I)
2590 IF FL% >= 0 THEN BS(JC(I)) = QA(IR(I), MZ%)
2600 NEXT I
2610 IN = 0
2620 FOR I = 1 TO N - 1
2630 FOR J = I + 1 TO N
2640 IF JO(J) >= JO(I) THEN 2660
2650 JT = JO(J): JO(J) = JO(I): JO(I) = JT: IN = IN + 1
2660 NEXT J, I
2670 IF 2 * INT(IN / 2) <> IN THEN DT = -DT
2680 IF FL% > 0 THEN RETURN
2690 FOR J = 1 TO N
2700 FOR I = 1 TO N
2710 VY(JC(I)) = QA(IR(I), J)
2720 NEXT I
2730 FOR I = 1 TO N
2740 QA(I, J) = VY(I): NEXT I
2750 NEXT J
2760 FOR I = 1 TO N
2770 FOR J = 1 TO N
2780 VY(IR(J)) = QA(I, JC(J)): NEXT J
2790 FOR J = 1 TO N
2800 QA(I, J) = VY(J): NEXT J
2810 NEXT I
2820 RETURN
2830 REM ref.1: Physical Chemistry On A Microcomputer by Joseph
H.Noggle,                Univ. of Delaware, 1985, chapter 4.
```

```
2840 REM ref.2: C.J.Cremers and R.C.Birkebak, Appl. Optics,5,1057(1966)
2850 REM ref.3: Theor. & Exper. Invest. of Ar ICP as a Spectrochemical
Source ,Ph.D. Thesis by R.G.Schleicher,U. of Mass., 1979,          see
P288-290,317-319.


3000 REM subroutine plot
3010 REM find ymin and ymax
3020 ymin = YY(1): YMAX = YY(1)
3030 FOR N = 1 TO NPTS
3040 IF YY(N) > YMAX THEN YMAX = YY(N)
3050 IF YY(N) < ymin THEN ymin = YY(N)
3060 NEXT N
3070 XMIN = XX(1): XMAX = XX(NPTS)
3080 REM plot
3090 SCREEN 2, 0, 0
3100 LINE (10, 10)-(630, 10)
3110 LINE (630, 10)-(630, 180)
3120 LINE (630, 180)-(10, 180)
3130 LINE (10, 180)-(10, 10)
3140 CX = 600 / (XMAX - XMIN)
3150 CY = 160 / (YMAX - ymin)
3160 X0 = 20
3170 Y0 = 175
3180 FOR N = 1 TO NPTS
3190 XL = (XX(N) - XMIN) * CX
3200 XL = XL + X0
3210 YL = (YY(N) - ymin) * CY
3220 YL = Y0 - YL
3230 PSET (XL, YL)
3240 NEXT N
3315 LOCATE 1, 35: PRINT "Temperature Profile"
3340 LOCATE 1, 1
3350 INPUT X$
3360 SCREEN 0, 0: RETURN
```

Procedure for Abel inverting data.

1) From Excel:

Save each line of view x data as follows:

26
0 0001
0.4 0002
0.8 0003
1.2 0004
to
10 0026

where 1st column is the view x position and the 2nd is the emission intensity.

2) Save these files as .csv files (comma delimited files)

3) Copy files to directory where Abel inversion program is i.e. a:\iitemp

4) From ms dos prompt type edit and name of file i.e. edit mxsol.csv

5) Delete commas and instead put a space between each data set.

6) Save files.

7) Exit

8) Run qbasic

9) Run sabel.bas program

10 Type in number of lines i.e. 26

11) Type in file name i.e. mxsol.csv

12) Press enter when prompted

13) Save output file as a comma delimited file. i.e. mx1.csv

14) Repeat Abel inversion for other data files

15) Exit qbasic

16) Run Excel. Open .csv files

17) To get data into two rows for plotting as graphs etc.: Highlight column, click on 'data' icon, click on 'text to columns' highlight 'fixed width', comma delimit, enter. Save as .xls files